

Drivers of plant nutrient acquisition and allocation strategies and their influence  
on plant responses to environmental change

by

Evan A. Perkowski, B.S.

A Dissertation

In

Biological Sciences

Submitted to the Graduate Faculty  
of Texas Tech University in  
Partial Fulfillment of  
the Requirements for  
the Degree of

Doctor of Philosophy

Approved

Nicholas G. Smith, Ph.D.  
Chair of Committee

Aimée T. Classen, Ph.D.

Natasja van Gestel, Ph.D.

Lindsey C. Slaughter, Ph.D.

Dylan W. Schwilk, Ph.D.

Mark Sheridan, Ph.D.  
Dean of the Graduate School

May 2023

Copyright 2023, Evan A. Perkowski

## Acknowledgements

This dissertation was made possible by the mentorship, collaboration, and friendship of many people. I am so thankful to be surrounded by such supportive and helpful mentors, peers, and friends that have made navigating through graduate school and finishing this dissertation an enjoyable experience. Specifically, I am thankful for the incredible mentorship of my advisor and committee chair, Dr. Nick Smith, who provided invaluable insight and tools that have helped shape me into the plant ecophysiological I claim to be today. I am also indebted to my committee members, Drs. Aimée Classen, Natasja van Gestel, Dylan Schwilk, and Lindsey Slaughter, for useful feedback, invaluable support, and encouragement as I planned and implemented experiments.

I am also thankful for past and present members of the EcoHealth lab for encouragement, support, and extracurricular activities that made time inside and outside the lab enjoyable and memorable. Particular thanks go to Dr. Lizz Waring, Dr. Xiulin Gao, Helen Scott, and Risa McNellis, Billi Jean Petermann, and the late Dr. Kris Petterson, all of whom were invaluable to helping me navigate my first year. I am especially thankful for the mentorship and friendship of Dr. Lizz Waring, as our weekly coffee chats were instrumental for helping me feel welcome in Lubbock and acclimate to life as a graduate student. I am also grateful for the friendship of Billi Jean Petermann and the late Dr. Kris Petterson for their encouragement and willingness to discuss microbial symbioses over coffee on random Saturday mornings.

Additional thanks go out to Isa Beltran, Snehanjana Chatterjee, Jeff Chi-

eppa, Peter Eludini, Zinny Ezekannagha, Hannah German, Eve Gray, Monika Kelley, Azaj Mahmud, Jorge Ochoa, Brad Posch, Avery Schoenherr, Christine Vanginault, and Jose Villeda for help with experiments or for lending an ear over puzzling results. I am also thankful for collaborators Dr. Christy Goodale and Dave Frey, who provided invaluable insight for the second experimental chapter.

I would like to thank my undergraduate advisor, Dr. Janice Krumm, for continued mentorship and friendship and for insightful advice about navigating graduate school, but most of all for helping me realize my career aspirations and pushing me to pursue this endeavor. Additional thanks go out to my family, particularly my parents, partner, and dog for continued support and distractions outside the lab. The experiments included here would not have been possible without their emotional and monetary support.

This work was made possible from funding by the NSF, USDA, Braun and Gresham, PLLC., and was a contribution to the LEMONTREE (Land Ecosystem Models based On New Theory, obseRvations and ExperimEnts) project. The LEMONTREE project is funded through the generosity of Eric and Wendy Schmidt by recommendation of the Schmidt Futures programme and the Imperial College initiative on Grand Challenges in Ecosystems and the Environment. This work was also funded by graduate student research awards from Texas Tech University and the Botanical Society of America.

I have inevitably missed mentioning folks that were instrumental to the completion of these experiments and contributed to my development as a plant ecophysiological. Please know that I am grateful and appreciative of our interactions.

## Table of Contents

<b>Acknowledgements . . . . .</b>	ii
<b>Abstract . . . . .</b>	ix
<b>List of Tables . . . . .</b>	xi
<b>List of Figures . . . . .</b>	xv
<b>1. Introduction . . . . .</b>	1
<b>2. Structural carbon costs to acquire nitrogen are determined by nitrogen and light availability in two species with different nitrogen acquisition strategies . . . . .</b>	7
2.1    Introduction . . . . .	7
2.2    Methods . . . . .	11
2.2.1 <i>Experiment setup</i> . . . . .	11
2.2.2 <i>Plant measurements and calculations</i> . . . . .	12
2.2.3 <i>Statistical analyses</i> . . . . .	13
2.3    Results . . . . .	15
2.3.1 <i>Carbon costs to acquire nitrogen</i> . . . . .	15
2.3.2 <i>Whole plant nitrogen biomass</i> . . . . .	18
2.3.3 <i>Root carbon biomass</i> . . . . .	20
2.3.4 <i>Root nodule biomass</i> . . . . .	22
2.4    Discussion . . . . .	26
2.4.1 <i>Carbon costs to acquire nitrogen increase with light availability and decrease with fertilization</i> . . . . .	26
2.4.2 <i>Modeling implications</i> . . . . .	28
2.4.3 <i>Study limitations</i> . . . . .	30
2.4.4 <i>Conclusions</i> . . . . .	32
<b>3. Soil nitrogen availability modifies leaf nitrogen economies in mature temperate deciduous forests: a direct test of photosynthetic least-cost theory . . . . .</b>	34
3.1    Introduction . . . . .	34

3.2	Methods	38
3.2.1	<i>Study site description</i>	38
3.2.2	<i>Experimental design</i>	39
3.2.3	<i>Leaf gas exchange and trait measurements</i>	39
3.2.4	$A_{net}/C_i$ curve-fitting and parameter estimation	42
3.2.5	<i>Proportion of leaf nitrogen allocated to photosynthesis and structure</i>	44
3.2.6	<i>Tradeoffs between nitrogen and water use</i>	45
3.2.7	<i>Soil nitrogen availability and pH</i>	46
3.2.8	<i>Statistical analyses</i>	48
3.3	Results	50
3.3.1	<i>Leaf nitrogen content</i>	50
3.3.2	<i>Net photosynthesis and leaf biochemistry</i>	53
3.3.3	<i>Leaf nitrogen allocation</i>	56
3.3.4	<i>Tradeoffs between nitrogen and water use</i>	59
3.4	Discussion	62
3.4.1	<i>Soil nitrogen availability modifies tradeoffs between nitrogen and water use</i>	63
3.4.2	<i>Soil pH did not modify tradeoffs between nitrogen and water usage</i>	65
3.4.3	<i>Species identity explains a large amount of variation in leaf and whole plant traits</i>	66
3.4.4	<i>Implications for photosynthetic least-cost theory model development</i>	67
3.4.5	<i>Conclusions</i>	69
4.	<b>The relative cost of resource use for photosynthesis drives variance in leaf nitrogen content across a climate and soil resource availability gradient</b>	70
4.1	Introduction	70
4.2	Methods	76
4.2.1	<i>Site descriptions and sampling methodology</i>	76

4.2.2 <i>Leaf trait measurements</i>	77
4.2.3 <i>Site climate data</i>	82
4.2.4 <i>Site edaphic characteristics</i>	82
4.2.5 <i>Plant functional group assignments</i>	84
4.2.6 <i>Data analysis</i>	85
4.3 Results	88
4.3.1 <i>Cost to acquire nitrogen relative to water</i>	88
4.3.2 <i>Leaf <math>C_i:C_a</math></i>	91
4.3.3 <i>Leaf nitrogen content</i>	94
4.3.4 <i>Structural equation model</i>	98
4.4 Discussion	101
4.4.1 <i>Negative effects of leaf <math>C_i:C_a</math> on <math>N_{area}</math> are driven by reductions in <math>M_{area}</math>, not <math>N_{mass}</math></i>	101
4.4.2 <i>Soil nitrogen availability increases <math>N_{area}</math> through changes in <math>\beta</math></i>	103
4.4.3 <i>Soil moisture increases <math>N_{area}</math> by facilitating increases in soil nitrogen availability</i>	104
4.4.4 <i>Indirect effects of climate on <math>N_{area}</math> are mediated through changes in leaf <math>C_i:C_a</math> and <math>\beta</math></i>	105
4.4.5 <i>Species identity traits modify effects of the environment on <math>\beta</math>, leaf <math>C_i:C_a</math>, and <math>N_{area}</math></i>	106
4.4.6 <i>Next steps for optimality model development</i>	107
4.4.7 <i>Conclusions</i>	108
5. Optimal resource investment to photosynthetic capacity maximizes nutrient allocation to whole plant growth under elevated CO <sub>2</sub>	109
5.1 Introduction	109
5.2 Methods	114
5.2.1 <i>Seed treatments and experimental design</i>	114
5.2.2 <i>Growth chamber conditions</i>	115
5.2.3 <i>Leaf gas exchange measurements</i>	117

5.2.4 <i>Leaf trait measurements</i> . . . . .	118
5.2.5 <i>A/C<sub>i</sub> curve fitting and parameter estimation</i> . . . . .	120
5.2.6 <i>Stomatal limitation</i> . . . . .	121
5.2.7 <i>Proportion of leaf nitrogen allocated to photosynthesis and structure</i> . . . . .	121
5.2.8 <i>Whole plant traits</i> . . . . .	123
5.2.9 <i>Statistical analyses</i> . . . . .	125
5.3 Results . . . . .	127
5.3.1 <i>Leaf nitrogen and chlorophyll content</i> . . . . .	127
5.3.2 <i>Leaf biochemistry and stomatal conductance</i> . . . . .	131
5.3.3 <i>Leaf nitrogen allocation</i> . . . . .	135
5.3.4 <i>Whole plant traits</i> . . . . .	139
5.3.5 <i>Nitrogen fixation</i> . . . . .	143
5.4 Discussion . . . . .	147
5.4.1 <i>Soil nitrogen fertilization has divergent effects on leaf and whole plant acclimation responses to CO<sub>2</sub></i> . . . . .	148
5.4.2 <i>Implications for future model development</i> . . . . .	151
5.4.3 <i>Study limitations and future directions</i> . . . . .	153
5.4.4 <i>Conclusions</i> . . . . .	154
6. Conclusions . . . . .	156
References . . . . .	166
Appendix A: Supplemental material for "Structural carbon costs to acquire nitrogen are determined by nitrogen and light availability in two species with different nitrogen acquisition strategies" . . . . .	203
Appendix B: Supplemental material for "Soil nitrogen availability modifies leaf nitrogen economies in mature temperate deciduous forests: a direct test of photosynthetic least-cost theory" . . . . .	207

<b>Appendix C: Supplemental material for "The relative cost of resource use for photosynthesis drives variance in leaf nitrogen content across a climate and soil resource availability gradient" . . . . .</b>	<b>212</b>
<b>Appendix D: Supplemental material for "Optimal resource investment to photosynthetic capacity maximizes nutrient allocation to whole plant growth under elevated CO<sub>2</sub>" . .</b>	<b>218</b>

## Abstract

Photosynthesis is the largest carbon flux between the atmosphere and is constrained by ecosystem carbon and nutrient cycle dynamics, which causes terrestrial biosphere models to be sensitive to the formulation of photosynthetic processes. Terrestrial biosphere models exhibit high divergence in simulated carbon and nitrogen fluxes under future environmental conditions, which may be due to uncertainty in the acclimation response of photosynthetic processes to environmental change. Photosynthetic least-cost theory provides a promising framework for understanding effects of climatic and edaphic factors on photosynthetic acclimation responses to changing environments. Yet, empirical tests of the theory are rare, limiting our ability to assess whether the theory is suitable for implementation in next-generation terrestrial biosphere models.

Here, I present four experiments designed to test assumptions of photosynthetic least-cost theory. Experiment chapters are flanked by a general introduction chapter and conclusions chapter. The first experimental chapter quantifies structural carbon costs to acquire nitrogen in *Glycine max* and *Gossypium hirsutum* grown under four nitrogen fertilization levels and four light availability levels in a full factorial greenhouse experiment. I find that carbon costs to acquire nitrogen in both species increase with increasing light availability and decrease with increasing fertilization, though responses to fertilization in *G. max* were markedly less than *G. hirsutum*. The second experimental chapter quantifies leaf nitrogen and photosynthetic traits in upper canopy leaves of deciduous trees growing in a 9-year nitrogen-by-sulfur field manipulation experiment. I find strong evi-

dence for nitrogen-water use tradeoffs with increasing soil nitrogen availability, evidenced through a strong negative relationship between leaf nitrogen content and leaf  $C_i:C_a$  and stronger increase in leaf nitrogen content with increasing soil nitrogen availability than leaf  $C_i:C_a$ . The third experiment investigates variance in leaf nitrogen content across a climate and soil resource availability gradient in Texan grasslands, showing that effects of soil resource availability and climate on leaf nitrogen content are driven by changes in leaf  $C_i:C_a$ . Finally, the fourth experiment quantifies leaf and whole plant acclimation responses in *G. max* grown under two atmospheric CO<sub>2</sub> levels, with and without inoculation with *Bradyrhizobium japonicum*, and across nine nitrogen fertilization treatments in a full factorial growth chamber experiment. I find that leaf acclimation responses to CO<sub>2</sub> were independent of soil nitrogen fertilization or inoculation treatment, though stimulations in whole plant growth under elevated CO<sub>2</sub> were enhanced with increasing soil nitrogen fertilization and in inoculated pots under low nitrogen fertilization.

Experiments included in this dissertation provide consistent support for patterns expected from photosynthetic least-cost theory. The use of multiple experimental approaches allowed me to examine mechanisms driving patterns expected from the theory and investigate whether these patterns occur in the field across environmental gradients. Findings from these chapters challenge common paradigms in plant ecophysiology, providing empirical evidence suggesting that including photosynthetic least-cost frameworks in terrestrial biosphere models may improve the longstanding observed divergence in simulated outcomes across terrestrial biosphere model products.

## List of Tables

2.1	Analysis of variance results exploring species-specific effects of light availability, nitrogen fertilization, and their interactions on carbon costs to acquire nitrogen, whole-plant nitrogen biomass, and root carbon biomass . . . . .	16
2.2	Analysis of variance results exploring effects of light availability, nitrogen fertilization, and their interactions on <i>G. max</i> root nodule biomass and the ratio of root nodule biomass to root biomass . . . . .	23
2.3	Slopes of the regression line describing the relationship between each dependent variable and nitrogen fertilization at each light level	24
3.1	Effects of soil nitrogen availability, soil pH, and species on leaf nitrogen content per unit leaf area, leaf nitrogen content per unit leaf mass, and leaf mass per unit leaf area . . . . .	51
3.2	Effects of soil nitrogen availability, soil pH, species, and $N_{\text{area}}$ on net photosynthesis, the maximum rate of Rubisco carboxylation, the maximum rate of RuBP regeneration, and the ratio of the maximum rate of RuBP regeneration to the maximum rate of Rubisco carboxylation . . . . .	54
3.3	Effects of soil nitrogen availability, soil pH, and species on the proportion of leaf nitrogen content allocated to photosynthesis, Rubisco, bioenergetics, and structure . . . . .	57

3.4 Effects of soil nitrogen availability, soil pH, species, and $N_{\text{area}}$ on $\chi$ , photosynthetic nitrogen use efficiency, leaf nitrogen content per unit $\chi$ , and maximum Rubisco carboxylation rate per unit $\chi$ . . . . .	60
4.1 Site locality information, sampling year, 2006-2020 mean annual precipitation, mean annual temperature, and water holding capacity	80
4.2 Effects of soil moisture, soil nitrogen availability, and plant functional group on $\beta$ . . . . .	89
4.3 Effects of soil moisture, soil nitrogen availability, and plant functional group on leaf $C_i:C_a$ . . . . .	92
4.4 Effects of soil moisture, soil nitrogen availability, plant functional group, and leaf $C_i:C_a$ on leaf nitrogen content per unit leaf area, leaf nitrogen content per unit leaf biomass, and leaf biomass per unit leaf area . . . . .	96
4.5 Structural equation model results investigating direct effects of climatic and soil resource availability on leaf nitrogen content . . . . .	99
5.1 Effects of soil nitrogen fertilization, inoculation, and $\text{CO}_2$ treatments on leaf nitrogen content per unit leaf area, leaf nitrogen content per unit leaf mass, leaf mass per unit leaf area, and chlorophyll content per unit leaf area . . . . .	129

5.2 Effects of soil nitrogen fertilization, inoculation, and CO <sub>2</sub> on the maximum rate of Rubisco carboxylation, the maximum rate of RuBP regeneration, dark respiration, the ratio of the maximum rate of RuBP regeneration to the maximum rate of Rubisco carboxylation, stomatal conductance, and stomatal limitation . . . . .	133
5.3 Effects of soil nitrogen fertilization, inoculation, and CO <sub>2</sub> on the fraction of leaf nitrogen allocated to Rubisco, bioenergetics, light harvesting proteins, photosynthesis, and structure . . . . .	137
5.4 Effects of CO <sub>2</sub> , fertilization, and inoculation on total leaf area, whole plant biomass, carbon costs to acquire nitrogen, belowground carbon biomass, and whole plant nitrogen biomass . . . . .	141
5.5 Effects of CO <sub>2</sub> , fertilization, and inoculation on root nodule biomass, plant investments in symbiotic nitrogen fixation, and percent nitrogen fixed from the atmosphere . . . . .	145
A1 Summary table containing volumes of compounds used to create modified Hoagland's solutions for each soil nitrogen fertilization treatment . . . . .	203
A2 Analysis of variance results exploring species-specific effects of light availability, nitrogen fertilization, and their interactions on the ratio of whole plant biomass to pot volume . . . . .	204
A3 Slopes of the regression line describing the relationship between each dependent variable and nitrogen fertilization at each light level	205

B1	Sample sizes of each species, abbreviated by their USDA NRCS PLANTS database code, within each plot at each site . . . . .	207
B2	Analysis of variance results exploring the linear effect of leaf temperature on net photosynthesis rate and stomatal conductance measured at 400 $\mu\text{mol mol}^{-1}$ CO <sub>2</sub> . . . . .	208
B3	Second order log-polynomial regression coefficients that described the effect of leaf temperature on net photosynthesis and stomatal conductance measured at 400 $\mu\text{mol mol}^{-1}$ CO <sub>2</sub> . . . . .	209
B4	Mean, standard error, and 95% confidence interval ranges of soil nitrogen availability estimates across all measured plots . . . . .	210
C1	List of sampled species and their plant functional group assignment	214
C2	List of sampled species and their plant functional group assignment (cont.) . . . . .	215
C3	Model selection results for soil moisture and vapor pressure deficit	216
D1	Summary table containing volumes of compounds used to create modified Hoagland's solutions for each soil nitrogen fertilization treatment . . . . .	218
D2	Summary of the daily growth chamber growing condition program	219
D3	Effects of CO <sub>2</sub> , fertilization, and inoculation on whole plant biomass: pot volume . . . . .	220

## List of Figures

2.1 Relationships between soil nitrogen fertilization and light availability on carbon costs to acquire nitrogen in <i>G. hirsutum</i> and <i>G. max</i> . . . . .	17
2.2 Relationships between soil nitrogen fertilization and light availability on whole-plant nitrogen biomass in <i>G. hirsutum</i> and <i>G. max</i> . . . . .	19
2.3 Relationships between soil nitrogen fertilization and light availability on root carbon biomass in <i>G. hirsutum</i> and <i>G. max</i> . . . . .	21
2.4 Effects of shade cover and nitrogen fertilization on root nodule biomass and the ratio of root nodule biomass to root biomass in <i>G. max</i> . . . . .	25
3.1 Effects of soil nitrogen availability and species on leaf nitrogen content per unit leaf area, leaf nitrogen content per unit leaf biomass, and leaf mass per leaf area . . . . .	52
3.2 Effects of soil nitrogen availability, species, and leaf nitrogen content on net photosynthesis, maximum Rubisco carboxylation rate, and maximum RuBP regeneration rate . . . . .	55
3.3 Effects of soil nitrogen availability, species, and leaf nitrogen content on the fraction of leaf nitrogen allocated to photosynthesis and structure . . . . .	58
3.4 Effects of soil N availability, species, and leaf N content on tradeoffs between nitrogen and water use . . . . .	61

4.1	Site locations along 2006-2020 mean annual precipitation and mean annual temperature gradients in Texas, USA. . . . .	81
4.2	Effects of soil nitrogen availability and soil moisture on the cost of acquiring and using nitrogen . . . . .	90
4.3	Effects of 4-day mean vapor pressure deficit, 2-day soil moisture (per water holding capacity), and soil nitrogen availability on leaf $C_i:C_a$ . . . . .	93
4.4	Effects of leaf $C_i:C_a$ , soil nitrogen availability, and soil moisture on leaf nitrogen content per unit leaf area, leaf nitrogen content per unit leaf biomass, and leaf mass per area. . . . .	97
4.5	Structural equation model results exploring drivers of $N_{\text{area}}$ . . . .	100
5.1	Effects of $\text{CO}_2$ , fertilization, and inoculation on leaf nitrogen per unit leaf area, leaf nitrogen content, leaf mass per unit leaf area, and chlorophyll content per unit leaf area . . . . .	130
5.2	Effects of $\text{CO}_2$ , fertilization, and inoculation on maximum rate of Rubisco carboxylation, the maximum rate of RuBP regeneration, and the ratio of the maximum rate of RuBP regeneration to the maximum rate of Rubisco carboxylation leaf mass per unit leaf area, dark respiration, stomatal conductance, and stomatal limitation .	134
5.3	Effects of $\text{CO}_2$ , fertilization, and inoculation on the relative fraction of leaf nitrogen allocated to photosynthesis and the fraction of leaf nitrogen allocated to structure . . . . .	138

5.4	Effects of CO <sub>2</sub> , fertilization, and inoculation on total leaf area, total biomass, and structural carbon costs to acquire nitrogen . . . . .	142
5.5	Effects of CO <sub>2</sub> , fertilization, and inoculation on nodule biomass, nodule biomass: root biomass, and percent nitrogen fixed from the atmosphere . . . . .	146
A1	Effects of shade cover and nitrogen fertilization on the ratio of plant biomass to rooting volume in <i>G. hirsutum</i> and <i>G. max</i> . . . . .	206
B1	Effects of leaf temperature on net photosynthesis rate and stomatal conductance values when measured at 400 μmol mol <sup>-1</sup> CO <sub>2</sub> . . .	211
C1	Model selection results exploring relevant timescales for soil moisture and vapor pressure deficit . . . . .	217
D1	Relationships between area-based leaf nitrogen content, mass-based leaf nitrogen content, and leaf mass per unit leaf area measured on the focal leaf used to generate $A_{\text{net}}/C_i$ curves and leaf nitrogen content measured on the leaf used for chlorophyll extractions . . .	221
D2	Effects of CO <sub>2</sub> , fertilization, and inoculation on the ratio of whole plant biomass to pot volume . . . . .	222

# 1 Chapter 1

## 2 Introduction

3 Photosynthesis represents the largest carbon flux between the atmosphere  
4 and biosphere, and is regulated by complex ecosystem carbon and nutrient cy-  
5 cles (Hungate et al. 2003; IPCC 2021). As a result, the inclusion of robust,  
6 empirically tested representations of photosynthetic processes is critical in order  
7 for terrestrial biosphere models to accurately and reliably simulate carbon and  
8 nutrient fluxes between the atmosphere and terrestrial biosphere (Oreskes et al.  
9 1994; Smith and Dukes 2013; Prentice et al. 2015; Wieder et al. 2015). Despite  
10 evidence that the inclusion of coupled carbon and nutrient cycles can improve  
11 model uncertainty, widespread divergence in predicted carbon and nutrient fluxes  
12 is still apparent across model products (Friedlingstein et al. 2014; Arora et al.  
13 2020; Davies-Barnard et al. 2020). Divergence in predicted carbon and nutrient  
14 fluxes across terrestrial biosphere models may be due to an incomplete under-  
15 standing of how plants acclimate to changing environments (Smith and Dukes  
16 2013; Davies-Barnard et al. 2020), as terrestrial biosphere models are sensitive to  
17 the formulation of photosynthetic processes (Bonan et al. 2011; Ziehn et al. 2011;  
18 Booth et al. 2012; Smith et al. 2016; Smith et al. 2017; Rogers et al. 2017).

Many terrestrial biosphere models predict leaf-level photosynthesis through linear relationships between area-based leaf nitrogen content and the maximum rate of Ribulose-1,5-bisphosphate carboxylase/oxygenase (“Rubisco”), following the idea that large fractions of leaf nitrogen content are allocated to the construction and maintenance of Rubisco and other photosynthetic enzymes (Evans

24 1989). The inclusion of coupled carbon and nutrient cycles in terrestrial bio-  
25 sphere models (Shi et al. 2016; Braghieri et al. 2022) allows for the prediction  
26 of leaf nitrogen content through soil nitrogen availability, which causes models to  
27 indirectly predict photosynthetic processes through shifts in soil nitrogen avail-  
28 ability (Smith et al. 2014; Lawrence et al. 2019). While these patterns are  
29 commonly observed in ecosystems globally (Brix 1971; Evans 1989; Firn et al.  
30 2019; Liang et al. 2020), this formulation does not allow for the prediction of  
31 leaf and whole plant acclimation responses to changing environments (Smith and  
32 Dukes 2013; Rogers et al. 2017; Harrison et al. 2021), and suggests that constant  
33 leaf nitrogen-photosynthesis relationships are ubiquitous across ecosystems.

34 Photosynthetic least-cost theory (Prentice et al. 2014; Wang et al. 2017;  
35 Smith et al. 2019; Paillassa et al. 2020; Scott and Smith 2022; Harrison et al.  
36 2021) provides a contemporary framework for predicting leaf and whole plant ac-  
37 climation responses to environmental change. The theory, which unifies optimal  
38 coordination (Chen et al. 1993; Maire et al. 2012) and least-cost (Wright et al.  
39 2003) theories, posits that plants optimize photosynthetic processes by minimizing  
40 the summed cost of nutrient and water use (i.e.,  $\beta$ ). The summed cost of nutrient  
41 and water use is predicted to be positively correlated with the ratio of intercellular  
42 CO<sub>2</sub> to atmospheric CO<sub>2</sub> (leaf  $C_i:C_a$ ). Leaf  $C_i:C_a$  is determined by factors that  
43 influence leaf nutrient demand, such as CO<sub>2</sub>, temperature, vapor pressure deficit,  
44 and light availability (Prentice et al. 2014; Wang et al. 2017; Smith et al. 2019;  
45 Stocker et al. 2020), and may change in response to changing edaphic charac-  
46 teristics through changes in  $\beta$  (Paillassa et al. 2020). Photosynthetic processes  
47 are optimized such that nutrients and water are allocated to photosynthetic en-

48 zymes to allow net photosynthesis rates to be equally co-limited by the maximum  
49 rate of Rubisco carboxylation and the maximum rate of Ribulose-1,5-bisphosphate  
50 (RuBP) regeneration (Chen et al. 1993; Maire et al. 2012). The theory indicates  
51 that costs of nutrient and water use are substitutable such that, in a given en-  
52 vironment, optimal photosynthesis rates can be achieved by sacrificing inefficient  
53 use of a relatively more abundant (and less costly to acquire) resource for more  
54 efficient use of a relatively less abundant (and more costly to acquire) resource.

55 Optimality models leveraging patterns expected from photosynthetic least-  
56 cost theory have been developed for both C<sub>3</sub> (Wang et al. 2017; Smith et al. 2019;  
57 Stocker et al. 2020) and more recently for C<sub>4</sub> species (Scott and Smith 2022).  
58 Such models show broad agreement with patterns observed across environmental  
59 gradients (Smith et al. 2019; Stocker et al. 2020; Paillassa et al. 2020; Querejeta  
60 et al. 2022; Westerband et al. 2023), and are capable of reconciling dynamic  
61 leaf nitrogen-photosynthesis relationships and acclimation responses to elevated  
62 CO<sub>2</sub>, temperature, light availability, and vapor pressure deficit (Dong et al. 2017;  
63 Dong et al. 2020; Smith and Keenan 2020; Luo et al. 2021; Peng et al. 2021;  
64 Dong et al. 2022; Dong et al. 2022; Querejeta et al. 2022; Westerband et al.  
65 2023). Current versions of optimality models that invoke patterns expected from  
66 photosynthetic least-cost theory hold  $\beta$  constant across growing environments.  
67 As growing evidence suggests that costs of nutrient use change across resource  
68 availability and climatic gradients in species with different nutrient acquisition  
69 strategies (Fisher et al. 2010; Brzostek et al. 2014; Terrer et al. 2018; Allen et al.  
70 2020), one might expect that  $\beta$  should dynamically change across environments  
71 and in species with different nutrient acquisition strategies.

72        Despite recent recognition that patterns expected from photosynthetic  
73 least-cost theory occur across broad environmental gradients, a limited number  
74 of studies have investigated how  $\beta$  varies across edaphic and climatic gradients  
75 and how variance in  $\beta$  might scale to influence leaf nutrient-water use tradeoffs  
76 (Lavergne et al. 2020; Paillassa et al. 2020). Furthermore, no previous study has  
77 investigated whether  $\beta$  varies in species with different nutrient acquisition strate-  
78 gies, or if changes in  $\beta$  due to changes in edaphic characteristics scale to influence  
79 leaf or whole plant acclimation responses to changing environments. The lack of  
80 such studies provided motivation for the experimental chapters included in this  
81 dissertation.

82        In this dissertation, I use a combination of greenhouse, field manipulation,  
83 environmental gradient, and growth chamber experiments to quantify leaf and  
84 whole plant acclimation responses across various climatic and edaphic conditions  
85 and different nutrient acquisition strategies. Together, these experiments eval-  
86 uated patterns expected from photosynthetic least-cost theory and test mechanisms  
87 predicted to drive responses expected from theory. The empirical data collected  
88 in these experiments provide important information needed to refine existing opti-  
89 mality models that include photosynthetic least-cost frameworks, and could help  
90 determine whether such models are suitable for implementing in next-generation  
91 terrestrial biosphere models. While theory suggests that plants acclimate across  
92 environments by minimizing the summed cost of nutrients relative to water, I chose  
93 to isolate effects of soil nitrogen availability on costs of nitrogen acquisition rela-  
94 tive to water for the sake of brevity. I acknowledge that patterns expected from  
95 theory may be modified by other nutrients (e.g., phosphorus) or other edaphic

96 characteristics (Smith et al. 2019; Paillassa et al. 2020; Westerband et al. 2023),  
97 and, though not included here, should also be investigated.

98 In the first experimental chapter, I re-analyze data from a greenhouse ex-  
99 periment that grew *Glycine max* and *Gossypium hirsutum* seedlings under full-  
100 factorial combinations of four light treatments and four fertilization treatments  
101 to examine effects of nitrogen and light availability on structural carbon costs to  
102 acquire nitrogen. In the second experimental chapter, I measure leaf physiological  
103 traits in the upper canopy of mature trees growing in a 9-year nitrogen-by-pH  
104 field manipulation experiment to assess whether changes in soil nitrogen availabil-  
105 ity or soil pH modify nitrogen-water use trade-offs expected from photosynthetic  
106 least-cost theory. The third experimental chapter leverages a broad precipitation  
107 and soil nitrogen availability gradient in Texan grasslands to investigate primary  
108 drivers of leaf nitrogen content. In the fourth experimental chapter, I use growth  
109 chambers to quantify leaf and whole plant acclimation responses to CO<sub>2</sub> across  
110 a soil nitrogen fertilization gradient, while also manipulating nutrient acquisition  
111 strategy by controlling whether seedlings were able to form associations with sym-  
112 biotic nitrogen-fixing bacteria.

113 Across experiments, I find strong and consistent support for patterns ex-  
114 pected from photosynthetic least-cost theory, showing that shifts in edaphic char-  
115 acteristics predictably alter  $\beta$ , and that shifts in  $\beta$  facilitate changes in leaf  
116 nitrogen-water use tradeoffs and leaf nitrogen-photosynthesis relationships. I also  
117 show that costs of nitrogen acquisition vary in species with different nitrogen  
118 acquisition strategies. Finally, I show strong evidence suggesting that leaf accli-  
119 mation responses to elevated CO<sub>2</sub> are decoupled from soil nitrogen availability and

120 inoculation with symbiotic nitrogen-fixing bacteria. It is my hope that these ex-  
121 periments will encourage future iterations of optimality models that adopt photo-  
122 synthetic least-cost frameworks to consider frameworks for implementing dynamic  
123  $\beta$  values across soil resource availability gradients and in species with different nu-  
124 trient acquisition strategies.

125 The four experimental chapters included in this dissertation are presented  
126 either as previously published journal articles or as manuscript drafts currently  
127 in preparation for journal submission. Specifically, the first experimental chapter  
128 was published in *Journal of Experimental Botany* in 2021 and the second chapter  
129 is currently in review, while the third and fourth chapters are each in preparation  
130 for journal submission. The dissertation concludes with a sixth chapter that sum-  
131 marizes experiment findings, briefly synthesizes common themes observed across  
132 experiments, and provides some suggestions for future experimentation.

133

## Chapter 2

134

Structural carbon costs to acquire nitrogen are determined by  
135 nitrogen and light availability in two species with different nitrogen  
136 acquisition strategies

137 Perkowski EA, EF Waring, NG Smith, "Root mass carbon costs to acquire nitro-  
138 gen are determined by nitrogen and light availability in two species with different  
139 nitrogen acquisition strategies", *Journal of Experimental Botany*, 2021, Volume  
140 72, Issue 15, Pages 5766-5776, by permission of Oxford University Press

141 2.1 Introduction

142 Carbon and nitrogen cycles are tightly coupled in terrestrial ecosystems. This  
143 tight coupling influences photosynthesis (Walker et al. 2014; Rogers et al. 2017),  
144 net primary productivity (LeBauer and Treseder 2008; Thomas et al. 2013), de-  
145 composition (Cornwell et al. 2008; Bonan et al. 2013; Sulman et al. 2019), and  
146 plant resource competition (Gill and Finzi 2016; Xu-Ri and Prentice 2017). Ter-  
147 restrial biosphere models are beginning to include connected carbon and nitrogen  
148 cycles to improve the realism of their simulations (Fisher et al. 2010; Brzostek  
149 et al. 2014; Wieder et al. 2015; Shi et al. 2016; Zhu et al. 2019). Simula-  
150 tions from these models indicate that coupling carbon and nitrogen cycles can  
151 drastically influence future biosphere-atmosphere feedbacks under global change,  
152 such as elevated carbon dioxide or nitrogen deposition (Thornton et al. 2007;  
153 Goll et al. 2012; Wieder et al. 2015; Wieder et al. 2019). Nonetheless, there  
154 are still limitations in our quantitative understanding of connected carbon and  
155 nitrogen dynamics (Thomas et al. 2015; Meyerholt et al. 2016; Rogers et al.  
156 2017; Exbrayat et al. 2018; Shi et al. 2019), forcing models to make potentially  
157 unreliable assumptions.

158 Plant nitrogen acquisition is a process in terrestrial ecosystems by which  
159 carbon and nitrogen are tightly coupled (Vitousek and Howarth 1991; Delaire  
160 et al. 2005; Brzostek et al. 2014). Plants must allocate photosynthetically de-  
161 rived carbon belowground to produce and maintain root systems or exchange with  
162 symbiotic soil microbes in order to acquire nitrogen (Högberg et al. 2008; Hög-  
163 berg et al. 2010). Thus, plants have an inherent carbon cost associated with  
164 acquiring nitrogen, which can include both direct energetic costs associated with  
165 nitrogen acquisition and indirect costs associated with building structures that  
166 support nitrogen acquisition (Gutschick 1981; Rastetter et al. 2001; Vitousek  
167 et al. 2002; Menge et al. 2008). Model simulations (Fisher et al. 2010; Brzostek  
168 et al. 2014; Shi et al. 2016; Allen et al. 2020) and meta-analyses (Terrer et al.  
169 2018) suggest that these carbon costs vary between species, particularly those  
170 with different nitrogen acquisition strategies. For example, simulations using iter-  
171 ations of the Fixation and Uptake of Nitrogen (FUN) model indicate that species  
172 that acquire nitrogen from non-symbiotic active uptake pathways (e.g. mass flow)  
173 generally have larger carbon costs to acquire nitrogen than species that acquire  
174 nitrogen through symbiotic associations with nitrogen-fixing bacteria (Brzostek  
175 et al. 2014; Allen et al. 2020).

176 Carbon costs to acquire nitrogen likely vary in response to changes in soil  
177 nitrogen availability. For example, if the primary mode of nitrogen acquisition  
178 is through non-symbiotic active uptake, then nitrogen availability could decrease  
179 carbon costs to acquire nitrogen as a result of increased per-root nitrogen up-  
180 take (Franklin et al. 2009; Wang et al. 2018). However, if the primary mode of  
181 nitrogen acquisition is through symbiotic active uptake, then nitrogen availabil-

182 ity may incur additional carbon costs to acquire nitrogen if it causes microbial  
183 symbionts to shift toward parasitism along the parasitism–mutualism continuum  
184 (Johnson et al. 1997; Hoek et al. 2016; Friel and Friesen 2019) or if it reduces  
185 the nitrogen acquisition capacity of a microbial symbiont (van Diepen et al. 2007;  
186 Soudzilovskaia et al. 2015; Muñoz et al. 2016). Species may respond to shifts in  
187 soil nitrogen availability by switching their primary mode of nitrogen acquisition  
188 to a strategy with lower carbon costs to acquire nitrogen in order to maximize  
189 the magnitude of nitrogen acquired from a belowground carbon investment and  
190 outcompete other individuals for soil resources (Rastetter et al. 2001; Menge et al.  
191 2008).

192 Environmental conditions that affect demand to acquire nitrogen to sup-  
193 port new and existing tissues could also be a source of variance in plant carbon  
194 costs to acquire nitrogen. For example, an increase in plant nitrogen demand could  
195 increase carbon costs to acquire nitrogen if this increases the carbon that must be  
196 allocated belowground to acquire a proportional amount of nitrogen (Kulmatiski  
197 et al. 2017; Noyce et al. 2019). This could be driven by a temporary state of  
198 diminishing return associated with investing carbon toward building and main-  
199 taining structures that are necessary to support enhanced nitrogen uptake, such  
200 as fine roots (Matamala and Schlesinger 2000; Norby et al. 2004; Arndal et al.  
201 2018), mycorrhizal hyphae (Saleh et al. 2020), or root nodules (Parvin et al.  
202 2020). Alternatively, if the environmental factor that increases plant nitrogen de-  
203 mand causes nitrogen to become more limiting in the system (e.g. atmospheric  
204 CO<sub>2</sub>) (Luo et al. 2004; LeBauer and Treseder 2008; Vitousek et al. 2010; Liang  
205 et al. 2016), species might switch their primary mode of nitrogen acquisition to

206 a strategy with lower relative carbon costs to acquire nitrogen in order to gain a  
207 competitive advantage over species with either different or more limited modes of  
208 nitrogen acquisition (Ainsworth and Long 2005; Taylor and Menge 2018).

209 Using a plant economics approach, I examined the influence of plant ni-  
210 trogen demand and soil nitrogen availability on plant carbon costs to acquire  
211 nitrogen. This was done by growing a species capable of forming associations  
212 with nitrogen-fixing bacteria (*Glycine max* L. (Merr)) and a species not capable  
213 of forming these associations (*Gossypium hirsutum* L.) under four levels of light  
214 availability (plant nitrogen demand proxy) and four levels of soil nitrogen fertil-  
215 ization (soil nitrogen availability proxy) in a full-factorial, controlled greenhouse  
216 experiment. I used this experimental set-up to test the following hypotheses:

- 217 1. An increase in plant nitrogen demand due to increasing light availability will  
218 increase carbon costs to acquire nitrogen through a proportionally larger  
219 increase in belowground carbon than whole-plant nitrogen acquisition. This  
220 will be the result of an increased investment of carbon toward belowground  
221 structures that support enhanced nitrogen uptake, but at a lower nitrogen  
222 return.
- 223 2. An increase in soil nitrogen availability will decrease carbon costs to acquire  
224 nitrogen as a result of increased per root nitrogen uptake in *G. hirsutum*.  
225 However, soil nitrogen availability will not affect carbon costs to acquire  
226 nitrogen in *G. max* because of the already high return of nitrogen supplied  
227 through nitrogen fixation.

**228** 2.2 Methods

**229** 2.2.1 *Experiment setup*

**230** *Gossypium hirsutum* and *G. max* were planted in individual 3 liter pots (NS-300; **231** Nursery Supplies, Orange, CA, USA) containing a 3:1 mix of unfertilized potting **232** mix (Sungro Sunshine Mix #2, Agawam, MA, USA) to native soil extracted from **233** an agricultural field most recently planted with *G. max* at the USDA-ARS Lab-**234** oratory in Lubbock, TX, USA (33.59°N, -101.90°W). The field soil was classified **235** as Amarillo fine sandy loam (75% sand, 10% silt, 15% clay). Upon planting, **236** all *G. max* pots were inoculated with *Bradyrhizobium japonicum* (Verdesian N-**237** Dure™ Soybean, Cary, NC, USA) to stimulate root nodulation. Individuals of **238** both species were grown under similar, unshaded, ambient greenhouse conditions **239** for 2 weeks to germinate and begin vegetative growth.

**240** Three blocks were set up in the greenhouse, each containing four light **241** treatments created using shade cloth that reduced incoming radiation by either 0 **242** (full sun), 30, 50, or 80%. Two weeks post-germination, individuals were randomly **243** placed in the four light treatments in each block. Individuals received one of four **244** nitrogen fertilization doses as 100mL of a modified Hoagland solution (Hoagland **245** and Arnon 1950) equivalent to either 0, 70, 210, or 630 ppm N twice per week **246** within each light treatment. Nitrogen fertilization doses were received as topical **247** agents to the soil surface. Each Hoagland solution was modified to keep concen-**248** trations of other macro- and micronutrients equivalent (Table A1). Plants were **249** routinely well watered to eliminate water stress.

**250** 2.2.2 *Plant measurements and calculations*

**251** Each individual was harvested after 5 weeks of treatment, and biomass was sepa-  
**252** rated by organ type (leaves, stems, and roots). Nodules on *G. max* roots were also  
**253** harvested. Except for the 0% shade cover and 630 ppm N treatment combination,  
**254** all treatment combinations in both species had lower average dry biomass:pot vol-  
**255** ume ratios than the 1:1 ratio recommended by Poorter et al. (2012) to minimize  
**256** the likelihood of pot volume-induced growth limitation (Table A2, A3; Fig. A1).

**257** All harvested material was dried, weighed, and ground by organ type.  
**258** Carbon and nitrogen content ( $\text{g g}^{-1}$ ) was determined by subsampling from ground  
**259** and homogenized biomass of each organ type using an elemental analyzer (Costech  
**260** 4010; Costech, Inc., Valencia, CA, USA). I scaled these values to total leaf, stem,  
**261** and root carbon and nitrogen biomass (g) by multiplying dry biomass of each  
**262** organ type by carbon or nitrogen content of each corresponding organ type. Whole  
**263** plant nitrogen biomass (g) was calculated as the sum of total leaf (g), stem (g),  
**264** and root (g) nitrogen biomass. Root nodule carbon biomass was not included in  
**265** the calculation of root carbon biomass; however, relative plant investment toward  
**266** root or root nodule standing stock was estimated as the ratio of root biomass to  
**267** root nodule biomass ( $\text{g g}^{-1}$ ), following similar metrics to those adopted by Dovrat  
**268** et al. (2018) and Dovrat et al. (2020).

**269** Carbon costs to acquire nitrogen ( $N_{\text{cost}}$ ;  $\text{gC gN}^{-1}$ ) were estimated as the  
**270** ratio of total root carbon biomass ( $C_{\text{bg}}$ ; gC) to whole-plant nitrogen biomass  
**271** ( $N_{\text{wp}}$ ; gN). This calculation quantifies the relationship between carbon spent on  
**272** nitrogen acquisition and whole plant nitrogen acquisition by using root carbon  
**273** biomass as a proxy for estimating the magnitude of carbon allocated toward ni-

274 trogen acquisition. This calculation therefore assumes that the magnitude of root  
275 carbon standing stock is proportional to carbon transferred to root nodules or my-  
276 corrhizae, or lost through root exudation or turnover. The assumption has been  
277 supported in species that associate with ectomycorrhizal fungi (Hobbie 2006; Hob-  
278 bie and Hobbie 2008), but is less clear in species that acquire nitrogen through  
279 non-symbiotic active uptake or symbiotic nitrogen fixation. It is also unclear  
280 whether relationships between root carbon standing stock and carbon transfer to  
281 root nodules are similar in magnitude to carbon lost through exudation or when  
282 allocated toward other active uptake pathways. Thus, because of the way mea-  
283 surements were calculated, proximal values of carbon costs to acquire nitrogen are  
284 underestimates.

285 2.2.3 *Statistical analyses*

286 I explored the effects of light and nitrogen availability on carbon costs to acquire  
287 nitrogen using separate linear mixed-effects models for each species. Models in-  
288 cluded shade cover, nitrogen fertilization, and interactions between shade cover  
289 and nitrogen fertilization as continuous fixed effects, and also included block as a  
290 random intercept term. Three separate models for each species were built with  
291 this independent variable structure for three different dependent variables: (i)  
292 carbon costs to acquire nitrogen ( $\text{gC gN}^{-1}$ ); (ii) whole plant nitrogen biomass  
293 (denominator of carbon cost to acquire nitrogen; gN); and (iii) belowground car-  
294 bon biomass (numerator of carbon cost to acquire nitrogen; gC). I constructed two  
295 additional models for *G. max* with the same model structure described above to  
296 investigate the effects of light availability and nitrogen fertilization on root nodule

297 biomass (g) and the ratio of root nodule biomass to root biomass (unitless).

298 I used Shapiro–Wilk tests of normality to determine whether species spe-  
299 cific linear mixed-effects model residuals followed a normal distribution. Zero  
300 models satisfied residual normality assumptions when models were fit using un-  
301 transformed data (Shapiro–Wilk:  $p < 0.05$  in all cases). I attempted to satisfy  
302 residual normality assumptions by first fitting models using dependent variables  
303 that were natural-log transformed. If residual normality assumptions were still  
304 not met (Shapiro–Wilk:  $p > 0.05$ ), then models were fit using dependent variables  
305 that were square root transformed. All residual normality assumptions were satis-  
306 fied when models were fit with either a natural-log or square root transformation  
307 (Shapiro–Wilk:  $p > 0.05$  in all cases). Specifically, I natural-log transformed *G.*  
308 *hirsutum* carbon costs to acquire nitrogen and *G. hirsutum* whole-plant nitrogen  
309 biomass. I also square root transformed *G. max* carbon costs to acquire nitrogen,  
310 *G. max* whole-plant nitrogen biomass, root carbon biomass in both species, *G.*  
311 *max* root nodule biomass, and the *G. max* ratio of root nodule biomass to root  
312 biomass. I used the ‘lmer’ function in the ‘lme4’ R package (Bates et al. 2015) to  
313 fit each model and the ‘Anova’ function in the ‘car’ R package (Fox and Weisberg  
314 2019) to calculate Wald’s  $\chi^2$  to determine the significance ( $\alpha = 0.05$ ) of each fixed  
315 effect coefficient. Finally, I used the ‘emmeans’ R package (Lenth 2019) to conduct  
316 post-hoc comparisons of our treatment combinations using Tukey’s tests. Degrees  
317 of freedom for all Tukey’s tests were approximated using the Kenward–Roger ap-  
318 proach (Kenward and Roger 1997). All analyses and plots were conducted in R  
319 version 4.0.1 (R Core Team 2021).

**320** 2.3 Results

**321** 2.3.1 *Carbon costs to acquire nitrogen*

**322** Carbon costs to acquire nitrogen in *G. hirsutum* increased with increasing light  
**323** availability ( $p<0.001$ ; Table 2.1; Fig. 2.1) and decreased with increasing nitrogen  
**324** fertilization ( $p<0.001$ ; Table 2.1; Fig. 2.1). There was no interaction between  
**325** light availability and nitrogen fertilization ( $p=0.486$ , Table 2.1; Fig. 2.1).

**326** Carbon costs to acquire nitrogen in *G. max* also increased with increasing  
**327** light availability ( $p<0.001$ , Table 2.1; Fig. 2.1) and decreased with increasing  
**328** nitrogen fertilization ( $p<0.001$ ; Table 2.1; Fig. 2.1). There was no interaction  
**329** between light availability and nitrogen fertilization ( $p=0.261$ , Table 2.1; Fig. 2.1).

**Table 2.1.** Analysis of variance results exploring species-specific effects of light availability, nitrogen fertilization, and their interactions on carbon costs to acquire nitrogen ( $N_{\text{cost}}$ ; gC gN $^{-1}$ ), whole plant nitrogen biomass ( $N_{\text{wp}}$ ; gN), and root carbon biomass ( $C_{\text{bg}}$ ; gC)

	$N_{\text{cost}}$			$N_{\text{wp}}$			$C_{\text{bg}}$			
	df	Coefficient	$\chi^2$	p	Coefficient	$\chi^2$	p	Coefficient	$\chi^2$	p
<i>G. hirsutum</i>										
Intercept		1.594	-	-	-3.232	-	-	0.432	-	-
Light (L)	1	-1.09E-02	56.494	<0.001	-6.41E-03	91.275	<0.001	-2.62E-03	169.608	<0.001
Nitrogen (N)	1	-1.34E-03	54.925	<0.001	1.83E-03	118.784	<0.001	1.15E-04	2.901	0.089
L*N	1	3.88E-06	0.485	0.486	-1.34E-05	10.721	0.001	-1.67E-06	3.140	0.076
<i>G. max</i>										
Intercept		1.877	-	-	0.239	-	-	0.438	-	-
Light (L)	1	-7.67E-03	174.156	<0.001	-6.72E-04	39.799	<0.001	-2.55E-03	194.548	<0.001
Nitrogen (N)	1	-2.35E-04	21.948	<0.001	1.55E-04	70.771	<0.001	2.52E-04	19.458	<0.001
L*N	1	-2.89E-06	1.262	0.261	-6.32E-07	1.435	0.231	-3.16E-06	10.803	0.001

16

330 \*Significance determined using Wald's  $\chi^2$  tests ( $p=0.05$ ).  $P$ -values less than 0.05 are in bold and  $p$ -values between  
 331 0.05 and 0.1 are italicized. Negative coefficients for light treatments indicate a positive effect of increasing light  
 332 availability on all response variables, as light availability is treated as percent shade cover in all linear mixed-effects  
 333 models.

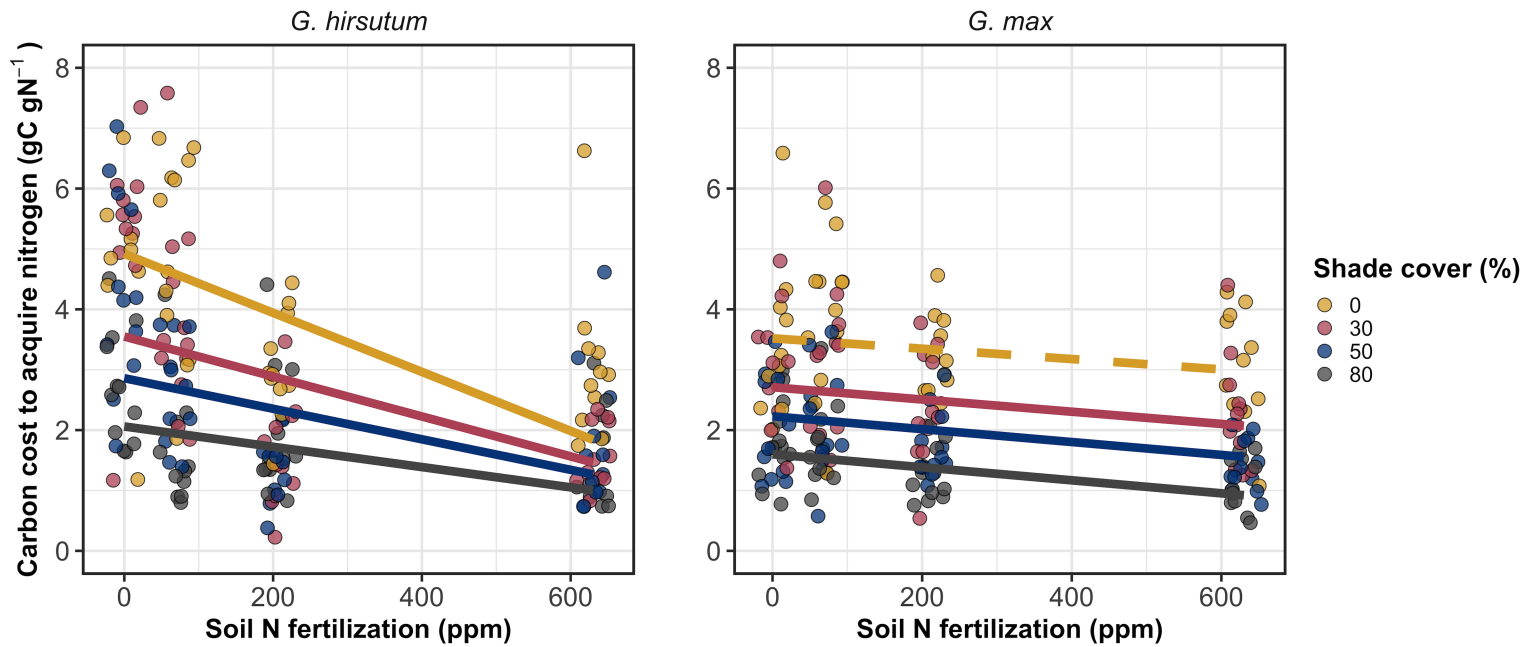


**Figure 2.1.** Relationships between soil nutrient fertilization and light availability on carbon costs to acquire nitrogen in *G. hirsutum* and *G. max*. Nitrogen fertilization treatments are represented on the x-axis. Shade cover treatments are represented through colored points and trendlines. Trendlines were created by back-transforming marginal mean slopes and intercepts from species-specific linear mixed-effects models. These values were calculated using the ‘emtrends’ and ‘emmeans’ functions in the ‘emmeans’ R package (Lenth, 2019). Yellow points and trendlines represent the 0% shade cover treatment, red points and trendlines represent the 30% shade cover treatment, blue points and trendlines represent the 50% shade cover treatment, and gray points and trendlines represent the 80% shade cover treatment. Solid trendlines indicate slopes that are significantly different from zero (Tukey:  $p < 0.05$ ), while dashed trendlines indicate slopes that are not statistically different from zero.

**334** 2.3.2 *Whole plant nitrogen biomass*

**335** Whole plant nitrogen biomass in *G. hirsutum* was driven by an interaction between  
**336** light availability and nitrogen fertilization ( $p=0.001$ ; Table 2.1; Fig. 2.2). This  
**337** interaction indicated a greater stimulation of whole-plant nitrogen biomass by  
**338** nitrogen fertilization as light levels increased (Table 2.1; Fig. 2.2).

**339** Whole plant nitrogen biomass in *G. max* increased with increasing light  
**340** availability ( $p<0.001$ ) and nitrogen fertilization ( $p<0.001$ ), with no interaction  
**341** between light availability and nitrogen fertilization ( $p=0.231$ ; Table 2.1; Fig. 2.2).

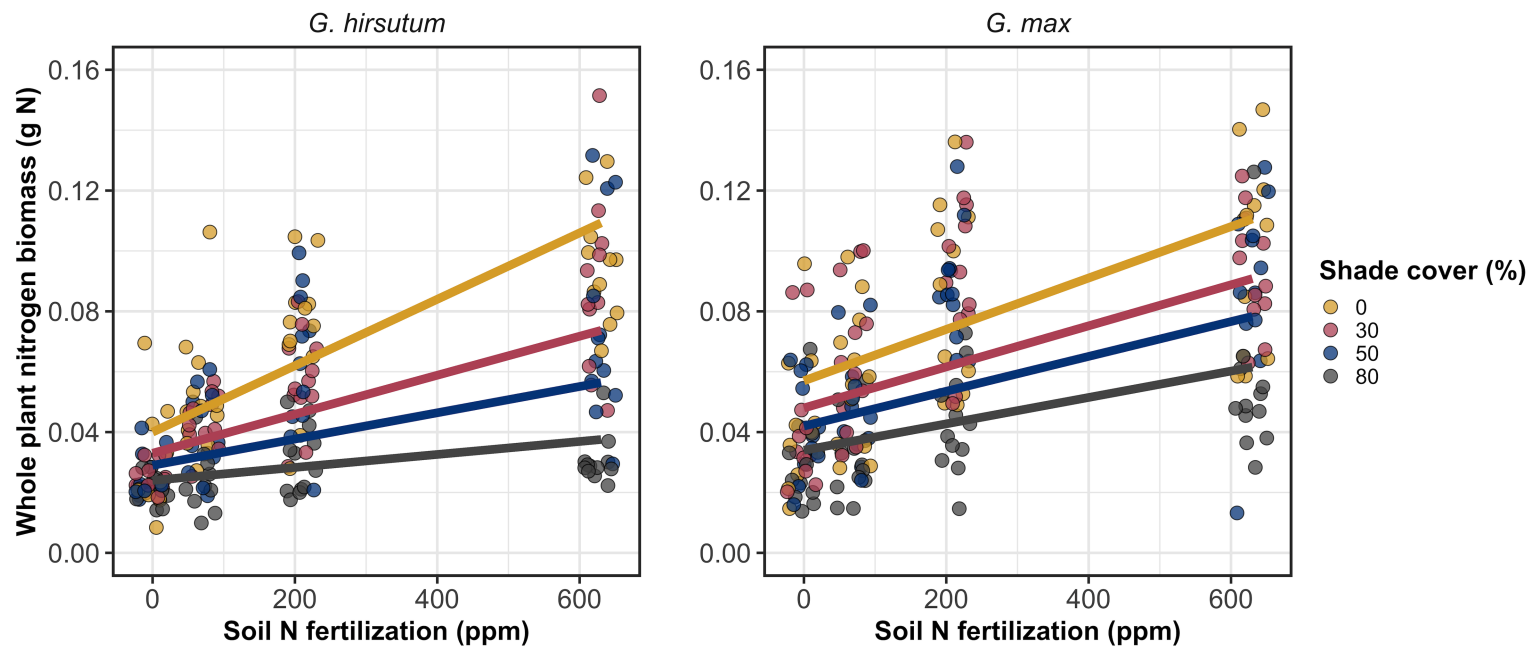


**Figure 2.2.** Relationships between soil nutrient fertilization and light availability on whole-plant nitrogen biomass in *G. hirsutum* and *G. max*. Whole-plant nitrogen biomass is the denominator of the carbon cost to acquire nitrogen calculation. Nitrogen fertilization treatments are represented on the x-axis. Shade cover treatments are represented through colored points and trendlines. Trendlines were created by back-transforming marginal mean slopes and intercepts from species-specific linear mixed-effects models. These values were calculated using the ‘emtrends’ and ‘emmeans’ functions in the ‘emmeans’ R package (Lenth 2019). Points are jittered for visibility. Colored points and trendlines are as explained in Fig. 2.1. Solid trendlines indicate slopes that are significantly different from zero (Tukey:  $p < 0.05$ ), while dashed trendlines indicate slopes that are not statistically different from zero.

**342** 2.3.3 *Root carbon biomass*

**343** Root carbon biomass in *G. hirsutum* significantly increased with increasing light availability ( $p<0.001$ ; Table 2.1; Fig. 2.3) and marginally increased with nitrogen fertilization ( $p=0.089$ ; Table 2.1; Fig. 2.3). There was also a marginal interaction between light availability and nitrogen fertilization ( $p=0.076$ ; Table 2.1), driven by an increase in the positive response of root carbon biomass to increasing nitrogen fertilization as light availability increased (Table 2.3). This resulted in significantly positive trends between root carbon biomass and nitrogen fertilization in the two highest light treatments (Tukey:  $p<0.05$  in both cases; Table 2.3; Fig. 2.3) and no effect of nitrogen fertilization in the two lowest light treatments (Tukey:  $p>0.05$  in both cases; Table 2.3; Fig. 2.3).

**353** There was an interaction between light availability and nitrogen fertilization on root carbon biomass in *G. max* ( $p=0.001$ ; Table 2.1; Fig. 2.3). Post-hoc analyses indicated that the positive effects of nitrogen fertilization on *G. max* root carbon biomass increased with increasing light availability (Table 2.3; Fig. 2.3). There were also positive individual effects of increasing nitrogen fertilization ( $p<0.001$ ; Table 2.3) and light availability ( $p<0.001$ ; Table 2.3) on *G. max* root carbon biomass (Table 2.1; Fig. 2.3).

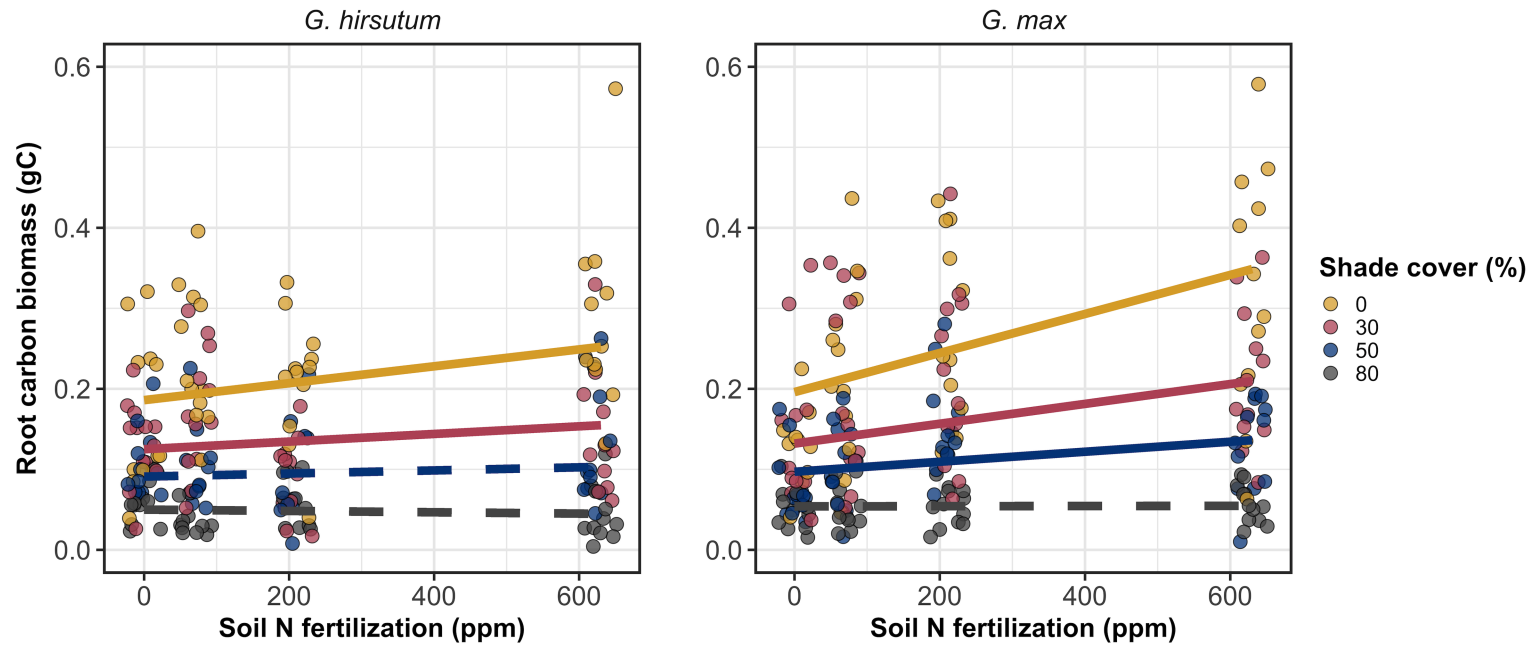


**Figure 2.3.** Relationships between soil nutrient fertilization and light availability on root carbon biomass in *G. hirsutum* and *G. max*. Root carbon biomass is the numerator of the carbon cost to acquire nitrogen calculation. Nitrogen fertilization treatments are represented on the x-axis. Colored points and trendlines are as explained in Fig. 2.1. Trendlines were created by back-transforming marginal mean slopes and intercepts from species-specific linear mixed-effects models. These values were calculated using the ‘emtrends’ and ‘emmeans’ functions in the ‘emmeans’ R package (Lenth 2019). Points are jittered for visibility. Colored points and trendlines are as explained in Fig. 2.1.

**360** 2.3.4 *Root nodule biomass*

**361** Root nodule biomass in *G. max* increased with increasing light availability ( $p <$   
**362** 0.001; Table 2.2; Fig. 2.4a) and decreased with increasing nitrogen fertilization  
**363** ( $p < 0.001$ ; Table 2.2; Fig. 2.4a). There was no interaction between nitrogen  
**364** fertilization and light availability ( $p = 0.133$ ; Table 2.2; Fig. 2.4a). The ratio of  
**365** root nodule biomass to root biomass did not change in response to light availability  
**366** ( $p = 0.481$ ; Table 2.2; Fig. 2.4b) but decreased with increasing nitrogen fertilization  
**367** ( $p < 0.001$ ; Table 2.2; Fig. 2.4b). There was no interaction between nitrogen  
**368** fertilization and light availability on the ratio of root nodule biomass to root  
**369** biomass ( $p = 0.621$ ; Table 2.2; Fig. 2.4b).

**Table 2.2.** Analysis of variance results exploring effects of light availability, nitrogen fertilization, and their interactions on *G. max* root nodule biomass (g) and the ratio of root nodule biomass to root biomass (g g<sup>-1</sup>)\*

	Nodule biomass			Nodule biomass: root biomass			<i>p</i>
	df	Coefficient	$\chi^2$	<i>p</i>	Coefficient	$\chi^2$	
(Intercept)		0.302	-	-	0.448	-	-
Light (L)	1	-1.81E-03	72.964	<0.001	-8.76E-05	0.496	0.481
Nitrogen (N)	1	-2.83E-04	115.377	<0.001	-5.09E-04	156.476	<0.001
L*N	1	1.14E-06	2.226	0.133	-7.30E-07	0.244	0.621

370 \*Significance determined using Wald's  $\chi^2$  tests ( $\alpha=0.05$ ). *P*-values less than 0.05 are in bold. Negative coefficients for  
 371 light treatments indicate a positive effect of increasing light availability on all response variables, as light availability  
 372 is treated as percent shade cover in all linear mixed-effects models. Root nodule biomass and nodule biomass: root  
 373 biomass models were only constructed for *G. max* because *G. hirsutum* was not inoculated with *B. japonicum* and  
 374 is not capable of forming root nodules.

**Table 2.3.** Slopes of the regression line describing the relationship between each dependent variable and nitrogen fertilization at each light level\*

Shade cover	Carbon cost to acquire nitrogen	Whole plant nitrogen biomass	Belowground carbon biomass	Root nodule biomass	Nodule biomass: root biomass
<i>G. hirsutum</i>					
0%	<b>-1.34E-03<sup>a</sup></b>	<b>1.83E-03<sup>a</sup></b>	<b>1.15E-04<sup>b</sup></b>	-	-
30%	<b>-1.22E-03<sup>a</sup></b>	<b>1.43E-03<sup>a</sup></b>	<b>1.17E-04<sup>b</sup></b>	-	-
50%	<b>-1.14E-03<sup>a</sup></b>	<b>1.17E-03<sup>a</sup></b>	3.12E-05 <sup>b</sup>	-	-
80%	<b>-1.02E-03<sup>a</sup></b>	<b>7.66E-04<sup>a</sup></b>	-1.89E-06 <sup>b</sup>	-	-
<i>G. max</i>					
0%	-2.35E-04 <sup>b</sup>	<b>1.55E-05<sup>b</sup></b>	<b>2.51E-04<sup>b</sup></b>	<b>-2.83E-04<sup>b</sup></b>	<b>-5.09E-04<sup>b</sup></b>
30%	<b>-3.22E-04<sup>b</sup></b>	<b>1.35E-05<sup>b</sup></b>	<b>1.57E-04<sup>b</sup></b>	<b>-2.49E-04<sup>b</sup></b>	<b>-5.31E-04<sup>b</sup></b>
50%	<b>-3.80E-04<sup>b</sup></b>	<b>1.23E-05<sup>b</sup></b>	<b>9.37E-05<sup>b</sup></b>	<b>-2.26E-04<sup>b</sup></b>	<b>-5.45E-04<sup>b</sup></b>
80%	<b>-4.66E-04<sup>b</sup></b>	<b>1.04E-05<sup>b</sup></b>	-9.95E-07 <sup>b</sup>	<b>-1.92E-04<sup>b</sup></b>	<b>-5.67E-04<sup>b</sup></b>

24

375 \* Slopes represent estimated marginal mean slopes from linear mixed-effects models described in the Methods. Slopes  
 376 were calculated using the ‘emmeans’ R package (Lenth 2019). Superscripts indicate slopes fit to natural-log (<sup>a</sup>) or  
 377 square root (<sup>b</sup>) transformed data. Slopes statistically different from zero (Tukey:  $p<0.05$ ) are indicated in bold.  
 378 Marginally significant slopes (Tukey:  $0.05< p<0.1$ ) are italicized.

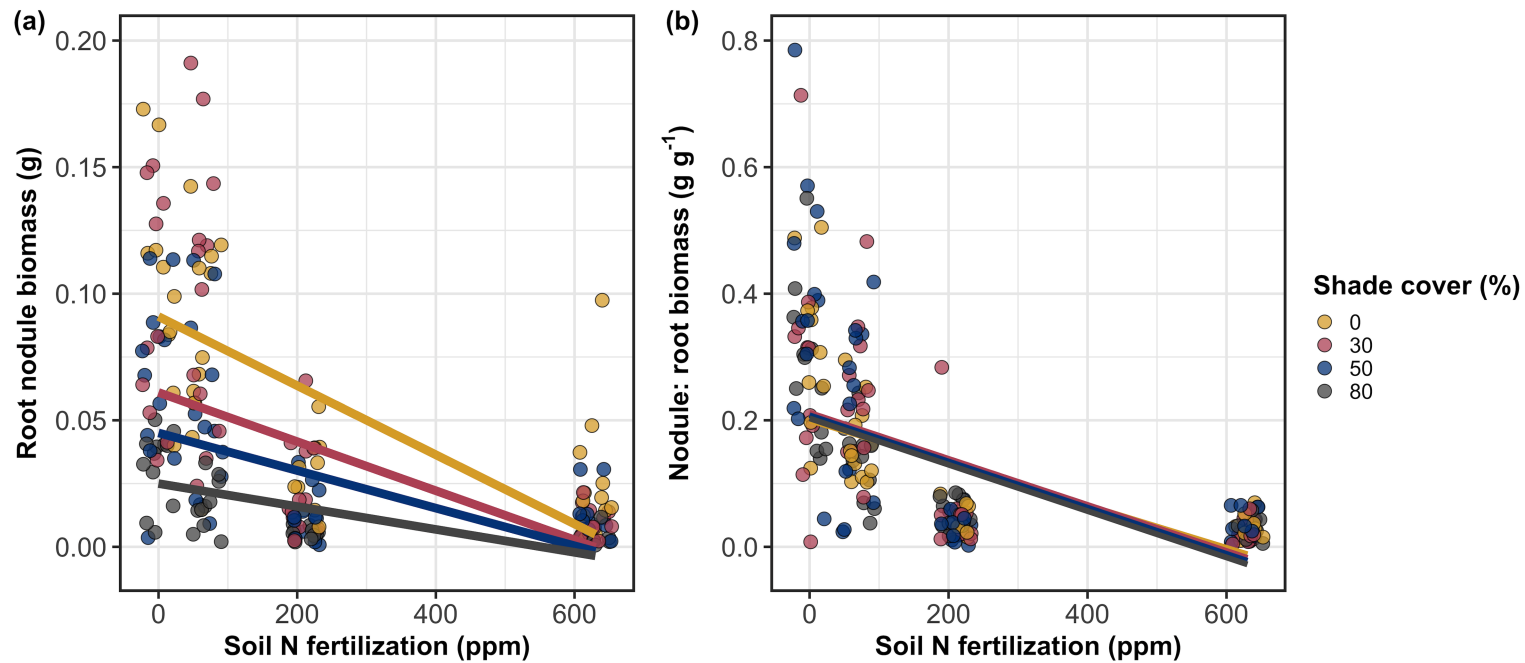


**Figure 2.4.** Effects of shade cover and nitrogen fertilization on root nodule biomass (a) and the ratio of root nodule biomass to root biomass (b) in *G. max*. Nitrogen fertilization treatments are represented on the x-axis. Shade cover treatments are represented through colored points and trendlines. Trendlines were created by back-transforming marginal mean slopes and intercepts from species-specific linear mixed-effects models. These values were calculated using the ‘emtrends’ and ‘emmeans’ functions in the ‘emmeans’ R package (Lenth 2019). Points are jittered for visibility. Yellow points and trendlines represent the 0% shade cover treatment, blue points and trendlines represent the 30% shade cover treatment, green points and trendlines represent the 50% shade cover treatment, and purple points and trendlines represent the 80% shade cover treatment. Solid trendlines indicate slopes that are significantly different from zero (Tukey:  $p < 0.05$ ), while dashed trendlines indicate slopes that are not statistically different from zero.

**379** 2.4 Discussion

**380** In this chapter, I determined the effects of light availability and soil nitrogen  
**381** fertilization on root mass carbon costs to acquire nitrogen in *G. hirsutum* and *G.*  
**382** *max*. In support of my hypotheses, I found that carbon costs to acquire nitrogen  
**383** generally increased with increasing light availability and decreased with increasing  
**384** soil nitrogen fertilization in both species. These findings suggest that carbon costs  
**385** to acquire nitrogen are determined by factors that influence plant nitrogen demand  
**386** and soil nitrogen availability. In contrast to my second hypothesis, root nodulation  
**387** data suggested that *G. max* and *G. hirsutum* achieved similar directional carbon  
**388** cost responses to nitrogen fertilization despite a likely shift in *G. max* allocation  
**389** from nodulation to root biomass along the nitrogen fertilization gradient.

**390** 2.4.1 *Carbon costs to acquire nitrogen increase with light availability and*  
**391** *decrease with fertilization*

**392** Both *G. max* and *G. hirsutum* experienced an increase in carbon costs to ac-  
**393** quire nitrogen due to increasing light availability. These patterns were driven by  
**394** a larger increase in root carbon biomass than whole-plant nitrogen biomass. In-  
**395** creases in root carbon biomass due to factors that increase plant nitrogen demand  
**396** are a commonly observed pattern, as carbon allocated belowground provides sub-  
**397** strate needed to produce and maintain structures that satisfy aboveground plant  
**398** nitrogen demand (Nadelhoffer and Raich 1992; Giardina et al. 2005; Raich et al.  
**399** 2014). Findings suggest that plants allocate relatively more carbon for acquiring  
**400** nitrogen when demand increases over short temporal scales, which may cause a  
**401** temporary state of diminishing return due to asynchrony between belowground

402 carbon and whole-plant nitrogen responses to plant nitrogen demand (Kulmatiski  
403 et al. 2017; Noyce et al. 2019). These responses might be attributed to a temporal  
404 lag associated with producing structures that enhance nitrogen acquisition. For  
405 example, fine roots (Matamala and Schlesinger 2000; Norby et al. 2004; Arndal  
406 et al. 2018) and root nodules (Parvin et al. 2020) take time to build and first  
407 require the construction of coarse roots. Thus, full nitrogen returns from these  
408 investments may not occur immediately (Kayler et al. 2010; Kayler et al. 2017),  
409 and may vary by species acquisition strategy. I speculate that increases in ni-  
410 trogen acquisition from a given carbon investment may occur beyond the 5-week  
411 scope of this experiment. A similar study conducted over a longer temporal scale  
412 would address this.

413 Increasing soil nitrogen fertilization generally decreased carbon costs to  
414 acquire nitrogen in both species. These patterns were driven by a larger increase  
415 in whole-plant nitrogen biomass than root carbon biomass. In *G. hirsutum*, re-  
416 ductions in carbon costs to acquire nitrogen may have been due to an increase in  
417 per-root nitrogen uptake, allowing individuals to maximize the amount of nitro-  
418 gen acquired from a belowground carbon investment. Interestingly, increased soil  
419 nitrogen fertilization increased whole-plant nitrogen biomass in *G. max* despite  
420 reductions in root nodule biomass that likely reduced the nitrogen-fixing capac-  
421 ity of *G. max* (Andersen et al. 2005; Muñoz et al. 2016). While reductions in  
422 root nodulation due to increased soil nitrogen availability are commonly observed  
423 (Gibson and Harper 1985; Fujikake et al. 2003), root nodulation responses were  
424 observed in tandem with increased root carbon biomass, implying that *G. max*  
425 shifted relative carbon allocation from nitrogen fixation to soil nitrogen acquisition

426 (Markham and Zekveld 2007; Dovrat et al. 2020). This was likely because there  
427 was a reduction in the carbon cost advantage of acquiring fixed nitrogen relative  
428 to soil nitrogen, and suggests that species capable of associating with symbiotic  
429 nitrogen-fixing bacteria shift their relative nitrogen acquisition pathway to opti-  
430 mize nitrogen uptake (Rastetter et al. 2001). Future studies should investigate  
431 these patterns with a larger quantity of phylogenetically related species, or differ-  
432 ent varieties of a single species that differ in their ability to form associations with  
433 symbiotic nitrogen-fixing bacteria to more directly test the impact of nitrogen  
434 fixation on the patterns observed in this study.

#### 435 2.4.2 *Modeling implications*

436 Carbon costs to acquire nitrogen are subsumed in the general discussion of eco-  
437 nomic analogies to plant resource uptake (Bloom et al. 1985; Rastetter et al.  
438 2001; Vitousek et al. 2002; Phillips et al. 2013; Terrer et al. 2018; Henneron  
439 et al. 2020). Despite this, terrestrial biosphere models rarely include costs of  
440 nitrogen acquisition within their framework for predicting plant nitrogen uptake.  
441 There is currently one plant resource uptake model, FUN, that quantitatively  
442 predicts carbon costs to acquire nitrogen within a framework for predicting plant  
443 nitrogen uptake for different nitrogen acquisition strategies (Fisher et al. 2010;  
444 Brzostek et al. 2014). Iterations of FUN are currently coupled to two terrestrial  
445 biosphere models: the Community Land Model 5.0 and the Joint UK Land En-  
446 vironment Simulator (Clark et al. 2011; Shi et al. 2016; Lawrence et al. 2019).  
447 Recent work suggests that coupling FUN to CLM 5.0 caused a large overpredic-  
448 tion of plant nitrogen uptake associated with nitrogen fixation (Davies-Barnard

449 et al. 2020) compared to other terrestrial biosphere model products. Thus, em-  
450 pirical data from manipulative experiments that explicitly quantify carbon costs  
451 to acquire nitrogen in species capable of associating with nitrogen-fixing bacteria  
452 across different environmental contexts is an important step toward identifying  
453 potential biases in models such as FUN.

454 These findings broadly support the FUN formulation of carbon costs to  
455 acquire nitrogen in response to soil nitrogen availability. FUN calculates carbon  
456 costs to acquire nitrogen based on the sum of carbon costs to acquire nitrogen  
457 via nitrogen fixation, mycorrhizal active uptake, non-mycorrhizal active uptake,  
458 and retranslocation (Fisher et al. 2010; Brzostek et al. 2014). Carbon costs to  
459 acquire nitrogen via mycorrhizal or non-mycorrhizal active uptake pathways are  
460 derived as a function of nitrogen availability, root biomass, and two parameterized  
461 values based on nitrogen acquisition strategy (Brzostek et al. 2014). Due to this,  
462 FUN simulates a net decrease in carbon costs to acquire nitrogen with increasing  
463 nitrogen availability for mycorrhizal and non-mycorrhizal active uptake pathways,  
464 assuming constant root biomass. This was a pattern I observed in *G. hirsutum* re-  
465 gardless of light availability. In contrast, FUN would not simulate a net change in  
466 carbon costs to acquire nitrogen via nitrogen fixation due to nitrogen availability.  
467 This is because carbon costs to acquire nitrogen via nitrogen fixation are derived  
468 from a well established function of soil temperature, which is independent of soil  
469 nitrogen availability (Houlton et al. 2008; Fisher et al. 2010). I observed a net  
470 reduction in carbon costs to acquire nitrogen in *G. max*, except when individu-  
471 als were grown under 0% shade cover. While a net reduction of carbon costs in  
472 response to nitrogen fertilization runs counter to nitrogen fixation carbon costs

473 simulated by FUN, these patterns were likely because *G. max* individuals switched  
474 their primary mode of nitrogen acquisition from symbiotic nitrogen fixation to a  
475 non-symbiotic active uptake pathway.

476 2.4.3 *Study limitations*

477 It should be noted that the metric used in this study to determine carbon costs  
478 to acquire nitrogen has several limitations. Most notably, this metric uses root  
479 carbon biomass as a proxy for estimating the amount of carbon spent on nitrogen  
480 acquisition. While it is true that most carbon allocated belowground has at least  
481 an indirect structural role in acquiring soil resources, it remains unclear whether  
482 this assumption holds true for species that acquire nitrogen via symbiotic nitro-  
483 gen fixation. I also cannot quantify carbon lost through root exudates or root  
484 turnover, which may increase due to factors that increase plant nitrogen demand  
485 (Tingey et al. 2000; Phillips et al. 2011), and can increase the magnitude of  
486 available nitrogen from soil organic matter through priming effects on soil micro-  
487 bial communities (Uselman et al. 2000; Bengtson et al. 2012). It is also not  
488 clear whether these assumptions hold under all environmental conditions, such  
489 as those that shift belowground carbon allocation toward a different mode of ni-  
490 trogen acquisition (Taylor and Menge 2018; Friel and Friesen 2019) or between  
491 species with different acquisition strategies. In this study, increasing soil nitrogen  
492 fertilization increased carbon investment to roots relative to carbon transferred to  
493 root nodules. By assuming that carbon allocated to root carbon was proportional  
494 to carbon allocated to root nodules across all treatment combinations, these ob-  
495 served responses to soil nitrogen fertilization were likely to be overestimated in *G.*

496 *max*. I encourage future research to quantify these carbon fates independently.

497 Researchers conducting pot experiments must carefully choose pot volume  
498 to minimize the likelihood of growth limitations induced by pot volume (Poorter  
499 et al. 2012). Poorter et al. (2012) indicate that researchers are likely to avoid  
500 growth limitations associated with pot volume if measurements are collected when  
501 the plant biomass:pot volume ratio is less than  $1 \text{ g L}^{-1}$ . In this experiment, all  
502 treatment combinations in both species had biomass:pot volume ratios less than  
503  $1 \text{ g L}^{-1}$  except for *G. max* and *G. hirsutum* that were grown under 0% shade  
504 cover and had received 630 ppm N. Specifically, *G. max* and *G. hirsutum* had  
505 average respective biomass:pot volume ratios of  $1.24 \pm 0.07 \text{ g L}^{-1}$  and  $1.34 \pm 0.13$   
506  $\text{g L}^{-1}$ , when grown under 0% shade cover and received 630 ppm N (Table A2,  
507 A3; Fig. A1). If growth in this treatment combination was limited by pot vol-  
508 ume, then individuals may have had larger carbon costs to acquire nitrogen than  
509 would be expected if they were grown in larger pots. This pot volume induced  
510 growth limitation could cause a reduction in per-root nitrogen uptake associated  
511 with more densely packed roots, which could reduce the positive effect of nitro-  
512 gen fertilization on whole-plant nitrogen biomass relative to root carbon biomass  
513 (Poorter et al. 2012).

514 Growth limitation associated with pot volume provides a possible expla-  
515 nation for the marginally insignificant effect of increasing nitrogen fertilization on  
516 *G. max* carbon costs to acquire nitrogen when grown under 0% shade cover. This  
517 is because the regression line describing the relationship between carbon costs to  
518 acquire nitrogen and nitrogen fertilization in *G. max* grown under 0% shade cover  
519 would have flattened if growth limitation had caused larger than expected carbon

520 costs to acquire nitrogen in the 0% shade cover, 630 ppm N treatment combi-  
521 nation. This may have been exacerbated by the fact that *G. max* likely shifted  
522 relative carbon allocation from nitrogen fixation to soil nitrogen acquisition, which  
523 could have increased the negative effect of more densely packed roots on nitrogen  
524 uptake. These patterns could have also occurred in *G. hirsutum* grown under 0%  
525 shade cover; however, there was no change in the effect of nitrogen fertilization on  
526 *G. hirsutum* carbon costs to acquire nitrogen grown under 0% shade cover relative  
527 to other shade cover treatments. Regardless, the possibility of growth limitation  
528 due to pot volume suggests that effects of increasing nitrogen fertilization on car-  
529 bon costs to acquire nitrogen in both species grown under 0% shade cover could  
530 have been underestimated. Follow-up studies using a similar experimental design  
531 with a larger pot volume would be necessary in order to determine whether these  
532 patterns were impacted by pot volume-induced growth limitation.

### 533 2.4.4 *Conclusions*

534 In conclusion, this chapter provides empirical evidence that carbon costs to ac-  
535 quire nitrogen are influenced by light availability and soil nitrogen fertilization  
536 in a species capable of acquiring nitrogen via symbiotic nitrogen fixation and a  
537 species not capable of forming such associations. We show that carbon costs to  
538 acquire nitrogen generally increase with increasing light availability and decrease  
539 with increasing nitrogen fertilization. This chapter provides important empirical  
540 data needed to evaluate the formulation of carbon costs to acquire nitrogen in  
541 terrestrial biosphere models, particularly carbon costs to acquire nitrogen that  
542 are associated with symbiotic nitrogen fixation. Findings broadly support the

543 general formulation of these carbon costs in the FUN biogeochemical model in  
544 response to shifts in nitrogen availability. However, there is a need for future  
545 studies to explicitly quantify carbon costs to acquire nitrogen under different en-  
546 vironmental contexts, over longer temporal scales, and using larger selections of  
547 phylogenetically related species. In addition, I suggest that future studies mini-  
548 mize the limitations associated with the metric used here by explicitly measuring  
549 belowground carbon fates independently.

550 Chapter 3

551 Soil nitrogen availability modifies leaf nitrogen economies in mature  
552 temperate deciduous forests: a direct test of photosynthetic least-cost  
553 theory

554 3.1 Introduction

Photosynthesis represents the largest carbon flux between the atmosphere and land surface (IPCC 2021), and plays a central role in biogeochemical cycling at multiple spatial and temporal scales (Vitousek and Howarth 1991; LeBauer and Treseder 2008; Kaiser et al. 2015; Wieder et al. 2015). Therefore, carbon and energy fluxes simulated by terrestrial biosphere models are sensitive to the formulation of photosynthetic processes (Ziehn et al. 2011; Bonan et al. 2011; Booth et al. 2012; Smith et al. 2016; Smith et al. 2017) and must be represented using robust, empirically tested processes (Prentice et al. 2015; Wieder et al. 2019). Current formulations of photosynthesis vary across terrestrial biosphere models (Smith and Dukes 2013; Rogers et al. 2017), which causes variation in modeled ecosystem processes (Knorr 2000; Knorr and Heimann 2001; Bonan et al. 2011; Friedlingstein et al. 2014) and casts uncertainty on the ability of these models to accurately predict terrestrial ecosystem responses and feedbacks to global change (Zaehle et al. 2005; Schaefer et al. 2012; Davies-Barnard et al. 2020).

Terrestrial biosphere models commonly represent C<sub>3</sub> photosynthesis through variants of the Farquhar et al. (1980) biochemical model (Smith and Dukes 2013; Rogers 2014; Rogers et al. 2017). This well-tested photosynthesis model estimates leaf-level carbon assimilation, or photosynthetic capacity, as a function of the maximum rate of Ribulose-1,5-bisphosphate carboxylase-oxygenase (Ru-

574 bisco) carboxylation ( $V_{cmax}$ ) and the maximum rate of Ribulose-1,5-bisphosphate  
575 (RuBP) regeneration ( $J_{max}$ ) (Farquhar et al. 1980). Many terrestrial biosphere  
576 models predict these model inputs based on plant functional group specific lin-  
577 ear relationships between leaf nutrient content and  $V_{cmax}$  (Smith and Dukes 2013;  
578 Rogers 2014; Rogers et al. 2017) under the tenet that a large fraction of leaf nutri-  
579 ents, and nitrogen in particular, are partitioned toward building and maintaining  
580 enzymes that support photosynthetic capacity, such as Rubisco (Brix 1971; Gul-  
581 mon and Chu 1981; Evans 1989; Kattge et al. 2009; Walker et al. 2014). Terres-  
582 trial biosphere models predict leaf nutrient content from soil nutrient availability  
583 based on the assumption that increasing soil nutrients generally increases leaf nu-  
584 trients (Firn et al. 2019; Li et al. 2020; Liang et al. 2020) which, in the case of  
585 nitrogen, generally corresponds with an increase in photosynthetic processes (Li  
586 et al. 2020; Liang et al. 2020).

587       Recent work calls the generality of relationships between soil nutrient avail-  
588 ability, leaf nutrient content, and photosynthetic capacity into question, suggest-  
589 ing instead that leaf nutrients and photosynthetic capacity are better predicted as  
590 an integrated product of aboveground climate, leaf traits, and soil nutrient avail-  
591 ability, rather than soil nutrient availability alone (Dong et al. 2017; Dong et al.  
592 2020; Dong et al. 2022; Firn et al. 2019; Smith et al. 2019; Peng et al. 2021).  
593 It has been reasoned that this result is because plants allocate added nutrients to  
594 growth and storage rather than alterations in leaf chemistry (Smith et al. 2019),  
595 perhaps as a result of nutrient limitation of primary productivity (LeBauer and  
596 Treseder 2008; Fay et al. 2015). Additionally, recent work suggests that relation-  
597 ships between leaf nutrient content and photosynthesis vary across environments,

598 and that the proportion of leaf nutrient content allocated to photosynthetic tis-  
599 sue varies over space and time with plant acclimation and adaptation responses  
600 to light availability, vapor pressure deficit, soil pH, soil nutrient availability, and  
601 environmental factors that influence leaf mass per area (Pons and Pearcy 1994;  
602 Niinemets and Tenhunen 1997; Evans and Poorter 2001; Hikosaka and Shigeno  
603 2009; Ghimire et al. 2017; Onoda et al. 2017; Luo et al. 2021). The use of linear  
604 relationships between leaf nutrient content and  $V_{cmax}$  to predict photosynthetic  
605 capacity, as commonly used in terrestrial biosphere models (Rogers 2014), is not  
606 capable of detecting such responses.

607 Photosynthetic least-cost theory provides an alternative framework for un-  
608 derstanding relationships between soil nutrient availability, leaf nutrient content,  
609 and photosynthetic capacity (Harrison et al. 2021). Leveraging a two-input mi-  
610 croeconomics approach (Wright et al. 2003), the theory posits that plants accli-  
611 mate to a given environment by optimizing leaf photosynthesis rates at the lowest  
612 summed cost of using nutrients and water (Prentice et al. 2014; Wang et al. 2017;  
613 Smith et al. 2019; Paillassa et al. 2020). Across resource availability gradients,  
614 the theory predicts that optimal photosynthetic rates can be achieved by trading  
615 less efficient use of a resource that is less costly to acquire (or more abundant)  
616 for more efficient use of a resource more costly to acquire (or less abundant). For  
617 example, an increase in soil nutrient availability should reduce the cost of acquir-  
618 ing and using nutrients (Bae et al. 2015; Eastman et al. 2021; Perkowski et al.  
619 2021), which could increase leaf nutrient investments in photosynthetic proteins to  
620 allow similar photosynthetic rates to be achieved with higher nutrient use (lower  
621 nutrient use efficiency) but lower water use (greater water use efficiency). The

622 theory suggests similar tradeoffs in response to increasing soil pH (Paillassa et al.  
623 2020), specifically, that increasing soil pH should reduce the cost of acquiring soil  
624 nutrients due to an increase in plant-available nutrient concentration (Paillassa  
625 et al. 2020; Dong et al. 2022). The theory is also capable of reconciling dynamic  
626 leaf nutrient-photosynthesis relationships at global scales (Luo et al. 2021).

627 Patterns expected from photosynthetic least-cost theory have recently re-  
628 ceived empirical support both in global environmental gradient (Smith et al.  
629 2019; Paillassa et al. 2020; Luo et al. 2021; Querejeta et al. 2022; Wester-  
630 band et al. 2023) and local manipulative invasion (Bialic-Murphy et al. 2021)  
631 studies. However, nutrient addition experiments that directly examine nutrient-  
632 water use tradeoffs expected from the theory are rare (but see Guerrieri et al.  
633 2011), and only global gradient studies testing the theory have considered soil pH  
634 in their analyses. As a result, there is a need to use nutrient addition and soil pH  
635 manipulation experiments to test mechanisms driving responses predicted by the  
636 theory.

637 In this study, I measured leaf responses to soil nitrogen availability in five  
638 deciduous tree species growing in the upper canopy of mature closed canopy tem-  
639 perate forests in the northeastern United States. Soil nitrogen availability and pH  
640 were manipulated through a nitrogen-by-pH field manipulation experiment with  
641 treatments applied since 2011, eight years prior to measurement. Two different soil  
642 nitrogen treatments were applied to increase nitrogen availability with opposing  
643 effects on soil pH. An additional nitrogen-free acidifying treatment was expected  
644 to decrease soil pH. I hypothesized that increased soil nitrogen availability would  
645 enable plants to increase nutrient uptake and create more photosynthetic enzymes

646 per leaf, allowing similar photosynthetic rates achieved with lower leaf C<sub>i</sub>:C<sub>a</sub> and  
647 increased leaf nitrogen content allocated to photosynthetic leaf tissue. I expected  
648 that this response would be driven by a reduction in the cost of acquiring nitrogen,  
649 which would cause trees to sacrifice efficient nitrogen use to enable more efficient  
650 use of other limiting resources (i.e., water). Finally, I hypothesized similar leaf  
651 responses to increasing soil pH.

652 3.2 Methods

653 3.2.1 *Study site description*

654 I conducted this study in summer 2019 at three stands located within a 20-km ra-  
655 dius of Ithaca, NY, USA (42.444 °N, 76.502 °W). All stands contain mature,  
656 closed-canopy forests dominated by deciduous tree species. Stands contained  
657 abundant sugar maple (*Acer saccharum* Marshall), American beech (*Fagus gran-*  
658 *difolia* Ehrh.), and white ash (*Fraxinus americana* L.), accounting for 43%, 15%,  
659 and 17% of the total aboveground biomass across the three stands, respectively,  
660 with less frequent red maple (*Acer rubrum* L.; 9% of total aboveground biomass)  
661 and red oak occurrences (*Quercus rubra* L.; 10% of total aboveground biomass).  
662 Soils at each site were broadly classified as a channery silt loam Inceptisols using  
663 the USDA NRCS Web Soil Survey data product (Soil Survey Staff 2022). Between  
664 2006 and 2020, study sites averaged 972 mm of precipitation per year and had an  
665 average temperature of 7.9 °C per a weather station located near the Cornell Uni-  
666 versity campus (42.449 °N, 76.449 °W) part of the NOAA NCEI Global Historical  
667 Climatology Network (Menne et al. 2012).

**668** 3.2.2 *Experimental design*

**669** Four 40 m x 40 m plots were set up at each site in 2009, each with an additional  
**670** 10 m buffer along plot perimeters (60 m x 60 m total). The plots were set up as a  
**671** nitrogen-by-pH field manipulation experiment, with one each of four treatments  
**672** at each site. Two nitrogen treatments were applied, both at  $50 \text{ kg N ha}^{-1} \text{ yr}^{-1}$ , as  
**673** either sodium nitrate ( $\text{NaNO}_3$ ) to raise soil pH, or ammonium sulfate ( $(\text{NH}_4)_2\text{SO}_4$ )  
**674** to acidify; an elemental sulfur treatment was selected to acidify without nitrogen,  
**675** applied at the same rate of S addition ( $57 \text{ kg S ha}^{-1} \text{ yr}^{-1}$ ); and control plots  
**676** received no additions. All amendments were added in pelletized form using hand-  
**677** held fertilizer spreaders to both the main plots and buffers. Amendments were  
**678** divided into three equal doses distributed across the growing season from 2011-  
**679** 2017 and added as a single dose from 2018 onward. During 2019, plots were  
**680** fertilized during the week of May 20.

**681** 3.2.3 *Leaf gas exchange and trait measurements*

**682** I sampled one leaf each from 6 to 10 individuals per plot between June 25 and July  
**683** 12, 2019 for gas exchange measurements (Table B1). Leaves were collected from  
**684** deciduous broadleaf trees represented across all sites and plots and were replicated  
**685** in efforts to mimic the species abundance of each plot at each site. I attempted  
**686** to collect leaves from the upper canopy to reduce differential shading effects on  
**687** leaf physiology. Leaves were accessed by pulling down small branches using an  
**688** arborist's slingshot and weighted beanbag attached to a throw line. Branches  
**689** were immediately recut under deionized water and remained submerged to reduce  
**690** stomatal closure and avoid xylem embolism, as done in Smith and Dukes (2018),

691 until gas exchange data were collected.

692 Randomly selected leaves with little to no visible external damage were  
693 attached to a Li-COR LI-6800 (Li-COR Bioscience, Lincoln, Nebraska, USA)  
694 portable photosynthesis machine to measure net photosynthesis ( $A_{\text{net}}$ ;  $\mu\text{mol m}^{-2}$   
695  $\text{s}^{-1}$ ), stomatal conductance ( $g_{\text{sw}}$ ;  $\text{mol m}^{-2} \text{s}^{-1}$ ), and intercellular  $\text{CO}_2$  concentra-  
696 tion ( $C_i$ ;  $\mu\text{mol mol}^{-1}$ ) at different reference  $\text{CO}_2$  concentrations ( $C_a$ ;  $\mu\text{mol mol}^{-1}$ )  
697 concentrations (i.e., an  $A_{\text{net}}/C_i$  curve) under saturating light conditions (2,000  
698  $\mu\text{mol m}^{-2} \text{s}^{-1}$ ). Reference  $\text{CO}_2$  concentrations followed the sequence: 400, 300,  
699 200, 100, 50, 400, 400, 600, 800, 1000, 1200, 1500, and 2000  $\mu\text{mol mol}^{-1} \text{CO}_2$ . Leaf  
700 temperatures were not controlled in the cuvette and ranged from 21.8 °C to 31.7  
701 °C (mean±SD: 27.2±2.2 °C). A linear and second order log-polynomial nonlinear  
702 regression suggested no effect of temperature on stomatal conductance measured  
703 at 400  $\mu\text{mol mol}^{-1} \text{CO}_2$  or net photosynthesis measured at 400  $\mu\text{mol mol}^{-1} \text{CO}_2$   
704 (Table B2, B3; Fig. B1). All  $A_{\text{net}}/C_i$  curves were generated within one hour of  
705 branch severance.

706 Leaf morphological and chemical traits were collected on the same leaf used  
707 to generate each  $A_{\text{net}}/C_i$  curve. Images of each leaf were taken using a flat-bed  
708 scanner to determine fresh leaf area using the ‘LeafArea’ R package (Katabuchi  
709 2015), which automates leaf area calculations using ImageJ software (Schneider  
710 et al. 2012). Each leaf was dried at 65°C for at least 48 hours, weighed, and  
711 ground using a Retsch MM200 ball mill grinder (Verder Scientific, Inc., Newtown,  
712 PA, USA) until homogenized. Leaf mass per unit leaf area ( $M_{\text{area}}$ ,  $\text{g m}^{-2}$ ) was  
713 calculated as the ratio of dry leaf biomass to fresh leaf area. Using a subsample  
714 of ground and homogenized leaf biomass, leaf nitrogen content ( $N_{\text{mass}}$ ;  $\text{gN g}^{-1}$ )

715 and leaf  $\delta^{13}\text{C}$  (‰, relative to Vienna Pee Dee Belemnite international reference  
 716 standard) were measured at the Cornell Stable Isotope Lab with an elemental  
 717 analyzer (NC 2500, CE Instruments, Wigan, UK) interfaced to an isotope ratio  
 718 mass spectrometer (Delta V Isotope Ratio Mass Spectrometer, ThermoFisher Sci-  
 719 entific, Waltham, MA, USA). Leaf nitrogen content per unit leaf area ( $N_{\text{area}}$ ; g N  
 720  $\text{m}^{-2}$ ) was calculated by multiplying  $N_{\text{mass}}$  by  $M_{\text{area}}$ .

721 I used leaf  $\delta^{13}\text{C}$  values to estimate  $\chi$  (unitless), which is an isotope-derived  
 722 estimate of the leaf  $C_i:C_a$  ratio. While intercellular and atmospheric  $\text{CO}_2$  concen-  
 723 trations were directly measured during each  $A_{\text{net}}/C_i$  curve, deriving  $\chi$  from  $\delta^{13}\text{C}$   
 724 provides a more integrative estimate of the leaf  $C_i:C_a$  over an individual leaf's  
 725 lifespan. I derived  $\chi$  following the approach of Farquhar et al. (1989) described  
 726 in Cernusak et al. (2013):

$$\chi = \frac{\Delta^{13}\text{C} - a}{b - a} \quad (3.1)$$

727 where  $\Delta^{13}\text{C}$  represents the relative difference between leaf  $\delta^{13}\text{C}$  (‰) and air  $\delta^{13}\text{C}$   
 728 (‰), and is calculated from the following equation:

$$\Delta^{13}\text{C} = \frac{\delta^{13}\text{C}_{\text{air}} - \delta^{13}\text{C}_{\text{leaf}}}{1 + \delta^{13}\text{C}_{\text{leaf}}} \quad (3.2)$$

729 where  $\delta^{13}\text{C}_{\text{air}}$  is assumed to be -8‰ (Keeling et al. 1979; Farquhar et al. 1989),  $a$   
 730 represents the fractionation between  $^{12}\text{C}$  and  $^{13}\text{C}$  due to diffusion in air, assumed  
 731 to be 4.4‰, and  $b$  represents the fractionation caused by Rubisco carboxylation,  
 732 assumed to be 27‰ (Farquhar et al. 1989).

**733** 3.2.4  $A_{net}/C_i$  curve-fitting and parameter estimation

**734** I fit  $A_{net}/C_i$  curves of each individual using the ‘fitaci’ function in the ‘plante-  
**735** cophys’ R package (Duursma 2015). This function estimates the maximum rate  
**736** of Rubisco carboxylation ( $V_{cmax}$ ;  $\mu\text{mol m}^{-2} \text{s}^{-1}$ ) and maximum rate of electron  
**737** transport for RuBP regeneration ( $J_{max}$ ;  $\mu\text{mol m}^{-2} \text{s}^{-1}$ ) based on the Farquhar,  
**738** von Caemmerer, and Berry biochemical model of C<sub>3</sub> photosynthesis (Farquhar  
**739** et al. 1980). For each curve fit, I included triose phosphate utilization (TPU)  
**740** limitation to avoid underestimating  $J_{max}$  (Gregory et al. 2021). Curves were  
**741** visually examined to confirm the likely presence of TPU limitation.

**742** I determined Michaelis-Menten coefficients for Rubisco affinity to CO<sub>2</sub> ( $K_c$ ;  
**743**  $\mu\text{mol mol}^{-1}$ ) and O<sub>2</sub> ( $K_o$ ;  $\mu\text{mol mol}^{-1}$ ), and the CO<sub>2</sub> compensation point ( $\Gamma^*$ ;  
**744**  $\mu\text{mol mol}^{-1}$ ) using leaf temperature and equations described in Medlyn et al.  
**745** (2002) and derived in Bernacchi et al. (2001). Specifically,  $K_c$  and  $K_o$  were  
**746** calculated as:

$$K_c = 404.9 * \exp^{\frac{79430(T_k - 298)}{298RT_k}} \quad (3.3)$$

**747** and

$$K_o = 278.4 * \exp^{\frac{36380(T_k - 298)}{298RT_k}} \quad (3.4)$$

**748** while  $\Gamma^*$  was calculated as:

$$\Gamma^* = 42.75 * \exp^{\frac{37830(T_k - 298)}{298RT_k}} \quad (3.5)$$

**749** In all three equations,  $T_k$  is the leaf temperature (in Kelvin) during each  $A_{\text{net}}/C_i$

**750** curve and R is the universal gas constant ( $8.314 \text{ J mol}^{-1} \text{ K}^{-1}$ ).

**751** I standardized  $V_{\text{cmax}}$  and  $J_{\text{max}}$  estimates to  $25^\circ\text{C}$  using a modified Arrhe-

**752** nius equation (Kattge and Knorr 2007):

$$k_{25} = \frac{k_{\text{obs}}}{e^{\frac{H_a(T_{\text{obs}} - T_{\text{ref}})}{T_{\text{ref}}RT_{\text{obs}}}} * \frac{1+e^{\frac{T_{\text{ref}}\Delta S - H_d}{T_{\text{obs}}\Delta S - H_d}}}{1+e^{\frac{T_{\text{obs}}\Delta S - H_d}{T_{\text{obs}}\Delta S - H_d}}}} \quad (3.6)$$

**753**  $k_{25}$  represents the standardized  $V_{\text{cmax}}$  or  $J_{\text{max}}$  rate at  $25^\circ\text{C}$ ,  $k_{\text{obs}}$  represents the

**754**  $V_{\text{cmax}}$  or  $J_{\text{max}}$  estimate at the average leaf temperature measured inside the cuvette

**755** during the  $A_{\text{net}}/C_i$  curve.  $H_a$  is the activation energy of  $V_{\text{cmax}}$  ( $71,513 \text{ J mol}^{-1}$ )

**756** Kattge and Knorr (2007) or  $J_{\text{max}}$  ( $49,884 \text{ J mol}^{-1}$ ) (Kattge and Knorr 2007).

**757**  $H_d$  represents the deactivation energy of both  $V_{\text{cmax}}$  and  $J_{\text{max}}$  ( $200,000 \text{ J mol}^{-1}$ )

**758** (Medlyn et al. 2002), and R represents the universal gas constant ( $8.314 \text{ J mol}^{-1}$

**759**  $\text{K}^{-1}$ ).  $T_{\text{ref}}$  represents the standardized temperature of  $298.15 \text{ K}$  ( $25^\circ\text{C}$ ) and  $T_{\text{obs}}$

**760** represents the mean leaf temperature (in K) during each  $A_{\text{net}}/C_i$  curve.  $\Delta S$  is an

**761** entropy term that (Kattge and Knorr 2007) derived as a linear relationship with

**762** average growing season temperature ( $T_g$ ;  $^\circ\text{C}$ ), where:

$$\Delta S_{v_{\text{cmax}}} = -1.07 T_g + 668.39 \quad (3.7)$$

**763** and

$$\Delta S_{j_{\text{max}}} = -0.75 T_g + 659.70 \quad (3.8)$$

**764** I estimated  $T_g$  in Equations 3.7 and 3.8 based on mean daily (24-hour) air tem-  
**765** perature of the 30 days leading up to the day of each sample collection using the  
**766** same weather station reported in the site description. I used  $V_{cmax25}$  and  $J_{max25}$   
**767** estimates to calculate the ratio of  $J_{max25}$  to  $V_{cmax25}$  ( $J_{max25}:V_{cmax25}$ ; unitless).

**768** 3.2.5 *Proportion of leaf nitrogen allocated to photosynthesis and structure*

**769** I used equations from Niinemets and Tenhunen (1997) to estimate the proportion  
**770** of leaf nitrogen content allocated to Rubisco and bioenergetics. The proportion of  
**771** leaf nitrogen allocated to Rubisco ( $\rho_{rubisco}$ ; gN gN<sup>-1</sup>) was calculated as a function  
**772** of  $V_{cmax25}$  and  $N_{area}$ :

$$\rho_{rubisco} = \frac{V_{cmax25} N_r}{V_{cr} N_{area}} \quad (3.9)$$

**773** where  $N_r$  is the amount of nitrogen in Rubisco, set to 0.16 gN (gN in Rubisco)<sup>-1</sup>  
**774** and  $V_{cr}$  is the maximum rate of RuBP carboxylation per unit Rubisco protein,  
**775** set to 20.5 μmol CO<sub>2</sub> (g Rubisco)<sup>-1</sup>. The proportion of leaf nitrogen allocated to  
**776** bioenergetics ( $\rho_{bioe}$ ; gN gN<sup>-1</sup>) was similarly calculated as a function of  $J_{max25}$  and  
**777**  $N_{area}$ :

$$\rho_{bioe} = \frac{J_{max25} N_b}{J_{mc} N_{area}} \quad (3.10)$$

**778** where  $N_b$  is the amount of nitrogen in cytochrome f, set to 0.12407 gN (μmol  
**779** cytochrome f)<sup>-1</sup> assuming a constant 1: 1: 1.2 cytochrome f: ferredoxin NADP  
**780** reductase: coupling factor molar ratio (Evans and Seemann 1989; Niinemets and  
**781** Tenhunen 1997), and  $J_{mc}$  is the capacity of electron transport per cytochrome f,

782 set to 156  $\mu\text{mol}$  electron ( $\mu\text{mol}$  cytochrome f) $^{-1}\text{s}^{-1}$ .

783 I estimated the proportion of leaf nitrogen content allocated to photosynthetic tissue ( $\rho_{\text{photo}}$ ;  $\text{gN gN}^{-1}$ ) as the sum of  $\rho_{\text{rubisco}}$  and  $\rho_{\text{bioe}}$ . This calculation  
784 is an underestimate of the proportion of leaf nitrogen allocated to photosynthetic  
785 tissue because it does not include nitrogen allocated to light harvesting proteins.  
786 This leaf nitrogen pool was not included because I did not perform chlorophyll  
787 extractions on focal leaves. However, the proportion of leaf nitrogen content al-  
788 located to light harvesting proteins tends to be small relative to  $\rho_{\text{rubisco}}$  and  $\rho_{\text{bioe}}$ ,  
789 and may scale with changes in  $\rho_{\text{rubisco}}$  and  $\rho_{\text{bioe}}$  (Niinemets and Tenhunen 1997).

791 Finally, the proportion of leaf nitrogen content allocated to structural tissue  
792 ( $\rho_{\text{structure}}$ ;  $\text{gN gN}^{-1}$ ) was estimated as:

$$\rho_{\text{structure}} = \frac{N_{\text{cw}}}{N_{\text{area}}} \quad (3.11)$$

793 where  $N_{\text{cw}}$  is the leaf nitrogen content allocated to cell walls ( $\text{gN m}^{-2}$ ), calculated  
794 as a function of  $M_{\text{area}}$  using an empirical equation from Onoda et al. (2017):

$$N_{\text{cw}} = 0.000355 * M_{\text{area}}^{1.39} \quad (3.12)$$

### 795 3.2.6 *Tradeoffs between nitrogen and water use*

796 Photosynthetic nitrogen use efficiency (PNUE;  $\mu\text{mol CO}_2 \text{ mol}^{-1} \text{ N s}^{-1}$ ) was cal-  
797 culated by dividing  $A_{\text{net}}$  by  $N_{\text{area}}$ , first converting  $N_{\text{area}}$  to  $\text{mol N m}^{-2}$  using the  
798 molar mass of nitrogen ( $14 \text{ g mol}^{-1}$ ). I used  $\chi$  as an indicator of water use effi-  
799 ciency, which exploratory analyses suggest had similar responses to soil nitrogen

800 availability and pH as intrinsic water use efficiency measured from gas exchange  
801 ( $A_{\text{net}}/g_{\text{sw}}$ ). Tradeoffs between nitrogen and water use were determined by cal-  
802 culating the ratio of  $N_{\text{area}}$  to  $\chi$  ( $N_{\text{area}}:\chi$ ; gN m<sup>-2</sup>) and  $V_{\text{cmax25}}$  to  $\chi$  ( $V_{\text{cmax25}}:\chi$ ;  
803  $\mu\text{mol m}^{-2} \text{ s}^{-1}$ ). This approach is similar to tradeoff calculations in which nitrogen-  
804 water use tradeoffs are measured as the ratio of  $N_{\text{area}}$  or  $V_{\text{cmax25}}$  to  $g_{\text{sw}}$  (Paillassa  
805 et al. 2020; Bialic-Murphy et al. 2021). In this chapter, I quantify these rela-  
806 tionships using  $\chi$  in lieu of  $g_{\text{sw}}$  because  $g_{\text{sw}}$  rapidly changes with environmental  
807 conditions and therefore may have been altered by recent tree branch severance  
808 and/or placement in the cuvette.

809 3.2.7 *Soil nitrogen availability and pH*

810 To characterize soil nitrogen availability at the time of our leaf gas exchange  
811 measurements, I used mixed bed resin bags to quantify mobile ammonium-N and  
812 nitrate-N concentrations in each plot. Lycra mesh bags were filled with 5 g of  
813 Dowex® Marathon MR-3 hydrogen and hydroxide form resin (MilliporeSigma,  
814 Burlington, MA USA) and sealed with a zip tie. Each bag was activated by  
815 soaking in 0.5 M HCl for 20 minutes, then in 2 M NaCl until pH of the saline  
816 solution stabilized, as described in Allison et al. (2008). Five resin bags were  
817 inserted about 10 cm below the soil surface at each plot on June 25, 2019: one  
818 near each of the four plot corners and one near the plot center. All resin bags  
819 were collected 24 days later on July 19, 2019 and were frozen until extracted.

820 Prior to anion and cation extraction, each resin bag was rinsed with ul-  
821 trapure water (MilliQ IQ 7000; Millipore Sigma, Burlington, MA) to remove any  
822 surface soil residues. Anions and cations were extracted from surface-cleaned

823 resin bags by individually soaking and shaking each bag in 100 mL of a 0.1 M  
824 HCl/2.0 M NaCl matrix for one hour. Using a microplate reader (Biotek Synergy  
825 H1; Biotek Instruments, Winooski, VT USA), I quantified nitrate-N concentra-  
826 tions spectrophotometrically at 540 nm with the end product of a single reagent  
827 vanadium (III) chloride reaction (Doane and Horwáth 2003), and ammonium-N  
828 concentrations quantified at 650 nm with the end product of a modified phenol-  
829 hypochlorite reaction (Weatherburn 1967; Rhine et al. 1998). Both the single  
830 reagent vanadium (III) chloride and modified phenol-hypochlorite methodologies  
831 are well established for determining nitrate-N and ammonium-N concentrations  
832 in resin bag extracts (Arnone 1997; Allison et al. 2008). I used a series of nega-  
833 tive and positive controls throughout each well plate to verify the accuracy and  
834 precision of our measurements, assaying each resin bag extract and control in  
835 triplicate. Soil nitrogen availability was estimated as the sum of the nitrate-N  
836 and ammonium-N concentration in each resin bag, normalized per g of resin and  
837 duration in the field ( $\mu\text{g N g}^{-1} \text{ resin d}^{-1}$ ), then subsequently averaged across all  
838 resin bags in a plot for a plot-level mean.

839 Soil pH was measured on 0-10 cm mineral soil samples collected prior to  
840 fertilization in 2019. Near each of the four plot corners, three 5.5 cm diameter soil  
841 cores were collected after first removing the forest floor where present. Each set  
842 of three cores was placed in a plastic bag, and later composited by hand mixing  
843 and sieved to 4mm. Soil pH was determined for a 1:2 soil:water slurry (10 g field-  
844 moist soil to 20 mL DI water) of each sample using an Accumet AB15 pH meter  
845 with flushable junction probe (Fisher Scientific; Hampton, NH, USA), and was  
846 estimated at the plot level as the mean soil pH within each plot.

**847** 3.2.8 *Statistical analyses*

**848** I built two separate series of linear mixed-effects models to explore effects of soil  
**849** nitrogen availability, soil pH, species, and leaf nitrogen content on leaf physiolog-  
**850** ical traits. In the first series of linear mixed-effects models, I explored the effect  
**851** of soil nitrogen availability, soil pH, and species on leaf nitrogen content, leaf  
**852** photosynthesis, stomatal conductance, and nitrogen-water use tradeoffs. Models  
**853** included plot-level soil nitrogen availability and plot-level soil pH as continuous  
**854** fixed effects, species as a categorical fixed effect, and site as a categorical ran-  
**855** dom intercept term. Interaction terms between fixed effects were not included  
**856** due to the small number of experimental plots. I built a series of separate mod-  
**857** els with this independent variable structure to quantify individual effects of soil  
**858** nitrogen availability, soil pH, and species on  $N_{\text{area}}$ ,  $M_{\text{area}}$ ,  $N_{\text{mass}}$ ,  $A_{\text{net}}$ ,  $V_{\text{cmax25}}$ ,  
**859**  $J_{\text{max25}}$ ,  $J_{\text{max25}}:V_{\text{cmax25}}$ ,  $\rho_{\text{rubisco}}$ ,  $\rho_{\text{bioenergetics}}$ ,  $\rho_{\text{photo}}$ ,  $\rho_{\text{structure}}$ ,  $\chi$ , PNUE,  $N_{\text{area}}:\chi$ , and  
**860**  $V_{\text{cmax25}}:\chi$ .

**861** A second series of linear mixed-effects models were built to investigate  
**862** relationships between leaf nitrogen content and photosynthetic parameters. Sta-  
**863** tistical models included  $N_{\text{area}}$  as a single continuous fixed effect with species and  
**864** site designated as individual random intercept terms. I used this independent  
**865** variable structure to quantify individual effects of leaf nitrogen content on  $A_{\text{net}}$ ,  
**866**  $V_{\text{cmax25}}$ ,  $J_{\text{max25}}$ ,  $J_{\text{max25}}:V_{\text{cmax25}}$ , and  $\chi$ .

**867** For all linear mixed-effects models, I used Shapiro-Wilk tests of normality  
**868** to determine whether linear mixed-effects models satisfied residual normality as-  
**869** sumptions. If residual normality assumptions were not met, then models were fit  
**870** using dependent variables that were natural log transformed. If residual normal-

871 ity assumptions were still not met (Shapiro-Wilk:  $p<0.05$ ), then models were fit  
872 using dependent variables that were square root transformed. All residual nor-  
873 mality assumptions for both sets of models that did not originally satisfy residual  
874 normality assumptions were met with either a natural log or square root data  
875 transformation (Shapiro-Wilk:  $p>0.05$  in all cases).

876 In the first series of models, models for  $N_{\text{area}}$ ,  $M_{\text{area}}$ ,  $N_{\text{mass}}$ ,  $V_{\text{cmax25}}$ ,  $J_{\text{max25}}$ ,  
877  $\chi$ ,  $N_{\text{area}}:\chi$ , and  $V_{\text{cmax25}}:\chi$ ,  $\rho_{\text{rubisco}}$ ,  $\rho_{\text{bioenergetics}}$ ,  $\rho_{\text{photo}}$ ,  $\rho_{\text{structure}}$  satisfied residual  
878 normality assumptions without data transformations (Shapiro-Wilk:  $p>0.05$  in  
879 all cases). The model for  $J_{\text{max25}}:V_{\text{cmax25}}$  satisfied residual normality assumptions  
880 with a natural log data transformation, while models for  $A_{\text{net}}$  and PNUE each  
881 satisfied residual normality assumptions with square root data transformations.  
882 In the second series of models, models for  $V_{\text{cmax25}}$ ,  $J_{\text{max25}}$ ,  $\chi$ , and  $V_{\text{cmax25}}:\chi$  satis-  
883 fied residual normality assumptions without data transformations (Shapiro-Wilk:  
884  $p>0.05$  in all cases). The model for  $J_{\text{max25}}:V_{\text{cmax25}}$  required a natural log data  
885 transformation and the model for  $A_{\text{net}}$  required a square root data transformation  
886 (Shapiro-Wilk:  $p>0.05$  in both cases).

887 In all models, I used the ‘lmer’ function in the ‘lme4’ R package (Bates  
888 et al. 2015) to fit each model and the ‘Anova’ function in the ‘car’ R package  
889 (Fox and Weisberg 2019) to calculate Type II Wald’s  $\chi^2$  and determine the signif-  
890 icance level ( $\alpha=0.05$ ) of each fixed effect coefficient. Finally, I used the ‘emmeans’  
891 R package (Lenth, 2019) to conduct post-hoc comparisons using Tukey’s tests,  
892 where degrees of freedom were approximated using the Kenward-Roger approach  
893 (Kenward and Roger 1997). All analyses and plots were conducted in R version  
894 4.1.1 (R Core Team 2021). All figure regression lines and associated 95% confi-

895 dence interval error bars were plotted using predictions generated across the soil  
896 nitrogen availability gradient using the ‘emmeans’ R package (Lenth 2019).

897 3.3 Results

898 3.3.1 *Leaf nitrogen content*

899 Increasing soil nitrogen availability generally increased  $N_{\text{area}}$  (Table 3.1; Fig. 3.1a).  
900 This pattern was driven by an increase in  $N_{\text{mass}}$  (Table 3.1; Fig. 3.1c) and a  
901 marginal increase in  $M_{\text{area}}$  (Table 3.1; Fig. 3.1e) with increasing soil nitrogen  
902 availability. There was no effect of soil pH on  $N_{\text{area}}$ ,  $N_{\text{mass}}$ , or  $M_{\text{area}}$  (Table 3.1);  
903 however, I also observed strong differences in  $N_{\text{area}}$  (Fig. 3.1b),  $N_{\text{mass}}$  (Fig. 3.1d),  
904 and  $M_{\text{area}}$  (Fig. 3.1e) between species (Table 3.1).

**Table 3.1.** Effects of soil nitrogen availability, soil pH, and species on leaf nitrogen content per unit leaf area ( $N_{\text{area}}$ ; gN m<sup>-2</sup>), leaf nitrogen content per unit leaf mass ( $N_{\text{mass}}$ ; gN g<sup>-1</sup>), and leaf mass per unit leaf area ( $M_{\text{area}}$ ; g m<sup>-2</sup>)\*

	$N_{\text{area}}$			$N_{\text{mass}}$			$M_{\text{area}}$			
	df	Coefficient	$\chi^2$	p	Coefficient	$\chi^2$	p	Coefficient	$\chi^2$	p
Intercept	-	9.03E-01	-	-	1.68E+00	-	-	4.60E+01	-	-
Soil N	1	1.68E-02	11.990	<b>0.001</b>	1.25E-02	6.902	<b>0.009</b>	4.87E-01	4.143	<b>0.042</b>
Soil pH	1	9.28E-02	0.836	0.361	8.08E-02	0.663	0.415	4.05E+00	0.653	0.419
Species	4	-	72.128	<0.001	-	35.074	<0.001	-	29.869	<0.001

905 \*Significance determined using Type II Wald  $\chi^2$  tests ( $\alpha=0.05$ ). P-values<0.05 are in bold.

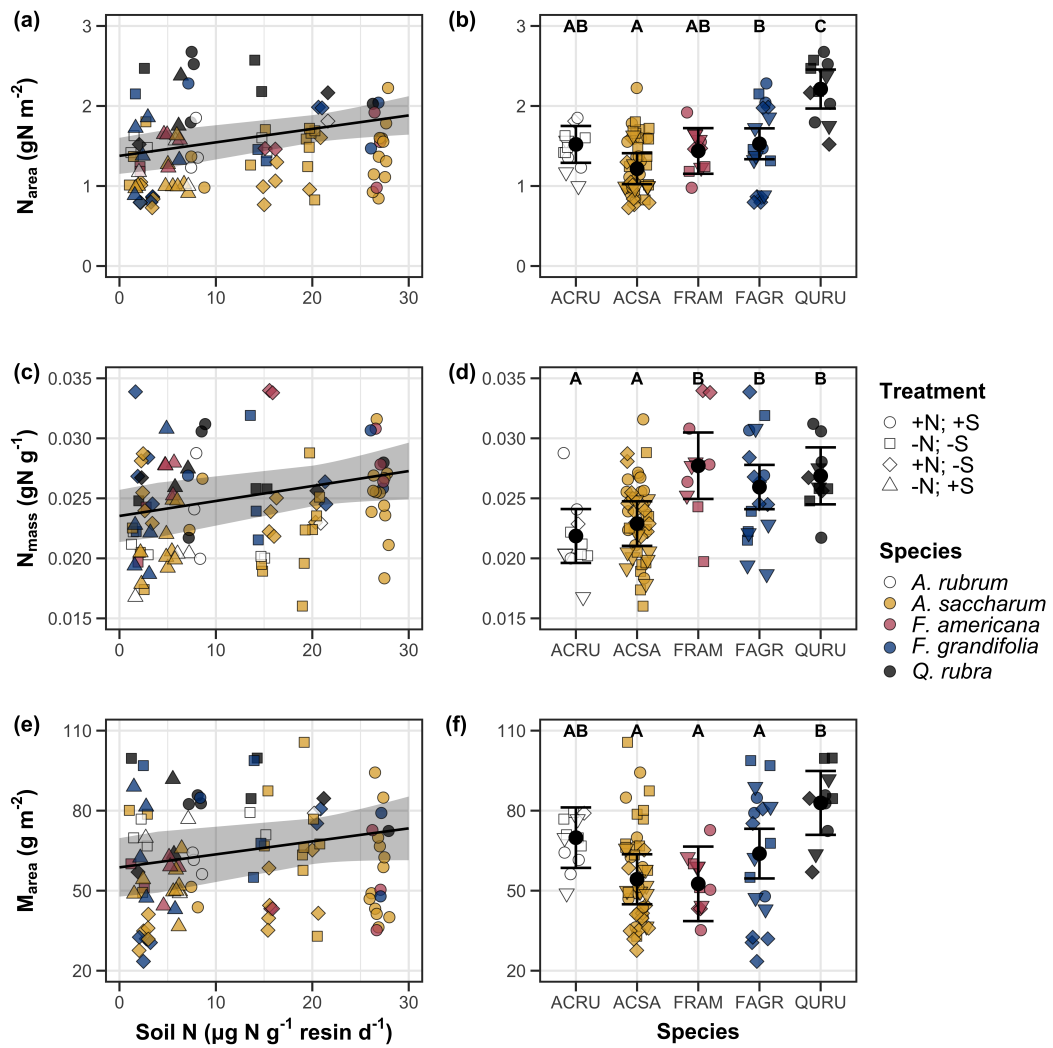


**Figure 3.1.** Effects of soil N availability and species on leaf nitrogen content per unit leaf area (a-b), leaf nitrogen content per unit leaf biomass (c-d), and leaf mass per unit leaf area (e-f). Soil nitrogen availability is represented on the x-axis in the left column of panels, while species is represented on the x-axis in the right column of panels. Tree species are represented as colored points and treatment plots are represented as shaped points, jittered for visibility. Species are abbreviated in the right column of panels through their assigned NRCS PLANTS Database symbol (USDA NRCS 2022), grouped along the x-axis per common mycorrhizal association, where the first three species commonly associate with arbuscular mycorrhizae (ACRU, ACSA, FAGR) and the second two species with ectomycorrhizae (FAGR, QURU). Trendlines are only included when the regression slope is statistically different from zero ( $p < 0.05$ ).

**906** 3.3.2 *Net photosynthesis and leaf biochemistry*

**907** Increasing soil nitrogen availability generally had no effect on  $A_{\text{net}}$ ,  $V_{\text{cmax25}}$ ,  $J_{\text{max25}}$ ,  
**908** or  $J_{\text{max25}}:V_{\text{cmax25}}$  (Table 3.2, Figs. 3.2a, 3.2d, 3.2g). I also observed strong species  
**909** effects on all measured leaf photosynthetic traits (Table 3.2; Figs. 3.2b, 3.2e, 3.2h).  
**910** Increasing soil pH had a marginal negative effect on  $A_{\text{net}}$ , but had no effect on  
**911**  $V_{\text{cmax25}}$ ,  $J_{\text{max25}}$ , or  $J_{\text{max25}}:V_{\text{cmax25}}$  (Table 3.2). There was a weak positive effect of  
**912** increasing  $N_{\text{area}}$  on  $A_{\text{net}}$  (Fig. 3.2c), but quite strong positive effects of increasing  
**913**  $N_{\text{area}}$  on  $V_{\text{cmax25}}$  and  $J_{\text{max25}}$  (Table 3.2; Fig. 3.2f and 3.2i).

**Table 3.2.** Effects of soil nitrogen availability, soil pH, species, and  $N_{\text{area}}$  on net photosynthesis ( $A_{\text{net}}$ ;  $\mu\text{mol m}^{-2} \text{s}^{-1}$ ), the maximum rate of Rubisco carboxylation ( $V_{\text{cmax25}}$ ;  $\mu\text{mol m}^{-2} \text{s}^{-1}$ ), the maximum rate of RuBP regeneration ( $J_{\text{max25}}$ ;  $\mu\text{mol m}^{-2} \text{s}^{-1}$ ), and the ratio of the maximum rate of RuBP regeneration to the maximum rate of Rubisco carboxylation ( $J_{\text{max25}}:V_{\text{cmax25}}$ ; unitless)\*

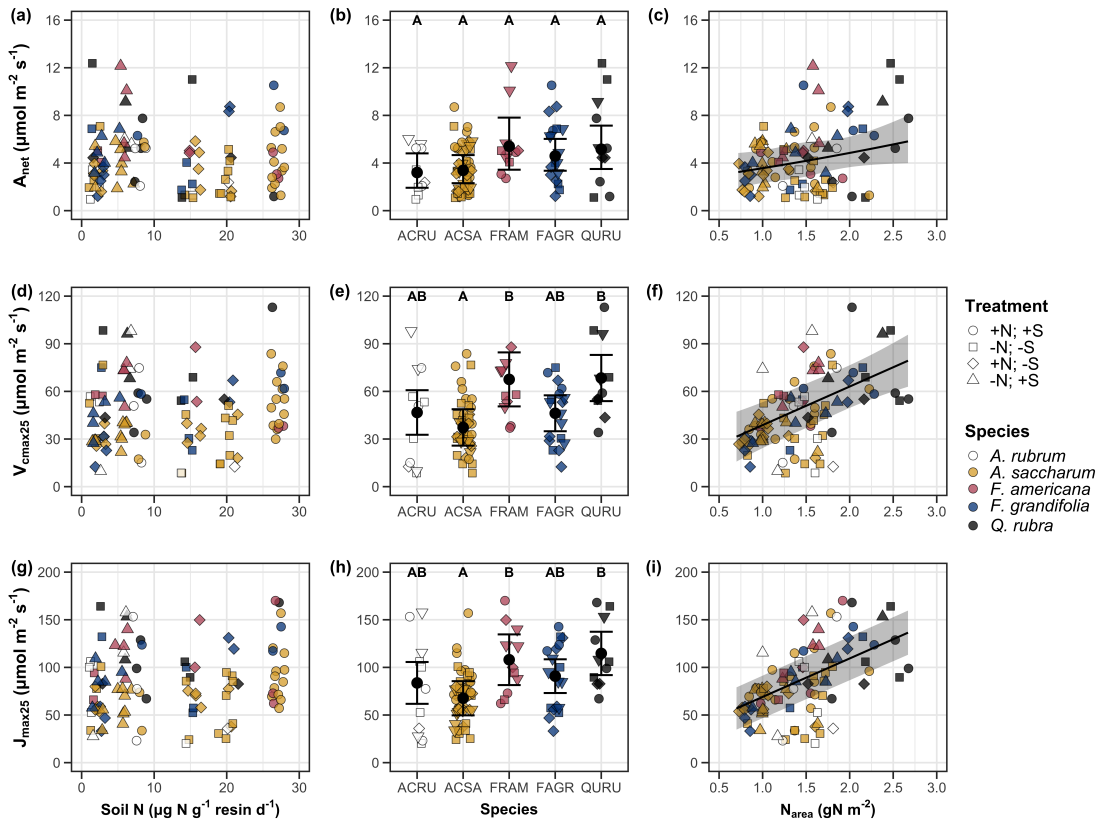
	$A_{\text{net}}$			$V_{\text{cmax25}}$			$J_{\text{max25}}$			
	df	Coefficient	$\chi^2$	p	Coefficient	$\chi^2$	p	Coefficient	$\chi^2$	p
(Intercept)	-	3.29E+00 <sup>b</sup>	-	-	6.38E+01	-	-	1.12E+02	-	-
Soil N	1	-1.23E-03 <sup>b</sup>	1.798	0.180	-3.84E-01	1.745	0.187	-6.70E-01	2.172	0.141
Soil pH	1	-3.09E-01 <sup>b</sup>	3.312	0.069	-4.91E+00	0.655	0.418	-8.18E+00	0.742	0.389
Species	4	-	11.838	<b>0.019</b>	-	31.748	<0.001	-	27.291	<0.001
( $N_{\text{area}}$ int.)	-	6.59E-01 <sup>b</sup>	-	-	1.45E-01	-	-	2.86E+01	-	-
$N_{\text{area}}$	4	3.13E-01 <sup>b</sup>	4.790	<b>0.029</b>	2.43E+01	22.616	<0.001	4.04E+01	28.259	<0.001

	$J_{\text{max25}}:V_{\text{cmax25}}$			
	df	Coefficient	$\chi^2$	p
(Intercept)	-	6.59E-01 <sup>a</sup>	-	-
Soil N	1	7.04E-04 <sup>a</sup>	0.088	0.767
Soil pH	1	-7.84E-03 <sup>a</sup>	0.025	0.874
Species	4	-	12.745	<b>0.013</b>
( $N_{\text{area}}$ int.)	-	6.69E-01 <sup>a</sup>	-	-
$N_{\text{area}}$	4	-4.69E-02 <sup>a</sup>	1.142	0.285

54

914 \*Significance determined using Type II Wald  $\chi^2$  tests ( $\alpha=0.05$ ). P-values less than 0.05 are in bold, while p-values  
 915 between 0.05 and 0.1 are italicized. Superscript letters indicate model coefficients fit to natural-log (<sup>a</sup>) or square-root  
 916 (<sup>b</sup>) transformed data. Relationships between  $N_{\text{area}}$  and each response variable were fit using the second series of  
 917 bivariate mixed-effects models, so model coefficients and results are independent of model coefficients and results  
 918 reported for relationships between soil nitrogen, soil pH, and species for each response variable.



**Figure 3.2.** Effects of soil nitrogen availability (left column of panels), species (middle column of panels), and leaf nitrogen content per unit leaf area (right column of panels) on net photosynthesis (a-c), maximum Rubisco carboxylation rate (d-f), and maximum RuBP regeneration rate (g-i). Soil nitrogen availability is represented on the x-axis in the left column of panels, species is represented on the x-axis in the middle column of panels, and leaf nitrogen content per unit leaf area is represented continuously on the x-axis in the right column of panels. Species abbreviations and position along the x-axis in the middle column of panels, colored points, shapes, and trendlines are as explained in Figure 3.1.

**919** 3.3.3 *Leaf nitrogen allocation*

**920** Neither soil nitrogen availability nor soil pH affected the proportion of leaf nitrogen  
**921** allocated to Rubisco or bioenergetics (Table 3.3; Fig. 3.3a, Fig. 3.3c). There was  
**922** also no effect of soil nitrogen availability or soil pH on the proportion of leaf  
**923** nitrogen allocated to photosynthesis (Table 3.3; Fig. 3.3f). I found no effect of  
**924** soil nitrogen availability or soil pH on the proportion of leaf nitrogen allocated to  
**925** structure (Table 3.3; Fig 3.3g). Species varied in the proportion of leaf nitrogen  
**926** allocated to Rubisco, photosynthesis, and structure (Fig 3.3b, Fig. 3.3f, Fig 3.3h),  
**927** with no detectable species effect on the proportion of leaf nitrogen allocated to  
**928** bioenergetics (Table 3.3, Fig. 3.3d).

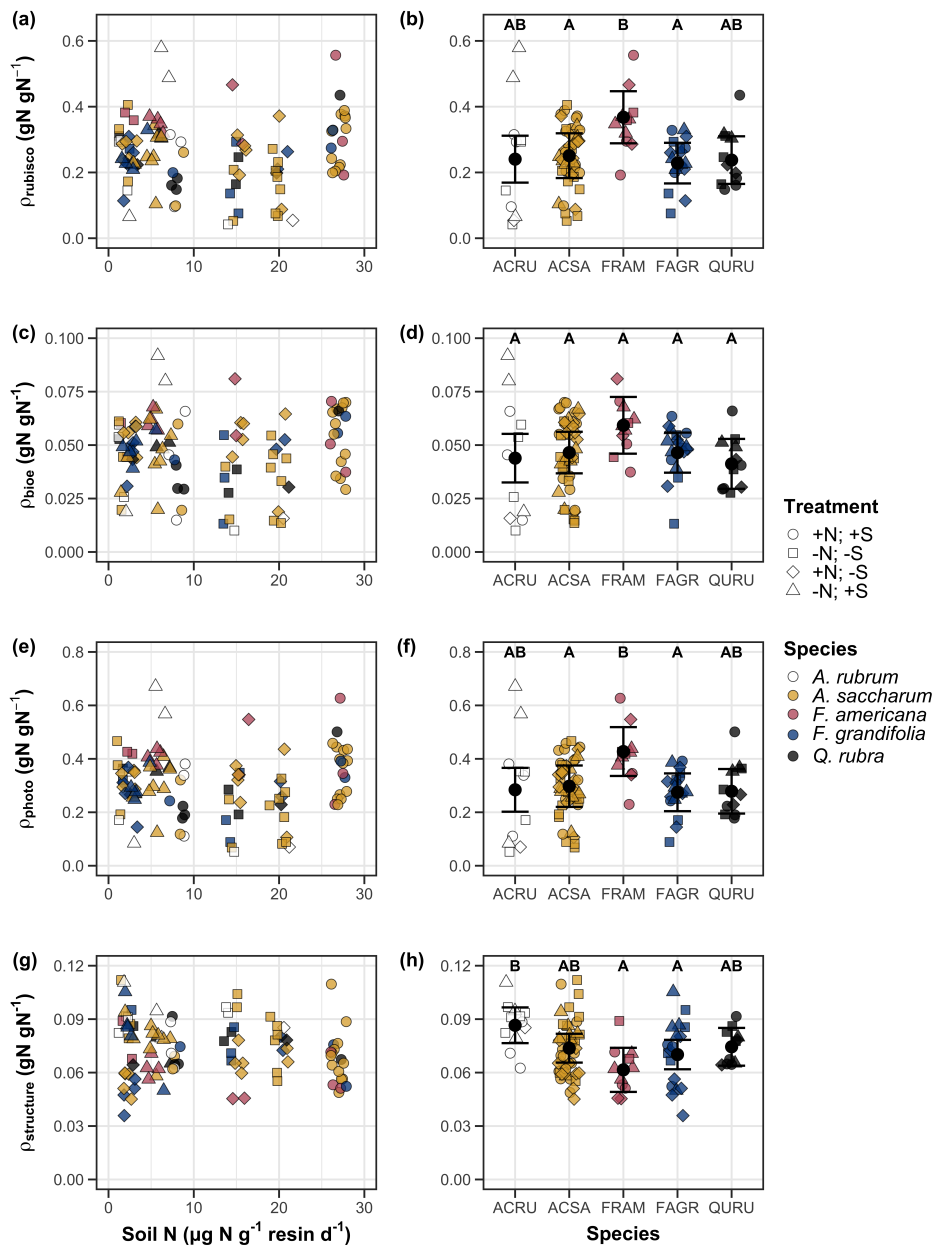
**Table 3.3.** Effects of soil nitrogen availability, soil pH, and species on the proportion of leaf nitrogen content allocated to photosynthesis ( $\rho_{\text{photo}}$ ; gN gN<sup>-1</sup>), Rubisco ( $\rho_{\text{rubisco}}$ ; gN gN<sup>-1</sup>), bioenergetics ( $\rho_{\text{bioe}}$ ; gN gN<sup>-1</sup>), and structure ( $\rho_{\text{structure}}$ ; gN gN<sup>-1</sup>)\*

	$\rho_{\text{photo}}$			$\rho_{\text{rubisco}}$			$\rho_{\text{bioe}}$			
	df	Coefficient	$\chi^2$	p	Coefficient	$\chi^2$	p	Coefficient	$\chi^2$	p
Intercept	-	4.93E-01	-	-	4.17E-01	-	-	7.64E-02	-	-
Soil N	1	-1.23E-03	0.521	0.470	-1.04E-03	0.501	0.479	-1.77E-04	0.557	0.455
Soil pH	1	-4.37E-02	1.581	0.209	-3.70E-02	1.511	0.219	-6.84E-03	1.941	0.164
Species	4	-	13.106	<b>0.011</b>	-	14.152	<b>0.007</b>	-	7.300	0.121

	$\rho_{\text{structure}}$			
	df	Coefficient	$\chi^2$	p
Intercept	-	9.77E-02	-	-
Soil N	1	-2.29E-04	1.165	0.280
Soil pH	1	-1.87E-03	0.179	0.672
Species	4	-	16.428	<b>0.002</b>

929 \*Significance determined using Type II Wald  $\chi^2$  tests ( $\alpha=0.05$ ). P-values less than 0.05 are in bold.



**Figure 3.3.** Effects of soil nitrogen availability and species on the proportion of leaf nitrogen content allocated to Rubisco (a-b), bioenergetics (c-d), photosynthesis (e-f), and structure (g-h). Soil nitrogen availability is represented on the x-axis in the left column of panels and species are represented on the x-axis in the right column of panels. Species abbreviations and position along the x-axis in the middle column of panels, colored points, shapes, trendlines, error bars, and compact lettering are as explained in Figure 3.1.

**930** 3.3.4 *Tradeoffs between nitrogen and water use*

**931** Although soil nitrogen availability did not affect  $\chi$  (Table 3.4; Fig. 3.4a), increasing  
**932** soil nitrogen availability decreased PNUE (Table 3.4; Fig. 3.4d) and increased  
**933** the ratio of  $N_{\text{area}}:\chi$  (Table 3.4; Fig. 3.4f). Specifically, this response yielded a  
**934** 26% reduction in PNUE and 37% stimulation in  $N_{\text{area}}:\chi$  across the soil nitrogen  
**935** availability gradient. There was no apparent effect of soil nitrogen availability on  
**936**  $V_{\text{cmax25}}:\chi$  (Table 3.4; Fig. 3.4h). Increasing soil pH had a weak marginal nega-  
**937** tive effect on PNUE, but did not influence  $\chi$ ,  $N_{\text{area}}:\chi$ , or  $V_{\text{cmax25}}:\chi$  (Table 3.4). I  
**938** observed differences in  $\chi$  (Fig. 3.4b), PNUE (Fig. 3.4e),  $N_{\text{area}}:\chi$  (Fig. 3.4g), and  
**939**  $V_{\text{cmax25}}:\chi$  (Fig. 3.4i) between species (Table 3.4). Finally, increasing  $N_{\text{area}}$  had a  
**940** strong negative effect on  $\chi$  (Table 3.4; Fig. 3.4c) and a strong positive effect on  
**941**  $V_{\text{cmax25}}:\chi$  (Table 3.4; Fig. 3.4j).

**Table 3.4.** Effects of soil nitrogen availability, soil pH, species, and  $N_{\text{area}}$  on  $\chi$  (unitless), photosynthetic nitrogen use efficiency (PNUE;  $\mu\text{mol CO}_2 \text{ mol}^{-1} \text{ N s}^{-1}$ ), leaf nitrogen content per unit  $\chi$  ( $N_{\text{area}}:\chi$ ;  $\text{gN m}^{-2}$ ), and maximum Rubisco carboxylation rate per unit  $\chi$  ( $V_{\text{cmax25}}:\chi$ ;  $\mu\text{mol m}^{-2} \text{ s}^{-1}$ )<sup>\*</sup>

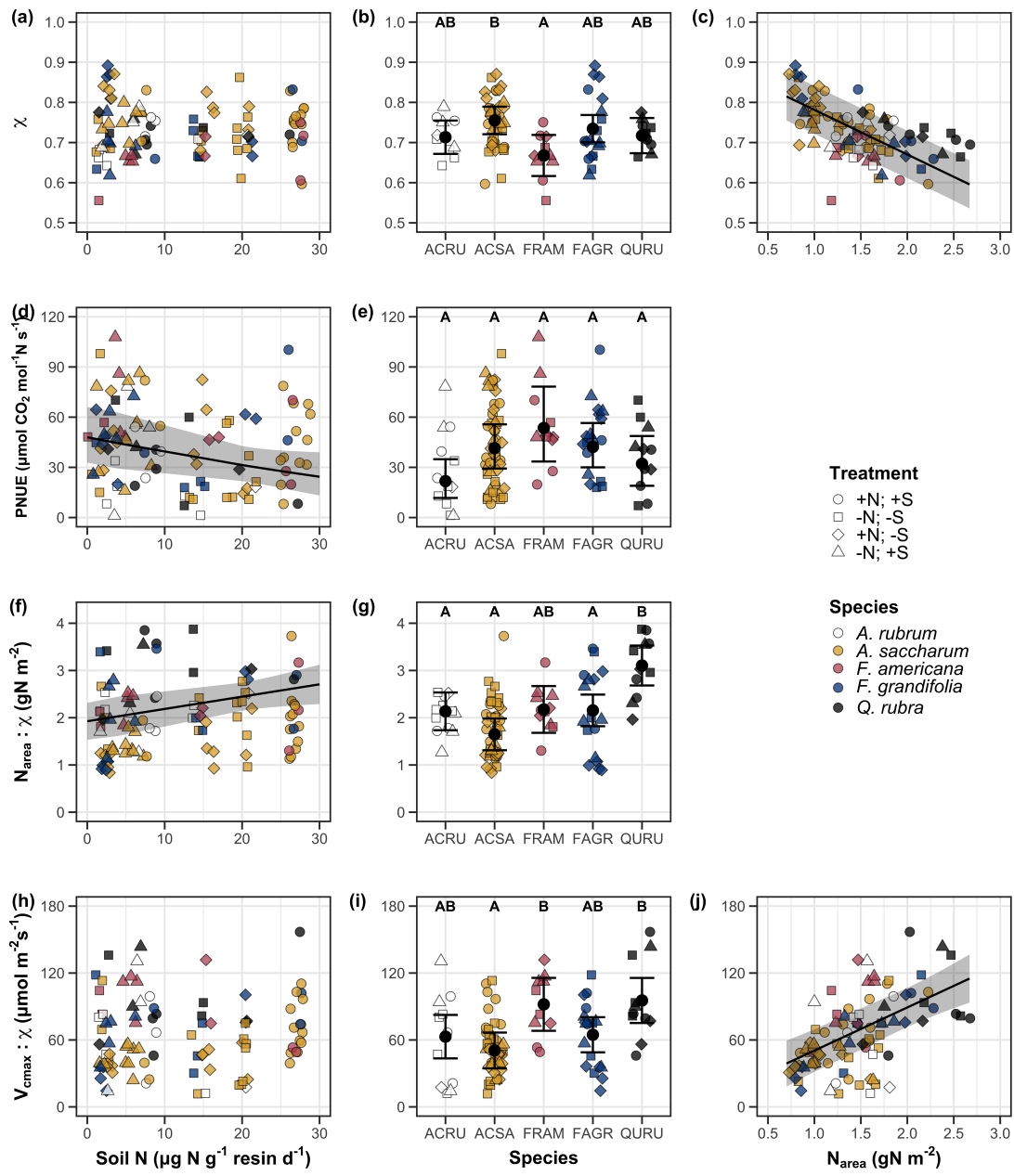
	$\chi$			PNUE			$N_{\text{area}}:\chi$			
	df	Coefficient	$\chi^2$	p	Coefficient	$\chi^2$	p	Coefficient	$\chi^2$	p
(Intercept)	-	8.12E-01	-	-	9.57E+00 <sup>b</sup>	-	-	9.19E-01	-	-
Soil N	1	-1.14E-03	1.698	0.193	-6.63E-02 <sup>b</sup>	6.396	<b>0.011</b>	2.60E-02	9.533	<b>0.002</b>
Soil pH	1	-1.91E-02	1.087	0.297	-9.25E-01 <sup>b</sup>	2.843	<i>0.092</i>	2.03E-01	1.321	0.250
Species	4	-	18.843	<b>0.001</b>	-	13.454	<b>0.009</b>	-	52.983	<b>&lt;0.001</b>
( $N_{\text{area}}$ int.)	-	8.93E-01	-	-	-	-	-	-	-	-
$N_{\text{area}}$	1	-1.11E-01	80.606	<b>&lt;0.001</b>	-	-	-	-	-	-

	$V_{\text{cmax25}}:\chi$			
	df	Coefficient	$\chi^2$	p
(Intercept)	-	7.20E+01	-	-
Soil N	1	3.99E-01	0.963	0.326
Soil pH	1	-3.12E+00	0.138	0.711
Species	4	-	31.450	<b>&lt;0.001</b>
( $N_{\text{area}}$ int.)	-	1.18E+01	-	-
$N_{\text{area}}$	4	3.87E+01	32.797	<b>&lt;0.001</b>

60

942 \*Significance determined using Type II Wald  $\chi^2$  tests ( $\alpha = 0.05$ ). P-values less than 0.05 are in bold, while p-values  
 943 between 0.05 and 0.1 are italicized. Superscript letters indicate model coefficients fit to natural-log (<sup>a</sup>) or square-root  
 944 (<sup>b</sup>) transformed data. Relationships between  $N_{\text{area}}$  and each response variable were fit using the second series of  
 945 bivariate mixed-effects models, so model coefficients and results are independent of model coefficients and results  
 946 reported for relationships between soil nitrogen, soil pH, and species for each response variable.



**Figure 3.4.** Effects of soil nitrogen availability and species on the proportion of leaf nitrogen content allocated to Rubisco (a-b), bioenergetics (c-d), photosynthesis (Rubisco + bioenergetics; e-f), and structure (g-h). Soil nitrogen availability is represented on the x-axis in the left column of panels and species are represented on the x-axis in the right column of panels. Species abbreviations and position along the x-axis in the middle column of panels, colored points, shapes, trendlines, error bars, and compact lettering are as explained in Figure 3.1.

**947** 3.4 Discussion

**948** Photosynthetic least-cost theory provides an explanation for understanding rela-  
**949** tionships between soil nutrient availability, leaf nutrient allocation, and photosyn-  
**950** thetic capacity. The theory suggests that plants acclimate to a given environment  
**951** by optimizing leaf photosynthesis rates at the lowest summed cost of using nu-  
**952** trients and water (Prentice et al. 2014; Wang et al. 2017; Smith et al. 2019;  
**953** Paillassa et al. 2020). The theory predicts that an increase in soil nutrient avail-  
**954** ability should allow similar photosynthesis rates to be achieved with increased leaf  
**955** nutrient content and photosynthetic capacity (i.e.,  $V_{cmax25}$  and  $J_{max25}$ ) at lower  
**956** leaf  $C_i:C_a$  ( $\chi$ ), resulting in an increase in water use efficiency, decrease in nutri-  
**957** ent use efficiency, and increase in both leaf nutrient content and photosynthetic  
**958** capacity per unit  $\chi$ . The theory predicts similar leaf responses to increasing soil  
**959** pH under acidic conditions, presumably due to generally faster nutrient cycle dy-  
**960** namics and consequent reductions in the cost of acquiring nutrients relative to  
**961** water with increasing soil pH (Wang et al. 2017; Paillassa et al. 2020; Dong et al.  
**962** 2020).

**963** Supporting the theory, increasing soil nitrogen availability was associated  
**964** with increased leaf nitrogen content, a pattern that reduced photosynthetic nitro-  
**965** gen use efficiency and increased leaf nitrogen content per unit  $\chi$ . Increasing soil  
**966** nitrogen coincided with slight, but non-significant decreases in  $\chi$  and increases  
**967** in  $V_{cmax25}$  and  $J_{max25}$  ( $p<0.2$ , Table 3.2). The positive trend between soil ni-  
**968** trogen availability and photosynthetic capacity was supported by the concurrent  
**969** strong increase in leaf nitrogen content with increasing soil nitrogen availability,  
**970** which resulted in no change in the proportion of leaf nitrogen content allocated to

971 photosynthesis across the soil nitrogen availability gradient. Additionally, leaf ni-  
972 trogen content exhibited a strong negative correlation with  $\chi$ , indicative of strong  
973 nitrogen-water use tradeoffs at the leaf level. Responses tended to vary more due  
974 to soil nitrogen availability than soil pH. Overall, these findings are consistent  
975 with the nutrient-water use tradeoffs predicted from theory.

976 3.4.1 *Soil nitrogen availability modifies tradeoffs between nitrogen and water use*  
977 In support of expected least-cost outcomes and past environmental gradient stud-  
978 ies (Dong et al. 2017; Paillassa et al. 2020), increasing soil nitrogen availability  
979 was associated with increased leaf nitrogen content. Soil nitrogen availability had  
980 smaller impacts on measures of net photosynthesis and  $\chi$ , which led to reductions  
981 in PNUE and increases in leaf nitrogen content per unit  $\chi$ , as expected from the-  
982 ory. Photosynthetic least-cost theory suggests that reductions in PNUE should  
983 be driven by an increase in the proportion of leaf nitrogen allocated to photosyn-  
984 thetic tissue, a pattern that should allow plants to achieve optimal photosynthetic  
985 rates with greater photosynthetic capacity to make better use of available light.  
986 Contrasting theory predictions, I found no effect of soil nitrogen availability on  
987 photosynthetic capacity. However, photosynthetic capacity did tend to increase  
988 with increasing soil nitrogen availability ( $p<0.20$ ; Table 3.2) resulting in no effect  
989 of soil nitrogen availability on the relative fraction of leaf nitrogen allocated to  
990 photosynthesis, Rubisco, or bioenergetics. These lines of evidence support the  
991 idea that trees use additional nitrogen to support increased leaf nitrogen alloca-  
992 tion toward photosynthetic tissue and enhance photosynthetic capacity (Wright  
993 et al. 2003).

994        Soil nitrogen availability had a stronger effect on leaf nitrogen than pho-  
995        tosynthetic capacity. This pattern suggests that additional plant nitrogen up-  
996        take due to increased soil nitrogen availability was also being used to support  
997        non-photosynthetic nitrogen pools, possibly to structural tissue or stress-induced  
998        amino acid and polyamine synthesis (Minocha et al. 2000; Onoda et al. 2004;  
999        Bubier et al. 2011). While I found no change in the proportion of leaf nitrogen  
1000      allocated to leaf structural tissue, the overall stimulation in leaf nitrogen content  
1001      with increasing soil nitrogen availability suggests an increase in the net amount of  
1002      nitrogen invested in leaf structural tissue along the nitrogen availability gradient.  
1003      Importantly, leaf nitrogen allocated to structure was calculated using an empiri-  
1004      cal relationship between  $M_{\text{area}}$  and the amount of leaf nitrogen allocated to cell  
1005      walls (Onoda et al. 2017). As the generality of relationships between  $M_{\text{area}}$  and  
1006      the amount of leaf nitrogen allocated to cell walls has been called into question  
1007      (Harrison et al. 2009), future work should consider explicitly measuring nitrogen  
1008      allocation to cell wall tissue and stress-induced amino acid synthesis to confirm  
1009      these patterns.

1010       In opposition to patterns expected from least-cost theory, increasing soil  
1011      nitrogen availability had no apparent effect on  $\chi$ . Interestingly, despite the null  
1012      effect of soil nitrogen availability on  $\chi$ , I observed a strong negative effect of in-  
1013      creasing  $N_{\text{area}}$  on  $\chi$ , consistent with the nitrogen-water use tradeoffs expected from  
1014      theory. The null response of  $\chi$  to increasing soil nitrogen availability may have  
1015      been due to a lack of water limitation in the system, given that the area received  
1016      approximately 20% more precipitation (1167 mm) during the 12-month period  
1017      leading up to our measurement period than normally expected (972 mm). How-

1018 ever, droughts can and do occur in temperate forests of the northeastern United  
1019 States (Sweet et al. 2017), so the observed increase in leaf nitrogen content with  
1020 increasing soil nitrogen availability could be a strategy that allows trees to hedge  
1021 bets against drier than normal growing seasons (Onoda et al. 2004; Onoda et al.  
1022 2017; Hallik et al. 2009). As was suggested in Paillassa et al. (2020), and more  
1023 recently by Querejeta et al. (2022), negative effects of soil nitrogen availabil-  
1024 ity on  $\chi$  may increase with increasing aridity. This strategy would be especially  
1025 advantageous if it allows individuals growing in arid regions to maintain carbon  
1026 assimilation rates with reduced water loss. Future work should attempt to quan-  
1027 tify interactive roles of climate and soil nitrogen availability on nitrogen-water use  
1028 tradeoffs, which could be done by leveraging coordinated and multifactor nutrient  
1029 (Borer et al. 2014) and water (Knapp et al. 2017) manipulation experiments  
1030 across broad climatic gradients.

1031 3.4.2 *Soil pH did not modify tradeoffs between nitrogen and water usage*

1032 While the primary purpose of this study was to examine the role of soil nitrogen  
1033 availability on nitrogen-water use tradeoffs, this experimental design manipulated  
1034 both soil nitrogen and pH, providing an opportunity to isolate the roles of these  
1035 variables. Previous correlational studies along environmental gradients have iden-  
1036 tified soil pH as a particularly important factor that can modify tradeoffs between  
1037 nutrient and water use (Smith et al. 2019; Paillassa et al. 2020; Westerband et al.  
1038 2023) and the proportion of leaf nitrogen allocated to photosynthesis (Luo et al.  
1039 2021). Such studies implied that these patterns may be driven by reductions in  
1040 the cost of acquiring nutrients relative to water with increasing pH, which may

**1041** be exacerbated in acidic soils.

**1042** Consistent with theory (Wright et al. 2003; Prentice et al. 2014), results  
**1043** indicate that increasing soil pH was negatively associated with PNUE. However,  
**1044** there was no effect of soil pH on leaf nitrogen content,  $\chi$ , or leaf nitrogen content  
**1045** per unit  $\chi$ , most likely because the experimental nitrogen additions increased soil  
**1046** nitrogen supply while both increasing (sodium nitrate) and decreasing (ammo-  
**1047** nium sulfate) soil pH. These results suggest that soil pH did not play a major  
**1048** role in modifying expected photosynthetic least-cost theory patterns, contrasting  
**1049** findings from Paillassa et al. (2020) and other gradient studies that note positive  
**1050** effects of increasing soil pH on leaf nitrogen content, Rubisco carboxylation, and  
**1051**  $\chi$  (Viet et al. 2013; Cornwell et al. 2018; Luo et al. 2021). Instead, null responses  
**1052** to soil pH show that leaf photosynthetic parameters depend more on soil nitrogen  
**1053** availability than pH per se, and that inferences from gradient studies might be  
**1054** confounding covariation between nitrogen availability and soil acidity.

**1055** 3.4.3 *Species identity explains a large amount of variation in leaf and whole*  
**1056** *plant traits*

**1057** Species generally explained a larger amount of variation in measured leaf traits  
**1058** than soil nitrogen availability or soil pH. Interspecies variation is an important  
**1059** factor to consider when deducing mechanisms that drive photosynthetic least-  
**1060** cost theory, particularly for species that form distinct mycorrhizal associations or  
**1061** have different photosynthetic pathways, growth forms, or leaf habit (Espelta et al.  
**1062** 2005; Adams et al. 2016; Bialic-Murphy et al. 2021; Scott and Smith 2022). The  
**1063** need to consider species may also be important when comparing nutrient-water

**1064** use tradeoffs in early and late successional species, or in species with different  
**1065** resource economic strategies (Abrams and Mostoller 1995; Ellsworth and Reich  
**1066** 1996; Wright et al. 2004; Reich 2014; Onoda et al. 2017; Ziegler et al. 2020).

**1067** A strength of the study design and sampling effort is that it controls for  
**1068** many species differences that should modify nitrogen-water use tradeoffs expected  
**1069** from theory. All tree species measured in this study shared the leaf habit of de-  
**1070** ciduous broadleaves, were growing in forests of similar successional stage, but  
**1071** differed in mycorrhizal association and consequent resource economic strategies.  
**1072** As stands tended to be dominated by trees that associate with arbuscular myc-  
**1073** orrhizae (*Fraxinus* and both *Acer* species made up roughly 70% of total above-  
**1074** ground biomass across stands), ecosystem biogeochemical cycle dynamics may be  
**1075** more closely aligned to the inorganic nutrient economy proposed in Phillips et al.  
**1076** (2013), which may promote stronger nitrogen-water use tradeoffs in tree species  
**1077** that associate with arbuscular mycorrhizae. This result was not observed here,  
**1078** as photosynthetic properties varied as much within as across the two mycorrhizal  
**1079** associations represented. Given the high variability in measured photosynthetic  
**1080** traits within and across species, effects of mycorrhizal association likely require  
**1081** more intensive sampling efforts to detect than were possible here.

**1082** 3.4.4 *Implications for photosynthetic least-cost theory model development*

**1083** In the field, soil nutrient availability is heterogeneous across time and space (Ta-  
**1084** ble B4). Unaccounted within-plot heterogeneity may have contributed to the low  
**1085** amount of variation explained by soil nitrogen availability in statistical models,  
**1086** as resin bags are a coarse surrogate for soil nitrogen availability. Despite this, I

1087 still observed evidence for nutrient-water use tradeoffs, suggesting that observed  
1088 responses reported here may be an underestimate toward the net effect of soil ni-  
1089 trogen availability on these tradeoffs. While I urge caution in the interpretation of  
1090 these results, they do provide a promising baseline for future studies investigating  
1091 patterns expected from photosynthetic least-cost theory at finer spatiotemporal  
1092 resolutions.

1093 The general stronger relationship between leaf nitrogen content and photo-  
1094 synthetic parameters versus between leaf nitrogen content and soil nitrogen avail-  
1095 ability suggests that leaf nitrogen content is more directly tied to photosynthesis  
1096 than soil nitrogen availability. While this could be due to the high spatiotemporal  
1097 heterogeneity of soil nitrogen availability, principles from photosynthetic least-  
1098 cost theory suggest that leaf nitrogen content is the downstream product of leaf  
1099 nutrient demand to build and maintain photosynthetic machinery, which is set by  
1100 aboveground environmental conditions such as light availability, CO<sub>2</sub>, tempera-  
1101 ture, or vapor pressure deficit (Smith et al. 2019; Paillassa et al. 2020; Peng et al.  
1102 2021; Westerband et al. 2023). The stronger relationship between leaf nitrogen  
1103 and photosynthetic parameters, paired with the strong negative relationship be-  
1104 tween leaf nitrogen and  $\chi$ , could indicate a relatively stronger effect of climate on  
1105 leaf nitrogen-photosynthesis relationships than soil resource availability. However,  
1106 the short distance between plots and across sites limited my ability to test this  
1107 mechanism.

1108 Variation in soil pH affected least cost responses less than variations in soil  
1109 nitrogen availability, in part because experimental treatments directly increased  
1110 soil nitrogen and affected soil pH in opposite directions. While soil pH has been

1111 shown to drive nitrogen-water tradeoffs in global gradient analyses (Viet et al.  
1112 2013; Paillassa et al. 2020), these responses may be due to covariations between  
1113 soil pH and nutrient cycling rather than a role of pH per se. The direct manipula-  
1114 tions of soil pH and soil nitrogen availability in this study partly disentangle these  
1115 factors and show that variation in nitrogen availability matters more for least-cost  
1116 tradeoffs than pH alone.

1117 3.4.5 *Conclusions*

1118 Increasing soil nitrogen availability generally increased leaf nitrogen content (both  
1119 area- and mass-based), but did not significantly influence  $\chi$ . This shift in leaf ni-  
1120 trogen led to a reduction in PNUE, and an increase in leaf nitrogen per unit  
1121  $\chi$  with increasing soil nitrogen availability. Despite null effects of soil nitrogen  
1122 availability on  $\chi$ , I observed a strong negative relationship between leaf nitrogen  
1123 content and  $\chi$ . These results provide empirical support for the nutrient-water use  
1124 tradeoffs expected from photosynthetic least-cost theory in response to increas-  
1125 ing soil nutrient availability, but suggest that all tenets of the theory may not  
1126 hold in every environment. These results experimentally test previous work sug-  
1127 gesting that leaf nitrogen-water economies vary across gradients of soil nutrient  
1128 availability and pH, and show that variations in nutrient availability matter more  
1129 for determining variation in leaf photosynthetic traits than soil pH.

1130

## Chapter 4

1131 The relative cost of resource use for photosynthesis drives variance in  
1132 leaf nitrogen content across a climate and soil resource availability  
1133 gradient

1134 4.1 Introduction

1135 Terrestrial biosphere models, which comprise the land surface component of Earth  
1136 system models, are sensitive to the formulation of photosynthetic processes (Knorr  
1137 and Heimann 2001; Ziehn et al. 2011; Booth et al. 2012; Walker et al. 2021).  
1138 This is because photosynthesis is the largest carbon flux between the atmosphere  
1139 and terrestrial biosphere (IPCC 2021), and is constrained by ecosystem carbon  
1140 and nutrient cycles (Hungate et al. 2003; LeBauer and Treseder 2008; Fay et al.  
1141 2015). Many terrestrial biosphere models formulate photosynthesis by parame-  
1142 terizing photosynthetic capacity within plant functional groups through empiri-  
1143 cal linear relationships between area-based leaf nitrogen content ( $N_{\text{area}}$ ) and the  
1144 maximum carboxylation rate of Ribulose-1,5-bisphosphate carboxylase/oxygenase  
1145 ( $V_{\text{cmax}}$ ) (Kattge et al. 2009; Rogers 2014; Rogers et al. 2017). Models are also  
1146 beginning to include connected carbon-nitrogen cycles (Wieder et al. 2015; Shi  
1147 et al. 2016; Davies-Barnard et al. 2020; Braghieri et al. 2022), which allows leaf  
1148 photosynthesis to be predicted directly through changes in  $N_{\text{area}}$  and indirectly  
1149 through changes in soil nitrogen availability (e.g., LPJ-GUESS, CLM5.0) (Smith  
1150 et al. 2014; Lawrence et al. 2019). Despite recent model developments, open  
1151 questions remain regarding the generality of ecological relationships between soil  
1152 nitrogen availability, leaf nitrogen content, and leaf photosynthesis across edaphic  
1153 and climatic gradients.

1154 Empirical support for positive relationships between soil nitrogen availabil-  
1155 ity and  $N_{\text{area}}$  is abundant (Firn et al. 2019; Liang et al. 2020), and is a result  
1156 often attributed to the high nitrogen cost of building and maintaining Rubisco  
1157 (Evans 1989; Evans and Seemann 1989; Onoda et al. 2004; Walker et al. 2014;  
1158 Onoda et al. 2017; Dong et al. 2020). Such patterns imply that positive relation-  
1159 ships between soil nitrogen availability and  $N_{\text{area}}$  should increase leaf photosyn-  
1160 thesis and photosynthetic capacity by increasing the maximum rate of Rubisco  
1161 carboxylation through increased investments to Rubisco construction and mainte-  
1162 nance. This integrated  $N_{\text{area}}$ -photosynthesis response to soil nitrogen availability  
1163 has been observed both in manipulative experiments and across environmental  
1164 gradients (Field and Mooney 1986; Evans 1989; Walker et al. 2014; Li et al.  
1165 2020), and is thought to be driven by ecosystem nitrogen limitation, which lim-  
1166 its primary productivity globally (LeBauer and Treseder 2008; Fay et al. 2015).  
1167 However, this response is not consistently observed, as recent studies note variable  
1168  $N_{\text{area}}$ -photosynthesis relationships across edaphic and climatic gradients (Liang  
1169 et al. 2020; Luo et al. 2021) and that aboveground growing conditions (e.g., light  
1170 availability, temperature, vapor pressure deficit) or species identity traits (e.g.,  
1171 photosynthetic pathway, nitrogen acquisition strategy) may be more important  
1172 for explaining variance in  $N_{\text{area}}$  and photosynthetic capacity across environmental  
1173 gradients (Adams et al. 2016; Dong et al. 2017; Smith et al. 2019; Dong et al.  
1174 2020; Peng et al. 2021; Dong et al. 2022; Westerband et al. 2023).

1175 One hypothesized mechanism to explain variance in  $N_{\text{area}}$  across environ-  
1176 mental gradients has been proposed via photosynthetic least-cost theory (Wright  
1177 et al. 2003; Prentice et al. 2014; Paillassa et al. 2020; Harrison et al. 2021).

1178 The theory predicts that plants acclimate to environments by optimizing photo-  
1179 synthetic assimilation rates at the lowest summed cost of nitrogen and water use  
1180 (Wright et al. 2003; Prentice et al. 2014). In a given environment, the theory  
1181 suggests that nitrogen and water use can be substituted for each other to maintain  
1182 the lowest summed cost of resource use, such that optimal photosynthetic rates  
1183 are achieved with less efficient use of the more abundant and less costly resource  
1184 to acquire in exchange for more efficient use of the less abundant and more costly  
1185 resource to acquire.

1186 Photosynthetic least-cost theory predicts that, all else equal, an increase in  
1187 soil nitrogen availability should decrease the cost of acquiring and using nitrogen  
1188 relative to water (a ratio referred to herein as  $\beta$ ), resulting in optimal photosyn-  
1189 thetic rates achieved with greater  $N_{\text{area}}$  at lower stomatal conductance and lower  
1190 leaf  $C_i:C_a$  (Wright et al. 2003; Prentice et al. 2014; Paillassa et al. 2020). Alter-  
1191 natively, an increase in soil moisture should reduce costs of water acquisition and  
1192 use, increasing  $\beta$  (Lavergne et al. 2020), stomatal conductance, and leaf  $C_i:C_a$ ,  
1193 resulting in optimal photosynthetic rates achieved with decreased  $N_{\text{area}}$ . The the-  
1194 ory also predicts variability in stomatal conductance and  $N_{\text{area}}$  in response to  
1195 climatic factors, suggesting that the optimal response to increased vapor pressure  
1196 deficit (VPD) should be a reduction in stomatal conductance and leaf  $C_i:C_a$  that  
1197 is counterbalanced by an increase in  $N_{\text{area}}$  to support the greater photosynthetic  
1198 capacity needed to maintain high assimilation at lower conductance (Grossiord  
1199 et al. 2020; Dong et al. 2020; López et al. 2021; Westerband et al. 2023).

1200 Leaf nitrogen allocation responses to changing climates or soil resource  
1201 availability may also depend on their mode of nutrient acquisition or photo-

**1202** synthetic pathway. For example, species that form associations with symbiotic  
**1203** nitrogen-fixing bacteria (referred as “N-fixing species” from this point forward)  
**1204** should, in theory, have access to less finite nitrogen supply than species not capa-  
**1205** ble of forming such associations (referred as “non-fixing species” from this point  
**1206** forward), which may result in lower  $\beta$  values in N-fixing species than non-fixing  
**1207** species. This result was previously shown in a greenhouse experiment, where a  
**1208** leguminous species generally had lower costs of nitrogen acquisition compared to a  
**1209** non-leguminous species, although these differences were generally stronger under  
**1210** increased nitrogen limitation (Perkowski et al. 2021). Lower  $\beta$  values could be an  
**1211** explanation for why N-fixing species commonly have greater leaf nitrogen content  
**1212** than non-fixing species (Adams et al. 2016; Dong et al. 2017).

**1213** Similarly, leaf nitrogen allocation patterns across environmental gradients  
**1214** may be dependent on photosynthetic pathway. Lower leaf  $C_i:C_a$  values in C<sub>4</sub>  
**1215** species suggests that C<sub>4</sub> species should have lower  $\beta$  values than C<sub>3</sub> species (Scott  
**1216** and Smith 2022), a pattern that could be the result of increased costs associated  
**1217** with water acquisition and use or reduced costs of nitrogen acquisition and use  
**1218** relative to C<sub>3</sub> species. Theory predicts that this response in C<sub>4</sub> species will cause  
**1219** C<sub>4</sub> species to have higher leaf nitrogen content on average compared to C<sub>3</sub> species,  
**1220** though ample evidence exists documenting general lower leaf nitrogen content in  
**1221** C<sub>4</sub> species (Schmitt and Edwards 1981; Sage and Pearcy 1987; Ghannoum et al.  
**1222** 2011). No study to date has directly quantified  $\beta$  in C<sub>4</sub> species aside from the  
**1223** initial parameterization of  $\beta$  in an optimality model for C<sub>4</sub> species (Scott and  
**1224** Smith 2022) using a global dataset of leaf  $\delta^{13}\text{C}$  values (Cornwell et al. 2018).

**1225** While photosynthetic least-cost theory provides a unified framework for

1226 understanding integrated effects of climate and soil resource availability on  $N_{\text{area}}$ ,  
1227 empirical tests of the theory are sparse. Previous work shows that increasing  
1228 soil nitrogen availability decreases costs of acquiring nutrients (Bae et al. 2015;  
1229 Perkowski et al. 2021; Lu et al. 2022), which can induce predictable nutrient-  
1230 water use tradeoffs expected from the theory across broad environmental gradients  
1231 (Paillassa et al. 2020; Querejeta et al. 2022; Westerband et al. 2023) and in  
1232 manipulation experiments (Bialic-Murphy et al. 2021). Additionally, increasing  
1233 vapor pressure deficit has been shown to have a positive effect on  $N_{\text{area}}$ , which is  
1234 commonly associated with reduced leaf  $C_i:C_a$  (Dong et al. 2017; Dong et al. 2020;  
1235 Firn et al. 2019; López et al. 2021).

1236 Despite evidence for patterns expected from photosynthetic least-cost the-  
1237 ory, studies have been restricted to exploring these patterns in C<sub>3</sub> species and,  
1238 while variance in  $N_{\text{area}}$  across environmental gradients has been shown to be driven  
1239 by strong negative relationships with leaf  $C_i:C_a$  (Dong et al. 2017; Paillassa et al.  
1240 2020; Westerband et al. 2023), no study has explicitly investigated effects of soil  
1241 resource availability or species identity on  $N_{\text{area}}$  using  $\beta$  as a direct predictor of  
1242 leaf  $C_i:C_a$ . Furthermore, as  $N_{\text{area}}$  can be broken down into structural (leaf mass  
1243 per area;  $M_{\text{area}}$ ; g m<sup>-2</sup>) and metabolic (mass-based leaf nitrogen content;  $N_{\text{mass}}$ ;  
1244 gN g<sup>-1</sup>) components (Dong et al. 2017), no study has investigated which compo-  
1245 nent of  $N_{\text{area}}$  drives the hypothesized response of  $N_{\text{area}}$  to leaf  $C_i:C_a$ , which limits  
1246 our ability to assess whether changes in  $N_{\text{area}}$  across environmental gradients are  
1247 driven by changes in leaf morphology (i.e.  $M_{\text{area}}$ ), leaf stoichiometry (i.e.  $N_{\text{mass}}$ ),  
1248 or both.

1249 In this study, I measured  $N_{\text{area}}$ ,  $N_{\text{mass}}$ ,  $M_{\text{area}}$ , leaf  $\delta^{13}\text{C}$ -derived estimates

1250 of leaf  $C_i:C_a$ , and leaf  $\delta^{13}\text{C}$ -derived estimates of  $\beta$  in 504 individuals spanning  
1251 52 species scattered across 24 grassland sites in Texas, USA. The state of Texas  
1252 contains a diverse climatic gradient, indicated by 2006-2020 mean annual precipi-  
1253 tation totals ranging from 204 to 1803 mm and 2006-2020 mean annual tempera-  
1254 ture ranging from  $11.8^\circ$  to  $24.6^\circ\text{C}$  within state boundaries (Fig. 4.1). Variability  
1255 in soil nitrogen availability and soil moisture was expected across sites, owing to  
1256 differences in soil texture and aboveground climate that would drive differential  
1257 rates of water retention and nitrogen transformations to plant-available nitrogen  
1258 substrate. I leveraged the expected climatic and soil resource variability across  
1259 sites to test the following hypotheses:

- 1260 1. Soil nitrogen availability will decrease  $\beta$  through a reduction in costs of  
1261 nitrogen acquisition and use, while soil moisture will increase  $\beta$  through a  
1262 reduction in costs of water acquisition and use. Following previous results, I  
1263 expected that N-fixing species would have lower  $\beta$  values and that  $C_4$  species  
1264 would have lower  $\beta$  values.
- 1265 2. Leaf  $C_i:C_a$  will be positively related to  $\beta$ , a pattern that will result in a  
1266 negative indirect effect of increasing soil nitrogen availability on leaf  $C_i:C_a$ ,  
1267 a positive indirect effect of increasing soil moisture on leaf  $C_i:C_a$ , and lower  
1268 leaf  $C_i:C_a$  in both N-fixing species and  $C_4$  species. I expected that leaf  
1269  $C_i:C_a$  would be negatively related to vapor pressure deficit, as increasing  
1270 atmospheric dryness would cause plants to close stomata to minimize water  
1271 loss.
- 1272 3.  $N_{\text{area}}$  will be negatively related to leaf  $C_i:C_a$ . This response will result in an  
1273 indirect positive and negative effect of increasing soil nitrogen availability

1274 and soil moisture, respectively, on  $N_{\text{area}}$ , and larger  $N_{\text{area}}$  values in N-fixing  
1275 species. While theory predicts that lower  $\beta$  values in C<sub>4</sub> species should  
1276 yield larger  $N_{\text{area}}$  in C<sub>4</sub> species, I expected that C<sub>4</sub> species would have lower  
1277  $N_{\text{area}}$  than C<sub>3</sub> species due to greater nitrogen use efficiency in C<sub>4</sub> species.  
1278 Additionally, I expected vapor pressure deficit to increase  $N_{\text{area}}$ , a pattern  
1279 that would be directly mediated through the reduction in leaf  $C_i:C_a$  with  
1280 increasing vapor pressure deficit.

1281 4.2 Methods

1282 4.2.1 *Site descriptions and sampling methodology*

1283 Leaf and soil samples were collected from 24 open canopy grassland sites scattered  
1284 across central and eastern Texas in summer 2020 and summer 2021 (Fig. 4.1).  
1285 Twelve sites were visited between June and July 2020 and 14 sites (11 unique from  
1286 2020) were visited between May and June 2021 (Table 4.1). Sites were chosen to  
1287 maximize precipitation and edaphic variability across sites (Table 4.1). No site  
1288 with personally communicated or anecdotal evidence of grazing or disturbance  
1289 (e.g., mowing, feral hog activity, etc.) was used. Leaf material was collected  
1290 from three individuals each of the five most abundant species at random locations  
1291 at each site, only selecting species that were broadly classified as graminoid or  
1292 forb/herb growth habits per the USDA PLANTS database (USDA NRCS 2022).  
1293 All collected leaves were fully expanded with no visible herbivory or other external  
1294 damage and also free from shading by nearby shrubs or trees. Five soil samples  
1295 were collected from 0-15 cm below the soil surface at each site near the leaf  
1296 collection sample locations. Soil samples were mixed together by hand to create

**1297** one composite soil sample per site.

**1298** 4.2.2 *Leaf trait measurements*

**1299** Images of each leaf were taken immediately following each site visit using a flat-  
**1300** bed scanner. Fresh leaf area was determined from each image using the ‘LeafArea’  
**1301** R package (Katabuchi 2015), which automates leaf area calculations using ImageJ  
**1302** software (Schneider et al. 2012). Each leaf was dried at 65°C for at least 48 hours  
**1303** to a constant mass, weighed, and manually ground in a mortar and pestle until  
**1304** homogenized. Leaf mass per area ( $M_{\text{area}}$ ; g m<sup>-2</sup>) was calculated as the ratio of  
**1305** dry leaf biomass to fresh leaf area. Subsamples of dried and homogenized leaf  
**1306** tissue were used to measure leaf nitrogen content ( $N_{\text{mass}}$ ; gN g<sup>-1</sup>) through ele-  
**1307** mental combustion analysis (Costech-4010, Costech Instruments, Valencia, CA).  
**1308** Leaf nitrogen content per unit leaf area ( $N_{\text{area}}$ ; gN m<sup>-2</sup>) was calculated as the  
**1309** product of  $N_{\text{mass}}$  and  $M_{\text{area}}$ .

**1310** Subsamples of dried and homogenized leaf tissue were sent to the University  
**1311** of California-Davis Stable Isotope Facility to determine leaf  $\delta^{13}\text{C}$ . Leaf  $\delta^{13}\text{C}$  values  
**1312** were determined using an elemental analyzer (PDZ Europa ANCA-GSL; Sercon  
**1313** Ltd., Chestshire, UK) interfaced to an isotope ratio mass spectrometer (PDZ  
**1314** Europa 20-20 Isotope Ratio Mass Spectrometer, Sercon Ltd., Chestshire, UK).  
**1315** I used leaf  $\delta^{13}\text{C}$  values (‰; relative to Vienna Pee Dee Belemnite international  
**1316** reference standard) to estimate the ratio of intercellular ( $C_i$ ) to extracellular ( $C_a$ )  
**1317** CO<sub>2</sub> ratio (leaf  $C_i:C_a$ ; unitless) following the approach of Farquhar et al. (1989)  
**1318** described in Cernusak et al. (2013). Specifically, I derived leaf  $C_i:C_a$  as:

$$C_i : C_a = \frac{\Delta^{13}C - a}{b - a} \quad (4.1)$$

**1319** where  $\Delta^{13}C$  represents the relative difference between leaf  $\delta^{13}\text{C}$  ( $\text{\textperthousand}$ ) and air  $\delta^{13}\text{C}$   
**1320** ( $\text{\textperthousand}$ ), calculated as:

$$\Delta^{13}C = \frac{\delta^{13}C_{air} - \delta^{13}C_{leaf}}{1 + \delta^{13}C_{leaf}} \quad (4.2)$$

**1321**  $\delta^{13}\text{C}_{air}$ , which is commonly assumed to be  $-8\text{\textperthousand}$  (Keeling et al. 1979; Farquhar  
**1322** et al. 1989), was calculated as a function of calendar year  $t$  using an empirical  
**1323** equation derived in Feng (1999):

$$\delta^{13}C_{air} = -6.429 - 0.006e^{0.0217(t-1740)} \quad (4.3)$$

**1324** Using this equation,  $\delta^{13}\text{C}_{air}$  values were set to  $-9.04\text{\textperthousand}$  and  $-9.09\text{\textperthousand}$  for 2020 and  
**1325** 2021, respectively. The parameter  $a$  represents the fractionation between  $^{12}\text{C}$   
**1326** and  $^{13}\text{C}$  due to diffusion in air, assumed to be  $4.4\text{\textperthousand}$ , while  $b$  represents the  
**1327** fractionation caused by Rubisco carboxylation, assumed to be  $27\text{\textperthousand}$  (Farquhar  
**1328** et al. 1989). For  $\text{C}_4$  species,  $b$  in Eqn. 4.1 was set to  $6.3\text{\textperthousand}$ , and was derived from:

$$b = c + (d \cdot \phi) \quad (4.4)$$

**1329** Where  $c$  was set to  $-5.7\text{\textperthousand}$  and  $d$  was set to  $30\text{\textperthousand}$  (Farquhar et al. 1989).  $\phi$ , which  
**1330** is the bundle sheath leakiness term, was set to 0.4. All leaf  $C_i:C_a$  values less than  
**1331** 0.1 and greater than 0.95 were assumed to be incorrect and removed from the

**1332** analysis.

**1333** I derived the unit cost of resource use ( $\beta$ ) using leaf  $C_i:C_a$  and site climate

**1334** data using equations first described in Prentice et al. (2014) and simplified in

**1335** Lavergne et al. (2020):

$$\beta = 1.6\eta^*VPD \frac{\chi - (\frac{\Gamma^*}{C_a})^2}{(1 - \chi)^2(K_m + \Gamma^*)} \quad (4.5)$$

**1336** where  $\eta^*$  is the viscosity of water relative to 25°C, calculated using elevation and

**1337** mean air temperature of the seven days leading up to each site visit following equa-

**1338** tions in Huber et al. (2009). VPD (Pa) was set to the mean vapor pressure deficit

**1339** of the seven days leading up to each site visit,  $C_a$  represents atmospheric CO<sub>2</sub>

**1340** concentration, arbitrarily set to 420  $\mu\text{mol mol}^{-1}$  CO<sub>2</sub>.  $K_m$  (Pa) is the Michaelis-

**1341** Menten coefficient for Rubisco affinity to CO<sub>2</sub> and O<sub>2</sub>, calculated as:

$$K_m = K_c \cdot \left(1 + \frac{O_i}{K_o}\right) \quad (4.6)$$

**1342** where  $K_c$  (Pa) and  $K_o$  (Pa) are the Michaelis-Menten coefficients for Rubisco

**1343** affinity to CO<sub>2</sub> and O<sub>2</sub>, respectively, and  $O_i$  is the intercellular O<sub>2</sub> concentration.

**1344**  $\Gamma^*$  (Pa) is the CO<sub>2</sub> compensation point in the absence of dark respiration.  $K_c$ ,  $K_o$ ,

**1345** and  $\Gamma^*$  were determined using equations described in Medlyn et al. (2002) and

**1346** derived in Bernacchi et al. (2001), invoking an elevation correction for atmospheric

**1347** pressure as explained in Stocker et al. (2020).

**Table 4.1.** Site locality information, sampling year, 2006-2020 mean annual precipitation (MAP; mm), mean annual temperature (MAT; °C), and water holding capacity (WHC; mm)\*

Site	Latitude	Longitude	Sampling year	MAP	MAT	WHC
Edwards_2019_17	29.95	-100.36	2020	563.5	19.0	224.7
Uvalde_2020_02	29.59	-100.09	2020, 2021	648.5	19.5	224.7
Menard_2020_01	30.91	-99.59	2020	641.9	18.3	220.2
Kerr_2020_03	30.06	-99.34	2021	672.4	18.3	237.5
Bandera_2020_03	29.85	-99.30	2021	789.4	18.8	235.1
Sansaba_2020_01	31.29	-98.62	2020	733.0	18.8	234.3
Comal_2020_21	29.79	-98.43	2020	878.5	19.9	220.7
Blanco_2019_16	29.99	-98.43	2020	833.0	19.2	222.2
Bexar_2019_13	29.24	-98.43	2020	759.3	21.5	206.0
Burnet_2020_14	30.84	-98.34	2021	763.3	19.5	217.8
Comal_2020_19	30.01	-98.32	2021	845.0	19.3	220.4
Hays_2020_54	29.96	-98.17	2021	861.3	20.0	225.6
Burnet_2020_12	30.82	-98.06	2021	815.1	19.4	245.3
Williamson_2019_09	30.71	-97.86	2020	867.7	19.7	270.2
Williamson_2019_10	30.54	-97.77	2020	819.5	19.9	239.8
Bell_2021_08	31.06	-97.55	2021	937.3	19.6	232.3
Fayette_2021_12	29.86	-97.21	2021	985.7	20.4	165.6
Fayette_2019_04	30.09	-96.78	2020	1017.4	20.6	226.9
Fayette_2020_09	29.86	-96.71	2021	1002.7	20.8	187.6
Washington_2020_08	30.28	-96.41	2021	1077.4	20.4	203.9
Austin_2020_03	29.78	-96.24	2021	1108.7	20.6	253.0
Brazos_2020_16	30.93	-96.23	2021	1078.0	20.1	202.2
Brazos_2020_18	30.52	-96.21	2020, 2021	1099.4	20.4	233.5
Harris_2020_03	29.88	-95.31	2020, 2021	1492.0	21.6	265.6

**1348** \* Rows are arranged by longitude to visualize precipitation variability across sites

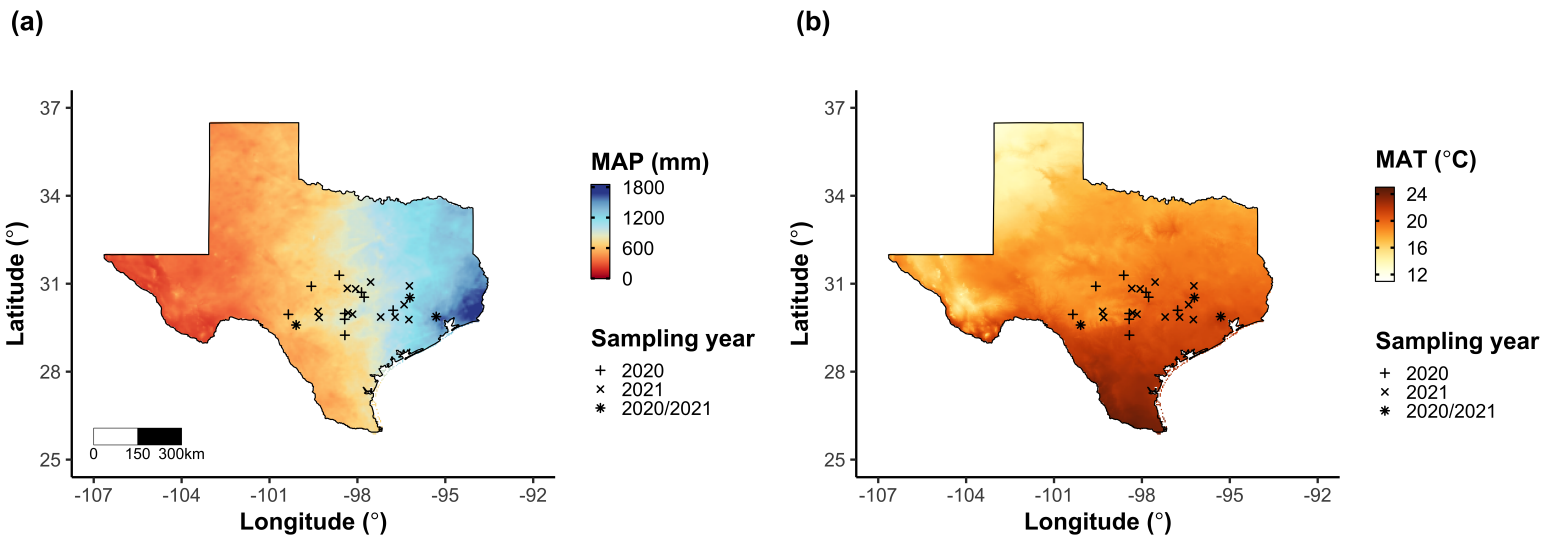


**Figure 4.1.** Site locations along 2006-2020 mean annual precipitation (a) and mean annual temperature (b) gradients in Texas, USA. Precipitation and temperature data were plotted using PRISM data at a 4-km grid resolution and are masked to include only grid cells that occur within the Texas state boundary of the United States. In both panels, addition signs refer to sites visited in 2020, multiplication signs to sites visited in 2021, and asterisks to sites visited in 2020 and 2021. The scale bar in (a) also applies to (b).

**1349** 4.2.3 *Site climate data*

**1350** I used the Parameter elevation Regressions on Independent Slopes Model (PRISM)  
**1351** (Daly et al. 2008) climate product to access gridded daily temperature and precip-  
**1352** itation data for the coterminous United States at a 4-km grid resolution between  
**1353** January 1, 2006 and July 31, 2021 (PRISM Climate Group, Oregon State Uni-  
**1354** versity, <https://prism.oregonstate.edu>, data created 4 Feb 2014, accessed 24  
**1355** Mar 2022). Mean daily air temperature, mean daily VPD, and total daily pre-  
**1356** cipitation data were extracted from the grid cell that contained the latitude and  
**1357** longitude of each property using the ‘extract’ function in the ‘terra’ R package  
**1358** (Hijmans 2022). PRISM data were used in lieu of local weather station data  
**1359** because several rural sites did not have a local weather station present within a  
**1360** 20-km radius of the site. Daily site climate data were used to estimate mean an-  
**1361** nual precipitation and mean annual temperature for each site between 2006 and  
**1362** 2020 (Table 4.1). I calculated total precipitation and mean daily VPD for the  
**1363** prior 1, 2, 3, 4, 5, 6, 7, 8, 9, 10, 15, 20, 25, 30, 60, and 90 days leading up to each  
**1364** site visit. Temperature was not included in any analysis due to the close range in  
**1365** mean annual temperature between sites (mean $\pm$ SD:  $19.8\pm0.9^{\circ}\text{C}$ ; Table 4.1).

**1366** 4.2.4 *Site edaphic characteristics*

**1367** Composted soil samples were sent to the Texas A&M Soil, Water and Forage  
**1368** Laboratory to quantify soil nitrate concentration ( $\text{NO}_3\text{-N}$ ; ppm). Soil  $\text{NO}_3\text{-N}$   
**1369** was determined by extracting composite soil samples in 1 M KCl, measuring  
**1370** absorbance values of extracts at 520 nm using the end product of a  $\text{NO}_3\text{-N}$  to  
**1371**  $\text{NO}_2\text{-N}$  cadmium reduction reaction (Kachurina et al. 2000; Keeney and Nelson

**1372** 1983). Soil texture data from 0-15 cm below the soil surface were accessed using  
**1373** the SoilGrids2.0 data product (Poggio et al. 2021) through the ‘fetchSoilGrids’  
**1374** function in the ‘soilDB’ R package (Beaudette et al. 2022). I used SoilGrids2.0  
**1375** to access soil texture data in lieu of analyses using the composite soil sample due  
**1376** to a lack of soil material from some sites after sending samples for soil NO<sub>3</sub>-N.

**1377** Soil moisture was not measured in the field, but was estimated using the  
**1378** ‘Simple Process-Led Algorithms for Simulating Habitats’ model (SPLASH) (Davis  
**1379** et al. 2017). This model, derived from the STASH model (Cramer and Prentice  
**1380** 1988), spins up a bucket model using Priestley-Taylor equations (Priestley and  
**1381** Taylor 1972) to calculate daily soil moisture ( $W_n$ ; mm) as a function of the previous  
**1382** day’s soil moisture ( $W_{n-1}$ ; mm), daily precipitation ( $P_n$ ; mm), condensation ( $C_n$ ;  
**1383** mm), actual evapotranspiration ( $E_n^a$ ; mm), and runoff (RO; mm):

$$W_n = W_{n-1} + P_n + C_n - E_n^a - RO \quad (4.7)$$

**1384** Models were spun up by equilibrating the previous day’s soil moisture using succes-  
**1385** sive model iterations with daily mean air temperature, daily precipitation total,  
**1386** the number of daily sunlight hours, and latitude as model inputs (Davis et al.  
**1387** 2017). Daily sunlight hours were estimated for each day at each site using the  
**1388** ‘getSunlightTimes’ function in the ‘suncalc’ R package, which estimated sunrise  
**1389** and sunset times of each property using date and site coordinates (Thieurmel and  
**1390** Elmarhraoui 2019). Water holding capacity (mm), or bucket size, was estimated  
**1391** as a function of soil texture using pedotransfer equations explained in Saxton and  
**1392** Rawls (2006), as done in Stocker et al. (2020) and Bloomfield et al. (2023). A

**1393** summary of these equations is included in Appendix C.1.

**1394** Daily soil moisture outputs from the SPLASH model for each site were  
**1395** used to calculate mean daily soil moisture for the prior 1, 2, 3, 4, 5, 6, 7, 8, 9,  
**1396** 10, 15, 20, 25, 30, 60, and 90 days leading up to each site visit. Mean daily  
**1397** soil moisture values were then expressed as a fraction of water holding capacity  
**1398** to normalize across sites with different bucket depths, as done in Stocker et al.  
**1399** (2018). Site water holding capacity values are referenced in Table 4.1.

**1400** 4.2.5 *Plant functional group assignments*

**1401** Plant functional group was assigned to each species and used as the primary de-  
**1402** scriptor of species identity. Specifically, plant functional groups were assigned  
**1403** based on photosynthetic pathway ( $C_3$ ,  $C_4$ ) and ability to form associations with  
**1404** symbiotic nitrogen-fixing bacteria (legume, nonlegume). The ability to form as-  
**1405** sociations with symbiotic nitrogen-fixing bacteria was assigned based on whether  
**1406** species were in the *Fabaceae* family, and photosynthetic pathway of each species  
**1407** was determined from past literature and confirmed through leaf  $\delta^{13}C$  values. I  
**1408** chose these plant functional groups based on *a priori* hypotheses regarding the  
**1409** functional role of nitrogen fixation and photosynthetic pathway on the sensitivity  
**1410** of plant nitrogen uptake and leaf nitrogen allocation to soil nitrogen availability  
**1411** and aboveground growing conditions. These plant functional group classifications  
**1412** resulted in three distinct plant functional groups within our dataset:  $C_3$  legumes  
**1413** (n=53),  $C_3$  nonlegumes (n=350), and  $C_4$  nonlegumes (n=117).

**1414** 4.2.6 *Data analysis*

**1415** All analyses and plotting were conducted in R version 4.1.1 (R Core Team 2021).

**1416** I constructed a series of separate linear mixed-effects models to investigate en-

**1417** vironmental drivers of  $\beta$ , leaf  $C_i:C_a$ ,  $N_{\text{area}}$ ,  $N_{\text{mass}}$ , and  $M_{\text{area}}$ , followed by a path

**1418** analysis using a piecewise structural equation model to investigate direct and

**1419** indirect effects of climate and soil resource availability on  $N_{\text{area}}$ .

**1420** To explore environmental drivers of  $\beta$ , I built a linear mixed-effects model

**1421** that included soil moisture, soil nitrogen availability, and plant functional group

**1422** as fixed effect coefficients. Species were designated as a random intercept term.

**1423** Interaction coefficients between all possible combinations of the three fixed effect

**1424** coefficients were also included.  $\beta$  was natural log transformed to linearize data.

**1425** I used an information-theoretic model selection approach to determine whether

**1426** 90-, 60-, 30-, 20-, 15-, 10-, 9-, 8-, 7-, 6-, 5-, 4-, 3-, 2-, or 1-day mean daily soil

**1427** moisture conferred the best model fit for  $\beta$ . To do this, I constructed 16 separate

**1428** linear mixed-effects models where log-transformed  $\beta$  was included as the response

**1429** variable and each soil moisture time step was separately included as a single

**1430** continuous fixed effect. Species were included as a random intercept term for all

**1431** models. I used corrected Akaike Information Criterion (AICc) to select the soil

**1432** moisture timescale that conferred the best model fit, indicated by the model with

**1433** the lowest AICc score (Table C3; Fig. C1).

**1434** To explore environmental drivers of leaf  $C_i:C_a$ , I constructed a second linear

**1435** mixed effects model that included VPD, soil moisture, soil nitrogen availability,

**1436** and plant functional group as fixed effect coefficients. Two-way interactions be-

**1437** tween plant functional group and VPD, soil nitrogen availability, or soil moisture

1438 were included as additional fixed effect coefficients, in addition to a three-way  
1439 interaction between soil moisture, soil nitrogen availability, and plant functional  
1440 group. Species were included as a random intercept term. I used an information-  
1441 theoretic model selection approach to determine whether 90-, 60-, 30-, 20-, 15-,  
1442 10-, 9-, 8-, 7-, 6-, 5-, 4-, 3-, 2-, or 1-day mean daily VPD conferred the best model  
1443 fit for leaf  $C_i:C_a$  using the same approach explained above for the soil moisture ef-  
1444 fect on  $\beta$ . The soil moisture timescale was set to the same timescale that conferred  
1445 the best fit for  $\beta$ .

1446 To explore environmental drivers of  $N_{\text{area}}$ ,  $N_{\text{mass}}$ , and  $M_{\text{area}}$ , I constructed  
1447 a linear mixed effects model for each trait, including leaf  $C_i:C_a$ , soil nitrogen  
1448 availability, soil moisture, and plant functional group as fixed effect coefficients  
1449 for each model. Two-way interactions between plant functional group and  $\beta$ , leaf  
1450  $C_i:C_a$ , soil nitrogen availability, or soil moisture were included as additional fixed  
1451 effect coefficients, in addition to a three-way interaction between soil nitrogen  
1452 availability, soil moisture, and plant functional group. Species were included as a  
1453 random intercept term, with the soil moisture timescale set to the same timescale  
1454 that conferred the best fit for  $\beta$ .

1455 In all linear mixed-effects models explained above, including those to select  
1456 relevant timescales, I used the ‘lmer’ function in the ‘lme4’ R package (Bates et al.  
1457 2015) to fit each model and the ‘Anova’ function in the ‘car’ R package (Fox and  
1458 Weisberg 2019) to calculate Type II Wald’s  $\chi^2$  and determine the significance  
1459 level ( $\alpha=0.05$ ) of each fixed effect coefficient. I used the ‘emmeans’ R package  
1460 (Lenth 2019) to conduct post-hoc comparisons using Tukey’s tests, where degrees  
1461 of freedom were approximated using the Kenward-Roger approach (Kenward and

**1462** Roger 1997). Trendlines and error ribbons for all plots were drawn using a series  
**1463** of ‘emmeans’ outputs across the range in plotted x-axis values.

**1464** Finally, I conducted a path analysis using a piecewise structural equation  
**1465** model to examine direct and indirect pathways that determined variance in  $N_{\text{area}}$ .  
**1466** Six separate linear mixed effects models were loaded into the piecewise structural  
**1467** equation model. Models were constructed per *a priori* hypotheses following pat-  
**1468** terns expected from photosynthetic least-cost theory. The first model regressed  
**1469**  $N_{\text{area}}$  against  $N_{\text{mass}}$  and  $M_{\text{area}}$ . The second model regressed  $M_{\text{area}}$  against leaf  
**1470**  $C_i:C_a$ . The third model regressed  $N_{\text{mass}}$  against leaf  $C_i:C_a$  and  $M_{\text{area}}$  (Dong et al.  
**1471** 2017; Dong et al. 2020). The fourth model regressed leaf  $C_i:C_a$  against  $\beta$  and  
**1472** VPD. The fifth model regressed  $\beta$  against soil nitrogen availability, soil moisture,  
**1473** ability to associate with symbiotic nitrogen-fixing bacteria, and photosynthetic  
**1474** pathway. The sixth model regressed soil nitrogen availability against soil mois-  
**1475** ture. All models included the relevant timescale selected in the individual linear  
**1476** mixed effect models explained above. Models included species as a random inter-  
**1477** cept term, were built using the ‘lme’ function in the ‘nlme’ R package (Pinheiro  
**1478** and Bates 2022), and subsequently loaded into the piecewise structural equation  
**1479** model using the ‘psem’ function in the ‘piecewiseSEM’ R package (Lefcheck 2016).

**1480** 4.3 Results

**1481** 4.3.1 *Cost to acquire nitrogen relative to water*

**1482** Model selection indicated that 90-day mean soil moisture conferred the best model

**1483** fit for  $\beta$  (AICc=1387.54; Table C3; Fig. C1).

**1484** Increasing soil nitrogen availability generally decreased  $\beta$  ( $p<0.001$ ; Table

**1485** 4.2; Fig. 4.2a), a pattern driven by a negative effect of increasing soil nitrogen on

**1486**  $\beta$  in C<sub>3</sub> nonlegumes (Tukey:  $p=0.005$ ) and C<sub>3</sub> legumes (Tukey:  $p=0.035$ ) despite

**1487** a null effect of increasing soil nitrogen on  $\beta$  in C<sub>4</sub> nonlegumes (Tukey:  $p=0.856$ ).

**1488** There was no effect of soil moisture on  $\beta$  ( $p=0.872$ ; Table 4.2; Fig. 4.2b). A func-

**1489** tional group effect ( $p<0.001$ ; Table 4.2) indicated that C<sub>4</sub> nonlegumes generally

**1490** had lower  $\beta$  values than both C<sub>3</sub> legumes and C<sub>3</sub> non-legumes (Tukey:  $p<0.001$

**1491** in both cases), while  $\beta$  values in C<sub>3</sub> legumes did not differ from C<sub>3</sub> nonlegumes

**1492** (Tukey:  $p=0.854$ ).

**Table 4.2.** Effects of soil moisture, soil nitrogen availability, and plant functional group on  $\beta$  (unitless)\*

	df	Coefficient	$\chi^2$	p
Intercept	-	3.39E+00	-	-
Soil moisture (SM <sub>90</sub> )	1	-1.96E-01	0.026	0.872
Soil N (N)	1	-1.42E-02	12.031	<b>&lt;0.001</b>
PFT	2	-	199.617	<b>&lt;0.001</b>
SM <sub>90</sub> *N	1	-3.02E-03	1.000	0.317
SM <sub>90</sub> *PFT	2	-	0.623	0.732
N*PFT	2	-	5.271	0.072
SM <sub>90</sub> *N*PFT	2	-	5.271	0.182

**1493** \*Significance determined using Type II Wald  $\chi^2$  tests ( $\alpha=0.05$ ). P-values<0.05  
**1494** are in bold. Model coefficients are expressed on the natural-log scale and are only  
**1495** included for continuous fixed effects. Key: df=degrees of freedom;  $\chi^2$ =Wald Type  
**1496** II chi-square test statistic

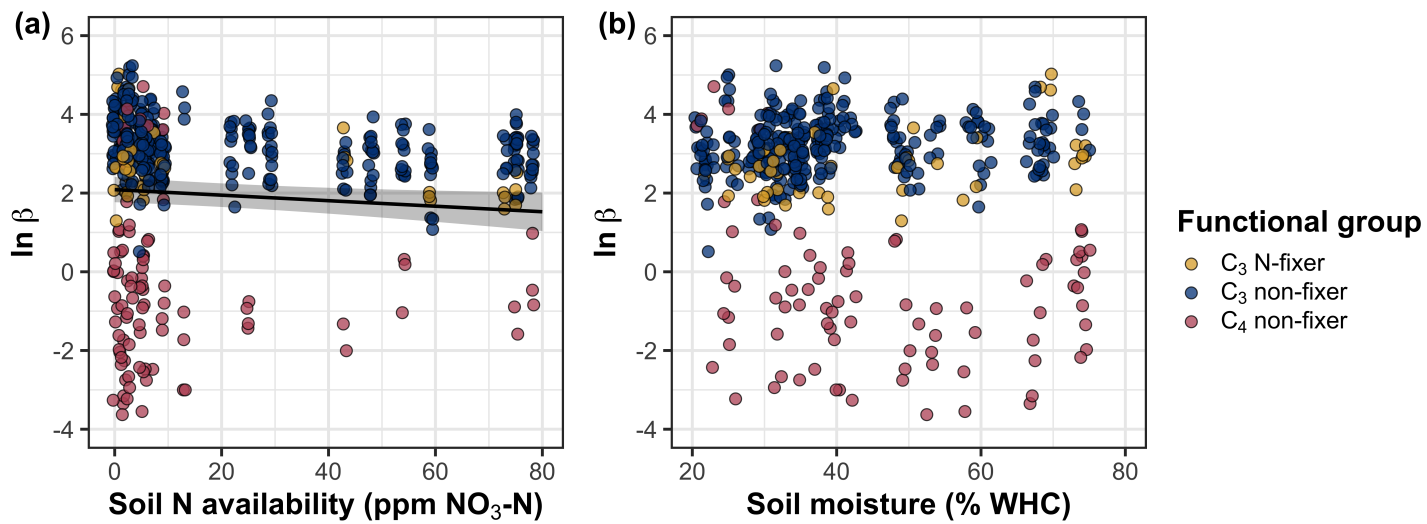


**Figure 4.2.** Effects of soil nitrogen availability (a) and soil moisture (b) on the cost of acquiring and using nitrogen ( $\beta$ ; unitless). Soil nitrogen availability is represented on the x-axis in (a), soil moisture is represented on the x-axis in (b) as a percent of site water holding capacity, and natural-log transformed  $\beta$  is represented on the y-axis for both panels. Yellow points represent C<sub>3</sub> legumes, blue points represent C<sub>3</sub> nonlegumes, and red points represent C<sub>4</sub> nonlegumes. Throughout, points are jittered for visibility. A black solid trendline is drawn to denote bivariate relationships where the slope is different from zero ( $p<0.05$ ), with error ribbons representing the upper and lower 95% confidence intervals.

**1497** 4.3.2 *Leaf C<sub>i</sub>:C<sub>a</sub>*

**1498** Model selection indicated that 4-day mean vapor pressure deficit was the timescale

**1499** that conferred the best model fit for leaf  $C_i:C_a$  (AICc=-755.81; Table C3; Fig. C1).

**1500** Model results revealed that increasing vapor pressure deficit generally de-

**1501** creased leaf  $C_i:C_a$  ( $p<0.001$ ; Table 4.3; Fig. 4.3a). There was no effect of soil

**1502** moisture ( $p=0.549$ ; Table 4.3; Fig. 4.3b) or soil nitrogen availability ( $p=0.549$ ; Ta-

**1503** ble 4.3; Fig. 4.3c) on leaf  $C_i:C_a$ . A strong plant functional group effect ( $p<0.001$ ;

**1504** Table 4.3) indicated that C<sub>4</sub> nonlegumes had lower leaf  $C_i:C_a$  than C<sub>3</sub> legumes

**1505** and C<sub>3</sub> nonlegumes (Tukey:  $p<0.001$  in both cases), with no difference between

**1506** C<sub>3</sub> legumes and C<sub>3</sub> nonlegumes (Tukey:  $p=0.866$ ).

**Table 4.3.** Effects of soil moisture, soil nitrogen availability, and plant functional group on leaf  $C_i:C_a$  (unitless)\*

	df	Coefficient	$\chi^2$	<i>p</i>
Intercept	-	1.32E+00	-	-
Vapor pressure deficit ( $VPD_4$ )	1	-4.53E-01	10.987	<b>&lt;0.001</b>
Soil moisture ( $SM_{90}$ )	1	-1.71E-01	0.039	0.843
Soil N (N)	1	-1.71E-03	0.043	0.549
PFT	2	-	205.274	<b>&lt;0.001</b>
$SM_{90}^*N$	1	7.29E-03	2.266	0.132
$VPD_4^*PFT$	2	-	0.887	0.642
$SM_{90}^*PFT$	2	-	0.814	0.666
$N^*PFT$	2	-	4.158	0.125
$SM_{90}^*N^*PFT$	2	-	3.465	0.177

**1507** \*Significance determined using Type II Wald  $\chi^2$  tests ( $\alpha=0.05$ ). *P*-values less  
**1508** than 0.05 are in bold and *p*-values where  $0.05 < p < 0.1$  are italicized. Leaf  $C_i:C_a$   
**1509** was not transformed prior to model fitting, so model coefficients are reported  
**1510** on the response scale. Model coefficients are only included for continuous fixed  
**1511** effects. Key: df=degrees of freedom;  $\chi^2$ =Wald Type II chi-square test statistic

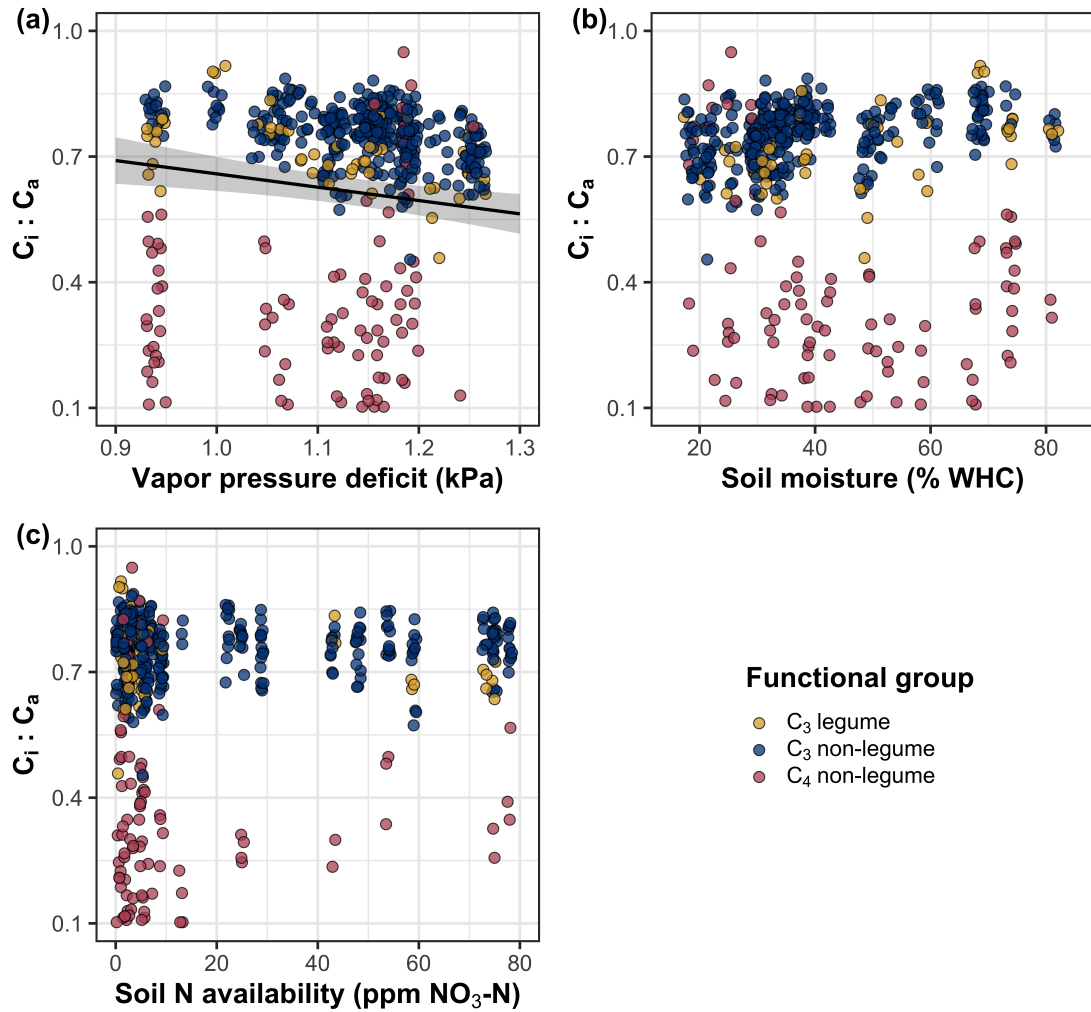


**Figure 4.3.** Effects of 4-day mean vapor pressure deficit (a), 90-day soil moisture (per water holding capacity; b), and soil nitrogen availability (c) on leaf  $C_i:C_a$ . Shading and trendlines are as explained in Figure 4.2. Points are jittered for visibility. Variably colored trendlines are only included if there is an interaction between the x-axis and plant functional group, where solid trendlines indicate slopes that are different from zero ( $p < 0.05$ ) and dashed trendlines indicate slopes that are not different from zero ( $p > 0.05$ ). Error ribbons represent the upper and lower 95% confidence intervals of each fitted trendline.

**1512** 4.3.3 *Leaf nitrogen content*

**1513** An interaction between leaf  $C_i:C_a$  and plant functional group ( $p<0.001$ ; Table 4.4) revealed that the negative effect of increasing leaf  $C_i:C_a$  on  $N_{area}$  ( $p<0.001$ ; Table 4.4) was driven by a negative effect of increasing leaf  $C_i:C_a$  on  $N_{area}$  in **1515**  $C_3$  nonlegumes and  $C_3$  legumes (Tukey:  $p<0.001$  in both cases), but not  $C_4$  **1517** nonlegumes (Tukey:  $p=0.786$ ; Fig. 4.4a). A marginal interaction between soil **1518** nitrogen availability and plant functional group ( $p=0.057$ ; Table 4.4) indicated **1519** that the positive effect of increasing soil nitrogen ( $p=0.007$ ; Table 4.4) was only **1520** apparent in  $C_3$  legumes (Tukey:  $p<0.001$ ; Table 4.4; Fig. 4.4d), but not  $C_3$  **1521** nonlegumes (Tukey:  $p=0.329$ ) or  $C_4$  nonlegumes (Tukey:  $p=0.682$ ). Increasing **1522** soil moisture increased  $N_{area}$  ( $p=0.011$ , Table 4.4). A plant functional group effect **1523** ( $p<0.001$ ; Table 4.4) indicated that  $C_4$  nonlegumes had lower  $N_{area}$  compared to **1524**  $C_3$  legumes and  $C_3$  nonlegumes (Tukey:  $p<0.001$  in both cases), while  $C_3$  legumes **1525** had lower  $N_{area}$  compared to  $C_3$  nonlegumes (Tukey:  $p=0.024$ ).

**1526** Leaf  $C_i:C_a$  had no effect on  $N_{mass}$  ( $p=0.455$ ; Table 4.4; Fig. 4.4b). Increasing **1527** soil nitrogen availability and soil moisture each had a positive effect on  $N_{mass}$  ( $p<0.001$  in both cases; Table 4.4; Fig. 4.4h). A plant functional group effect **1528** ( $p<0.001$ ; Table 4.4) indicated that  $C_4$  nonlegumes had lower  $N_{mass}$  compared to **1529**  $C_3$  legumes and  $C_3$  nonlegumes (Tukey:  $p=0.001$  in both cases), while  $N_{mass}$  did **1530** not differ between  $C_3$  legumes and  $C_3$  nonlegumes (Tukey:  $p=0.323$ ).

**1532** Variance in  $M_{area}$  was driven by a three-way interaction between soil nitrogen availability, soil moisture, and plant functional group ( $p=0.018$ ; Table 4.4). **1533** This interaction indicated that increasing soil moisture increased the positive effect **1534** of increasing soil nitrogen availability on  $M_{area}$  in  $C_3$  legumes (Tukey:  $p=0.028$ )

**1536** but did not modify the negative effect of increasing soil nitrogen availability on  
**1537**  $M_{\text{area}}$  in C<sub>4</sub> nonlegumes (Tukey:  $p=0.806$ ) or C<sub>3</sub> nonlegumes (Tukey:  $p=0.998$ ).  
**1538** There was otherwise no effect of soil moisture on  $M_{\text{area}}$  ( $p=0.436$ ; Table 4.4). An  
**1539** interaction between leaf  $C_i:C_a$  and plant functional group ( $p<0.001$ ; Table 4.4;  
**1540** Fig. 4.4c) indicated that the negative effect of increasing leaf  $C_i:C_a$  on  $M_{\text{area}}$   
**1541** ( $p<0.001$ ; Table 4.4) was driven by a negative effect of increasing leaf  $C_i:C_a$  on  
**1542**  $M_{\text{area}}$  in C<sub>3</sub> legumes (Tukey:  $p<0.001$ ) and C<sub>3</sub> nonlegumes (Tukey:  $p=0.003$ ), but  
**1543** not C<sub>4</sub> nonlegumes (Tukey:  $p=0.257$ ; Fig. 4.4c).

**Table 4.4.** Effects of soil moisture, soil nitrogen availability, plant functional group, and leaf  $C_i:C_a$  on leaf nitrogen content per unit leaf area ( $N_{\text{area}}$ ; gN m $^{-2}$ ), leaf nitrogen content per unit leaf biomass ( $N_{\text{mass}}$ ; gN g $^{-1}$ ), and leaf biomass per unit leaf area ( $M_{\text{area}}$ ; g m $^{-2}$ )

		$N_{\text{area}}$			$N_{\text{mass}}$			$M_{\text{area}}$		
	df	Coefficient	$\chi^2$	p	Coefficient	$\chi^2$	p	Coefficient	$\chi^2$	p
(Intercept)	-	2.41E+00	-	-	7.72E-02	-	-	6.91E+00	-	-
$C_i:C_a$	1	-2.32E+00	6.841	<b>0.009</b>	7.91E-01	0.558	0.455	-3.13E+00	15.913	<0.001
Soil N (N)	1	1.26E-02	7.072	<b>0.011</b>	1.21E-02	87.457	<0.001	-2.66E-02	41.791	<0.001
Soil moisture (SM <sub>90</sub> )	1	5.60E-01	6.493	<b>0.011</b>	7.94E-01	10.889	<0.001	-2.54E-01	0.605	0.437
PFT	1		-	49.273	<0.001	-	21.786	<0.001	-	6.673
SM <sub>90</sub> *N	1	5.45E-02	0.482	0.488	-2.18E-02	2.606	0.106	8.16E-02	0.791	0.374
$C_i:C_a$ *PFT	1		-	24.380	<0.001	-	5.367	0.068	-	30.073
N*PFT	1		-	5.713	0.057	-	1.286	0.526	-	19.405
SM <sub>90</sub> *PFT	1		-	3.487	0.175	-	0.889	0.641	-	2.998
SM <sub>90</sub> *N*PFT	1		-	3.523	0.172	-	0.161	0.923	-	7.996

96

1544 \*Significance determined using Type II Wald  $\chi^2$  tests ( $\alpha=0.05$ ). P-values less than 0.05 are in bold and p-values  
 1545 where  $0.05 < p < 0.1$  are italicized. Coefficients are reported on the natural-log scale for all traits and are only included  
 1546 for continuous fixed effects. Key: df=degrees of freedom;  $\chi^2$ =Wald Type II chi-square test statistic

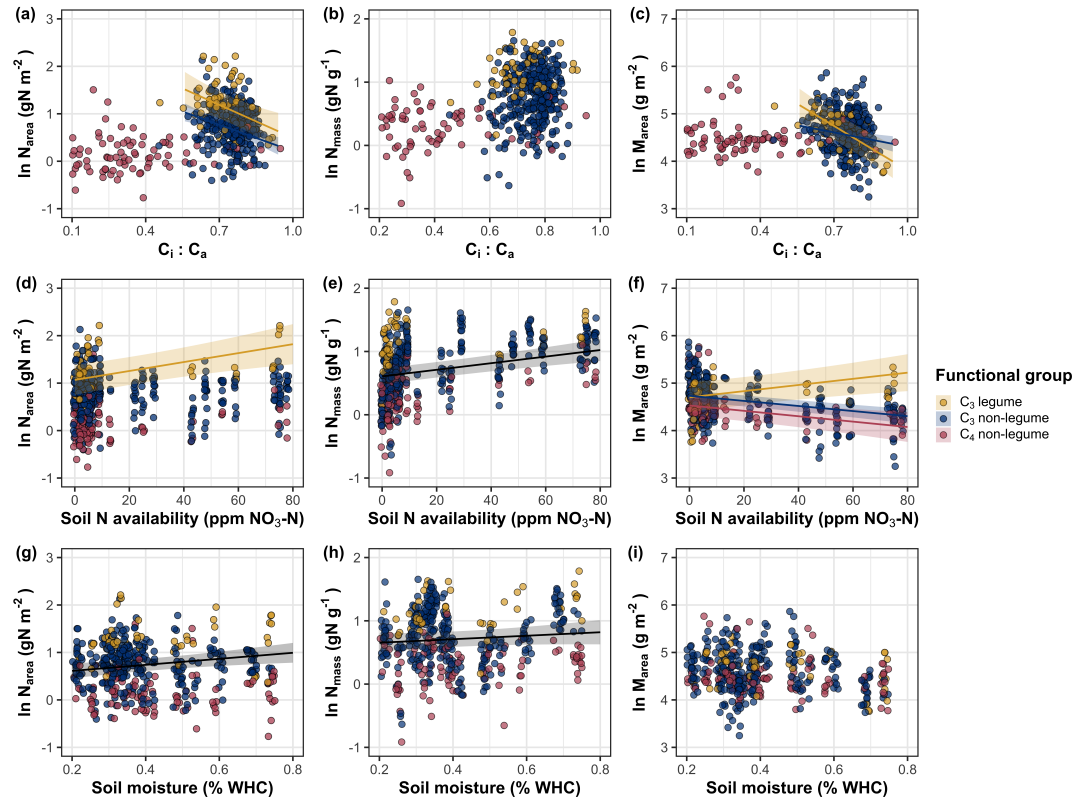


**Figure 4.4.** Effects of leaf  $C_i:C_a$  (a-c), soil nitrogen availability (d-f), and soil moisture (g-i) on leaf nitrogen content per unit leaf area (a, d, g), leaf nitrogen content per unit leaf biomass (b, e, h), and leaf mass per area (c, f, i). Yellow points and trendlines indicate  $C_3$  legumes, blue points and trendlines indicate  $C_3$  nonlegumes, and red points and trendlines indicate  $C_4$  nonlegumes. Points are jittered for visibility. Variably colored trendlines are only included if there is an interaction between plant functional group and the x-axis. Black solid trendlines denote bivariate slopes that are different from zero ( $p < 0.05$ ) where there is no apparent interaction between plant functional group and the x-axis.

**1547** 4.3.4 *Structural equation model*

**1548** The piecewise structural equation model explained 89%, 56%, 57%, 82%, and  
**1549** 38% of variance in  $N_{\text{area}}$ ,  $N_{\text{mass}}$ ,  $M_{\text{area}}$ , leaf  $C_i:C_a$ , and  $\beta$ , respectively (Table  
**1550** 4.5; Fig. 4.5). Variance in  $N_{\text{area}}$  was driven by a positive effect of increasing  
**1551**  $N_{\text{mass}}$  and  $M_{\text{area}}$  ( $p < 0.001$  in both cases; Table 4.5; Fig. 4.5). Model results  
**1552** indicated that an indirect negative effect of  $C_i:C_a$  on  $N_{\text{area}}$  was driven by a strong  
**1553** reduction in  $M_{\text{area}}$  with increasing leaf  $C_i:C_a$  ( $p < 0.001$ ; Table 4.5) paired with no  
**1554** effect of increasing  $C_i:C_a$  on  $N_{\text{mass}}$  ( $p = 0.153$ ; Table 4.5). However, there was a  
**1555** strong negative effect of increasing  $M_{\text{area}}$  on  $N_{\text{mass}}$  ( $p < 0.001$ ; Table 4.5; Fig. 4.5).  
**1556** Leaf  $C_i:C_a$  increased with increasing  $\beta$  ( $p < 0.001$ ; Table 4.5) and decreased with  
**1557** increasing vapor pressure deficit ( $p < 0.001$ ; Table 4.5; Fig. 4.5). Variance in  $\beta$   
**1558** was driven by a negative effect of increasing soil nitrogen availability ( $p < 0.001$ ;  
**1559** Table 4.5) and was generally higher in C<sub>3</sub> species ( $p < 0.001$ ; Table 4.5; Fig. 4.5).  
**1560** However,  $\beta$  did not change with soil moisture ( $p = 0.895$ ; Table 4.5) or with ability  
**1561** to acquire nitrogen via symbiotic nitrogen fixation ( $p = 0.495$ ; Table 4.5). Finally,  
**1562** soil nitrogen availability was positively associated with increasing soil moisture  
**1563** ( $p = 0.003$ ; Table 4.5; Fig. 4.5).

**Table 4.5.** Structural equation model results investigating direct effects of climatic and soil resource availability on leaf nitrogen content ( $N_{\text{area}}$ ; g m<sup>-2</sup>)\*

Predictor	Coefficient	<i>p</i>
$N_{\text{area}}$ ( $R^2_c=0.89$ )		
$M_{\text{area}}$	0.714	<b>&lt;0.001</b>
$N_{\text{mass}}$	0.778	<b>&lt;0.001</b>
$N_{\text{mass}}$ ( $R^2_c=0.56$ )		
Leaf $C_i:C_a$	0.086	0.153
$M_{\text{area}}$	-0.256	<b>&lt;0.001</b>
$M_{\text{area}}$ ( $R^2_c=0.57$ )		
Leaf $C_i:C_a$	-0.250	<b>&lt;0.001</b>
Leaf $C_i:C_a$ ( $R^2_c=0.82$ )		
$\beta$	0.308	<b>&lt;0.001</b>
$\text{VPD}_4$	-0.111	<b>&lt;0.001</b>
$\beta$ ( $R^2_c=0.38$ )		
Soil N	-0.207	<b>&lt;0.001</b>
$\text{SM}_{90}$	-0.006	0.895
Photo. pathway	0.446	<b>&lt;0.001</b>
N-fixing ability	-0.059	0.519
Soil N ( $R^2_c=0.35$ )		
$\text{SM}_{90}$	-0.148	<b>0.003</b>

1564 \*Coefficients are standardized across the structural equation model. *P*-values less  
 1565 than 0.05 are noted in bold. Positive coefficients for photosynthetic pathway  
 1566 indicate generally larger values in C<sub>3</sub> species, while positive coefficients for N-  
 1567 fixing ability indicate generally larger values in N-fixing species. Key: df=degrees  
 1568 of freedom;  $\chi^2$ =Wald Type II chi-square test statistic;  $R^2_c$ =conditional R<sup>2</sup> value;  
 1569  $N_{\text{mass}}$ =leaf nitrogen content per unit leaf biomass (gN g<sup>-1</sup>);  $M_{\text{area}}$ =leaf mass per  
 1570 unit leaf biomass (g m<sup>-2</sup>);  $\beta$ =cost of acquiring nitrogen relative to water (unitless);  
 1571  $\text{VPD}_4$ =4-day mean vapor pressure deficit (kPa);  $\text{SM}_{90}$ =90-day mean soil moisture  
 1572 (mm)

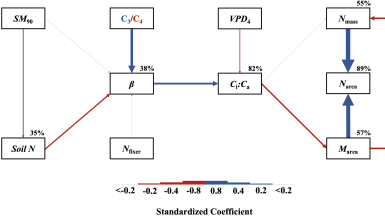


**Figure 4.5.** Structural equation model results exploring drivers of  $N_{\text{area}}$ . Boxes indicate measured edaphic factors, climatic factors, and leaf traits. Solid arrows indicate bivariate relationships where  $p < 0.05$ , while dashed arrows indicate relationships where  $p > 0.05$ . Positive model coefficients are indicated through blue arrows, negative model coefficients are indicated through red arrows, and insignificant coefficients are indicated through gray dashed arrows. Arrow thickness scales with the standardized model coefficient of each bivariate relationship. A positive coefficient for photosynthetic pathway indicates larger values in  $C_3$  species, while a positive coefficient for  $N_{\text{fixer}}$  indicates larger values in  $N$ -fixing species. Standardized model coefficients and associated  $p$ -values are reported in Table 4.5, with conditional  $R^2$  values for each response variable reported on the top right of each box.

**1573** 4.4 Discussion

**1574** In this study, I quantified direct and indirect effects of edaphic and climatic char-  
**1575** acteristics on  $N_{\text{area}}$  and components of  $N_{\text{area}}$  ( $N_{\text{mass}}$  and  $M_{\text{area}}$ ) in 520 individuals  
**1576** spanning across a soil resource availability and climate gradient in Texas, USA.  
**1577** Strong and consistent patterns emerged in support of those expected from photo-  
**1578** synthetic least-cost theory, a result driven by a strong direct negative relationship  
**1579** between leaf  $C_i:C_a$  and  $N_{\text{area}}$ . In further support of patterns expected from theory,  
**1580** increasing soil nitrogen availability had a strong negative effect on  $\beta$ , resulting in  
**1581** an indirect stimulation in  $N_{\text{area}}$  mediated through a positive relationship between  
**1582**  $\beta$  and  $C_i:C_a$ . Increasing VPD also indirectly increased  $N_{\text{area}}$  through a direct  
**1583** negative effect of increasing VPD on leaf  $C_i:C_a$ , following hypotheses and pat-  
**1584** terns expected from theory. Interestingly, a strong positive association between  
**1585** soil moisture and  $N_{\text{area}}$  was driven by covariance between soil moisture and soil  
**1586** nitrogen availability and was not associated with a direct effect of soil moisture  
**1587** on  $\beta$ . Overall, results provide strong and consistent support for patterns expected  
**1588** from photosynthetic least-cost theory, showing that both soil resource availability  
**1589** and climate drive variance in  $N_{\text{area}}$  through changes in leaf  $C_i:C_a$ .

**1590** 4.4.1 *Negative effects of leaf  $C_i:C_a$  on  $N_{\text{area}}$  are driven by reductions in  $M_{\text{area}}$ ,*  
**1591** *not  $N_{\text{mass}}$*

**1592** A strong negative effect of increasing leaf  $C_i:C_a$  on  $N_{\text{area}}$  was detected in both  
**1593** the linear mixed effect and piecewise structural equation models. The negative  
**1594** response of  $N_{\text{area}}$  to increasing leaf  $C_i:C_a$  is consistent with previous environmental  
**1595** gradient (Dong et al. 2017; Querejeta et al. 2022) and manipulation experiments

1596 (3.4c), showing strong support for the nitrogen-water use tradeoffs expected from  
1597 photosynthetic least cost theory (Wright et al. 2003; Prentice et al. 2014). Neg-  
1598 ative effects of increasing leaf  $C_i:C_a$  on  $N_{\text{area}}$  were driven by a strong negative  
1599 effect of increasing  $C_i:C_a$  on  $M_{\text{area}}$ , with no apparent effect of leaf  $C_i:C_a$  on  $N_{\text{mass}}$ ,  
1600 suggesting that changes in  $N_{\text{area}}$  were driven by changes in leaf structure and not  
1601 leaf chemistry. However, increasing  $M_{\text{area}}$  was negatively associated with  $N_{\text{mass}}$ ,  
1602 indicating that an increase in  $N_{\text{mass}}$  was associated with larger, thinner leaves (i.e.  
1603 lower  $M_{\text{area}}$ ). These results are consistent with patterns reported from previous  
1604 studies indicating that variance in  $N_{\text{area}}$  is driven by changes in  $M_{\text{area}}$  across envi-  
1605 ronmental gradients, and that part of this response is due to negative covariance  
1606 between  $M_{\text{area}}$  and  $N_{\text{mass}}$  (Dong et al. 2017; Dong et al. 2020). Negative co-  
1607 variance between  $M_{\text{area}}$  and  $N_{\text{mass}}$  could be a response associated with tradeoffs  
1608 between leaf longevity and leaf productivity (Wright et al. 2004; Dong et al. 2017;  
1609 Dong et al. 2022; Querejeta et al. 2022; Wang et al. 2023).

1610 The negative relationship between leaf  $C_i:C_a$  and  $M_{\text{area}}$  could also be a re-  
1611 sponse that allows leaves to maximize productivity in shorter-lived leaves. Trade-  
1612 offs between leaf longevity and leaf productivity are commonly observed and are  
1613 included in a continuum of coordinated leaf traits that position individuals along  
1614 a fast- or slow-growing leaf economics spectrum (Wright et al. 2003; Onoda et al.  
1615 2004; Reich 2014; Onoda et al. 2017; Wang et al. 2023). Negative relationships  
1616 between leaf  $C_i:C_a$  and  $M_{\text{area}}$  indicate that increased stomatal conductance and  
1617 reduced water use efficiency were associated with thinner, larger leaves (i.e., lower  
1618  $M_{\text{area}}$ ). These patterns, combined with the negative covariance between  $M_{\text{area}}$  and  
1619  $N_{\text{mass}}$  mentioned above, may have allowed individuals to maximize light intercep-

1620 tion and productivity by exploiting high light environments, though this comes  
1621 at the expense of increased water loss and decreased water-use efficiency. This  
1622 strategy may be especially advantageous for fast-growing species in open canopy  
1623 systems. In this study, C<sub>3</sub> legumes and C<sub>3</sub> nonlegumes dominated the dataset  
1624 (78% of total sampling effort), of which 22% (17% of total sampling effort) were  
1625 classified as annual species with short growing seasons. We observed no effect of  
1626 leaf  $C_i:C_a$  on  $N_{\text{area}}$  or  $M_{\text{area}}$  in C<sub>4</sub> nonlegumes, which made up 22% of the sampling  
1627 effort and were generally classified as warm season graminoid species with slower  
1628 growth rates and longer growing seasons. These patterns indicate that stronger  
1629 tradeoffs between nitrogen and water use may be more apparent in fast-growing  
1630 species with high demand for building and maintaining productive leaf tissues.

1631 4.4.2 *Soil nitrogen availability increases  $N_{\text{area}}$  through changes in  $\beta$*   
1632 Structural equation model results indicated that soil nitrogen availability had a  
1633 null effect of soil nitrogen availability on  $N_{\text{area}}$ , a pattern that was driven by  
1634 positive and negative respective effects of increasing soil nitrogen availability on  
1635  $N_{\text{mass}}$  and  $M_{\text{area}}$  that were equal in magnitude. The null response of  $N_{\text{area}}$  to  
1636 soil nitrogen availability occurred alongside a negative effect of increasing soil  
1637 nitrogen availability on  $\beta$ , paired with the negative relationship between leaf  $C_i:C_a$   
1638 and  $M_{\text{area}}$  and null effect of leaf Ci:Ca on  $N_{\text{mass}}$ . These patterns suggest that  
1639 positive effects of increasing soil nitrogen availability on  $N_{\text{area}}$  were likely driven  
1640 by reductions in the cost of acquiring nitrogen, supporting previous work (Bae  
1641 et al. 2015; Eastman et al. 2021; Perkowski et al. 2021; Lu et al. 2022) and  
1642 patterns expected from photosynthetic least-cost theory (Paillassa et al. 2020).

1643 The null effect of leaf  $C_i:C_a$  on  $N_{\text{mass}}$  and negative effect of leaf  $C_i:C_a$  on  
1644  $M_{\text{area}}$  suggests that the positive indirect effect of increasing soil nitrogen avail-  
1645 ability on  $N_{\text{area}}$  was driven by increased leaf nitrogen content allocated to leaf  
1646 structural tissue (Onoda et al. 2004; Onoda et al. 2017; Dong et al. 2020). While  
1647 this implies a null effect of soil nitrogen availability on leaf nitrogen content al-  
1648 located to photosynthetic leaf tissue, leaf nitrogen allocation to photosynthetic  
1649 tissue could not be quantified due to a lack of gas exchange data. Relationships  
1650 between soil nitrogen availability and  $N_{\text{area}}$  are complex in terrestrial ecosystems  
1651 across environmental gradients; however, our results indicate that photosynthetic  
1652 least-cost frameworks are capable of detecting predictable variance in  $N_{\text{area}}$  and  
1653 tradeoffs between nitrogen and water use across soil nitrogen availability gradients.

1654 4.4.3 *Soil moisture increases  $N_{\text{area}}$  by facilitating increases in soil nitrogen  
1655 availability*

1656 Increasing soil moisture had a positive effect on  $N_{\text{area}}$ , a response that was asso-  
1657 ciated with a null effect of soil moisture on  $\beta$ . These results contrast patterns  
1658 expected from theory, where increasing soil moisture is expected to indirectly de-  
1659 crease  $N_{\text{area}}$  through an increase in  $\beta$  due to a reduction in costs associated with  
1660 water acquisition and use (Wright et al. 2003; Prentice et al. 2014; Lavergne  
1661 et al. 2020). Interestingly, structural equation model results revealed a strong  
1662 positive association between soil moisture and soil nitrogen availability, indicat-  
1663 ing an indirect positive effect of increasing soil moisture on  $N_{\text{area}}$  mediated by  
1664 the negative effect of increasing soil nitrogen availability on  $\beta$ . In Texan grass-  
1665 lands, productivity and nutrient uptake are often co-limited by precipitation and  
1666 nutrient availability (Yahdjian et al. 2011; Wang et al. 2017). Thus, increases  
1667 in soil moisture may have facilitated more favorable and productive environments

1668 for soil microbial communities (Reichman et al. 1966; Stark and Firestone 1995;  
1669 Paul et al. 2003), or alternatively greater nitrogen mobility in soil solution. As  
1670 discussed above, the positive indirect response of  $N_{\text{area}}$  to increasing soil nitrogen  
1671 availability as mediated through reductions in  $\beta$  follow patterns expected from  
1672 theory.

1673 4.4.4 *Indirect effects of climate on  $N_{\text{area}}$  are mediated through changes in leaf*  
1674  *$C_i:C_a$  and  $\beta$*

1675 In support of hypotheses and patterns expected from theory, increasing vapor  
1676 pressure deficit indirectly increased  $N_{\text{area}}$ , mediated through the negative effect  
1677 of increasing vapor pressure deficit on leaf  $C_i:C_a$ . These responses are consistent  
1678 with previous work noting strong reductions in stomatal conductance with increas-  
1679 ing vapor pressure deficit (Oren et al. 1999; Novick et al. 2016; Sulman et al.  
1680 2016; Grossiord et al. 2020; López et al. 2021), a response that allows plants  
1681 to minimize water loss as a result of high atmospheric water demand. Results  
1682 also support findings from previous experiments across environmental gradients,  
1683 where increasing vapor pressure deficit generally increases  $N_{\text{area}}$  at lower stomatal  
1684 conductance across environmental gradients (Dong et al. 2017; Dong et al. 2022;  
1685 Paillassa et al. 2020; Westerband et al. 2023). These responses provide another  
1686 line of evidence that suggests leaf nitrogen content is a deterministic acclima-  
1687 tion response to changing aboveground climate, allowing plants to satisfy demand  
1688 to build and maintain photosynthetic enzymes and optimize photosynthetic pro-  
1689 cesses by maximizing resource use efficiency (Paillassa et al. 2020; Peng et al.  
1690 2021; Dong et al. 2022; Westerband et al. 2023).

**1691** 4.4.5 *Species identity traits modify effects of the environment on  $\beta$ , leaf  $C_i:C_a$ ,*  
**1692** *and  $N_{area}$*

**1693** N-fixing species had greater  $N_{area}$  values on average compared to non-fixing species,  
**1694** a pattern driven by a stronger stimulation in  $N_{mass}$  in N-fixing species coupled with  
**1695** no change in  $M_{area}$  between species with different N-fixation ability. There was  
**1696** no evidence to suggest that N-fixing species had different  $\beta$  or leaf  $C_i:C_a$  values  
**1697** compared to non-fixing species across the environmental gradient. These results  
**1698** follow patterns from previous environmental gradient experiments that investi-  
**1699** gate variance in leaf nitrogen allocation in N-fixing species (Adams et al. 2016;  
**1700** Dong et al. 2017; Dong et al. 2020), and that increases in  $N_{mass}$  and  $N_{area}$  in  
**1701** N-fixing species are not necessarily correlated to increases in water use efficiency  
**1702** or reductions in leaf  $C_i:C_a$  (Adams et al. 2016). While results are consistent with  
**1703** results from previous environmental gradient experiments, they do not support  
**1704** hypotheses presented here or patterns expected from theory, which predicts that  
**1705** stimulations in  $N_{area}$  by N-fixing species should be driven by a reduction in  $\beta$   
**1706** relative to non-fixing species, and that this response should decrease stomatal  
**1707** conductance and leaf  $C_i:C_a$ .

**1708**  $C_4$  species had reduced  $\beta$ , leaf  $C_i:C_a$ , and  $N_{area}$  than  $C_3$  species. Reduced  
**1709**  $\beta$  and leaf  $C_i:C_a$  values in  $C_4$  species follow hypotheses listed above, a pattern  
**1710** that could be the result of either reduced costs of nitrogen acquisition and use,  
**1711** increased costs of water acquisition and use, or both (Wright et al. 2003; Prentice  
**1712** et al. 2014). Results also indicate that  $\beta$  in  $C_4$  nonlegumes was unresponsive to  
**1713** changes in soil nitrogen availability despite an apparent negative effect of increas-  
**1714** ing soil nitrogen availability on  $\beta$  in  $C_3$  legumes and  $C_3$  nonlegumes. Combined  
**1715** with a general null response of  $\beta$  to soil moisture regardless of plant functional

1716 group, these patterns imply that reduced  $\beta$  values in C<sub>4</sub> species may be the re-  
1717 sult of lower costs of nitrogen acquisition and use relative to C<sub>3</sub> species. While  
1718 lower  $\beta$  values in C<sub>4</sub> species provides a possible explanation for why C<sub>4</sub> species  
1719 often have lower leaf  $C_i:C_a$  and greater water use efficiency, theory predicts that  
1720 this response should cause C<sub>4</sub> species to have greater  $N_{area}$  values compared to  
1721 C<sub>3</sub> species, though C<sub>4</sub> species commonly exhibit lower  $N_{area}$  and higher nitrogen  
1722 use efficiency than C<sub>3</sub> species (Schmitt and Edwards 1981; Sage and Pearcy 1987;  
1723 Ghannoum et al. 2011). We speculate that lowered costs of nitrogen acquisition  
1724 and use in C<sub>4</sub> species could be driven by more efficient Rubisco carboxylation effi-  
1725 ciency in C<sub>4</sub> species associated with CO<sub>2</sub> concentrating mechanisms that eliminate  
1726 photorespiration (Ghannoum et al. 2011), which could reduce or eliminate the  
1727 need to sacrifice inefficient nitrogen use for efficient water use to achieve optimal  
1728 photosynthesis rates.

1729 4.4.6 *Next steps for optimality model development*

1730 Optimality models for both C<sub>3</sub> and C<sub>4</sub> species have been developed using principles  
1731 from photosynthetic least-cost theory (Prentice et al. 2014; Wang et al. 2017;  
1732 Smith et al. 2019; Stocker et al. 2020; Scott and Smith 2022). In both C<sub>3</sub> and C<sub>4</sub>  
1733 model variants,  $\beta$  values are held constant using global datasets of leaf  $\delta^{13}\text{C}$  (Wang  
1734 et al. 2017; Cornwell et al. 2018). Specifically, the C<sub>3</sub> optimality model initially  
1735 assumed a constant  $\beta$  value of 240 (Wang et al. 2017), later corrected to 146  
1736 (Stocker et al. 2020), while the C<sub>4</sub> optimality model assumes a constant  $\beta$  value of  
1737 166 (Scott and Smith 2022). These results, which build on findings from Paillassa  
1738 et al. (2020) and Lavergne et al. (2020), demonstrate high variability in calculated  
1739  $\beta$  values across the environmental gradient. Specifically,  $\beta$  values in C<sub>3</sub> species

**1740** ranged from 1.7 to 188.0 (mean: 30.2; median: 23.1; standard deviation: 25.4),  
**1741** while ranged from 0.1 to 110.6 in C<sub>4</sub> species (mean: 7.2; median: 0.7; standard  
**1742** deviation: 18.6). Mean  $\beta$  values in both C<sub>3</sub> and C<sub>4</sub> species were consistently lower  
**1743** than values currently implemented in optimality models, though this was likely  
**1744** the result of increased water limitation across sites relative to global averages.  
**1745** Regardless, the high degree of  $\beta$  variability across this environmental gradient,  
**1746** together with findings from Lavergne et al. (2020) and Paillassa et al. (2020),  
**1747** suggests that the use of constant  $\beta$  values may contribute to erroneous errors when  
**1748** conducting optimality model simulations. Results from this experiment build  
**1749** on suggestions from Wang et al. (2017), suggesting that future photosynthetic  
**1750** least-cost optimality model developments should consider adopting frameworks  
**1751** for dynamically calculating  $\beta$ .

**1752** 4.4.7 *Conclusions*

**1753** To summarize, variability in  $N_{\text{area}}$  across an environmental gradient in Texan  
**1754** grasslands was driven by indirect effects of climate and soil resource availability  
**1755** mediated by changes in  $\beta$  and leaf  $C_i:C_a$ . Results from this experiment provide  
**1756** strong and consistent support for patterns expected from photosynthetic least-  
**1757** cost theory, demonstrating that negative relationships between  $C_i:C_a$  and  $N_{\text{area}}$   
**1758** unify expected effects of climatic and edaphic characteristics on  $N_{\text{area}}$  across en-  
**1759** vironmental gradients. Results reported here also demonstrate a need to consider  
**1760** the dynamic nature of the relative cost of nitrogen versus water uptake ( $\beta$ ) across  
**1761** environmental gradients in optimality models that leverage principles of photo-  
**1762** synthetic least-cost theory.

1763

## Chapter 5

1764     Optimal resource investment to photosynthetic capacity maximizes  
1765       nutrient allocation to whole plant growth under elevated CO<sub>2</sub>

1766     5.1   Introduction

1767     Terrestrial ecosystems are regulated by complex carbon and nitrogen cycles. As  
1768     a result, terrestrial biosphere models, which are beginning to include coupled  
1769     carbon and nitrogen cycles (Shi et al. 2016; Davies-Barnard et al. 2020; Braghieri  
1770     et al. 2022), must accurately represent these cycles under different environmental  
1771     scenarios to reliably simulate carbon and nitrogen atmosphere-biosphere fluxes  
1772     (Hungate et al. 2003; Prentice et al. 2015). While the inclusion of coupled carbon  
1773     and nitrogen cycles tends to reduce model uncertainty (Arora et al. 2020), large  
1774     uncertainty in role of soil nitrogen availability and nitrogen acquisition strategy  
1775     on leaf and whole plant acclimation responses to CO<sub>2</sub> remains (Smith and Dukes  
1776     2013; Terrer et al. 2018; Smith and Keenan 2020). This source of uncertainty  
1777     likely contributes to the widespread divergence in future carbon and nitrogen flux  
1778     simulations across terrestrial biosphere models (Friedlingstein et al. 2014; Zaehle  
1779     et al. 2014; Meyerholt et al. 2020).

1780           Plants grown under elevated CO<sub>2</sub> generally have less leaf nitrogen content  
1781     than those grown under ambient CO<sub>2</sub>, a response that often corresponds with  
1782     reductions in photosynthetic capacity and stomatal conductance at the leaf-level  
1783     and biomass stimulation over time at the whole plant level (Curtis 1996; Drake  
1784     et al. 1997; Ainsworth et al. 2002; Makino 2003; Morgan et al. 2004; Ainsworth  
1785     and Long 2005; Ainsworth and Rogers 2007; Smith and Dukes 2013; Poorter et al.  
1786     2022). As net primary productivity is generally limited by nitrogen availability

1787 (Vitousek and Howarth 1991; LeBauer and Treseder 2008; Fay et al. 2015), and  
1788 soil nitrogen availability is often positively correlated with leaf nitrogen content  
1789 and photosynthetic capacity (Field and Mooney 1986; Evans and Seemann 1989;  
1790 Evans 1989; Walker et al. 2014; Firn et al. 2019; Liang et al. 2020), some  
1791 have hypothesized that leaf and whole plant acclimation responses to CO<sub>2</sub> are  
1792 constrained by soil nitrogen availability.

1793 The progressive nitrogen limitation hypothesis predicts that elevated CO<sub>2</sub>  
1794 will increase plant nitrogen demand, which will increase plant nitrogen uptake and  
1795 progressively deplete soil nitrogen if soil nitrogen supply does not exceed plant  
1796 nitrogen demand (Luo et al. 2004). The hypothesis predicts that this response  
1797 should result in strong acute stimulations in whole plant growth and primary  
1798 productivity that diminish over time as nitrogen becomes more limiting. Assuming  
1799 a positive relationship between soil nitrogen availability, leaf nitrogen content, and  
1800 photosynthetic capacity, this hypothesis also implies that progressive reductions in  
1801 soil nitrogen availability should be the mechanism that drives the downregulation  
1802 of leaf nitrogen content and photosynthetic capacity under elevated CO<sub>2</sub>. This  
1803 hypothesis has received some support from free air CO<sub>2</sub> enrichment experiments  
1804 (Reich et al. 2006; Norby et al. 2010), although is not consistently observed across  
1805 experiments (Finzi et al. 2006; Moore et al. 2006; Liang et al. 2016).

1806 While possible that progressive nitrogen limitation may determine leaf and  
1807 whole plant acclimation responses to CO<sub>2</sub>, growing evidence indicates that leaf ni-  
1808 trogen and photosynthetic capacity are more strongly determined through above-  
1809 ground growing conditions than by soil resource availability (Dong et al. 2017;  
1810 Dong et al. 2020; Dong et al. 2022; Smith et al. 2019; Smith and Keenan 2020;

1811 Paillassa et al. 2020; Peng et al. 2021; Querejeta et al. 2022; Westerband et al.  
1812 2023), and satellite-derived chlorophyll fluorescence data indicate that increasing  
1813 atmospheric CO<sub>2</sub> may decrease leaf and canopy demand for nitrogen (Dong et al.  
1814 2022). Together, results from these studies suggest that the downregulation in  
1815 leaf nitrogen content and photosynthetic capacity due to increasing CO<sub>2</sub> may not  
1816 be as tightly linked to progressive nitrogen limitation as previously hypothesized.

1817 A unification of optimal coordination and least-cost theories predicts that  
1818 leaves acclimate to elevated CO<sub>2</sub> by downregulating nitrogen allocation to Ribulose-  
1819 1,5-bisphosphate (RuBP) carboxylase/oxygenase (Rubisco) to optimize resource  
1820 use efficiencies at the leaf level, which allows for greater resource allocation to  
1821 whole plant growth (Drake et al. 1997; Wright et al. 2003; Prentice et al. 2014;  
1822 Smith et al. 2019). The theory predicts that the downregulation in nitrogen  
1823 allocation to Rubisco results in a stronger downregulation in the maximum rate  
1824 of Rubisco carboxylation ( $V_{cmax}$ ) than the maximum rate of RuBP regeneration  
1825 ( $J_{max}$ ), which maximizes photosynthetic efficiency by allowing net photosynthesis  
1826 rates to be equally co-limited by Rubisco carboxylation and RuBP regeneration  
1827 (Chen et al. 1993; Maire et al. 2012). This acclimation response allows plants to  
1828 make more efficient use of available light while avoiding overinvestment in Rubisco,  
1829 which has high nitrogen and energetic costs of building and maintaining (Evans  
1830 1989; Evans and Clarke 2019). Instead, additional acquired resources not needed  
1831 to optimize leaf photosynthesis are allocated to the maintenance of structures that  
1832 support whole plant growth (e.g., total leaf area, whole plant biomass, etc.) or  
1833 to allocation processes not related to leaf photosynthesis or growth, such as plant  
1834 defense mechanisms. Regardless, optimized resource allocation at the leaf level

1835 should allow for greater resource allocation to whole plant growth. The theory  
1836 indicates that leaf acclimation responses to CO<sub>2</sub> should be independent of changes  
1837 in soil nitrogen availability. While this leaf acclimation response maximizes nitro-  
1838 gen allocation to structures that support whole plant growth, the theory suggests  
1839 that the positive effect of elevated CO<sub>2</sub> on whole plant growth may be further  
1840 stimulated by soil nitrogen availability through reductions in the cost of acquiring  
1841 nitrogen (Bae et al. 2015; Perkowski et al. 2021; Lu et al. 2022).

1842 Plants acquire nitrogen by allocating photosynthetically derived carbon be-  
1843 lowground in exchange for nitrogen through different nitrogen acquisition strate-  
1844 gies. These nitrogen acquisition strategies can include direct uptake pathways  
1845 such as mass flow or diffusion (Barber 1962), symbioses with mycorrhizal fungi or  
1846 symbiotic nitrogen-fixing bacteria (Vance and Heichel 1991; Marschner and Dell  
1847 1994; Smith and Read 2008; Udvardi and Poole 2013), or through the release  
1848 of root exudates that prime free-living soil microbial communities (Phillips et al.  
1849 2011; Wen et al. 2022). Plants cannot acquire nitrogen without first allocating  
1850 carbon belowground, which implies an inherent carbon cost to the plant for acquir-  
1851 ing nitrogen regardless of nitrogen acquisition strategy. Carbon costs to acquire  
1852 nitrogen often vary in species with different nitrogen acquisition strategies and  
1853 are dependent on external environmental factors such as atmospheric CO<sub>2</sub>, light  
1854 availability, and soil nitrogen availability (Brzostek et al. 2014; Terrer et al. 2016;  
1855 Terrer et al. 2018; Allen et al. 2020; Perkowski et al. 2021; Lu et al. 2022). These  
1856 patterns suggest that acquisition strategy may at least partially determine the net  
1857 effect of soil nitrogen availability on leaf and whole plant acclimation responses to  
1858 elevated CO<sub>2</sub>.

1859 A recent meta-analysis using data across 20 grassland and forest CO<sub>2</sub> en-  
1860 richment experiments suggested that species which acquire nitrogen from sym-  
1861 biotic nitrogen-fixing bacteria had reduced costs of nitrogen acquisition under  
1862 elevated CO<sub>2</sub> (Terrer et al. 2018). Though these analyses only included data  
1863 from two experimental sites, findings from this meta-analysis indicated that re-  
1864 ductions in costs of nitrogen acquisition in species that form associations with  
1865 symbiotic nitrogen-fixing bacteria under elevated CO<sub>2</sub> may drive stronger stim-  
1866 ulations in whole plant growth and downregulations in  $V_{cmax}$  than species that  
1867 associate with arbuscular mycorrhizal fungi (Smith and Keenan 2020), which gen-  
1868 erally have greater costs of nitrogen acquisition under elevated CO<sub>2</sub> (Terrer et al.  
1869 2018). However, plant investments in symbiotic nitrogen fixation generally de-  
1870 cline with increasing nitrogen availability (Dovrat et al. 2018; Perkowski et al.  
1871 2021), a response that has been previously inferred to be the result of a shift in  
1872 the dominant mode of nitrogen acquisition to direct uptake pathways as costs of  
1873 direct uptake decrease with increasing soil nitrogen availability (Rastetter et al.  
1874 2001; Perkowski et al. 2021). Thus, effects of symbiotic nitrogen fixation on plant  
1875 acclimation responses to CO<sub>2</sub> should decline with increasing soil nitrogen avail-  
1876 ability, although manipulative experiments that directly test these patterns are  
1877 rare.

1878 Here, I conducted a 7-week growth chamber experiment using *Glycine max*  
1879 L. (Merr.) to examine the effects of soil nitrogen fertilization and inoculation with  
1880 symbiotic nitrogen-fixing bacteria on leaf and whole plant acclimation responses  
1881 to elevated CO<sub>2</sub>. Following patterns expected from theory, I hypothesized that in-  
1882 dividual leaves should acclimate to elevated CO<sub>2</sub> by more strongly downregulating

1883  $V_{cmax}$  relative to  $J_{max}$ , allowing leaf photosynthesis to approach optimal coordi-  
1884 nation. I expected this response to correspond with a stronger downregulation in  
1885 leaf nitrogen content than  $V_{cmax}$  and  $J_{max}$ , which would increase the fraction of  
1886 leaf nitrogen content allocated to photosynthesis and photosynthetic nitrogen use  
1887 efficiency. At the whole-plant level, I hypothesized that plants would acclimate  
1888 to elevated CO<sub>2</sub> by stimulating whole plant growth and productivity, a response  
1889 that would be driven by a strong positive response of total leaf area and above-  
1890 ground biomass to elevated CO<sub>2</sub>. I predicted that leaf acclimation responses to  
1891 elevated CO<sub>2</sub> would be independent of soil nitrogen fertilization and inoculation  
1892 with symbiotic nitrogen-fixing bacteria; however, I expected that increasing soil  
1893 nitrogen fertilization would increase the positive effect of elevated CO<sub>2</sub> on mea-  
1894 sures of whole plant growth due to a stronger reduction in the cost of acquiring  
1895 nitrogen under elevated CO<sub>2</sub> with increasing fertilization. I also expected stronger  
1896 stimulations in whole plant growth due to inoculation, but that this effect would  
1897 only be apparent under low fertilization due to a reduction in root nodulation  
1898 with increasing fertilization.

1899 5.2 Methods

1900 5.2.1 *Seed treatments and experimental design*

1901 *Glycine max* L. (Merr) seeds were planted in 144 6-liter surface sterilized pots (NS-  
1902 600, Nursery Supplies, Orange, CA, USA) containing a steam-sterilized 70:30 v:v  
1903 mix of Sphagnum peat moss (Premier Horticulture, Quakertown, PA, USA) to  
1904 sand (Pavestone, subsidiary of Quikrete Companies, Atlanta, GA, USA). Before  
1905 planting, all *G. max* seeds were surface sterilized in 2% sodium hypochlorite for 3

1906 minutes, followed by three separate 3-minute washes with ultrapure water (MilliQ  
1907 7000; MilliporeSigma, Burlington, MA USA). A subset of surface sterilized seeds  
1908 were inoculated with *Bradyrhizobium japonicum* (Verdesian N-Dure<sup>TM</sup> Soybean,  
1909 Cary, NC, USA) in a slurry following manufacturer recommendations (3.12 g  
1910 inoculant and 241 g deionized water per 1 kg seed).

1911 Seventy-two pots were randomly planted with surface-sterilized seeds inoc-  
1912 ulated with *B. japonicum*, while the remaining 72 pots were planted with surface-  
1913 sterilized uninoculated seeds. Thirty-six pots within each inoculation treatment  
1914 were randomly placed in one of two atmospheric CO<sub>2</sub> treatments (ambient and  
1915 1000  $\mu\text{mol mol}^{-1}$  CO<sub>2</sub>). Pots within each unique inoculation-by-CO<sub>2</sub> treatment  
1916 combination randomly received one of nine soil nitrogen fertilization treatments  
1917 equivalent to 0, 35, 70, 105, 140, 210, 280, 350, or 630 ppm N. Nitrogen fertil-  
1918 ization treatments were created using a modified Hoagland solution (Hoagland  
1919 and Arnon 1950) designed to keep concentrations of other macronutrients and  
1920 micronutrients equivalent across treatments (Table D1). Pots received the same  
1921 fertilization treatment throughout the entire duration experiment, which were ap-  
1922 plied twice per week in 150 mL doses as topical agents to the soil surface. This  
1923 experimental design yielded a fully factorial experiment with four replicates per  
1924 unique fertilization-by-inoculation-by-CO<sub>2</sub> combination.

### 1925 5.2.2 *Growth chamber conditions*

1926 Upon experiment initiation, pots were randomly placed in one of six Percival  
1927 LED-41L2 growth chambers (Percival Scientific Inc., Perry, IA, USA) over two  
1928 experimental iterations due to chamber space limitation. Two iterations were

1929 conducted such that one iteration included all elevated CO<sub>2</sub> pots and the second  
1930 iteration included all ambient CO<sub>2</sub> pots. Mean ( $\pm$  SD) CO<sub>2</sub> concentrations across  
1931 chambers throughout the experiment were  $439 \pm 5 \mu\text{mol mol}^{-1}$  CO<sub>2</sub> for the ambient  
1932 CO<sub>2</sub> treatment and  $989 \pm 4 \mu\text{mol mol}^{-1}$  CO<sub>2</sub> for the elevated CO<sub>2</sub> treatment.

1933 Daytime growing conditions were simulated using a 16-hour photoperiod,  
1934 with incoming light radiation set to chamber maximum (mean  $\pm$  SD:  $1240 \pm 32$   
1935  $\mu\text{mol m}^{-2} \text{s}^{-1}$  across chambers), air temperature set to 25°C, and relative humid-  
1936 ity set to 50%. The remaining 8 hours simulated nighttime growing conditions,  
1937 with incoming light radiation set to 0  $\mu\text{mol m}^{-2} \text{s}^{-1}$ , chamber temperature set  
1938 to 17°C, and relative humidity set to 50%. Transitions between daytime and  
1939 nighttime growing conditions were simulated by ramping incoming light radiation  
1940 in 45-minute increments and temperature in 90-minute increments over a 3-hour  
1941 period (Table D2).

1942 Including the two, 3-hour ramping periods, pots grew under average ( $\pm$  SD)  
1943 daytime light intensity of  $1049 \pm 27 \mu\text{mol m}^{-2} \text{s}^{-1}$ . In the elevated CO<sub>2</sub> iteration,  
1944 pots grew under  $24.0 \pm 0.2^\circ\text{C}$  during the day,  $16.4 \pm 0.8^\circ\text{C}$  during the night, and  
1945 51.6  $\pm 0.4\%$  relative humidity. In the ambient CO<sub>2</sub> iteration, pots grew under  
1946  $23.9 \pm 0.2^\circ\text{C}$  during the day,  $16.0 \pm 1.4^\circ\text{C}$  during the night, and 50.3  $\pm 0.2\%$  relative  
1947 humidity. I accounted for any climatic differences across the six chambers by  
1948 shuffling the same group of pots daily throughout the growth chambers. This  
1949 process was done by iteratively moving the group of pots on the top rack of a  
1950 chamber to the bottom rack of the same chamber, while simultaneously moving  
1951 the group of pots on the bottom rack of a chamber to the top rack of the adjacent  
1952 chamber. I moved pots within and across chambers every day throughout the

1953 course of each experiment iteration.

1954 5.2.3 *Leaf gas exchange measurements*

1955 Gas exchange measurements were collected for all individuals on the seventh week

1956 of development. All gas exchange measurements were collected on the center leaf

1957 of the most recent fully expanded trifoliate leaf set. Specifically, I measured net

1958 photosynthesis ( $A_{\text{net}}$ ;  $\mu\text{mol m}^{-2} \text{s}^{-1}$ ), stomatal conductance ( $g_{\text{sw}}$ ;  $\text{mol m}^{-2} \text{s}^{-1}$ ),

1959 and intercellular  $\text{CO}_2$  ( $C_i$ ;  $\mu\text{mol mol}^{-1}$ ) concentrations across a range of atmo-

1960 spheric  $\text{CO}_2$  concentrations (i.e., an  $A_{\text{net}}/C_i$  curve) using the Dynamic Assimila-

1961 tion Technique<sup>TM</sup>. The Dynamic Assimilation Technique<sup>TM</sup> has been shown to

1962 correspond well with traditional steady-state  $\text{CO}_2$  response curves in *G. max*

1963 (Saathoff and Welles 2021).  $A_{\text{net}}/C_i$  curves were generated along a reference  $\text{CO}_2$

1964 ramp down from  $420 \mu\text{mol mol}^{-1} \text{CO}_2$  to  $20 \mu\text{mol mol}^{-1} \text{CO}_2$ , followed by a ramp

1965 up from  $420 \mu\text{mol mol}^{-1} \text{CO}_2$  to  $1620 \mu\text{mol mol}^{-1} \text{CO}_2$  after a 90-second wait

1966 period at  $420 \mu\text{mol mol}^{-1} \text{CO}_2$ . The ramp rate for each curve was set to  $200$

1967  $\mu\text{mol mol}^{-1} \text{min}^{-1}$ , logging every five seconds, which generated 96 data points per

1968 response curve. All  $A_{\text{net}}/C_i$  curves were generated after  $A_{\text{net}}$  and  $g_{\text{sw}}$  stabilized

1969 in a LI-6800 cuvette set to a  $500 \text{ mol s}^{-1}$ , 10,000 rpm mixing fan speed, 1.5 kPa

1970 vapor pressure deficit,  $25^\circ\text{C}$  leaf temperature,  $2000 \mu\text{mol m}^{-2} \text{s}^{-1}$  incoming light

1971 radiation, and initial reference  $\text{CO}_2$  set to  $420 \mu\text{mol mol}^{-1}$ .

1972 With the same focal leaf used to generate  $A_{\text{net}}/C_i$  curves, I measured dark

1973 respiration ( $R_{d25}$ ;  $\mu\text{mol m}^{-2} \text{s}^{-1}$ ) following at least a 30-minute period of darkness.

1974 Measurements were collected on a 5-second log interval for 60 seconds after stabi-

1975 lizing in a LI-6800 cuvette set to a  $500 \text{ mol s}^{-1}$ , 10,000 rpm mixing fan speed, 1.5

1976 kPa vapor pressure deficit, 25°C leaf temperature, and 420  $\mu\text{mol mol}^{-1}$  reference  
1977 CO<sub>2</sub> concentration (for both CO<sub>2</sub> concentrations), with incoming light radiation  
1978 set to 0  $\mu\text{mol m}^{-2} \text{s}^{-1}$ . A single dark respiration value was determined for each  
1979 focal leaf by calculating the mean dark respiration value (i.e. the absolute value  
1980 of  $A_{\text{net}}$  during the logging period) across the logging interval.

1981 5.2.4 *Leaf trait measurements*

1982 The focal leaf used to generate  $A_{\text{net}}/C_i$  curves and dark respiration was harvested  
1983 immediately following gas exchange measurements. Images of each focal leaf were  
1984 curated using a flat-bed scanner to determine wet leaf area using the ‘LeafArea’ R  
1985 package (Katabuchi 2015), which automates leaf area calculations using ImageJ  
1986 software (Schneider et al. 2012). Each leaf was dried at 65°C for at least 48  
1987 hours, and subsequently weighed and ground until homogenized. Leaf mass per  
1988 area ( $M_{\text{area}}$ ; g  $\text{m}^{-2}$ ) was calculated as the ratio of dry leaf biomass to fresh leaf  
1989 area. Using subsamples of ground and homogenized leaf tissue, I measured leaf  
1990 nitrogen content ( $N_{\text{mass}}$ ; gN  $\text{g}^{-1}$ ) through elemental combustion analysis (Costech-  
1991 4010, Costech, Inc., Valencia, CA, USA). Leaf nitrogen content per unit leaf area  
1992 ( $N_{\text{area}}$ ; gN  $\text{m}^{-2}$ ) was calculated by multiplying  $N_{\text{mass}}$  and  $M_{\text{area}}$ . Subsamples of  
1993 ground and homogenized leaf tissue were also sent to the UC-Davis Stable Isotope  
1994 Facility to quantify leaf  $\delta^{15}\text{N}$ , later used to estimate the fraction of leaf nitrogen  
1995 derived from the atmosphere.

1996 I extracted chlorophyll content from a second leaf in the same trifoliolate  
1997 leaf set as the focal leaf used to generate  $A_{\text{net}}/C_i$  curves. Prior to chlorophyll  
1998 extraction, I used a cork borer to punch between 3 and 5 0.6 cm<sup>2</sup> disks from the

**1999** leaf. Separate images of each punched leaf and set of leaf disks were curated using  
**2000** a flat-bed scanner to determine wet leaf area, again quantified using the ‘LeafArea’  
**2001** R package (Katabuchi 2015). The punched leaf was dried and weighed after at  
**2002** least 65°C in the drying oven to determine  $M_{\text{area}}$  of the chlorophyll leaf.

**2003** Leaf disks were shuttled into a test tube containing 10mL dimethyl sulfoxide, vortexed, and incubated at 65°C for 120 minutes (Barnes et al. 1992). Incubated test tubes were vortexed again before loaded in 150  $\mu\text{L}$  triplicate aliquots to a 96-well plate. Dimethyl sulfoxide was also loaded in a 150  $\mu\text{L}$  triplicate aliquot as a blank. Absorbance measurements at 649.1 nm ( $A_{649.1}$ ) and 665.1 nm ( $A_{665.1}$ ) were read in each well using a plate reader (Bioteck Synergy H1; Bioteck Instruments, Winooski, VT USA) (Wellburn 1994), with triplicates subsequently averaged and corrected by the mean of the blank absorbance value. Blank-corrected absorbance values were used to estimate  $Chl_a$  ( $\mu\text{g mL}^{-1}$ ) and  $Chl_b$  ( $\mu\text{g mL}^{-1}$ ) following equations from Wellburn (1994):

$$Chl_a = 12.47A_{665.1} - 3.62A_{649.1} \quad (5.1)$$

**2013** and

$$Chl_b = 25.06A_{665.1} - 6.50A_{649.1} \quad (5.2)$$

**2014**  $Chl_a$  and  $Chl_b$  were converted to mmol  $\text{mL}^{-1}$  using the molar mass of chlorophyll a (893.51 g  $\text{mol}^{-1}$ ) and the molar mass of chlorophyll b (907.47 g  $\text{mol}^{-1}$ ), then added together to calculate total chlorophyll content in the dimethyl sulfoxide extractant (mmol  $\text{mL}^{-1}$ ). Total chlorophyll content was multiplied by the volume of the dimethyl sulfoxide extractant (10 mL) and converted to area-based chlorophyll

2019 content by dividing by the total area of the leaf disks ( $Chl_{area}$ ; mmol m<sup>-2</sup>). Mass-  
2020 based chlorophyll content ( $Chl_{mass}$ ; mmol g<sup>-1</sup>) was calculated by dividing  $Chl_{area}$   
2021 by the leaf mass per area of the punched leaf.

2022 5.2.5 *A/C<sub>i</sub> curve fitting and parameter estimation*

2023 I fit  $A_{net}/C_i$  curves of each individual using the ‘fitaci’ function in the ‘plante-  
2024 cophys’ R package (Duursma 2015). This function estimates the maximum rate  
2025 of Rubisco carboxylation ( $V_{cmax}$ ;  $\mu\text{mol m}^{-2} \text{s}^{-1}$ ) and maximum rate of electron  
2026 transport for RuBP regeneration ( $J_{max}$ ;  $\mu\text{mol m}^{-2} \text{s}^{-1}$ ) based on the Farquhar  
2027 biochemical model of C<sub>3</sub> photosynthesis (Farquhar et al. 1980). Triose phosphate  
2028 utilization (TPU) limitation was included in all curve fits, and all curve fits in-  
2029 cluded measured dark respiration values. As  $A_{net}/C_i$  curves were generated using  
2030 a common leaf temperature, curves were fit using Michaelis-Menten coefficients  
2031 for Rubisco affinity to CO<sub>2</sub> ( $K_c$ ;  $\mu\text{mol mol}^{-1}$ ) and O<sub>2</sub> ( $K_o$ ;  $\mu\text{mol mol}^{-1}$ ), and the  
2032 CO<sub>2</sub> compensation point ( $\Gamma^*$ ;  $\mu\text{mol mol}^{-1}$ ) reported in Bernacchi et al. (2001).  
2033 Specifically,  $K_c$  was set to 404.9  $\mu\text{mol mol}^{-1}$ ,  $K_o$  was set to 278.4  $\mu\text{mol mol}^{-1}$ ,  
2034 and  $\Gamma^*$  was set to 42.75  $\mu\text{mol mol}^{-1}$ . All curve fits were visually examined for  
2035 goodness-of-fit. The use of a common leaf temperature across curves and dark  
2036 respiration measurements eliminated the need to temperature standardize rate  
2037 estimates. For clarity, I reference  $V_{cmax}$ ,  $J_{max}$ , and  $R_d$  estimates throughout the  
2038 rest of the chapter as  $V_{cmax25}$ ,  $J_{max25}$ , and  $R_{d25}$ .

**2039** 5.2.6 *Stomatal limitation*

**2040** I quantified the extent by which stomatal conductance limited photosynthesis ( $l$ ;

**2041** unitless) following equations originally described in Farquhar and Sharkey (1982).

**2042** Stomatal limitation was calculated as:

$$l = 1 - \frac{A_{net}}{A_{mod}} \quad (5.3)$$

**2043** where  $A_{mod}$  represents the photosynthetic rate where  $C_i = C_a$ .  $A_{mod}$  was calculated

**2044** as:

$$A_{mod} = V_{cmax25} - \frac{420 - \Gamma^*}{420 + K_m} - R_{d25} \quad (5.4)$$

**2045**  $K_m$  is the Michaelis-Menten coefficient for Rubisco-limited photosynthesis, calcu-

**2046** lated as:

$$K_m = K_c \cdot \left(1 + \frac{O_i}{K_o}\right) \quad (5.5)$$

**2047** where  $O_i$  refers to leaf intercellular  $O_2$  concentrations, set to  $210 \mu\text{mol mol}^{-1}$ .

**2048** 5.2.7 *Proportion of leaf nitrogen allocated to photosynthesis and structure*

**2049** I used equations from Niinemets and Tenhunen (1997) to estimate the proportion

**2050** of leaf nitrogen content allocated to Rubisco, bioenergetics, and light harvesting

**2051** proteins. The proportion of leaf nitrogen allocated to Rubisco ( $\rho_{rubisco}$ ;  $\text{gN gN}^{-1}$ )

**2052** was calculated as a function of  $V_{cmax25}$  and  $N_{area}$ :

$$\rho_{rubisco} = \frac{V_{cmax25} N_r}{V_{cr} N_{area}} \quad (5.6)$$

2053 where  $N_r$  is the amount of nitrogen in Rubisco, set to 0.16 gN (gN in Rubisco) $^{-1}$   
 2054 and  $V_{cr}$  is the maximum rate of RuBP carboxylation per unit Rubisco protein,  
 2055 set to 20.5  $\mu\text{mol CO}_2$  (g Rubisco) $^{-1}$ . The proportion of leaf nitrogen allocated to  
 2056 bioenergetics ( $\rho_{bioe}$ ; gN gN $^{-1}$ ) was similarly calculated as a function of  $J_{max25}$  and  
 2057  $N_{area}$ :

$$\rho_{bioe} = \frac{J_{max25} N_b}{J_{mc} N_{area}} \quad (5.7)$$

2058 where  $N_b$  is the amount of nitrogen in cytochrome f, set to 0.12407 gN ( $\mu\text{mol}$   
 2059 cytochrome f) $^{-1}$  assuming a constant 1: 1: 1.2 cytochrome f: ferredoxin NADP  
 2060 reductase: coupling factor molar ratio (Evans and Seemann 1989; Niinemets and  
 2061 Tenhunen 1997), and  $J_{mc}$  is the capacity of electron transport per cytochrome f,  
 2062 set to 156  $\mu\text{mol electron}$  ( $\mu\text{mol cytochrome f}$ ) $^{-1}\text{s}^{-1}$ .

2063 The proportion of leaf nitrogen allocated to light harvesting proteins ( $\rho_{light}$ ;  
 2064 gN gN $^{-1}$ ) was calculated as a function of  $Chl_{mass}$  and  $N_{mass}$ :

$$\rho_{light} = \frac{Chl_{mass}}{N_{mass} c_b} \quad (5.8)$$

2065 where  $c_b$  is the stoichiometry of the light-harvesting chlorophyll complexes of  
 2066 photosystem II, set to 2.75 mmol chlorophyll (gN in chlorophyll) $^{-1}$ . I used the  
 2067  $N_{mass}$  value of the focal leaf used to generate  $A_{net}/C_i$  curves instead of the leaf  
 2068 used to extract chlorophyll content, as the two leaves are from the same trifoliolate  
 2069 leaf set and are highly correlated (Figure D1).

2070 The proportion of leaf nitrogen content allocated to photosynthetic tissue  
 2071 ( $\rho_{photo}$ ; gN gN $^{-1}$ ) was estimated as the sum of  $\rho_{rubisco}$ ,  $\rho_{bioe}$ , and  $\rho_{light}$ . Finally,  
 2072 the proportion of leaf nitrogen content allocated to structural tissue ( $\rho_{structure}$ ; gN

2073  $\text{gN}^{-1}$ ) was estimated as:

$$\rho_{structure} = \frac{N_{cw}}{N_{area}} \quad (5.9)$$

2074 where  $N_{cw}$  is the leaf nitrogen content allocated to cell walls ( $\text{gN m}^{-2}$ ), calculated

2075 as a function of  $M_{area}$  using an empirical equation from Onoda et al. (2017):

$$N_{cw} = 0.000355 * M_{area}^{1.39} \quad (5.10)$$

2076 5.2.8 *Whole plant traits*

2077 Seven weeks after experiment initiation and immediately following gas exchange

2078 measurements, I harvested all experimental individuals and separated biomass of

2079 each experimental individual into major organ types (leaves, stems, roots, and

2080 nodules when present). Fresh leaf area of all harvested leaves was measured using

2081 an LI-3100C (Li-COR Biosciences, Lincoln, Nebraska, USA). Total fresh leaf area

2082 ( $\text{cm}^2$ ) was calculated as the sum of all leaf areas, including the focal leaf used to

2083 collect gas exchange data and the focal leaf used to extract chlorophyll content. All

2084 harvested material was dried in an oven set to  $65^\circ\text{C}$  for at least 48 hours, weighed,

2085 and ground to homogeneity. Leaves and nodules were manually ground with a

2086 mortar and pestle, while stems and roots were ground using a Wiley mill (E3300

2087 Mini Mill; Eberbach Corp., MI, USA). Total dry biomass (g) was calculated as

2088 the sum of dry leaf (including focal leaf for both the  $A_{net}/C_i$  curve and leaf used

2089 to extract chlorophyll content), stem, root, and root nodule biomass. I quantified

2090 carbon and nitrogen content of each respective organ type through elemental

2091 combustion (Costech-4010, Costech, Inc., Valencia, CA, USA) using subsamples

2092 of ground and homogenized organ tissue.

2093        Following the approach explained in the first experimental chapter, I calcu-  
 2094        lated structural carbon costs to acquire nitrogen as the ratio of total belowground  
 2095        carbon biomass to whole plant nitrogen biomass ( $N_{cost}$ ; gC gN<sup>-1</sup>). Belowground  
 2096        carbon biomass ( $C_{bg}$ ; gC) was calculated as the sum of root carbon biomass  
 2097        and root nodule carbon biomass. Root carbon biomass and root nodule carbon  
 2098        biomass was calculated as the product of the organ biomass and the respective  
 2099        organ carbon content. Whole plant nitrogen biomass ( $N_{wp}$ ; gN) was similarly  
 2100        calculated as the sum of total leaf, stem, root, and root nodule nitrogen biomass,  
 2101        including the focal leaf used for  $A_{net}/C_i$  curve and chlorophyll extractions. Leaf,  
 2102        stem, root, and root nodule nitrogen biomass was calculated as the product of  
 2103        the organ biomass and the respective organ nitrogen content. This calculation  
 2104        only quantifies plant structural carbon costs to acquire nitrogen and does not  
 2105        include any additional costs of nitrogen acquisition associated with respiration,  
 2106        root exudation, or root turnover. An explicit explanation of the limitations for  
 2107        interpreting this calculation can be found in Perkowski et al. (2021) and Terrer  
 2108        et al. (2018).

2109        Finally, plant investments in nitrogen fixation were calculated as the ratio  
 2110        of root nodule biomass to root biomass, where increasing values indicate an in-  
 2111        crease in plant investments to nitrogen fixation (Dovrat et al. 2018; Dovrat et al.  
 2112        2020; Perkowski et al. 2021). I also calculated the percent of leaf nitrogen ac-  
 2113        quired from the atmosphere (% $N_{dfa}$ ; %) using leaf δ<sup>15</sup>N and the following equation  
 2114        from Andrews et al. (2011):

$$\%N_{dfa} = \frac{\delta^{15}N_{reference} - \delta^{15}N_{sample}}{\delta^{15}N_{reference} - B} \quad (5.11)$$

2115 where  $\delta^{15}\text{N}_{\text{reference}}$  refers to a reference plant that exclusively acquires nitrogen via  
2116 direct uptake,  $\delta^{15}\text{N}_{\text{sample}}$  refers to an individual's leaf  $\delta^{15}\text{N}$ , and B refers to individuals  
2117 that are entirely reliant on nitrogen fixation. Within each unique nitrogen  
2118 fertilization treatment-by-CO<sub>2</sub> treatment combination, I calculated the mean leaf  
2119  $\delta^{15}\text{N}$  for individuals growing in the non-inoculated treatment for  $\delta^{15}\text{N}_{\text{reference}}$ . Any  
2120 individuals with visual confirmation of root nodule formation were omitted from  
2121 the calculation of  $\delta^{15}\text{N}_{\text{reference}}$ . Following recommendations from Andrews et al.  
2122 (2011) I calculated B within each CO<sub>2</sub> treatment using the mean leaf  $\delta^{15}\text{N}$  of  
2123 inoculated individuals that received 0 ppm N. I did not calculate B within each  
2124 unique soil nitrogen-by-CO<sub>2</sub> treatment combination, as previous studies suggest  
2125 decreased reliance on nitrogen fixation with increasing soil nitrogen availability  
2126 (Perkowski et al. 2021).

2127 5.2.9 *Statistical analyses*

2128 Uninoculated pots that had substantial root nodule formation (nodule biomass:  
2129 root biomass values greater than 0.05 g g<sup>-1</sup>) were removed from all analyses, as  
2130 pots were assumed to have been colonized by symbiotic nitrogen-fixing bacteria  
2131 from outside sources. This decision resulted in the removal of sixteen pots from  
2132 analyses: two pots in the elevated CO<sub>2</sub> treatment that received 35 ppm N, three  
2133 pots in the elevated CO<sub>2</sub> treatment that received 70 ppm N, one pot in the elevated  
2134 CO<sub>2</sub> treatment that received 210 ppm N, two pots in the elevated CO<sub>2</sub> treatment  
2135 that received 280 ppm N, two pots in the ambient CO<sub>2</sub> treatment that received  
2136 0 ppm N, three pots in the ambient CO<sub>2</sub> treatment that received 70 ppm N, two  
2137 pots in the ambient CO<sub>2</sub> treatment that received 105 ppm N, and one pot in the

2138 ambient CO<sub>2</sub> treatment that received 280 ppm N.

2139 I built a series of linear mixed effects models to investigate the impacts of  
2140 CO<sub>2</sub> concentration, soil nitrogen fertilization, and inoculation with *B. japonicum*  
2141 on *G. max* gas exchange, tradeoffs between nitrogen and water use, whole plant  
2142 growth, and investment in nitrogen fixation. All models included CO<sub>2</sub> treatment  
2143 as a categorical fixed effect, inoculation treatment as a categorical fixed effect,  
2144 soil nitrogen fertilization as a continuous fixed effect, with interaction terms be-  
2145 tween all three fixed effects. All models also accounted for climatic difference  
2146 between chambers across experiment iterations by including a random intercept  
2147 term that nested starting chamber rack by CO<sub>2</sub> treatment. Models with this  
2148 independent variable structure were created for each of the following dependent  
2149 variables:  $N_{\text{area}}$ ,  $M_{\text{area}}$ ,  $N_{\text{mass}}$ ,  $Chl_{\text{area}}$ ,  $V_{\text{cmax25}}$ ,  $J_{\text{max25}}$ ,  $J_{\text{max25}}:V_{\text{cmax25}}$ ,  $R_{\text{d25}}$ ,  $g_{\text{sw}}$ ,  
2150 stomatal limitation,  $\rho_{\text{rubisco}}$ ,  $\rho_{\text{bioe}}$ ,  $\rho_{\text{light}}$ ,  $\rho_{\text{photo}}$ ,  $\rho_{\text{structure}}$ , total biomass, total leaf  
2151 area,  $N_{\text{cost}}$ ,  $C_{\text{bg}}$ ,  $N_{\text{wp}}$ , nodule biomass, the ratio of nodule biomass to root biomass,  
2152 and % $N_{\text{dfa}}$ .

2153 I used Shapiro-Wilk tests of normality to determine whether linear mixed  
2154 effects models satisfied residual normality assumptions. If residual normality as-  
2155 sumptions were not met (Shapiro-Wilk:  $p < 0.05$ ), then models were fit using de-  
2156 pendent variables that were natural log transformed. If residual normality as-  
2157 sumptions were still not met (Shapiro-Wilk:  $p < 0.05$ ), then models were fit using  
2158 dependent variables that were square root transformed. All residual normality  
2159 assumptions that did not originally satisfy residual normality assumptions were  
2160 met with either a natural log or square root data transformation (Shapiro-Wilk:  
2161  $p > 0.05$  in all cases). Specifically, models for  $N_{\text{area}}$ ,  $N_{\text{mass}}$ ,  $Chl_{\text{area}}$ ,  $V_{\text{cmax25}}$ ,  $J_{\text{max25}}$ ,

**2162**  $J_{\max25}$ :  $V_{\text{cmax}25}$ ,  $R_{d25}$ ,  $g_{sw}$ , stomatal limitation,  $\rho_{\text{rubisco}}$ ,  $\rho_{\text{bioe}}$ ,  $\rho_{\text{light}}$ ,  $\rho_{\text{photo}}$ , total leaf  
**2163** area,  $N_{\text{cost}}$  satisfied residual normality assumptions without data transformation.  
**2164** Models for  $M_{\text{area}}$ ,  $\rho_{\text{structure}}$ ,  $C_{bg}$ , and total biomass satisfied residual normality as-  
**2165** sumptions with a natural log data transformation, while models for  $N_{wp}$ , nodule  
**2166** biomass, nodule biomass: root biomass, and  $\%N_{dfa}$  satisfied residual normality  
**2167** assumptions with a square root data transformation.

**2168** In all statistical models, I used the ‘lmer’ function in the ‘lme4’ R package  
**2169** (Bates et al. 2015) to fit each model and the ‘Anova’ function in the ‘car’ R  
**2170** package (Fox and Weisberg 2019) to calculate Type II Wald’s  $\chi^2$  and determine  
**2171** the significance ( $\alpha=0.05$ ) of each fixed effect coefficient. I used the ‘emmeans’  
**2172** R package (Lenth 2019) to conduct post-hoc comparisons using Tukey’s tests,  
**2173** where degrees of freedom were approximated using the Kenward-Roger approach  
**2174** (Kenward and Roger 1997). All analyses and plots were conducted in R version  
**2175** 4.2.0 (R Core Team 2021).

## **2176** 5.3 Results

### **2177** 5.3.1 Leaf nitrogen and chlorophyll content

**2178** Elevated CO<sub>2</sub> reduced  $N_{\text{area}}$ ,  $N_{\text{mass}}$ , and  $Chl_{\text{area}}$  by 29%, 50%, and 31%, respec-  
**2179** tively, and stimulated  $M_{\text{area}}$  by 44% ( $p<0.001$  in all cases; Table 5.1). An inter-  
**2180** action between fertilization and CO<sub>2</sub> (CO<sub>2</sub>-by-fertilization interaction:  $p_{N_{\text{area}}}=$   
**2181** 0.017,  $p_{N_{\text{mass}}}<0.001$ ,  $p_{Chl_{\text{area}}}=0.083$ ; Table 5.1) indicated that the positive effect  
**2182** of increasing fertilization on  $N_{\text{area}}$ ,  $N_{\text{mass}}$ , and  $Chl_{\text{area}}$  ( $p<0.001$  in all cases; Table  
**2183** 5.1) was stronger under ambient CO<sub>2</sub> (Tukey <sub>$N_{\text{area}}$</sub> :  $p=0.026$ ; Tukey <sub>$N_{\text{mass}}$</sub> :  $p<0.001$ ;  
**2184** Tukey <sub>$Chl_{\text{area}}$</sub> :  $p=0.065$ ; Table 5.1; Figs. 5.1a, 5.1b, 5.1d). An interaction between

2185 fertilization and CO<sub>2</sub> on  $M_{\text{area}}$  (CO<sub>2</sub>-by-fertilization interaction:  $p=0.006$ ; Ta-  
2186 ble 5.1) indicated that the positive effect of increasing fertilization on  $M_{\text{area}}$  was  
2187 stronger under elevated CO<sub>2</sub> (Tukey:  $p=0.009$ ; Fig. 5.1c). Overall, interactions  
2188 between fertilization and CO<sub>2</sub> resulted in stronger reductions in  $N_{\text{area}}$ ,  $N_{\text{mass}}$ , and  
2189  $Chl_{\text{area}}$ , and a stronger stimulation in  $M_{\text{area}}$  under elevated CO<sub>2</sub> with increasing  
2190 fertilization.

2191 An interaction between inoculation and CO<sub>2</sub> on  $N_{\text{area}}$  (CO<sub>2</sub>-by-inoculation  
2192 interaction:  $p=0.030$ ; Table 5.1) indicated that the positive effect of inoculation  
2193 on  $N_{\text{area}}$  ( $p<0.001$ ; Table 5.1) was stronger under elevated CO<sub>2</sub> (45% increase;  
2194 Tukey:  $p<0.001$ ) than under ambient CO<sub>2</sub> (18% increase; Tukey:  $p<0.001$ ), a  
2195 result that increased the reduction in  $N_{\text{area}}$  in inoculated pots under elevated  
2196 CO<sub>2</sub>. Inoculation treatment did not modify the downregulation in  $N_{\text{mass}}$  (CO<sub>2</sub>-  
2197 by-inoculation interaction:  $p=0.148$ ; Table 5.1) and  $Chl_{\text{area}}$  ( $p = 0.147$ ; Table  
2198 5.1) or the stimulation in  $M_{\text{area}}$  ( $p=0.866$ ; Table 5.1) under elevated CO<sub>2</sub>. How-  
2199 ever, interactions between fertilization and inoculation on  $N_{\text{area}}$ ,  $N_{\text{mass}}$ ,  $M_{\text{area}}$ ,  
2200 and  $Chl_{\text{area}}$  (fertilization-by-inoculation interaction:  $p_{N_{\text{area}}}<0.001$ ,  $p_{N_{\text{mass}}}=0.001$ ,  
2201  $p_{M_{\text{area}}}=0.025$ ,  $p_{Chl_{\text{area}}}=0.083$ ; Table 5.1) indicated that the positive effect of in-  
2202 creasing fertilization on each trait was stronger in uninoculated pots (Tukey <sub>$N_{\text{area}}$</sub> :  
2203  $p<0.001$ ; Tukey <sub>$N_{\text{mass}}$</sub> :  $p=0.001$ ; Tukey <sub>$M_{\text{area}}$</sub> :  $p=0.031$ ; Tukey <sub>$Chl_{\text{area}}$</sub> :  $p<0.001$ ;  
2204 Figs. 5.1a-d).

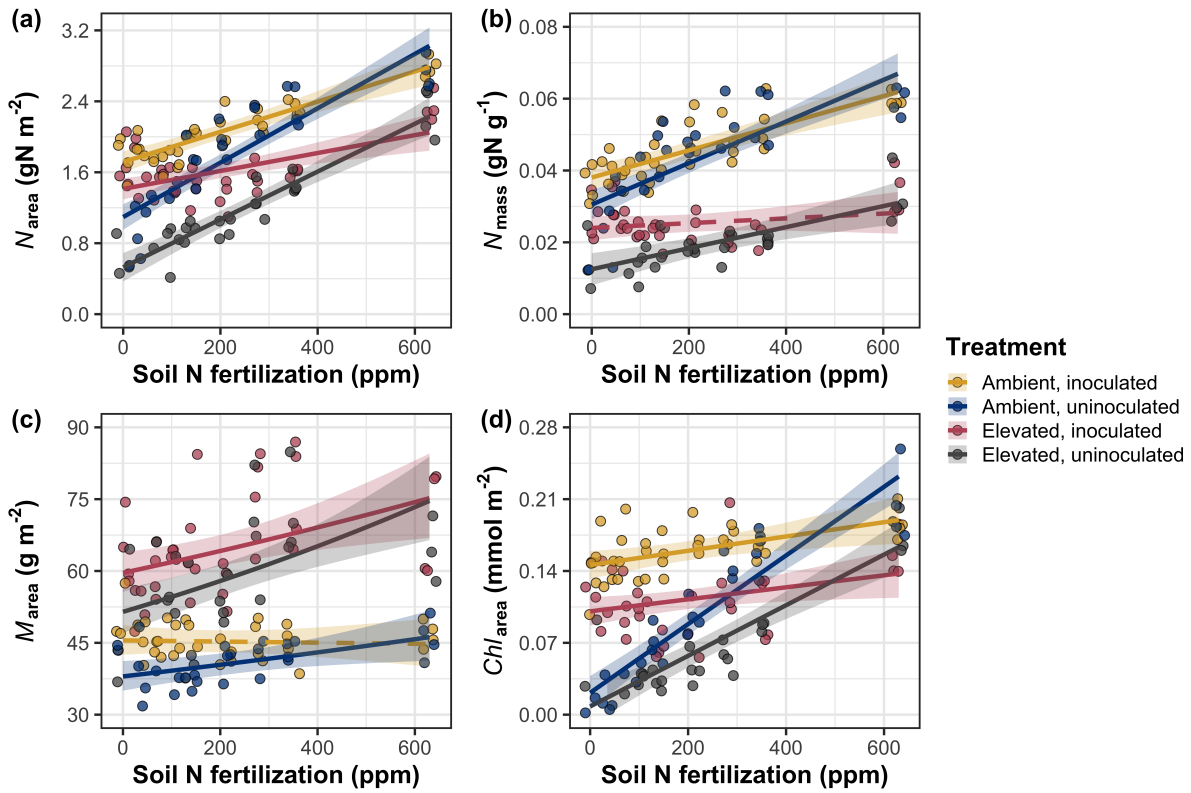
**Table 5.1.** Effects of soil nitrogen fertilization, inoculation, and CO<sub>2</sub> treatments on leaf nitrogen content per unit leaf area ( $N_{\text{area}}$ ; gN m<sup>-2</sup>), leaf nitrogen content per unit leaf mass ( $N_{\text{mass}}$ , gN g<sup>-1</sup>), leaf mass per unit leaf area ( $M_{\text{area}}$ ; g m<sup>-2</sup>), and chlorophyll content per unit leaf area ( $Chl_{\text{area}}$ ; mmol m<sup>-2</sup>)<sup>\*</sup>

	$N_{\text{area}}$			$N_{\text{mass}}$			$M_{\text{area}}^a$			
	df	Coefficient	$\chi^2$	p	Coefficient	$\chi^2$	p	Coefficient	$\chi^2$	p
(Intercept)	-	1.10E+00	-	-	3.05E-02	-	-	3.64E+00	-	-
CO <sub>2</sub>	1	-5.67E-01	155.908	<0.001	-1.80E-02	272.362	<0.001	3.04E-01	151.319	<0.001
Inoculation (I)	1	6.21E-01	86.029	<0.001	7.54E-03	15.576	<0.001	1.81E-01	19.158	<0.001
Fertilization (N)	1	3.06E-03	316.408	<0.001	5.78E-05	106.659	<0.001	3.10E-04	21.440	<0.001
CO <sub>2</sub> *I	1	2.63E-01	4.729	<b>0.030</b>	3.96E-03	2.025	0.155	-3.37E-02	0.029	0.866
CO <sub>2</sub> *N	1	-3.68E-04	5.723	<b>0.017</b>	-2.85E-05	22.542	<0.001	2.80E-04	7.619	<b>0.006</b>
I*N	1	-1.36E-03	43.381	<0.001	-2.00E-05	11.137	<b>0.001</b>	-3.36E-04	5.022	<b>0.025</b>
CO <sub>2</sub> *I*N	1	-3.23E-04	0.489	0.484	-2.59E-06	0.041	0.839	1.15E-04	0.208	0.649

	$Chl_{\text{area}}$			
	df	Coefficient	$\chi^2$	p
(Intercept)	-	2.13E-02	-	-
CO <sub>2</sub>	1	-1.33E-02	69.233	<0.001
Inoculation (I)	1	1.24E-01	136.341	<0.001
Fertilization (N)	1	3.35E-04	163.111	<0.001
CO <sub>2</sub> *I	1	-3.18E-02	2.102	0.147
CO <sub>2</sub> *N	1	-8.79E-05	2.999	0.083
I*N	1	-2.65E-04	75.769	<0.001
CO <sub>2</sub> *I*N	1	7.68E-05	2.144	0.147

2205 \*Significance determined using Type II Wald  $\chi^2$  tests ( $\alpha=0.05$ ). P-values less than 0.05 are in bold, while p-values  
 2206 between 0.05 and 0.1 are italicized. A superscript “a” is included after trait labels to indicate if models were fit with  
 2207 natural log transformed response variables. Key: df=degrees of freedom,  $\chi^2$ =Wald Type II chi-square test statistic.



**Figure 5.1.** Effects of  $\text{CO}_2$ , fertilization, and inoculation on leaf nitrogen per unit leaf area (a), leaf nitrogen content (b), leaf mass per unit leaf area (c), and chlorophyll content per unit leaf area (d). Soil nitrogen fertilization is represented on the x-axis in all panels. Yellow points and trendlines indicate inoculated individuals grown under ambient  $\text{CO}_2$ , blue points and trendlines indicate uninoculated individuals grown under ambient  $\text{CO}_2$ , red points and trendlines indicate inoculated individuals grown under elevated  $\text{CO}_2$ , and grey points indicate uninoculated individuals grown under elevated  $\text{CO}_2$ . Solid trendlines indicate regression slopes that are different from zero ( $p < 0.05$ ), while dashed trendlines indicate slopes that are not distinguishable from zero ( $p > 0.05$ ).

**2208** 5.3.2 *Leaf biochemistry and stomatal conductance*

**2209** Elevated CO<sub>2</sub> resulted in plants with 16% lower  $V_{cmax25}$  ( $p<0.001$ ; Table 5.2) and  
**2210** 10% lower  $J_{max25}$  ( $p=0.014$ ; Table 5.2) compared to those grown under ambient  
**2211** CO<sub>2</sub>. However, CO<sub>2</sub> concentration did not influence  $R_{d25}$  ( $p=0.613$ ; Table 5.2;  
**2212** Fig. 5.2d). A relatively stronger downregulation in  $V_{cmax25}$  than  $J_{max25}$  resulted  
**2213** in an 8% stimulation in  $J_{max25}:V_{cmax25}$  under elevated CO<sub>2</sub> ( $p<0.001$ ; Table 5.2).  
**2214** The downregulatory effect of CO<sub>2</sub> on  $V_{cmax25}$  and  $J_{max25}$  was not modified across  
**2215** the fertilization gradient (CO<sub>2</sub>-by-fertilization interaction:  $p=0.185$  and  $p=0.389$   
**2216** for  $V_{cmax25}$  and  $J_{max25}$ , respectively; Table 5.2; Figs. 5.2a, 5.2b) or between in-  
**2217** oculation treatments (CO<sub>2</sub>-by-inoculation interaction:  $p=0.799$  and  $p=0.714$  for  
**2218**  $V_{cmax25}$  and  $J_{max25}$ , respectively; Table 5.2). However, a strong interaction between  
**2219** fertilization and inoculation (fertilization-by-inoculation interaction:  $p\leq0.001$  in  
**2220** all cases; Table 5.2) indicated that the positive effect of increasing fertilization  
**2221** on  $V_{cmax25}$  ( $p<0.001$ ; Table 5.2),  $J_{max25}$  ( $p<0.001$ ; Table 5.2), and  $R_{d25}$  ( $p=0.015$ ;  
**2222** Table 5.2) was only observed in uninoculated pots (Tukey:  $p\leq0.001$  in all cases;  
**2223** Figs. 5.2a, 5.2b). A stronger positive effect of increasing fertilization on  $V_{cmax25}$   
**2224** than  $J_{max25}$  resulted in a reduction in  $J_{max25}:V_{cmax25}$  with increasing fertilization  
**2225** ( $p<0.001$ ; Table 5.2), though this pattern was only observed in uninoculated pots  
**2226** (fertilization-by-inoculation interaction:  $p=0.002$ ; Table 5.2; Fig. 5.2c).  
**2227** Elevated CO<sub>2</sub> reduced stomatal conductance by 20% ( $p<0.001$ ; Table 5.2;  
**2228** Fig. 5.2e), but this downregulation did not influence stomatal limitation of pho-  
**2229** tosynthesis ( $p=0.355$ ; Table 5.2; Fig. 5.2f). As with  $V_{cmax25}$  and  $J_{max25}$ , the down-  
**2230** regulation of stomatal conductance due to elevated CO<sub>2</sub> was not modified across  
**2231** the fertilization gradient (CO<sub>2</sub>-by-fertilization interaction:  $p=0.141$ ; Table 5.2) or

**2232** between inoculation treatments ( $\text{CO}_2$ -by-inoculation interaction:  $p=0.179$ ; Table  
**2233** 5.2). Fertilization also did not modify the null effect of  $\text{CO}_2$  on stomatal limitation  
**2234** ( $\text{CO}_2$ -by-fertilization interaction:  $p=0.554$ ; Table 5.2), although an interaction  
**2235** between  $\text{CO}_2$  and inoculation ( $\text{CO}_2$ -by-inoculation interaction:  $p=0.043$ ; Table  
**2236** 5.2) indicated that inoculation increased stomatal limitation under ambient  $\text{CO}_2$   
**2237** (Tukey:  $p=0.021$ ), but not under elevated  $\text{CO}_2$  (Tukey:  $p>0.999$ ). An interaction  
**2238** between inoculation and fertilization on stomatal conductance (fertilization-by-  
**2239** inoculation interaction:  $p<0.001$ ; Table 5.2) indicated that increasing fertilization  
**2240** increased stomatal conductance in uninoculated pots (Tukey:  $p=0.003$ ) but de-  
**2241** creased stomatal conductance in inoculated pots (Tukey:  $p=0.021$ ). The similar  
**2242** in magnitude, but opposite direction, trend in the effect of increasing fertiliza-  
**2243** tion on stomatal conductance between inoculation treatments likely drove a null  
**2244** response of stomatal conductance to increasing fertilization ( $p=0.642$ ; Table 5.2).

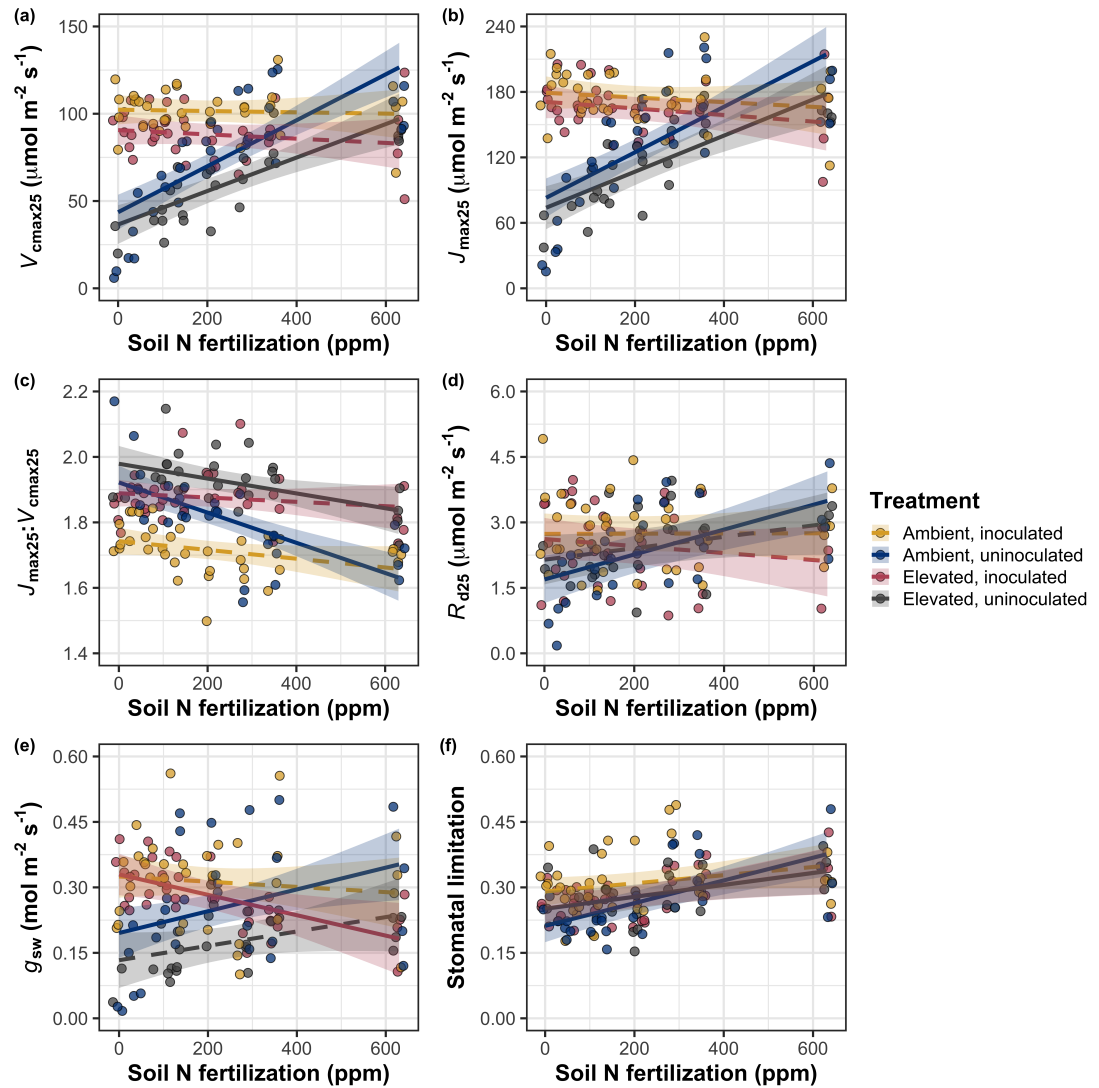
**Table 5.2.** Effects of soil nitrogen fertilization, inoculation, and CO<sub>2</sub> on the maximum rate of Rubisco carboxylation ( $V_{\text{cmax}25}$ ;  $\mu\text{mol m}^{-2} \text{s}^{-1}$ ), the maximum rate of RuBP regeneration ( $J_{\text{max}25}$ ;  $\mu\text{mol m}^{-2} \text{s}^{-1}$ ), dark respiration ( $R_{\text{d}25}$ ;  $\mu\text{mol m}^{-2} \text{s}^{-1}$ ), the ratio of the maximum rate of RuBP regeneration to the maximum rate of Rubisco carboxylation ( $J_{\text{max}25}:V_{\text{cmax}25}$ ; unitless), stomatal conductance ( $g_{\text{sw}}$ ;  $\text{mol m}^{-2} \text{s}^{-1}$ ), and stomatal limitation (unitless)\*

	$V_{\text{cmax}25}$			$J_{\text{max}25}$			$R_{\text{d}25}$			
	df	Coefficient	$\chi^2$	p	Coefficient	$\chi^2$	p	Coefficient	$\chi^2$	p
(Intercept)	-	4.36E+01	-	-	8.30E+01	-	-	1.69E+00	-	-
CO <sub>2</sub>	1	-7.05E+00	18.039	<0.001	-9.11E+00	6.042	0.014	4.53E-01	0.256	0.613
Inoculation (I)	1	5.87E+01	98.579	<0.001	9.62E+01	85.064	<0.001	1.04E+00	3.094	0.079
Fertilization (N)	1	1.32E-01	37.053	<0.001	2.09E-01	25.356	<0.001	2.86E-03	5.965	0.015
CO <sub>2</sub> *I	1	-4.65E+00	0.065	0.799	7.84E-01	0.667	0.414	-5.71E-01	2.563	0.109
CO <sub>2</sub> *N	1	-3.58E-02	1.758	0.185	-4.33E-02	0.742	0.389	-1.55E-03	2.675	0.102
I*N	1	-1.35E-01	60.394	<0.001	-2.30E-01	57.410	<0.001	-2.84E-03	12.083	0.001
CO <sub>2</sub> *I*N	1	2.73E-02	0.748	0.387	3.46E-02	0.377	0.539	7.21E-04	0.244	0.622

	$J_{\text{max}25}:V_{\text{cmax}25}$			$g_{\text{sw}}$			Stomatal limitation			
	df	Coefficient	$\chi^2$	p	Coefficient	$\chi^2$	p	Coefficient	$\chi^2$	p
(Intercept)	-	1.92E+00	-	-	1.95E-01	-	-	2.12E-01	-	-
CO <sub>2</sub>	1	5.71E-02	92.010	<0.001	-6.23E-02	9.718	0.002	3.91E-02	0.856	0.355
Inoculation (I)	1	-1.79E-01	27.768	<0.001	1.30E-01	22.351	<0.001	7.87E-02	4.582	0.032
Fertilization (N)	1	-4.61E-04	28.147	<0.001	2.50E-04	0.066	0.797	2.60E-04	32.218	<0.001
CO <sub>2</sub> *I	1	8.94E-02	2.916	0.088	6.69E-02	1.810	0.179	-7.84E-02	4.093	0.043
CO <sub>2</sub> *N	1	2.35E-04	3.210	0.073	-8.50E-05	2.165	0.141	-1.24E-04	0.350	0.554
I*N	1	3.27E-04	9.607	0.002	-3.09E-04	14.696	<0.001	-1.67E-04	2.547	0.110
CO <sub>2</sub> *I*N	1	-1.66E-04	1.102	0.294	-8.89E-05	0.234	0.629	1.67E-04	2.231	0.135

2245 \*Significance determined using Type II Wald  $\chi^2$  tests ( $\alpha=0.05$ ). P-values less than 0.05 are in bold, while p-values  
 2246 between 0.05 and 0.1 are italicized. Key: df=degrees of freedom;  $\chi^2$ =Wald Type II chi-square test statistic.



**Figure 5.2.** Effects of CO<sub>2</sub>, fertilization, and inoculation on maximum rate of Rubisco carboxylation (a), the maximum rate of RuBP regeneration (b), and the ratio of the maximum rate of RuBP regeneration to the maximum rate of Rubisco carboxylation leaf mass per unit leaf area (c), dark respiration (d), stomatal conductance (e), and stomatal limitation (f). Soil nitrogen fertilization is represented on the x-axis in all panels. Colored points and trendlines are as explained in Figure 5.1.

**2247** 5.3.3 *Leaf nitrogen allocation*

**2248** A relatively stronger downregulation in  $N_{\text{area}}$  than  $V_{\text{cmax}25}$  and  $J_{\text{max}25}$  resulted in  
**2249** an 20% and 29% respective stimulation in  $\rho_{\text{rubisco}}$  and  $\rho_{\text{bioe}}$  under elevated CO<sub>2</sub>  
**2250** ( $p<0.001$  in both cases; Table 5.3). There was no effect of CO<sub>2</sub> on  $\rho_{\text{light}}$  ( $p=0.700$ ;  
**2251** Table 5.3), but the stimulation in  $\rho_{\text{rubisco}}$  and  $\rho_{\text{bioe}}$  resulted in a 21% stimulation  
**2252** of  $\rho_{\text{photo}}$  under elevated CO<sub>2</sub> ( $p<0.001$ ; Table 5.3; Fig. 5.3a). The stimulation  
**2253** of  $\rho_{\text{rubisco}}$ ,  $\rho_{\text{bioe}}$ , and  $\rho_{\text{photo}}$  under elevated CO<sub>2</sub> was not modified across the fer-  
**2254** tilization gradient (CO<sub>2</sub>-by-fertilization interaction:  $p_{\text{rubisco}}=0.269$ ,  $p_{\text{bioe}}=0.298$ ,  
**2255**  $p_{\text{photo}}=0.281$ ; Table 5.3). A marginal interaction between inoculation and CO<sub>2</sub> on  
**2256**  $\rho_{\text{rubisco}}$  and  $\rho_{\text{photo}}$  (CO<sub>2</sub>-by-inoculation interaction:  $p_{\text{rubisco}}=0.057$ ,  $p_{\text{photo}}=0.055$ ;  
**2257** Table 5.3) indicated that the positive effect of inoculation on  $\rho_{\text{rubisco}}$  and  $\rho_{\text{photo}}$   
**2258** ( $p<0.001$  in both cases; Table 5.3) was only apparent under ambient CO<sub>2</sub> (Tukey:  
**2259**  $p<0.001$  in both cases). Inoculation did not modify the stimulation of  $\rho_{\text{bioe}}$  un-  
**2260** der elevated CO<sub>2</sub> (CO<sub>2</sub>-by-inoculation interaction:  $p=0.122$ ; Table 5.3) or the  
**2261** null effect of CO<sub>2</sub> on  $\rho_{\text{bioe}}$  (CO<sub>2</sub>-by-inoculation interaction:  $p=0.298$ ; Table 5.3).  
**2262** An interaction between fertilization and inoculation on  $\rho_{\text{rubisco}}$ ,  $\rho_{\text{bioe}}$ , and  $\rho_{\text{photo}}$   
**2263** (fertilization-by-inoculation interaction:  $p<0.001$  in all cases; Table 5.3) indicated  
**2264** that the negative effect of increasing fertilization on each trait ( $p<0.001$  in all  
**2265** cases; Table 5.3) was only observed in inoculated pots (Tukey:  $p<0.001$  in all  
**2266** cases). An additional interaction between fertilization and inoculation on  $\rho_{\text{light}}$   
**2267** (fertilization-by-inoculation interaction:  $p<0.001$ ; Table 5.3) indicated a negative  
**2268** effect of increasing fertilization on  $\rho_{\text{light}}$  in inoculated pots (Tukey:  $p=0.041$ ), but  
**2269** a positive effect of increasing fertilization in uninoculated pots (Tukey:  $p<0.001$ ).  
**2270** The stimulation in  $M_{\text{area}}$  under elevated CO<sub>2</sub> resulted in an 133% stimu-

2271 lation of  $\rho_{\text{structure}}$  ( $p<0.001$ ; Table 5.3; Fig 5.3b). An interaction between fertil-  
2272 ization and CO<sub>2</sub> (CO<sub>2</sub>-by-fertilization interaction:  $p=0.039$ ; Table 5.3) indicated  
2273 that the negative effect of increasing fertilization ( $p<0.001$ ; Table 5.3) on  $\rho_{\text{structure}}$   
2274 was marginally stronger under ambient CO<sub>2</sub> (Tukey:  $p=0.055$ ). A marginal inter-  
2275 action between inoculation and CO<sub>2</sub> (CO<sub>2</sub>-by-inoculation interaction:  $p=0.057$ ;  
2276 Table 5.3) indicated that the positive effect of inoculation on  $\rho_{\text{structure}}$  ( $p<0.001$ ;  
2277 Table 5.3) was only observed under elevated CO<sub>2</sub> (Tukey:  $p<0.001$ ), with no ap-  
2278 parent inoculation effect observed under ambient CO<sub>2</sub> (Tukey:  $p=0.513$ ). Finally,  
2279 an interaction between fertilization and inoculation (fertilization-by-inoculation  
2280 interaction:  $p<0.001$ ; Table 5.3) indicated that, while increasing fertilization in-  
2281 creased  $\rho_{\text{structure}}$  ( $p<0.001$ ; Table 5.3), this response was stronger in uninoculated  
2282 pots (Tukey:  $p=0.001$ ; Fig. 5.3b).

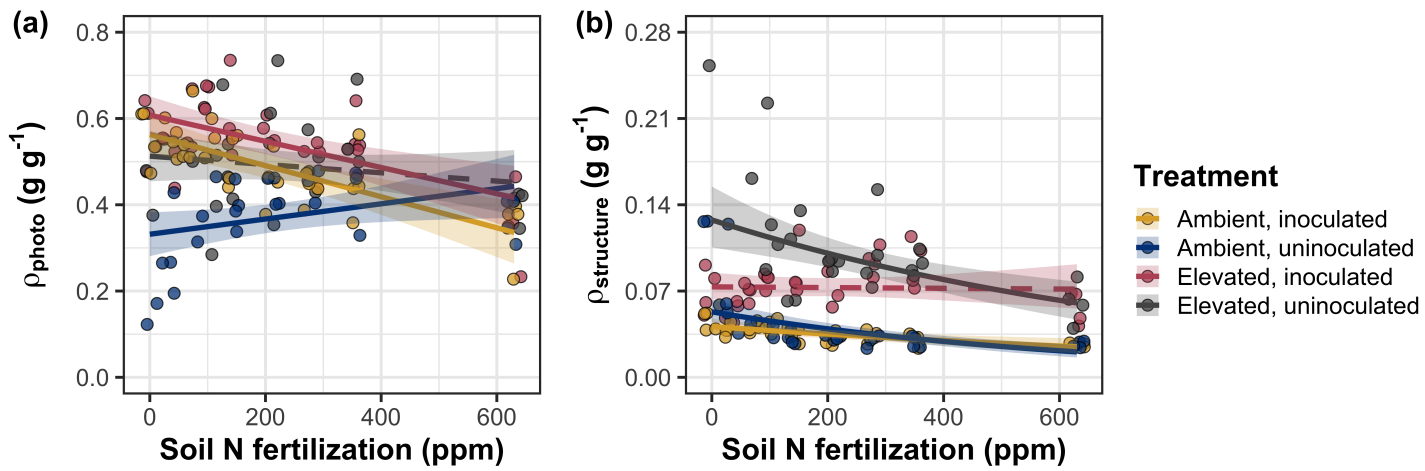
**Table 5.3.** Effects of soil nitrogen fertilization, inoculation, and CO<sub>2</sub> on the fraction of leaf nitrogen allocated to Rubisco ( $\rho_{\text{rubisco}}$ ; gN gN<sup>-1</sup>), bioenergetics ( $\rho_{\text{bioe}}$ ; gN gN<sup>-1</sup>), light harvesting proteins ( $\rho_{\text{light}}$ ; gN gN<sup>-1</sup>), photosynthesis ( $\rho_{\text{photo}}$ ; gN gN<sup>-1</sup>), and structure ( $\rho_{\text{structure}}$ ; gN gN<sup>-1</sup>)\*

	$\rho_{\text{rubisco}}$			$\rho_{\text{bioe}}$			$\rho_{\text{light}}$			
	df	Coefficient	$\chi^2$	p	Coefficient	$\chi^2$	p	Coefficient	$\chi^2$	p
(Intercept)	-	2.70E-01	-	-	5.26E-02	-	-	8.48E-03	-	-
CO <sub>2</sub>	1	1.42E-01	23.510	<0.001	3.00E-02	53.899	<0.001	2.03E-03	0.149	0.700
Inoculation (I)	1	1.83E-01	23.475	<0.001	2.80E-02	13.860	<0.001	2.04E-02	147.234	<0.001
Fertilization (N)	1	1.35E-04	16.609	<0.001	1.22E-05	26.827	<0.001	3.22E-05	19.378	<0.001
CO <sub>2</sub> *I	1	-1.07E-01	3.629	0.057	-1.67E-02	2.390	0.122	-5.33E-03	0.684	0.408
CO <sub>2</sub> *N	1	-2.16E-04	1.223	0.269	-3.59E-05	1.085	0.298	-7.01E-06	0.351	0.553
I*N	1	-4.26E-04	20.045	<0.001	-6.87E-05	15.458	<0.001	-4.37E-05	64.042	<0.001
CO <sub>2</sub> *I*N	1	2.50E-04	3.327	0.068	4.08E-05	2.651	0.103	1.74E-05	3.735	0.053

	$\rho_{\text{photo}}$			$\rho_{\text{structure}}^a$			
	df	Coefficient	$\chi^2$	p	Coefficient	$\chi^2$	p
(Intercept)	-	3.32E-01	-	-	-2.93E+00	-	-
CO <sub>2</sub>	1	1.81E-01	27.651	<0.001	8.77E-01	229.571	<0.001
Inoculation (I)	1	2.31E-01	26.238	<0.001	-2.55E-01	13.872	<0.001
Fertilization (N)	1	1.76E-04	15.899	<0.001	-1.51E-03	38.128	<0.001
CO <sub>2</sub> *I	1	-1.36E-01	3.671	0.055	-2.99E-01	3.622	0.057
CO <sub>2</sub> *N	1	-2.72E-04	1.163	0.281	3.14E-04	4.266	0.039
I*N	1	-5.37E-04	21.355	<0.001	7.00E-04	11.025	0.001
CO <sub>2</sub> *I*N	1	3.29E-04	4.009	0.045	4.52E-04	0.669	0.413

2283 \*Significance determined using Type II Wald  $\chi^2$  tests ( $\alpha=0.05$ ). P-values less than 0.05 are in bold, while p-values  
 2284 between 0.05 and 0.1 are italicized. A superscript “a” is included after trait labels to indicate if models were fit with  
 2285 natural log transformed response variable. Key: df=degrees of freedom;  $\chi^2$ =Wald Type II chi-square test statistic.



**Figure 5.3.** Effects of  $\text{CO}_2$ , fertilization, and inoculation on the relative fraction of leaf nitrogen allocated to photosynthesis (a) and the fraction of leaf nitrogen allocated to structure (b). Soil nitrogen fertilization is represented on the x-axis in both panels. Colored points and trendlines are as explained in Figure 5.1.

**2286** 5.3.4 *Whole plant traits*

**2287** Total leaf area and total biomass were 51% and 102% greater under elevated CO<sub>2</sub>,  
**2288** respectively ( $p<0.001$  in both cases; Table 5.4). The stimulation in total leaf area  
**2289** and total biomass under elevated CO<sub>2</sub> was enhanced by increasing fertilization  
**2290** (CO<sub>2</sub>-by-fertilization interaction:  $p<0.001$  in both cases; Table 5.4; Figs. 5.4a,  
**2291** 5.4b) but was not modified across inoculation treatments (CO<sub>2</sub>-by-inoculation  
**2292** interaction:  $p_{total\_leaf\_area}=0.151$ ,  $p_{total\_biomass}=0.472$ ; Table 5.4). The positive  
**2293** effect of increasing fertilization on total leaf area and total biomass was modified by  
**2294** inoculation treatment (fertilization-by-inoculation interaction:  $p<0.001$  in both  
**2295** cases; Table 5.4), indicating a stronger positive effect of increasing fertilization in  
**2296** uninoculated pots (Tukey:  $p_{total\_leaf\_area}=0.002$ ,  $p_{total\_biomass}=0.001$ , Figs. 5.4a,  
**2297** 5.4b).

**2298** A 62% stimulation in  $N_{cost}$  under elevated CO<sub>2</sub> was modified through a  
**2299** strong three-way interaction between CO<sub>2</sub>, fertilization, and inoculation (CO<sub>2</sub>-  
**2300** by-inoculation-by-fertilization interaction:  $p<0.001$ ; Table 5.4; Fig. 5.4). This  
**2301** interaction revealed a general negative effect of increasing fertilization on  $N_{cost}$   
**2302** ( $p<0.001$ ; Table 5.4) that was observed in all treatment combinations (Tukey:  
**2303**  $p<0.001$  in all cases) except for inoculated pots grown under elevated CO<sub>2</sub> (Tukey:  
**2304**  $p=0.779$ ; Fig. 5.4c). This response also resulted in stronger negative effects of in-  
**2305** creasing fertilization on  $N_{cost}$  in uninoculated pots grown under elevated CO<sub>2</sub> than  
**2306** uninoculated pots grown under ambient CO<sub>2</sub> (Tukey:  $p=0.001$ ) and inoculated  
**2307** pots grown under either ambient CO<sub>2</sub> (Tukey:  $p<0.001$ ) or elevated CO<sub>2</sub> (Tukey:  
**2308**  $p<0.001$ ), while uninoculated pots grown under ambient CO<sub>2</sub> had stronger nega-  
**2309** tive effects of increasing fertilization on  $N_{cost}$  than inoculated pots grown under

**2310** elevated CO<sub>2</sub> (Tukey:  $p=0.002$ ), but not inoculated pots grown under ambient  
**2311** CO<sub>2</sub> (Tukey:  $p=0.216$ ; Fig. 5.4). The reduction in  $N_{\text{cost}}$  with increasing fertiliza-  
**2312** tion and in uninoculated pots were driven by a stronger positive effect of increasing  
**2313** fertilization on  $N_{\text{wp}}$  (denominator of  $N_{\text{cost}}$ ) than  $C_{\text{bg}}$  (numerator of  $N_{\text{cost}}$ ), while  
**2314** the stimulation in  $N_{\text{cost}}$  under elevated CO<sub>2</sub> was driven by a stronger positive  
**2315** effect of elevated CO<sub>2</sub> on  $C_{\text{bg}}$  than  $N_{\text{wp}}$  (Table 5.4).

**Table 5.4.** Effects of CO<sub>2</sub>, fertilization, and inoculation on total leaf area (cm<sup>2</sup>), whole plant biomass (g), carbon costs to acquire nitrogen ( $N_{\text{cost}}$ ; gC gN<sup>-1</sup>), belowground carbon biomass ( $C_{\text{bg}}$ ; gC), and whole plant nitrogen biomass ( $N_{\text{wp}}$ ; gN)\*

	Total leaf area			Total biomass <sup>b</sup>			<i>N</i> <sub>cost</sub>			
	df	Coefficient	$\chi^2$	p	Coefficient	$\chi^2$	p	Coefficient	$\chi^2$	p
(Intercept)	-	8.78E+01	-	-	9.96E-01	-	-	8.67E+00	-	-
CO <sub>2</sub>	1	3.36E+01	69.291	<0.001	5.07E-01	131.477	<0.001	8.75E+00	88.189	<0.001
Inoculation (I)	1	1.88E+02	35.715	<0.001	7.96E-01	34.264	<0.001	-1.68E+00	136.343	<0.001
Fertilization (N)	1	9.35E-01	274.199	<0.001	3.14E-03	269.046	<0.001	-8.50E-03	80.501	<0.001
CO <sub>2</sub> *I	1	6.44E+01	2.064	0.151	-7.69E-02	0.518	0.472	-8.38E+00	85.237	<0.001
CO <sub>2</sub> *N	1	5.05E-01	18.655	<0.001	1.61E-03	16.877	<0.001	-9.17E-03	1.050	0.306
I*N	1	-3.84E-01	10.804	0.001	-1.45E-03	15.779	<0.001	4.20E-03	46.489	<0.001
CO <sub>2</sub> *I*N	1	-2.97E-03	<0.001	0.990	-1.14E-04	0.023	0.880	1.32E-02	18.125	<0.001

141

	$C_{\text{bg}}^{\text{a}}$		$N_{\text{wp}}^{\text{b}}$				
	df	Coefficient	$\chi^2$	p	Coefficient	$\chi^2$	p
(Intercept)	-	-1.70E+00	-	-	1.24E-01	-	-
CO <sub>2</sub>	1	9.21E-01	84.134	<0.001	-3.41E-03	23.890	<0.001
Inoculation (I)	1	1.18E+00	41.030	<0.001	1.68E-01	134.460	<0.001
N fertilization (N)	1	3.38E-03	152.248	<0.001	6.69E-04	529.021	<0.001
CO <sub>2</sub> * I	1	-6.18E-01	8.965	<b>0.003</b>	3.68E-02	1.190	0.275
CO <sub>2</sub> * N	1	-3.66E-05	1.188	0.276	1.58E-04	5.915	<b>0.015</b>
I * N	1	-2.22E-03	22.648	<0.001	-3.20E-04	55.562	<0.001
CO <sub>2</sub> * I * N	1	8.09E-04	1.109	0.292	-7.54E-05	0.620	0.431

**2316** \*Significance determined using Type II Wald  $\chi^2$  tests ( $\alpha=0.05$ ). *P*-values less than 0.05 are in bold. Superscripts  
**2317** included after trait labels indicate if models were fit with natural log (<sup>a</sup>) or square root (<sup>b</sup>) transformed response  
**2318** variables. Key: df=degrees of freedom;  $\chi^2$ =Wald Type II chi-square test statistic.

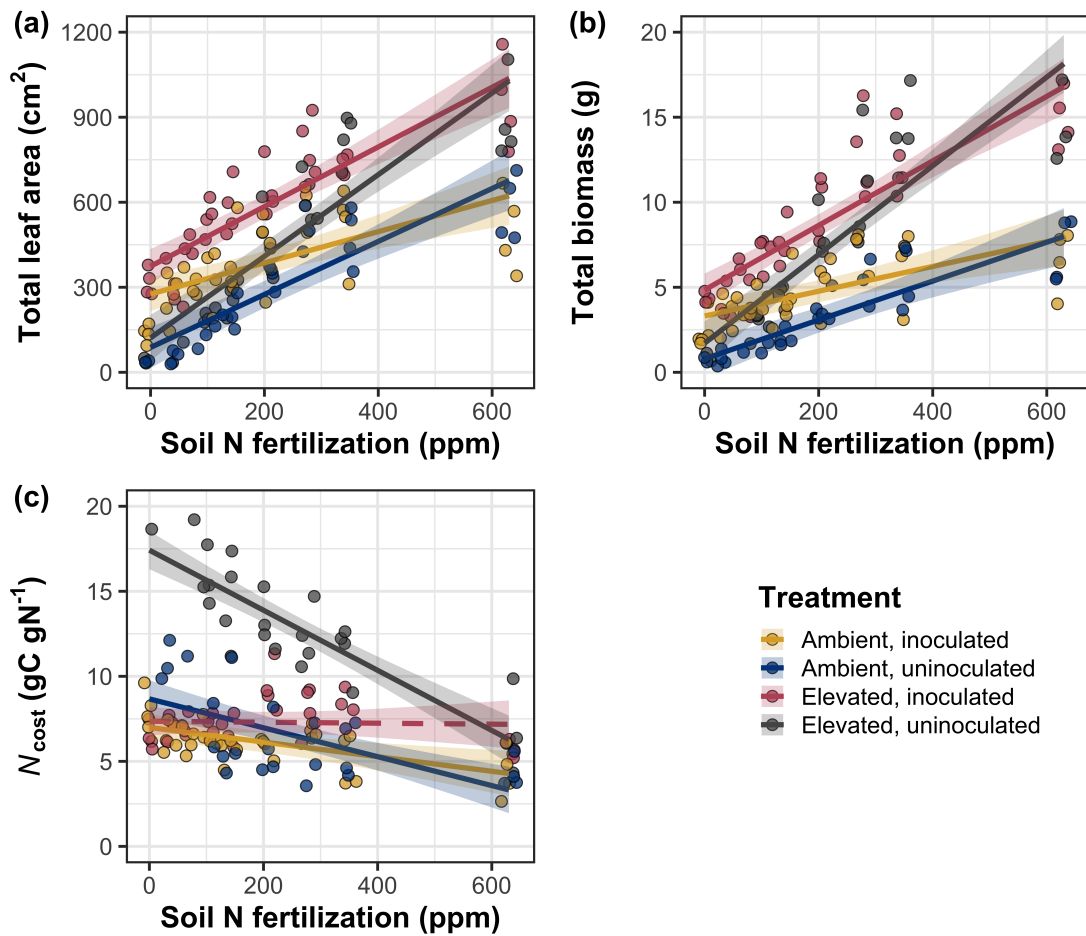


**Figure 5.4.** Effects of CO<sub>2</sub>, fertilization, and inoculation on total leaf area (a), total biomass (b), and structural carbon costs to acquire nitrogen (c). Soil nitrogen fertilization is represented on the x-axis in all panels. Colored points and trendlines are as explained in Figure 5.1.

**2319** 5.3.5 *Nitrogen fixation*

**2320** Nodule biomass was stimulated by 30% under elevated CO<sub>2</sub> ( $p<0.001$ ; Table 5.5),  
**2321** a pattern that was modified across the fertilization gradient (CO<sub>2</sub>-by-fertilization  
**2322** interaction:  $p=0.479$ ; Table 5.5), but not between inoculation treatments (CO<sub>2</sub>-  
**2323** by-inoculation interaction:  $p=0.404$ ; Table 5.5). Specifically, the negative effect  
**2324** of increasing fertilization on nodule biomass ( $p<0.001$ ; Table 5.5) was stronger  
**2325** under elevated CO<sub>2</sub> (Tukey:  $p<0.001$ ; Fig. 5.5a). An interaction between fertil-  
**2326** ization and inoculation (fertilization-by-inoculation interaction:  $p<0.001$ ; Table  
**2327** 5.5) indicated a stronger negative effect of increasing fertilization in inoculated  
**2328** pots (Tukey:  $p<0.001$ ; Fig. 5.5a).

**2329** There was no effect of CO<sub>2</sub> on nodule: root biomass ( $p=0.767$ ; Table 5.5),  
**2330** although an interaction between CO<sub>2</sub> and inoculation (CO<sub>2</sub>-by-inoculation in-  
**2331** teraction:  $p<0.001$ ; Table 5.5) indicated that the positive effect of inoculation  
**2332** on nodule: root biomass ( $p<0.001$ ; Table 5.5) was stronger under ambient CO<sub>2</sub>  
**2333** (3129% increase; Tukey:  $p<0.001$ ) than elevated CO<sub>2</sub> (379% increase; Tukey:  
**2334**  $p<0.001$ ; Fig. 5.5b). The null effect of CO<sub>2</sub> on nodule: root biomass was consis-  
**2335** tently observed across the fertilization gradient (CO<sub>2</sub>-by-fertilization interaction:  
**2336**  $p=0.183$ ; Table 5.5; Fig. 5.5b). An interaction between fertilization and inocula-  
**2337** tion (fertilization-by-inoculation interaction:  $p<0.001$ ; Table 5.5) indicated that  
**2338** the negative effect of increasing fertilization on nodule: root biomass ( $p<0.001$ ;  
**2339** Table 5.5) was stronger in inoculated pots (Tukey:  $p<0.001$ ; Fig. 5.5b).

**2340** There was no effect of CO<sub>2</sub> on %N<sub>dfa</sub> ( $p=0.472$ ; Table 5.5), a pattern  
**2341** that was not modified by inoculation (CO<sub>2</sub>-by-inoculation interaction:  $p=0.156$ ;  
**2342** Table 5.5) or fertilization (CO<sub>2</sub>-by-fertilization interaction:  $p=0.099$ ; Table 5.5).

- 2343** An interaction between fertilization and inoculation (fertilization-by-inoculation  
**2344** interaction:  $p<0.001$ ; Table 5.5) indicated that the negative effect of increasing  
**2345** fertilization on  $\%N_{dfa}$  ( $p<0.001$ ; Table 5.5) was only observed in inoculated pots  
**2346** (Tukey:  $p<0.001$ ; Fig. 5.5c).

**Table 5.5.** Effects of CO<sub>2</sub>, fertilization, and inoculation on root nodule biomass (g), plant investments in symbiotic nitrogen fixation (unitless), and percent nitrogen fixed from the atmosphere (%N<sub>dfa</sub>; unitless)\*

	Root nodule biomass <sup>b</sup>			Root nodule: root biomass <sup>b</sup>			%N <sub>dfa</sub> <sup>b</sup>			
	df	Coefficient	$\chi^2$	p	Coefficient	$\chi^2$	p	Coefficient	$\chi^2$	p
(Intercept)	-	9.41E-03	-	-	1.33E-02	-	-	7.48E-01	-	-
CO <sub>2</sub>	1	1.20E-01	19.258	<b>&lt;0.001</b>	9.94E-02	0.087	0.768	-1.00E-01	0.518	0.472
Inoculation (I)	1	5.74E-01	755.020	<b>&lt;0.001</b>	5.40E-01	903.691	<b>&lt;0.001</b>	9.01E+00	955.570	<b>&lt;0.001</b>
Fertilization (N)	1	7.71E-06	84.376	<b>&lt;0.001</b>	-5.99E-06	258.099	<b>&lt;0.001</b>	3.64E-04	292.938	<b>&lt;0.001</b>
CO <sub>2</sub> *I	1	-4.68E-02	0.950	0.330	-1.38E-01	20.614	<b>&lt;0.001</b>	-1.44E-01	2.010	0.156
CO <sub>2</sub> *N	1	-1.59E-04	2.106	0.147	-1.73E-04	1.773	0.183	-6.21E-05	2.716	0.099
I*N	1	-5.82E-04	44.622	<b>&lt;0.001</b>	-7.45E-04	133.918	<b>&lt;0.001</b>	-1.58E-02	231.290	<b>&lt;0.001</b>
CO <sub>2</sub> *I*N	1	7.26E-05	0.196	0.658	1.76E-04	2.359	0.125	2.77E-03	2.119	0.145

2347 \*Significance determined using Type II Wald  $\chi^2$  tests ( $\alpha=0.05$ ). P-values less than 0.05 are in bold, while p-values  
 2348 between 0.05 and 0.1 are italicized. Superscript letters indicate model coefficients fit to square-root (<sup>b</sup>) transformed  
 2349 data. Key: df=degrees of freedom;  $\chi^2$ =Wald Type II chi-square test statistic.

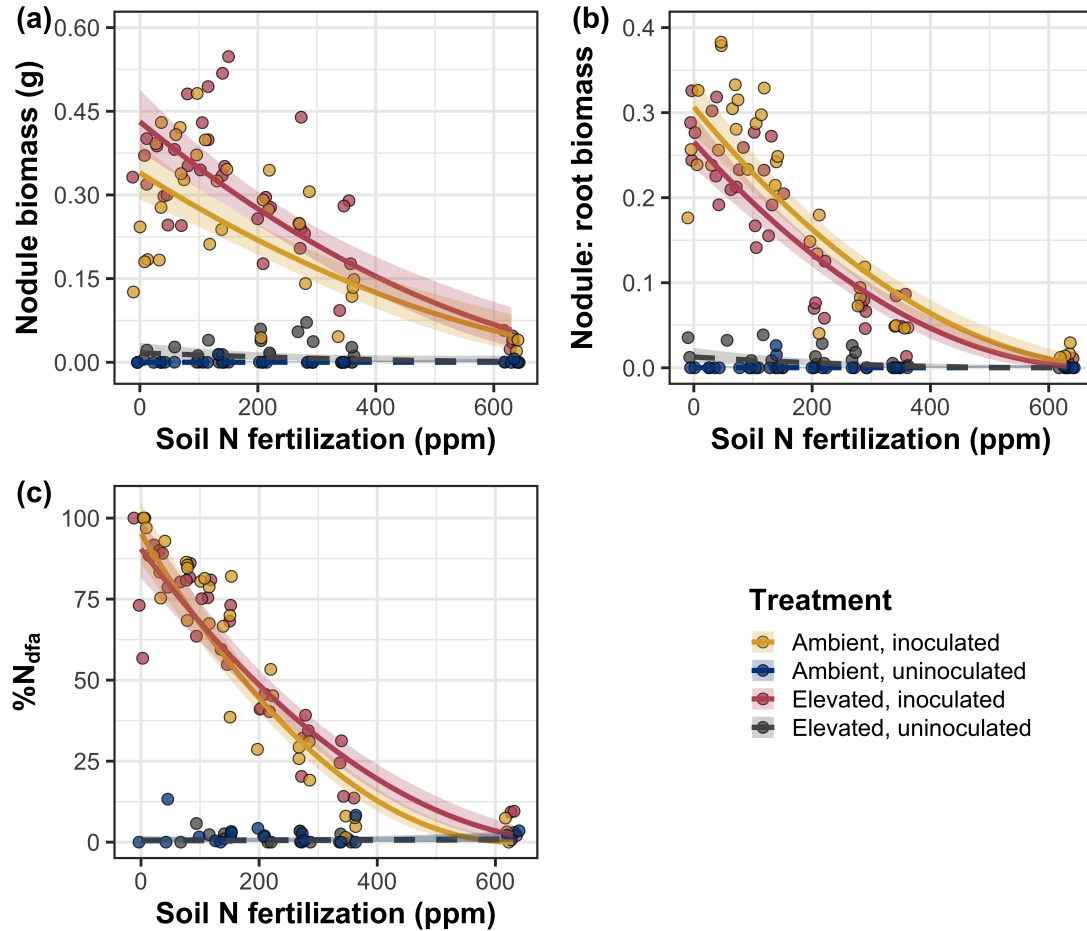


**Figure 5.5.** Effects of CO<sub>2</sub>, fertilization, and inoculation on nodule biomass (a), nodule biomass: root biomass (b), and percent nitrogen fixed from the atmosphere (c). Soil nitrogen fertilization is represented on the x-axis. Colored points and trendlines are as explained in Figure 5.1. Curvilinear trendlines occur as a result of back-transforming models where response variables received either a natural log or square root transformation prior to fitting.

**2350** 5.4 Discussion

**2351** In this study, I determined leaf and whole plant acclimation responses of 7-week *G.*  
**2352** *max* seedlings grown under two CO<sub>2</sub> concentrations, two inoculation treatments,  
**2353** and nine soil nitrogen fertilization treatments in a full-factorial growth chamber  
**2354** experiment. In support of hypotheses and patterns expected from theory, elevated  
**2355** CO<sub>2</sub> reduced  $N_{\text{area}}$ ,  $V_{\text{cmax25}}$ , and  $J_{\text{max25}}$ . The relatively stronger downregulation in  
**2356**  $V_{\text{cmax25}}$  than  $J_{\text{max25}}$  under elevated CO<sub>2</sub> resulted in a stimulation in  $J_{\text{max25}}:V_{\text{cmax25}}$   
**2357** under elevated CO<sub>2</sub>. The downregulation of  $V_{\text{cmax25}}$  and  $J_{\text{max25}}$  under elevated  
**2358** CO<sub>2</sub> was similar across fertilization and inoculation treatments, indicating that  
**2359** the CO<sub>2</sub> responses were not associated with nitrogen limitation. Interestingly,  
**2360** results indicate that elevated CO<sub>2</sub> increased the fraction of leaf nitrogen allocated  
**2361** to photosynthesis and structure, leading to a stimulation in nitrogen use efficiency  
**2362** under elevated CO<sub>2</sub> despite the apparent downregulation in  $N_{\text{area}}$ ,  $V_{\text{cmax25}}$ , and  
**2363**  $J_{\text{max25}}$ .

**2364** The downregulation in leaf photosynthetic processes under elevated CO<sub>2</sub>  
**2365** corresponded with a strong stimulation in total leaf area and total biomass. Strong  
**2366** stimulations in whole plant growth due to elevated CO<sub>2</sub> were generally enhanced  
**2367** with increasing fertilization and were negatively related to structural carbon costs  
**2368** to acquire nitrogen. Inoculation generally did not modify whole plant responses  
**2369** to elevated CO<sub>2</sub> across the fertilization gradient, likely due to a strong reduc-  
**2370** tion in root nodulation with increasing fertilization. However, strong positive  
**2371** effects of inoculation on whole plant growth were observed under low fertilization,  
**2372** consistent with hypotheses. Overall, observed leaf and whole plant acclimation  
**2373** responses to CO<sub>2</sub> support hypotheses and patterns expected from photosynthetic

2374 least-cost theory, showing that leaf acclimation responses to CO<sub>2</sub> were decoupled  
2375 from soil nitrogen availability and ability to acquire nitrogen via symbiotic nitro-  
2376 gen fixation. Instead, leaf and whole plant acclimation responses to CO<sub>2</sub> were  
2377 driven by optimal resource investment to photosynthetic capacity, where optimal  
2378 resource investment at the leaf level maximized nitrogen allocation to structures  
2379 that support whole plant growth.

2380 5.4.1 *Soil nitrogen fertilization has divergent effects on leaf and whole plant*  
2381 *acclimation responses to CO<sub>2</sub>*

2382 Elevated CO<sub>2</sub> reduced  $N_{\text{area}}$ ,  $V_{\text{cmax25}}$ ,  $J_{\text{max25}}$ , and stomatal conductance by 29%,  
2383 16%, 10%, and 20%, respectively. The larger downregulation of  $V_{\text{cmax25}}$  than  
2384  $J_{\text{max25}}$  led to an 8% stimulation in  $J_{\text{max25}}:V_{\text{cmax25}}$ , while the larger downregulation  
2385 of  $N_{\text{area}}$  than  $V_{\text{cmax25}}$  resulted in a 21% stimulation in the fraction of leaf nitro-  
2386 gen allocated to photosynthesis under elevated CO<sub>2</sub>. These acclimation responses  
2387 are directionally consistent with previous studies that have investigated or re-  
2388 viewed leaf acclimation responses to CO<sub>2</sub> (Drake et al. 1997; Makino et al. 1997;  
2389 Ainsworth et al. 2002; Ainsworth and Long 2005; Ainsworth and Rogers 2007;  
2390 Smith and Dukes 2013; Smith and Keenan 2020; Poorter et al. 2022), and fol-  
2391 low patterns expected from photosynthetic least-cost theory (Wright et al. 2003;  
2392 Prentice et al. 2014; Smith et al. 2019; Smith and Keenan 2020). Together, the  
2393 stimulation in  $J_{\text{max25}}:V_{\text{cmax25}}$  and the fraction of leaf nitrogen allocated to pho-  
2394 tosynthesis under elevated CO<sub>2</sub> provide strong support for the idea that leaves  
2395 were downregulating  $V_{\text{cmax25}}$  in response to elevated CO<sub>2</sub> in order to optimally co-  
2396 ordinate photosynthesis such that net photosynthesis rates approached becoming

**2397** equally co-limited by Rubisco carboxylation and RuBP regeneration (Chen et al.  
**2398** 1993; Maire et al. 2012) while optimizing resource use efficiency.

**2399** Increasing fertilization and inoculation induced strong positive effects on  
**2400**  $N_{\text{area}}$ ,  $V_{\text{cmax25}}$ ,  $J_{\text{max25}}$ . The general positive response of  $N_{\text{area}}$  to increasing fertiliza-  
**2401** tion and in inoculated pots was enhanced under ambient CO<sub>2</sub>, which, paired with  
**2402** the general downregulation of  $N_{\text{area}}$  under elevated CO<sub>2</sub>, resulted in a stronger  
**2403** downregulation of  $N_{\text{area}}$  under elevated CO<sub>2</sub> with increasing fertilization and in  
**2404** inoculated pots. These patterns suggest that  $N_{\text{area}}$  responses to CO<sub>2</sub> were at least  
**2405** partially dependent on soil nitrogen fertilization and nitrogen acquisition strat-  
**2406** egy. However, the general stimulation in the fraction of leaf nitrogen allocated to  
**2407** Rubisco, bioenergetics, or photosynthesis under elevated CO<sub>2</sub> was not modified  
**2408** across the fertilization gradient and was only marginally enhanced in inoculated  
**2409** pots. These patterns suggest that the increased downregulation of  $N_{\text{area}}$  under  
**2410** elevated CO<sub>2</sub> with increasing fertilization was not necessarily associated with a  
**2411** change in relative investment to photosynthetic tissue, providing another line of  
**2412** evidence suggesting that leaf acclimation responses to CO<sub>2</sub> are decoupled from  
**2413** changes in soil nitrogen availability.

**2414** Leaf acclimation responses to elevated CO<sub>2</sub> corresponded with a 62% and  
**2415** 100% stimulation in total leaf area and total biomass, respectively. The stimula-  
**2416** tion in total leaf area and total biomass under elevated CO<sub>2</sub> corresponded with  
**2417** generally larger structural carbon costs to acquire nitrogen, a pattern driven by  
**2418** a stimulation in belowground carbon biomass and reduction in whole plant ni-  
**2419** trogen biomass. This result suggests that elevated CO<sub>2</sub> reduces plant nitrogen  
**2420** uptake efficiency, which does not explain why plants grown under elevated CO<sub>2</sub>

2421 generally had higher biomass and total leaf area, unless growth stimulations un-  
2422 der elevated CO<sub>2</sub> were driven by reductions in per-tissue nitrogen demand (Dong  
2423 et al. 2022). Interestingly, strong negative effects of increasing fertilization on  
2424 structural carbon costs to acquire nitrogen, which were generally similar between  
2425 CO<sub>2</sub> concentrations, were driven by stronger increases in whole plant nitrogen  
2426 biomass than belowground carbon biomass. This response allowed plants to in-  
2427 crease nitrogen uptake efficiency with increasing fertilization, which could be the  
2428 mechanism that drove the enhanced growth stimulation under elevated CO<sub>2</sub> with  
2429 increasing fertilization.

2430 Interestingly, results indicate that the stimulation in total leaf area and  
2431 whole plant growth under elevated CO<sub>2</sub> was not modified by inoculation despite  
2432 an apparent general negative effect of inoculation on  $N_{cost}$ . This response could  
2433 have been due to strong negative effect of increasing fertilization on nodulation,  
2434 which may have caused the strong increase in the positive effect of elevated CO<sub>2</sub> on  
2435 whole plant growth with increasing fertilization to mask any increase in the posi-  
2436 tive effect of elevated CO<sub>2</sub> on whole plant growth due to inoculation. Reductions  
2437 in nodulation with increasing fertilization are commonly observed patterns that  
2438 have been inferred to be a response that allows species optimize nitrogen uptake  
2439 efficiency as costs to acquire nitrogen via direct uptake become more similar (Gib-  
2440 son and Harper 1985; Rastetter et al. 2001). In this study, pairwise comparisons  
2441 indicated strong positive effects of inoculation on total leaf area and total biomass  
2442 (158% increase in total leaf area, 119% increase in total biomass) under elevated  
2443 CO<sub>2</sub> at 0 ppm N ( $p < 0.05$  in both cases), but no observable inoculation effect on  
2444 total leaf area or total biomass under elevated CO<sub>2</sub> at 350 ppm N or 630 ppm N

2445 ( $p>0.05$  in both cases). While these responses did not generally differ from those  
2446 observed under ambient CO<sub>2</sub>, they do confirm the hypothesis that positive effects  
2447 of inoculation on whole plant growth responses to elevated CO<sub>2</sub> would decrease  
2448 with increasing fertilization.

2449 Combined, results reported here suggest that soil nitrogen availability plays  
2450 divergent roles in shaping leaf and whole plant acclimation responses to CO<sub>2</sub>. Leaf  
2451 acclimation responses were generally decoupled from fertilization, while whole  
2452 plant acclimation responses relied heavily on an increase in nitrogen uptake ef-  
2453 ficiency and consequent reduction in costs of acquiring nitrogen associated with  
2454 increasing fertilization. Whole plant responses to CO<sub>2</sub> indicated that fertilization  
2455 may play a more important role in determining whole plant acclimation responses  
2456 to CO<sub>2</sub> than nitrogen acquisition strategy, although any inoculation effect was  
2457 likely masked by the strong reduction in root nodulation with increasing fertil-  
2458 ization. These results suggest that plants acclimate to CO<sub>2</sub> in nitrogen-limited  
2459 systems by minimizing the number of optimally coordinated leaves, and that  
2460 downregulations in leaf nitrogen content under elevated CO<sub>2</sub> are not driven by  
2461 changes in soil nitrogen availability as has been previously implied.

2462 5.4.2 *Implications for future model development*

2463 Many terrestrial biosphere models predict photosynthetic capacity through plant  
2464 functional group-specific linear regressions between  $N_{\text{area}}$  and  $V_{\text{cmax}}$  (Rogers 2014;  
2465 Rogers et al. 2017), which assumes that leaf nitrogen-photosynthesis relation-  
2466 ships are constant across growing environments. These results build on previ-  
2467 ous work suggesting that leaf nitrogen-photosynthesis relationships dynamically  
2468 change across growing environments (Luo et al. 2021; Dong et al. 2022), showing

that CO<sub>2</sub> concentration increases the fraction of leaf nitrogen content allocated to photosynthesis independent of fertilization or acquisition strategy. Additionally, increasing fertilization strongly decreased the fraction of leaf nitrogen allocated to photosynthesis, a response that was largely determined by acquisition strategy. Specifically, reductions in the fraction of leaf nitrogen allocated to photosynthesis with increasing fertilization were only observed in inoculated pots that had less finite access to nitrogen, suggesting that constant leaf nitrogen-photosynthesis relationships may only be apparent in environments where nitrogen is limiting. Terrestrial biosphere models that parameterize photosynthetic capacity through linear relationships between  $N_{\text{area}}$  and  $V_{\text{cmax}}$  (Rogers 2014; Rogers et al. 2017) may therefore be overestimating photosynthetic capacity in systems where nitrogen is not as limiting. Such models are also not capable of detecting stimulations in the fraction of leaf nitrogen allocated to photosynthesis with increasing CO<sub>2</sub> concentration. The inability of models to predict these responses likely contributes to the widespread divergence of model simulations under future environmental scenarios (Friedlingstein et al. 2014; Davies-Barnard et al. 2020), and should therefore be a target for resolving in future generations of terrestrial biosphere models.

These results demonstrate that optimal resource investment to photosynthetic capacity defines leaf acclimation responses to elevated CO<sub>2</sub>, and that these responses were independent of fertilization or inoculation treatment. Current model approaches for simulating photosynthetic responses to CO<sub>2</sub> generally invoke patterns expected from progressive nitrogen limitation, where the downregulation in  $N_{\text{area}}$ , and therefore photosynthetic capacity, due to elevated CO<sub>2</sub> is formulated as a function of progressive reductions in soil nitrogen availability. Results

2493 reported here contradict this formulation, suggesting that the leaf acclimation re-  
2494 sponse is driven by optimal resource investment to photosynthetic capacity and  
2495 is independent of soil resource supply. Optimality models that leverage prin-  
2496 ciples from optimal coordination and photosynthetic least-cost theories (Wang  
2497 et al. 2017; Stocker et al. 2020; Scott and Smith 2022) are capable of capturing  
2498 such acclimation responses to CO<sub>2</sub> (Smith and Keenan 2020), suggesting that the  
2499 implementation of these models may improve the simulation of photosynthetic  
2500 processes in terrestrial biosphere models under increasing CO<sub>2</sub> concentrations.

2501 5.4.3 *Study limitations and future directions*

2502 There are two study limitations that must be addressed to contextualize patterns  
2503 observed in this study. First, restricting the volume of belowground substrate  
2504 via a potted experiment does not adequately replicate belowground environments  
2505 of natural systems, and therefore may modify effects of soil resource availability  
2506 and inoculation on plant nitrogen uptake. This limitation may be particularly  
2507 relevant if pot size limits whole plant growth (Poorter et al. 2012). I attempted  
2508 to minimize the extent of pot size limitation experienced in the first experimen-  
2509 tal chapter while accounting for the expected stimulation in whole plant growth  
2510 under elevated CO<sub>2</sub> by using 6-liter pots. Despite attempts to minimize growth  
2511 limitation imposed by pot volume, fertilization and CO<sub>2</sub> treatments increased the  
2512 biomass: pot volume ratio such that all treatment combinations to exceed 1 g L<sup>-1</sup>  
2513 biomass: pot volume under high fertilization (Table D3; Fig. D2). The 1 g L<sup>-1</sup>  
2514 biomass: pot volume recommendation from Poorter et al. (2012) was designated  
2515 to avoid growth limitation imposed by pot volume. However, if pot size limita-

2516 tion indeed limited whole plant growth, then structural carbon costs to acquire  
2517 nitrogen, belowground carbon biomass, whole plant nitrogen biomass, and whole  
2518 plant biomass should each exhibit strong saturation points with increasing fertil-  
2519 ization, which was not observed here. Importantly, leaf acclimation responses to  
2520 CO<sub>2</sub> observed in this study are consistent with findings reported in (Smith and  
2521 Keenan 2020), who used data from field manipulation experiments that did not  
2522 have any belowground space limitation.

2523 Second, this study evaluated leaf and whole plant responses to CO<sub>2</sub> in 7-  
2524 week seedlings. Given the long-term scale of the progressive nitrogen limitation  
2525 hypothesis, patterns observed here should be validated in longer-term nitrogen  
2526 manipulation experiments. Previous work in free air CO<sub>2</sub> enrichment experiments  
2527 show some support for patterns expected from the progressive nitrogen limitation  
2528 hypothesis (Reich et al. 2006; Norby et al. 2010), although results are not consis-  
2529 tent across experimental sites (Finzi et al. 2006; Moore et al. 2006; Liang et al.  
2530 2016). I found some support for patterns expected by the progressive nitrogen  
2531 limitation hypothesis, namely the increase in plant nitrogen uptake under elevated  
2532 CO<sub>2</sub> (Luo et al. 2004), though leaf acclimation responses to CO<sub>2</sub> were strongly  
2533 indicative of optimal resource investment to photosynthetic capacity as expected  
2534 from photosynthetic least-cost theory (Prentice et al. 2014; Smith et al. 2019;  
2535 Smith and Keenan 2020).

2536 5.4.4 *Conclusions*

2537 This study provides strong evidence suggesting that leaf acclimation responses  
2538 to elevated CO<sub>2</sub> did not vary with soil nitrogen fertilization or ability to acquire  
2539 nitrogen through symbiotic nitrogen fixation. However, whole plant acclimation

2540 responses to CO<sub>2</sub> were dependent on fertilization, where increasing fertilization  
2541 increased the positive effect of whole plant growth under elevated CO<sub>2</sub>. Results  
2542 also indicate that fertilization played a relatively more important role in modify-  
2543 ing whole plant responses to CO<sub>2</sub> than inoculation with symbiotic nitrogen-fixing  
2544 bacteria, perhaps due to a reduction in nodulation across the fertilization gra-  
2545 dient. These patterns strongly support the hypothesis that leaf and whole plant  
2546 acclimation responses are driven by optimal resource investment to photosynthetic  
2547 capacity, and that leaf acclimation responses to CO<sub>2</sub> were not modified by changes  
2548 in soil nitrogen availability. These results build on previous work suggesting that  
2549 constant leaf nitrogen-photosynthesis relationships are dynamic and change across  
2550 growing environments, calling the current formulation of photosynthetic processes  
2551 used in many terrestrial biosphere models into question.

2552

## Chapter 6

2553

### Conclusions

2554 The experiments included in this dissertation test mechanisms that drive patterns  
2555 expected from photosynthetic least-cost theory across various edaphic and climatic  
2556 gradients. Specifically, I investigate environmental drivers of carbon costs to ac-  
2557 quire nitrogen, tradeoffs between nitrogen and water use, and plant acclimation  
2558 responses to CO<sub>2</sub>. These experiments provide important empirical data needed to  
2559 test assumptions made in optimality models that leverage photosynthetic least-  
2560 cost frameworks, and are among the first manipulative experiments to show sup-  
2561 port for patterns expected from theory. Below, I summarize main findings of each  
2562 chapter, synthesize common patterns observed across experiments, and conclude  
2563 with a few study ideas that I think will help refine our understanding of plant  
2564 nutrient acquisition and allocation responses to environmental change leveraging  
2565 patterns predicted by photosynthetic least-cost theory.

2566 In the first experimental chapter, I quantified carbon costs to acquire ni-  
2567 trogen in a species capable of forming associations with symbiotic nitrogen-fixing  
2568 bacteria (*Glycine max*) and a species not capable of forming such associations  
2569 (*Gossypium hirsutum*) grown under four soil nitrogen fertilization treatments and  
2570 four light availability treatments in a full factorial greenhouse experiment. Sup-  
2571 porting hypotheses, increasing light availability increased carbon costs to acquire  
2572 nitrogen in both species due to a larger increase in belowground carbon biomass  
2573 than whole plant nitrogen biomass. In further support of hypotheses, increasing  
2574 fertilization decreased carbon costs to acquire nitrogen due to a larger increase in

2575 whole plant nitrogen biomass than belowground carbon biomass. Root nodulation  
2576 data indicated that *G. max* shifted relative carbon allocation from nitrogen fixa-  
2577 tion to direct uptake with increasing fertilization, which may explain the reduced  
2578 responsiveness of *G. max* carbon costs to acquire nitrogen across the fertilization  
2579 gradient.

2580 Despite evidence that reductions in the response of *G. max* carbon costs  
2581 to acquire nitrogen to increasing fertilization may have been driven by shifts away  
2582 from nitrogen fixation with increasing fertilization, I urge caution in assigning  
2583 causality to the differential response of carbon costs to acquire nitrogen between  
2584 species. This is because *G. max* and *G. hirsutum* are not phylogenetically related  
2585 and have different life histories. Differences in life history between the two species  
2586 limit my ability to assess whether reductions in the negative effect of increasing  
2587 fertilization on carbon costs to acquire nitrogen in *G. max* were driven by shifts  
2588 to direct uptake with increasing fertilization. However, these patterns were later  
2589 confirmed in the fourth experimental chapter, where similar weaker negative ef-  
2590 fects of increasing fertilization on carbon costs to acquire nitrogen were observed  
2591 in *G. max* that were inoculated with symbiotic nitrogen-fixing bacteria compared  
2592 to *G. max* that were left uninoculated across a similar soil nitrogen fertilization  
2593 gradient.

2594 In the second experimental chapter, I assessed whether changes in soil  
2595 nitrogen availability or soil pH drove changes in nitrogen-water use tradeoffs pre-  
2596 dicted by photosynthetic least-cost theory. I measured leaf traits of mature upper  
2597 canopy deciduous trees growing in a nine-year nitrogen-by-sulfur field manipula-  
2598 tion experiment, where experimental sulfur additions were added with intent to

2599 acidify plots. Following patterns expected from the theory, increasing soil nitrogen  
2600 availability was associated with increased leaf nitrogen content, but not net photo-  
2601 tosynthesis, resulting in an increase in photosynthetic nitrogen use efficiency. In  
2602 further support of theory, increasing soil nitrogen availability exhibited slight, but  
2603 nonsignificant, decreases in leaf  $C_i:C_a$  and increases in measures of photosynthetic  
2604 capacity. Perhaps the strongest evidence for the theory was a strong negative  
2605 relationship between leaf nitrogen content and leaf  $C_i:C_a$ , of which increased with  
2606 increasing soil nitrogen availability through a stronger increase in leaf nitrogen  
2607 content than leaf  $C_i:C_a$ .

2608 I found no effect of soil pH on nitrogen-water use tradeoffs aside from a  
2609 marginal reduction in net photosynthesis rates that marginally reduced photosyn-  
2610 thetic nitrogen use efficiency with increasing soil pH. Directionally, reductions in  
2611 photosynthetic nitrogen use efficiency with increasing soil pH were expected per  
2612 theory; however, this response was driven by no change in leaf nitrogen content  
2613 and a reduction in net photosynthesis. Theory predicts that these tradeoffs should  
2614 be driven by no change in net photosynthesis and an increase in leaf nitrogen con-  
2615 tent. The general null leaf response to changing soil pH may have been due to  
2616 experimental treatments directly increased soil nitrogen availability and affected  
2617 soil pH in opposite patterns, suggesting that soil nitrogen availability may be more  
2618 important in dictating nitrogen-water use tradeoffs than soil pH per se.

2619 In the third experimental chapter, I quantified variance in leaf nitrogen  
2620 content across a precipitation and soil resource availability gradient in Texan  
2621 grasslands. Specifically, I measured area-based leaf nitrogen content, components  
2622 of area-based leaf nitrogen content (leaf mass per unit leaf area, leaf nitrogen per

2623 unit dry biomass), leaf  $C_i:C_a$ , and the unit cost of acquiring nitrogen relative to  
2624 water in 520 individuals comprising 57 species. I found that variance in area-  
2625 based leaf nitrogen content was positively associated with increasing soil nitrogen  
2626 availability, soil moisture, vapor pressure deficit, and was negatively related to  
2627 increasing leaf  $C_i:C_a$ . Following patterns expected from theory, a path analysis  
2628 revealed that the positive soil nitrogen-leaf nitrogen relationship was driven by a  
2629 positive relationship between soil nitrogen availability and the unit cost of acquir-  
2630 ing and using nitrogen relative to water, a positive relationship between the unit  
2631 cost of acquiring and using nitrogen relative to water, and negative relationship  
2632 between leaf  $C_i:C_a$  and leaf mass per unit leaf area. Interestingly, there was no  
2633 effect of  $C_i:C_a$  on leaf nitrogen content per unit dry biomass, indicating that vari-  
2634 ance in area-based leaf nitrogen content across the environmental gradient was  
2635 driven by a change in leaf morphology and not leaf chemistry.

2636 In the fourth experimental chapter, I quantified leaf and whole plant accli-  
2637 mation responses in *G. max* grown under two atmospheric CO<sub>2</sub> levels, with and  
2638 without inoculation with *Bradyrhizobium japonicum*, and across nine nitrogen fer-  
2639 tilization treatments in a full factorial growth chamber experiment. I found strong  
2640 evidence that leaf nitrogen content,  $V_{cmax}$ , and  $J_{max}$  were each downregulated un-  
2641 der elevated CO<sub>2</sub>. A stronger downregulation in  $V_{cmax}$  than  $J_{max}$  and stronger  
2642 downregulation in leaf nitrogen content than  $V_{cmax}$  or  $J_{max}$  provided strong sup-  
2643 port suggesting that leaves were acclimating to elevated CO<sub>2</sub> by optimizing leaf  
2644 photosynthetic resource use efficiency to achieve optimal coordination. In striking  
2645 support of my hypotheses, I find strong evidence suggesting that leaf acclimation  
2646 responses to elevated CO<sub>2</sub> were decoupled from soil nitrogen fertilization and in-

**2647** oculation treatment, despite apparent strong increases in leaf nitrogen content,  
**2648**  $V_{\text{cmax}}$ , and  $J_{\text{max}}$  with increasing fertilization and in inoculated pots. These find-  
**2649** ings contrast the current formulation of photosynthetic processes in terrestrial  
**2650** biosphere models, where many models simulate downregulations in leaf nitrogen  
**2651** content under elevated CO<sub>2</sub> as a function of progressive nitrogen limitation.

**2652** There are currently two iterations of optimality models that employ the  
**2653** use of patterns expected from photosynthetic least-cost theory, one for C<sub>3</sub> species  
**2654** (Wang et al. 2017; Smith et al. 2019; Stocker et al. 2020) and one more recently  
**2655** developed for C<sub>4</sub> species (Scott and Smith 2022). In both model variants, costs  
**2656** to acquire and use nitrogen relative to water are held constant using a global  
**2657** dataset of δ<sup>13</sup>C (Cornwell et al. 2018). Throughout experiments, I show strong  
**2658** evidence suggesting that costs to acquire and use nitrogen are dynamic and vary  
**2659** predictably across environmental gradients, and that changes in these costs scale  
**2660** to alter leaf nitrogen-water use tradeoffs and acclimation responses to changing  
**2661** environments in ways predicted through photosynthetic least-cost theory. Thus,  
**2662** while optimality model simulations show good agreement with measured data  
**2663** (Smith et al. 2019; Stocker et al. 2020), such models may not be capturing an  
**2664** important source of variability in leaf nitrogen-water use tradeoffs by holding costs  
**2665** of resource use constant across environmental gradients.

**2666** First principles of photosynthetic least-cost theory suggest that, in a given  
**2667** environment, plants optimize photosynthesis rates by sacrificing inefficient use of  
**2668** a relatively more abundant (and less costly to acquire) resource for more efficient  
**2669** use of a relatively less abundant (and more costly to acquire) resource. Through-  
**2670** out experimental chapters, I show strong support for these patterns across ex-

2671 periments, where increasing soil nitrogen fertilization generally decreased the cost  
2672 of acquiring nitrogen relative to water, a pattern that scaled to influence leaf  
2673 nitrogen-water use tradeoffs. I did not find evidence to suggest that soil moisture  
2674 influenced nitrogen-water use tradeoffs, though this was due to strong covariation  
2675 between soil moisture and soil nitrogen availability. Overall, findings across exper-  
2676 iments provide empirical validation of photosynthetic least-cost theory needed to  
2677 further develop optimality models and eventually implement such models in ter-  
2678 restrial biosphere model products. Many terrestrial biosphere model products do  
2679 not include robust frameworks for simulating acclimation responses to changing  
2680 environmental conditions, and empirical findings shown here provide some support  
2681 that optimality models that leverage photosynthetic least-cost theory predictions  
2682 may improve the ability of terrestrial biosphere models to accurately simulate  
2683 photosynthetic processes.

2684       Many terrestrial biosphere models predict photosynthetic capacity through  
2685 plant functional group-specific linear regressions between area-based leaf nitrogen  
2686 content and  $V_{cmax}$  (Rogers 2014; Rogers et al. 2017), which assumes that leaf  
2687 nitrogen-photosynthesis relationships are constant across growing environments.  
2688 I found constant leaf nitrogen-photosynthesis relationships with increasing soil ni-  
2689 trogen availability in the nitrogen-by-sulfur field manipulation experiment. How-  
2690 ever, results from the CO<sub>2</sub>-by-nitrogen-by-inoculation manipulation experiment  
2691 indicated that leaf nitrogen-photosynthesis responses to soil nitrogen availability  
2692 were dependent on whether nitrogen was limiting. Further investigation regard-  
2693 ing the effect of soil nitrogen availability in modifying leaf nitrogen-photosynthesis  
2694 relationships is warranted to better understand the generality of leaf nitrogen pho-

**2695** tosynthesis relationships across environmental gradients. However, findings from  
**2696** these experiments suggest that representing photosynthetic processes through pos-  
**2697** itive relationships between soil nitrogen availability, leaf nitrogen, and photosyn-  
**2698** thetic capacity are likely contributing to erroneous errors in model simulations and  
**2699** may explain the high degree of divergence in simulated processes across terrestrial  
**2700** biosphere models (Friedlingstein et al. 2014; Davies-Barnard et al. 2020).

**2701** The experiments included in this dissertation have provided a strong foun-  
**2702** dation for me to continue growing as a plant physiological ecologist. I envision  
**2703** five primary avenues for future research that build on the work presented here,  
**2704** which are briefly summarized below:

- 2705** 1. Manipulative and environmental gradient experiments included here were  
**2706** designed to provide empirical data needed to test photosynthetic least-cost  
**2707** theory assumptions. While these results show promising patterns for pat-  
**2708** terns expected from photosynthetic least-cost theory, they do not necessarily  
**2709** address whether these patterns follow those simulated by optimality models  
**2710** that leverage photosynthetic least-cost principles. Thus, a clear future di-  
**2711** rection of these experiments would be to conduct model-data comparisons  
**2712** using data collected here (or similar experiments) to compare against opti-  
**2713** mality model simulations.
  
- 2714** 2. Experiments included here explicitly quantify effects of symbiotic nitrogen  
**2715** fixation on carbon costs to acquire nitrogen, nitrogen-water use tradeoffs,  
**2716** and leaf nitrogen-photosynthesis relationships. However, carbon costs to ac-  
**2717** quire nitrogen also vary in species that associate with different mycorrhizal  
**2718** types (Brzostek et al. 2014; Terrer et al. 2018), and dominant mycorrhizal

2719 type in an ecosystem has been shown to determine net biogeochemical cycle  
2720 dynamics in deciduous forests of the northeastern United States (Phillips  
2721 et al. 2013). Thus, future work should consider conducting similar experi-  
2722 ments while manipulating mycorrhizal association to better understand how  
2723 microbial symbioses modify leaf and whole plant acclimation responses to  
2724 changing environments.

2725 3. Recent work indicates a high degree of variance in symbiotic nitrogen fixa-  
2726 tion rates across terrestrial biosphere models (Meyerholt et al. 2016; Davies-  
2727 Barnard et al. 2020), perhaps due to nitrogen fixation rates that are im-  
2728 plemented across terrestrial biosphere models as a function of temperature  
2729 (Houlton et al. 2008). While energetic costs of nitrogen fixation are de-  
2730 pendent on temperature, I show that structural carbon costs to acquire  
2731 nitrogen via symbiotic nitrogen fixation are driven by factors that influence  
2732 demand to acquire nitrogen (i.e. CO<sub>2</sub>, light) and are modified by soil ni-  
2733 tragen supply. The light-by-nitrogen greenhouse experiment was published  
2734 in *Journal of Experimental Botany*, and a reviewer encouraged future work  
2735 to include a model-data comparison comparing structural carbon costs to  
2736 acquire nitrogen measured in the experiment to carbon costs to acquire ni-  
2737 tragen simulated by the FUN biogeochemical model (Fisher et al. 2010;  
2738 Brzostek et al. 2014; Allen et al. 2020). Conveniently, FUN calculates car-  
2739 bon costs to acquire nitrogen following the same calculation used in the first  
2740 and fourth experimental chapter. Conducting such a model-data comparison  
2741 would be a useful step toward identifying biases in the FUN biogeochemi-  
2742 cal model, which is currently coupled to several terrestrial biosphere models

2743 (Clark et al. 2011; Shi et al. 2016; Lawrence et al. 2019; Davies-Barnard  
2744 et al. 2020).

2745 4. Carbon costs to acquire nitrogen relative to water were quantified at the  
2746 leaf level as a function of  $\delta^{13}\text{C}$  and vapor pressure deficit, while structural  
2747 carbon costs to acquire nitrogen were quantified at the whole plant level  
2748 as the ratio of belowground carbon allocation per unit whole plant nitro-  
2749 gen biomass. As increasing soil nitrogen availability decreases both leaf and  
2750 whole plant estimates of costs to acquire and use nitrogen, one might expect  
2751 leaf and whole plant carbon cost to acquire nitrogen estimates to covary. Fu-  
2752 ture work should consider investigating if leaf and whole plant estimates of  
2753 carbon costs to acquire nitrogen covary and evaluate whether environmental  
2754 conditions (or species acquisition strategy) modifies any of this possible co-  
2755 variance. Strong covariance between leaf and whole plant costs of nitrogen  
2756 acquisition could be a possible avenue to implement frameworks for allowing  
2757 costs of nitrogen acquisition to vary in optimality models, as the FUN model  
2758 calculates carbon costs of nitrogen acquisition at the whole plant level.

2759 5. While experiments included here target effects of soil nitrogen availability  
2760 on carbon costs to acquire nitrogen and associated leaf nitrogen-water use  
2761 tradeoffs, photosynthetic least-cost theory predicts that plants acclimate  
2762 their photosynthetic processes by minimizing the summed cost of nutrient  
2763 (not just nitrogen) and water use. Therefore, the theory would predict  
2764 similar leaf acclimation responses across soil phosphorus or other nutrient  
2765 availability gradients. Recent iterations of the FUN biogeochemical cycle  
2766 includes a framework for determining the carbon and nitrogen cost of ac-

**2767** quiring and using phosphorus, which similarly varies in species with different  
**2768** nutrient acquisition strategies (Allen et al. 2020). The implementation of  
**2769** this model in a terrestrial biosphere model (E3SM) was also recently shown  
**2770** to improve model performance of ecosystem nutrient limitation (Braghieri  
**2771** et al. 2022). As nitrogen and phosphorus commonly co-limit leaf photo-  
**2772** synthesis and primary productivity, extending experiments reported here to  
**2773** investigate carbon and nitrogen costs of phosphorus use, and whether these  
**2774** patterns scale to leaf nutrient-water use tradeoffs would be a useful next  
**2775** step in understanding extensions and limitations of photosynthetic least-  
**2776** cost theory.

**2777** The experiments included in this dissertation and the proposed experiments sum-  
**2778** marized above provide a snapshot view of the things that I have learned through-  
**2779** out my time as a graduate student. I am excited to continue learning and growing  
**2780** as a plant ecophysiologicalist, ecologist, and scientist, and look forward to continuing  
**2781** along my journey of investigating nutrient acquisition and allocation responses to  
**2782** global change.

**2783**

**References**

- 2784** Abrams, M. D. and S. A. Mostoller (1995). Gas exchange, leaf structure and  
**2785** nitrogen in contrasting successional tree species growing in open and under-  
**2786** story sites during a drought. *Tree Physiology* 15(6), 361–370.
- 2787** Adams, M. A., T. L. Turnbull, J. I. Sprent, and N. Buchmann (2016). Legumes  
**2788** are different: Leaf nitrogen, photosynthesis, and water use efficiency. *Pro-  
**2789** ceedings of the National Academy of Sciences of the United States of Amer-  
**2790** ica* 113(15), 4098–4103.
- 2791** Ainsworth, E. A., P. A. Davey, C. J. Bernacchi, O. C. Dermody, E. A. Heaton,  
**2792** D. J. Moore, P. B. Morgan, S. L. Naidu, H. S. Y. Ra, X. G. Zhu, P. S. Curtis,  
**2793** and S. P. Long (2002). A meta-analysis of elevated [CO<sub>2</sub>] effects on soybean  
**2794** (*Glycine max*) physiology, growth and yield. *Global Change Biology* 8(8),  
**2795** 695–709.
- 2796** Ainsworth, E. A. and S. P. Long (2005). What have we learned from 15 years of  
**2797** free-air CO<sub>2</sub> enrichment (FACE)? A meta-analytic review of the responses  
**2798** of photosynthesis, canopy properties and plant production to rising CO<sub>2</sub>.  
**2799** *New Phytologist* 165(2), 351–372.
- 2800** Ainsworth, E. A. and A. Rogers (2007). The response of photosynthesis and  
**2801** stomatal conductance to rising [CO<sub>2</sub>]: mechanisms and environmental in-  
**2802** teractions. *Plant, Cell and Environment* 30(3), 258–270.
- 2803** Allen, K., J. B. Fisher, R. P. Phillips, J. S. Powers, and E. R. Brzostek (2020).  
**2804** Modeling the carbon cost of plant nitrogen and phosphorus uptake across  
**2805** temperate and tropical forests. *Frontiers in Forests and Global Change* 3,

- 2806 1–12.
- 2807 Allison, S. D., C. I. Czimczik, and K. K. Treseder (2008). Microbial activity  
2808 and soil respiration under nitrogen addition in Alaskan boreal forest. *Global  
2809 Change Biology* 14(5), 1156–1168.
- 2810 Andersen, M. K., H. Hauggaard-Nielsen, P. Ambus, and E. S. Jensen (2005).  
2811 Biomass production, symbiotic nitrogen fixation and inorganic N use in dual  
2812 and tri-component annual intercrops. *Plant and Soil* 266(1-2), 273–287.
- 2813 Andrews, M., E. K. James, J. I. Sprent, R. M. Boddey, E. Gross, and F. B. dos  
2814 Reis (2011). Nitrogen fixation in legumes and actinorhizal plants in natural  
2815 ecosystems: Values obtained using  $^{15}\text{N}$  natural abundance. *Plant Ecology  
2816 and Diversity* 4(2-3), 117–130.
- 2817 Arndal, M. F., A. Tolver, K. S. Larsen, C. Beier, and I. K. Schmidt (2018). Fine  
2818 root growth and vertical distribution in response to elevated CO<sub>2</sub>, warming  
2819 and drought in a mixed heathland–grassland. *Ecosystems* 21(1), 15–30.
- 2820 Arnone, J. A. (1997). Indices of plant N availability in an alpine grassland under  
2821 elevated atmospheric CO<sub>2</sub>. *Plant and Soil* 190(1), 61–66.
- 2822 Arora, V. K., A. Katavouta, R. G. Williams, C. D. Jones, V. Brovkin,  
2823 P. Friedlingstein, J. Schwinger, L. Bopp, O. Boucher, P. Cadule, M. A.  
2824 Chamberlain, J. R. Christian, C. Delire, R. A. Fisher, T. Hajima, T. Ilyina,  
2825 E. Joetzjer, M. Kawamiya, C. D. Koven, J. P. Krasting, R. M. Law, D. M.  
2826 Lawrence, A. Lenton, K. Lindsay, J. Pongratz, T. Raddatz, R. Séférian,  
2827 K. Tachiiri, J. F. Tjiputra, A. Wiltshire, T. Wu, and T. Ziehn (2020).  
2828 Carbon-concentration and carbon-climate feedbacks in CMIP6 models and  
2829 their comparison to CMIP5 models. *Biogeosciences* 17(16), 4173–4222.

- 2830 Bae, K., T. J. Fahey, R. D. Yanai, and M. Fisk (2015). Soil nitrogen availability affects belowground carbon allocation and soil respiration in northern  
2831 hardwood forests of New Hampshire. *Ecosystems* 18(7), 1179–1191.
- 2832
- 2833 Barber, S. A. (1962). A diffusion and mass-flow concept of soil nutrient availability. *Soil Science* 93(1), 39–49.
- 2834
- 2835 Barnes, J. D., L. Balaguer, E. Manrique, S. Elvira, and A. W. Davison (1992).  
2836 A reappraisal of the use of DMSO for the extraction and determination  
2837 of chlorophylls a and b in lichens and higher plants. *Environmental and  
2838 Experimental Botany* 32(2), 85–100.
- 2839
- 2840 Bates, D., M. Mächler, B. Bolker, and S. Walker (2015). Fitting linear mixed-  
2841 effects models using lme4. *Journal of Statistical Software* 67(1), 1–48.
- 2842
- 2843 Beaudette, D., J. Skovlin, S. Roeker, and A. Brown (2022). soilDB: Soil  
2844 Database Interface.
- 2845
- 2846 Bengtson, P., J. Barker, and S. J. Grayston (2012). Evidence of a strong cou-  
2847 pling between root exudation, C and N availability, and stimulated SOM  
2848 decomposition caused by rhizosphere priming effects. *Ecology and Evolu-  
2849 tion* 2(8), 1843–1852.
- 2850
- 2851 Bernacchi, C. J., E. L. Singsaas, C. Pimentel, A. R. Portis, and S. P. Long  
2852 (2001). Improved temperature response functions for models of Rubisco-  
limited photosynthesis. *Plant, Cell and Environment* 24(2), 253–259.
- 2853
- 2854 Bialic-Murphy, L., N. G. Smith, P. Voothuluru, R. M. McElderry, M. D.  
2855 Roche, S. T. Cassidy, S. N. Kivlin, and S. Kalisz (2021). Invasion-induced  
2856 root–fungal disruptions alter plant water and nitrogen economies. *Ecology*

- 2853** *Letters* 24(6), 1145–1156.
- 2854** Bloom, A. J., F. S. Chapin, and H. A. Mooney (1985). Resource limitation  
**2855** in plants - an economic analogy. *Annual Review of Ecology and Systemat-*  
**2856** *ics* 16(1), 363–392.
- 2857** Bloomfield, K. J., B. D. Stocker, T. F. Keenan, and I. C. Prentice (2023).  
**2858** Environmental controls on the light use efficiency of terrestrial gross primary  
**2859** production. *Global Change Biology* 29(4), 0–2.
- 2860** Bonan, G. B., M. D. Hartman, W. J. Parton, and W. R. Wieder (2013). Eval-  
**2861** uating litter decomposition in earth system models with long-term litter  
**2862** bag experiments: an example using the Community Land Model version 4  
**2863** (CLM4). *Global Change Biology* 19(3), 957–974.
- 2864** Bonan, G. B., P. J. Lawrence, K. W. Oleson, S. Levis, M. Jung, M. Reich-  
**2865** stein, D. M. Lawrence, and S. C. Swenson (2011). Improving canopy pro-  
**2866** cesses in the Community Land Model version 4 (CLM4) using global flux  
**2867** fields empirically inferred from FLUXNET data. *Journal of Geophysical Re-*  
**2868** *search* 116(G2), G02014.
- 2869** Booth, B. B. B., C. D. Jones, M. Collins, I. J. Totterdell, P. M. Cox, S. Sitch,  
**2870** C. Huntingford, R. A. Betts, G. R. Harris, and J. Lloyd (2012). High sen-  
**2871** sitivity of future global warming to land carbon cycle processes. *Environ-*  
**2872** *mental Research Letters* 7(2), 024002.
- 2873** Borer, E. T., W. S. Harpole, P. B. Adler, E. M. Lind, J. L. Orrock, E. W.  
**2874** Seabloom, and M. D. Smith (2014). Finding generality in ecology: A model  
**2875** for globally distributed experiments. *Methods in Ecology and Evolution* 5(1),  
**2876** 65–73.

- 2877** Braghieri, R. K., J. B. Fisher, K. Allen, E. Brzostek, M. Shi, X. Yang, D. M.
- 2878** Ricciuto, R. A. Fisher, Q. Zhu, and R. P. Phillips (2022). Modeling global
- 2879** carbon costs of plant nitrogen and phosphorus acquisition. *Journal of Ad-*
- 2880** *vances in Modeling Earth Systems* 14(8), 1–23.
- 2881** Brix, H. (1971). Effects of nitrogen fertilization on photosynthesis and respi-
- 2882** ration in Douglas-fir. *Forest Science* 17(4), 407–414.
- 2883** Brzostek, E. R., J. B. Fisher, and R. P. Phillips (2014). Modeling the carbon
- 2884** cost of plant nitrogen acquisition: Mycorrhizal trade-offs and multipath
- 2885** resistance uptake improve predictions of retranslocation. *Journal of Geo-*
- 2886** *physical Research: Biogeosciences* 119, 1684–1697.
- 2887** Bubier, J. L., R. Smith, S. Juutinen, T. R. Moore, R. Minocha, S. Long, and
- 2888** S. Minocha (2011). Effects of nutrient addition on leaf chemistry, morphol-
- 2889** ogy, and photosynthetic capacity of three bog shrubs. *Oecologia* 167(2),
- 2890** 355–368.
- 2891** Cernusak, L. A., N. Ubierna, K. Winter, J. A. M. Holtum, J. D. Marshall, and
- 2892** G. D. Farquhar (2013). Environmental and physiological determinants of
- 2893** carbon isotope discrimination in terrestrial plants. *New Phytologist* 200(4),
- 2894** 950–965.
- 2895** Chen, J.-L., J. F. Reynolds, P. C. Harley, and J. D. Tenhunen (1993). Coor-
- 2896** dination theory of leaf nitrogen distribution in a canopy. *Oecologia* 93(1),
- 2897** 63–69.
- 2898** Clark, D. B., L. M. Mercado, S. Sitch, C. D. Jones, N. Gedney, M. J. Best,
- 2899** M. Pryor, G. G. Rooney, R. L. H. Essery, E. Blyth, O. Boucher, R. J.
- 2900** Harding, C. Huntingford, and P. M. Cox (2011). The Joint UK Land Envi-

- 2901 ronment Simulator (JULES), model description. Part 2: Carbon fluxes and  
2902 vegetation dynamics. *Geoscientific Model Development* 4(3), 701–722.
- 2903 Cornwell, W. K., J. H. C. Cornelissen, K. Amatangelo, E. Dorrepaal, V. T.  
2904 Eviner, O. Godoy, S. E. Hobbie, B. Hoorens, H. Kurokawa, N. Pérez-  
2905 Harguindeguy, H. M. Quested, L. S. Santiago, D. A. Wardle, I. J. Wright,  
2906 R. Aerts, S. D. Allison, P. van Bodegom, V. Brovkin, A. Chatain, T. V.  
2907 Callaghan, S. Díaz, E. Garnier, D. E. Gurvich, E. Kazakou, J. A. Klein,  
2908 J. Read, P. B. Reich, N. A. Soudzilovskaia, M. V. Vaieretti, and M. Westoby  
2909 (2008). Plant species traits are the predominant control on litter decompo-  
2910 sition rates within biomes worldwide. *Ecology Letters* 11(10), 1065–1071.
- 2911 Cornwell, W. K., I. J. Wright, J. Turner, V. Maire, M. M. Barbour, L. A.  
2912 Cernusak, T. E. Dawson, D. S. Ellsworth, G. D. Farquhar, H. Griffiths,  
2913 C. Keitel, A. Knohl, P. B. Reich, D. G. Williams, R. Bhaskar, J. H. C. Cor-  
2914 nelissen, A. Richards, S. Schmidt, F. Valladares, C. Körner, E.-D. Schulze,  
2915 N. Buchmann, and L. S. Santiago (2018). Climate and soils together regulate  
2916 photosynthetic carbon isotope discrimination within C<sub>3</sub> plants worldwide.  
2917 *Global Ecology and Biogeography* 27(9), 1056–1067.
- 2918 Cramer, W. and I. C. Prentice (1988). Simulation of regional soil moisture  
2919 deficits on a European scale. *Norsk Geografisk Tidsskrift - Norwegian Jour-*  
2920 *nal of Geography* 42(2-3), 149–151.
- 2921 Curtis, P. S. (1996). A meta-analysis of leaf gas exchange and nitrogen in trees  
2922 grown under elevated carbon dioxide. *Plant, Cell and Environment* 19(2),  
2923 127–137.
- 2924 Daly, C., M. Halbleib, J. I. Smith, W. P. Gibson, M. K. Doggett, G. H. Taylor,

- 2925 J. Curtis, and P. P. Pasteris (2008). Physiographically sensitive mapping  
2926 of climatological temperature and precipitation across the conterminous  
2927 United States. *International Journal of Climatology* 28(15), 2031–2064.
- 2928 Davies-Barnard, T., J. Meyerholt, S. Zaehle, P. Friedlingstein, V. Brovkin,  
2929 Y. Fan, R. A. Fisher, C. D. Jones, H. Lee, D. Peano, B. Smith, D. Wårlind,  
2930 and A. J. Wiltshire (2020). Nitrogen cycling in CMIP6 land surface models:  
2931 progress and limitations. *Biogeosciences* 17(20), 5129–5148.
- 2932 Davis, T. W., I. C. Prentice, B. D. Stocker, R. T. Thomas, R. J. Whitley,  
2933 H. Wang, B. J. Evans, A. V. Gallego-Sala, M. T. Sykes, and W. Cramer  
2934 (2017). Simple process-led algorithms for simulating habitats (SPLASH  
2935 v.1.0): robust indices of radiation, evapotranspiration and plant-available  
2936 moisture. *Geoscientific Model Development* 10, 689–708.
- 2937 Delaire, M., E. Frak, M. Sigogne, B. Adam, F. Beaujard, and X. Le Roux  
2938 (2005). Sudden increase in atmospheric CO<sub>2</sub> concentration reveals strong  
2939 coupling between shoot carbon uptake and root nutrient uptake in young  
2940 walnut trees. *Tree Physiology* 25(2), 229–235.
- 2941 Doane, T. A. and W. R. Horwáth (2003). Spectrophotometric determination of  
2942 nitrate with a single reagent. *Analytical Letters* 36(12), 2713–2722.
- 2943 Dong, N., I. C. Prentice, B. J. Evans, S. Caddy-Retalic, A. J. Lowe, and I. J.  
2944 Wright (2017). Leaf nitrogen from first principles: field evidence for adaptive  
2945 variation with climate. *Biogeosciences* 14(2), 481–495.
- 2946 Dong, N., I. C. Prentice, I. J. Wright, B. J. Evans, H. F. Togashi, S. Caddy-  
2947 Retalic, F. A. McInerney, B. Sparrow, E. Leitch, and A. J. Lowe (2020).  
2948 Components of leaf-trait variation along environmental gradients. *New Phy-*

- 2949** *tologist* 228(1), 82–94.
- 2950** Dong, N., I. C. Prentice, I. J. Wright, H. Wang, O. K. Atkin, K. J. Bloomfield,
- 2951** T. F. Domingues, S. M. Gleason, V. Maire, Y. Onoda, H. Poorter, and N. G.
- 2952** Smith (2022). Leaf nitrogen from the perspective of optimal plant function.
- 2953** *Journal of Ecology* 110(11), 2585–2602.
- 2954** Dong, N., I. J. Wright, J. M. Chen, X. Luo, H. Wang, T. F. Keenan, N. G.
- 2955** Smith, and I. C. Prentice (2022). Rising CO<sub>2</sub> and warming reduce global
- 2956** canopy demand for nitrogen. *New Phytologist* 235(5), 1692–1700.
- 2957** Dovrat, G., H. Bakhshian, T. Masci, and E. Sheffer (2020). The nitrogen eco-
- 2958** nomic spectrum of legume stoichiometry and fixation strategy. *New Phytol-*
- 2959** *ogist* 227(2), 365–375.
- 2960** Dovrat, G., T. Masci, H. Bakhshian, E. Mayzlish Gati, S. Golan, and E. Shef-
- 2961** fer (2018). Drought-adapted plants dramatically downregulate dinitrogen
- 2962** fixation: Evidences from Mediterranean legume shrubs. *Journal of Ecol-*
- 2963** *ogy* 106(4), 1534–1544.
- 2964** Drake, B. G., M. A. Gonzàlez-Meler, and S. P. Long (1997). More efficient
- 2965** plants: a consequence of rising atmospheric CO<sub>2</sub>? *Annual Review of Plant*
- 2966** *Biology* 48, 609–639.
- 2967** Duursma, R. A. (2015). Plantecophys - An R package for analyzing and mod-
- 2968** elling leaf gas exchange data. *PLOS ONE* 10(11), e0143346.
- 2969** Eastman, B. A., M. B. Adams, E. R. Brzostek, M. B. Burnham, J. E. Carrara,
- 2970** C. Kelly, B. E. McNeil, C. A. Walter, and W. T. Peterjohn (2021). Altered
- 2971** plant carbon partitioning enhanced forest ecosystem carbon storage after 25

- 2972 years of nitrogen additions. *New Phytologist* 230(4), 1435–1448.
- 2973 Ellsworth, D. S. and P. B. Reich (1996). Photosynthesis and leaf nitrogen in five
- 2974 Amazonian tree species during early secondary succession. *Ecology* 77(2),
- 2975 581–594.
- 2976 Espelta, J. M., P. Cortés, M. Mangirón, and J. Retana (2005). Differences
- 2977 in biomass partitioning, leaf nitrogen content, and water use efficiency  $\delta^{13}$
- 2978 result in similar performance of seedlings of two Mediterranean oaks with
- 2979 contrasting leaf habit. *Ecoscience* 12(4), 447–454.
- 2980 Evans, J. R. (1989). Photosynthesis and nitrogen relationships in leaves of C<sub>3</sub>
- 2981 plants. *Oecologia* 78(1), 9–19.
- 2982 Evans, J. R. and V. C. Clarke (2019). The nitrogen cost of photosynthesis.
- 2983 *Journal of Experimental Botany* 70(1), 7–15.
- 2984 Evans, J. R. and H. Poorter (2001). Photosynthetic acclimation of plants to
- 2985 growth irradiance: the relative importance of specific leaf area and nitrogen
- 2986 partitioning in maximizing carbon gain. *Plant, Cell and Environment* 24(8),
- 2987 755–767.
- 2988 Evans, J. R. and J. R. Seemann (1989). The allocation of protein nitrogen in
- 2989 the photosynthetic apparatus: costs, consequences, and control. *Photosyn-*
- 2990 *thesis* 8, 183–205.
- 2991 Exbrayat, J.-F., A. A. Bloom, P. Falloon, A. Ito, T. L. Smallman, and
- 2992 M. Williams (2018). Reliability ensemble averaging of 21<sup>st</sup> century projec-
- 2993 tions of terrestrial net primary productivity reduces global and regional
- 2994 uncertainties. *Earth System Dynamics* 9(1), 153–165.

- 2995** Farquhar, G. D., J. R. Ehleringer, and K. T. Hubick (1989). Carbon isotope  
**2996** discrimination and photosynthesis. *Annual Review of Plant Physiology and*  
**2997** *Plant Molecular Biology* 40(1), 503–537.
- 2998** Farquhar, G. D. and T. D. Sharkey (1982). Stomatal conductance and photo-  
**2999** synthesis. *Annual Review of Plant Physiology* 33(1), 317–345.
- 3000** Farquhar, G. D., S. von Caemmerer, and J. A. Berry (1980). A biochemical  
**3001** model of photosynthetic CO<sub>2</sub> assimilation in leaves of C<sub>3</sub> species.  
**3002** *Planta* 149(1), 78–90.
- 3003** Fay, P. A., S. M. Prober, W. S. Harpole, J. M. H. Knops, J. D. Bakker, E. T.  
**3004** Borer, E. M. Lind, A. S. MacDougall, E. W. Seabloom, P. D. Wragg, P. B.  
**3005** Adler, D. M. Blumenthal, Y. M. Buckley, C. Chu, E. E. Cleland, S. L.  
**3006** Collins, K. F. Davies, G. Du, X. Feng, J. Firn, D. S. Gruner, N. Hagenah,  
**3007** Y. Hautier, R. W. Heckman, V. L. Jin, K. P. Kirkman, J. A. Klein, L. M.  
**3008** Ladwig, Q. Li, R. L. McCulley, B. A. Melbourne, C. E. Mitchell, J. L. Moore,  
**3009** J. W. Morgan, A. C. Risch, M. Schütz, C. J. Stevens, D. A. Wedin, and  
**3010** L. H. Yang (2015). Grassland productivity limited by multiple nutrients.  
**3011** *Nature Plants* 1(7), 15080.
- 3012** Feng, X. (1999). Trends in intrinsic water-use efficiency of natural trees for the  
**3013** past 100-200 years: A response to atmospheric CO<sub>2</sub> concentration. *Geochim-  
ica et Cosmochimica Acta* 63(13-14), 1891–1903.
- 3015** Field, C. B. and H. A. Mooney (1986). The photosynthesis-nitrogen relationship  
**3016** in wild plants. In T. J. Givnish (Ed.), *On the Economy of Plant Form and*  
**3017** *Function*, pp. 25–55. Cambridge: Cambridge University Press.
- 3018** Finzi, A. C., D. J. P. Moore, E. H. DeLucia, J. Lichter, K. S. Hofmockel, R. B.

- 3019 Jackson, H. S. Kim, R. Matamala, H. R. McCarthy, R. Oren, J. S. Pippen,  
3020 and W. H. Schlesinger (2006). Progressive nitrogen limitation of ecosystem  
3021 processes under elevated CO<sub>2</sub> in a warm-temperate forest. *Ecology* 87(1),  
3022 15–25.
- 3023 Firn, J., J. M. McGree, E. Harvey, H. Flores Moreno, M. Schutz, Y. M. Buckley,  
3024 E. T. Borer, E. W. Seabloom, K. J. La Pierre, A. M. MacDougall, S. M.  
3025 Prober, C. J. Stevens, L. L. Sullivan, E. Porter, E. Ladouceur, C. Allen,  
3026 K. H. Moromizato, J. W. Morgan, W. S. Harpole, Y. Hautier, N. Eisen-  
3027 hauer, J. P. Wright, P. B. Adler, C. A. Arnillas, J. D. Bakker, L. Biederman,  
3028 A. A. D. Broadbent, C. S. Brown, M. N. Bugalho, M. C. Caldeira, E. E. Cle-  
3029 land, A. Ebeling, P. A. Fay, N. Hagenah, A. R. Kleinhesselink, R. Mitchell,  
3030 J. L. Moore, C. Nogueira, P. L. Peri, C. Roscher, M. D. Smith, P. D. Wragg,  
3031 and A. C. Risch (2019). Leaf nutrients, not specific leaf area, are consistent  
3032 indicators of elevated nutrient inputs. *Nature Ecology and Evolution* 3(3),  
3033 400–406.
- 3034 Fisher, J. B., S. Sitch, Y. Malhi, R. A. Fisher, C. Huntingford, and S.-Y. Tan  
3035 (2010). Carbon cost of plant nitrogen acquisition: A mechanistic, globally  
3036 applicable model of plant nitrogen uptake, retranslocation, and fixation.  
3037 *Global Biogeochemical Cycles* 24(1), 1–17.
- 3038 Fox, J. and S. Weisberg (2019). *An R companion to applied regression* (Third  
3039 edit ed.). Thousand Oaks, California: Sage.
- 3040 Franklin, O., R. E. McMurtrie, C. M. Iversen, K. Y. Crous, A. C. Finzi, D. Tis-  
3041 sue, D. S. Ellsworth, R. Oren, and R. J. Norby (2009). Forest fine-root  
3042 production and nitrogen use under elevated CO<sub>2</sub>: contrasting responses

- 3043** in evergreen and deciduous trees explained by a common principle. *Global  
3044 Change Biology* 15(1), 132–144.
- 3045** Friedlingstein, P., M. Meinshausen, V. K. Arora, C. D. Jones, A. Anav, S. K.  
**3046** Liddicoat, and R. Knutti (2014). Uncertainties in CMIP5 climate projections  
**3047** due to carbon cycle feedbacks. *Journal of Climate* 27(2), 511–526.
- 3048** Friel, C. A. and M. L. Friesen (2019). Legumes modulate allocation to rhizobial  
**3049** nitrogen fixation in response to factorial light and nitrogen manipulation.  
**3050** *Frontiers in Plant Science* 10, 1316.
- 3051** Fujikake, H., A. Yamazaki, N. Ohtake, K. Sueoshi, S. Matsuhashi, T. Ito,  
**3052** C. Mizuniwa, T. Kume, S. Hoshimoto, N.-S. Ishioka, S. Watanabe, A. Osa,  
**3053** T. Sekine, H. Uchida, A. Tsuji, and T. Ohyama (2003). Quick and reversible  
**3054** inhibition of soybean root nodule growth by nitrate involves a decrease in  
**3055** sucrose supply to nodules. *Journal of Experimental Botany* 54(386), 1379–  
**3056** 1388.
- 3057** Ghannoum, O., J. R. Evans, and S. von Caemmerer (2011). Nitrogen and water  
**3058** use efficiency of C<sub>4</sub> plants. In A. S. Raghavendra and R. F. Sage (Eds.), *C<sub>4</sub>  
3059 Photosynthesis and Related CO<sub>2</sub> Concentrating Mechanisms*, Chapter 8, pp.  
**3060** 129–146. Springer.
- 3061** Ghimire, B., W. J. Riley, C. D. Koven, J. Kattge, A. Rogers, P. B. Reich, and  
**3062** I. J. Wright (2017). A global trait-based approach to estimate leaf nitrogen  
**3063** functional allocation from observations:. *Ecological Applications* 27(5),  
**3064** 1421–1434.
- 3065** Giardina, C. P., M. D. Coleman, J. E. Hancock, J. S. King, E. A. Lilleskov,  
**3066** W. M. Loya, K. S. Pregitzer, M. G. Ryan, and C. C. Trettin (2005). The

- 3067** response of belowground carbon allocation in forests to global change. In  
**3068** D. Binkley and O. Manyailo (Eds.), *Tree Species Effects on Soils: Implica-*  
**3069** *tions for Global Change* (Volume 55 ed.), Chapter Chapter 7, pp. 119–154.  
**3070** Berlin/Heidelberg: Springer-Verlag.
- 3071** Gibson, A. H. and J. E. Harper (1985). Nitrate effect on nodulation of soybean  
**3072** by *Bradyrhizobium japonicum*. *Crop Science* 25(3), 497–501.
- 3073** Gill, A. L. and A. C. Finzi (2016). Belowground carbon flux links biogeochemical  
**3074** cycles and resource-use efficiency at the global scale. *Ecology Letters* 19(12),  
**3075** 1419–1428.
- 3076** Goll, D. S., V. Brovkin, B. R. Parida, C. H. Reick, J. Kattge, P. B. Reich, P. M.  
**3077** van Bodegom, and Ü. Niinemets (2012). Nutrient limitation reduces land  
**3078** carbon uptake in simulations with a model of combined carbon, nitrogen  
**3079** and phosphorus cycling. *Biogeosciences Discussions* 9(3), 3173–3232.
- 3080** Gregory, L. M., A. M. McClain, D. M. Kramer, J. D. Pardo, K. E. Smith, O. L.  
**3081** Tessmer, B. J. Walker, L. G. Ziccardi, and T. D. Sharkey (2021, oct). The  
**3082** triose phosphate utilization limitation of photosynthetic rate: Out of global  
**3083** models but important for leaf models. *Plant, Cell and Environment* 44(10),  
**3084** 3223–3226.
- 3085** Grossiord, C., T. N. Buckley, L. A. Cernusak, K. A. Novick, B. Poulter, R. T. W.  
**3086** Siegwolf, J. S. Sperry, and N. G. McDowell (2020). Plant responses to rising  
**3087** vapor pressure deficit. *New Phytologist* 226(6), 1550–1566.
- 3088** Gulmon, S. L. and C. C. Chu (1981). The effects of light and nitrogen on pho-  
**3089** tosynthesis, leaf characteristics, and dry matter allocation in the chaparral  
**3090** shrub, *Diplacus aurantiacus*. *Oecologia* 49(2), 207–212.

- 3091 Gutschick, V. P. (1981). Evolved strategies in nitrogen acquisition by plants.
- 3092 *The American Naturalist* 118(5), 607–637.
- 3093 Hallik, L., Ü. Niinemets, and I. J. Wright (2009). Are species shade and drought
- 3094 tolerance reflected in leaf-level structural and functional differentiation in
- 3095 Northern Hemisphere temperate woody flora? *New Phytologist* 184(1), 257–
- 3096 274.
- 3097 Harrison, M. T., E. J. Edwards, G. D. Farquhar, A. B. Nicotra, and J. R.
- 3098 Evans (2009). Nitrogen in cell walls of sclerophyllous leaves accounts for
- 3099 little of the variation in photosynthetic nitrogen-use efficiency. *Plant, Cell*
- 3100 and *Environment* 32(3), 259–270.
- 3101 Harrison, S. P., W. Cramer, O. Franklin, I. C. Prentice, H. Wang,
- 3102 Å. Bränström, H. de Boer, U. Dieckmann, J. Joshi, T. F. Keenan,
- 3103 A. Lavergne, S. Manzoni, G. Mengoli, C. Morfopoulos, J. Peñuelas,
- 3104 S. Pietsch, K. T. Rebel, Y. Ryu, N. G. Smith, B. D. Stocker, and I. J.
- 3105 Wright (2021). Eco-evolutionary optimality as a means to improve vegeta-
- 3106 tion and land-surface models. *New Phytologist* 231(6), 2125–2141.
- 3107 Henneron, L., P. Kardol, D. A. Wardle, C. Cros, and S. Fontaine (2020). Rhizo-
- 3108 sphere control of soil nitrogen cycling: a key component of plant economic
- 3109 strategies. *New Phytologist* 228(4), 1269–1282.
- 3110 Hijmans, R. J. (2022). terra: Spatial Data Analysis.
- 3111 Hikosaka, K. and A. Shigeno (2009). The role of Rubisco and cell walls in the
- 3112 interspecific variation in photosynthetic capacity. *Oecologia* 160(3), 443–
- 3113 451.

- 3114** Hoagland, D. R. and D. I. Arnon (1950). The water culture method for growing  
**3115** plants without soil. *California Agricultural Experiment Station: 347* 347(2),  
**3116** 1–32.
- 3117** Hobbie, E. A. (2006). Carbon allocation to ectomycorrhizal fungi correlates  
**3118** with belowground allocation in culture studies. *Ecology* 87(3), 563–569.
- 3119** Hobbie, E. A. and J. E. Hobbie (2008). Natural abundance of  $^{15}\text{N}$  in nitrogen-  
**3120** limited forests and tundra can estimate nitrogen cycling through mycorrhizal  
**3121** fungi: a review. *Ecosystems* 11(5), 815–830.
- 3122** Hoek, T. A., K. Axelrod, T. Biancalani, E. A. Yurtsev, J. Liu, and J. Gore  
**3123** (2016). Resource availability modulates the cooperative and competitive na-  
**3124** nature of a microbial cross-feeding mutualism. *PLOS Biology* 14(8), e1002540.
- 3125** Höglberg, M. N., M. J. I. Briones, S. G. Keel, D. B. Metcalfe, C. Campbell, A. J.  
**3126** Midwood, B. Thornton, V. Hurry, S. Linder, T. Näsholm, and P. Höglberg  
**3127** (2010). Quantification of effects of season and nitrogen supply on tree below-  
**3128** ground carbon transfer to ectomycorrhizal fungi and other soil organisms in  
**3129** a boreal pine forest. *New Phytologist* 187(2), 485–493.
- 3130** Höglberg, P., M. N. Höglberg, S. G. Göttlicher, N. R. Betson, S. G. Keel, D. B.  
**3131** Metcalfe, C. Campbell, A. Schindlbacher, V. Hurry, T. Lundmark, S. Linder,  
**3132** and T. Näsholm (2008). High temporal resolution tracing of photosynthate  
**3133** carbon from the tree canopy to forest soil microorganisms. *New Phytolo-*  
**3134** *gist* 177(1), 220–228.
- 3135** Houlton, B. Z., Y.-P. Wang, P. M. Vitousek, and C. B. Field (2008). A uni-  
**3136** fying framework for dinitrogen fixation in the terrestrial biosphere. *Na-*  
**3137** *ture* 454(7202), 327–330.

- 3138** Huber, M. L., R. A. Perkins, A. Laesecke, D. G. Friend, J. V. Sengers, M. J.  
**3139** Assael, I. N. Metaxa, E. Vogel, R. Mareš, and K. Miyagawa (2009). New  
**3140** international formulation for the viscosity of H<sub>2</sub>O. *Journal of Physical and*  
**3141** *Chemical Reference Data* 38(2), 101–125.
- 3142** Hungate, B. A., J. S. Dukes, M. R. Shaw, Y. Luo, and C. B. Field (2003).  
**3143** Nitrogen and climate change. *Science* 302(5650), 1512–1513.
- 3144** IPCC (2021). *Climate Change 2021: The Physical Science Basis. Contribution*  
**3145** *of Working Group I to the Sixth Assessment Report of the Intergovernmental*  
**3146** *Panel on Climate Change*, Volume In Press. Cambridge, United Kingdom  
**3147** and New York, NY, USA: Cambridge University Press.
- 3148** Johnson, N. C., J. H. Graham, and F. A. Smith (1997). Functioning of mycor-  
**3149** rhizal associations along the mutualism-parasitism continuum. *New Phytol-*  
**3150** *ogist* 135(4), 575–585.
- 3151** Kachurina, O. M., H. Zhang, W. R. Raun, and E. G. Krenzer (2000). Simul-  
**3152** taneous determination of soil aluminum, ammonium- and nitrate- nitrogen  
**3153** using 1 M potassium chloride. *Communications in Soil Science and Plant*  
**3154** *Analysis* 31(7-8), 893–903.
- 3155** Kaiser, C., M. R. Kilburn, P. L. Clode, L. Fuchsleger, M. Koranda, J. B. Cliff,  
**3156** Z. M. Solaiman, and D. V. Murphy (2015). Exploring the transfer of recent  
**3157** plant photosynthates to soil microbes: mycorrhizal pathway vs direct root  
**3158** exudation. *New Phytologist* 205(4), 1537–1551.
- 3159** Katabuchi, M. (2015). LeafArea: An R package for rapid digital analysis of leaf  
**3160** area. *Ecological Research* 30(6), 1073–1077.

- 3161** Kattge, J. and W. Knorr (2007). Temperature acclimation in a biochemical  
**3162** model of photosynthesis: a reanalysis of data from 36 species. *Plant, Cell*  
**3163** and *Environment* 30(9), 1176–1190.
- 3164** Kattge, J., W. Knorr, T. Raddatz, and C. Wirth (2009). Quantifying photosyn-  
**3165** thetic capacity and its relationship to leaf nitrogen content for global-scale  
**3166** terrestrial biosphere models. *Global Change Biology* 15(4), 976–991.
- 3167** Kayler, Z., A. Gessler, and N. Buchmann (2010). What is the speed of link  
**3168** between aboveground and belowground processes? *New Phytologist* 187(4),  
**3169** 885–888.
- 3170** Kayler, Z., C. Keitel, K. Jansen, and A. Gessler (2017). Experimental evidence  
**3171** of two mechanisms coupling leaf-level C assimilation to rhizosphere CO<sub>2</sub>  
**3172** release. *Environmental and Experimental Botany* 135, 21–26.
- 3173** Keeling, C. D., W. G. Mook, and P. P. Tans (1979, jan). Recent trends in the  
**3174** <sup>13</sup>C:<sup>12</sup>C ratio of atmospheric carbon dioxide. *Nature* 277(5692), 121–123.
- 3175** Keeney, D. R. and D. W. Nelson (1983). Nitrogen—Inorganic Forms. In A. L.  
**3176** Page (Ed.), *Methods of Soil Analysis* (2nd ed.), Chapter 33, pp. 643–698.  
**3177** Madison, WI, USA: ASA and SSSA.
- 3178** Kenward, M. G. and J. H. Roger (1997). Small sample inference for fixed effects  
**3179** from restricted maximum likelihood. *Biometrics* 53(3), 983.
- 3180** Knapp, A. K., M. L. Avolio, C. Beier, C. J. W. Carroll, S. L. Collins, J. S.  
**3181** Dukes, L. H. Fraser, R. J. Griffin-Nolan, D. L. Hoover, A. Jentsch, M. E.  
**3182** Loik, R. P. Phillips, A. K. Post, O. E. Sala, I. J. Slette, L. Yahdjian, and  
**3183** M. D. Smith (2017). Pushing precipitation to the extremes in distributed

- 3184 experiments: recommendations for simulating wet and dry years. *Global  
3185 Change Biology* 23(5), 1774–1782.
- 3186 Knorr, W. (2000). Annual and interannual CO<sub>2</sub> exchanges of the  
3187 terrestrial biosphere: process-based simulations and uncertainties. *Global  
3188 Ecology and Biogeography* 9(3), 225–252.
- 3189 Knorr, W. and M. Heimann (2001). Uncertainties in global terrestrial biosphere  
3190 modeling: 1. A comprehensive sensitivity analysis with a new photosynthesis  
3191 and energy balance scheme. *Global Biogeochemical Cycles* 15(1), 207–225.
- 3192 Kulmatiski, A., P. B. Adler, J. M. Stark, and A. T. Tredennick (2017). Water  
3193 and nitrogen uptake are better associated with resource availability than  
3194 root biomass. *Ecosphere* 8(3), e01738.
- 3195 Lavergne, A., D. Sandoval, V. J. Hare, H. Graven, and I. C. Prentice (2020).  
3196 Impacts of soil water stress on the acclimated stomatal limitation of pho-  
3197 tosynthesis: Insights from stable carbon isotope data. *Global Change Biol-  
3198 ogy* 26(12), 7158–7172.
- 3199 Lawrence, D. M., R. A. Fisher, C. D. Koven, K. W. Oleson, S. C. Swen-  
3200 son, G. B. Bonan, N. Collier, B. Ghimire, L. Kampenhout, D. Kennedy,  
3201 E. Kluzek, P. J. Lawrence, F. Li, H. Li, D. L. Lombardozzi, W. J. Riley,  
3202 W. J. Sacks, M. Shi, M. Vertenstein, W. R. Wieder, C. Xu, A. A. Ali,  
3203 A. M. Badger, G. Bisht, M. Broeke, M. A. Brunke, S. P. Burns, J. Buzan,  
3204 M. Clark, A. Craig, K. M. Dahlin, B. Drewniak, J. B. Fisher, M. Flanner,  
3205 A. M. Fox, P. Gentine, F. M. Hoffman, G. Keppel-Aleks, R. Knox, S. Ku-  
3206 mar, J. Lenaerts, L. R. Leung, W. H. Lipscomb, Y. Lu, A. Pandey, J. D.  
3207 Pelletier, J. Perket, J. T. Randerson, D. M. Ricciuto, B. M. Sanderson,

- 3208** A. Slater, Z. M. Subin, J. Tang, R. Q. Thomas, M. Val Martin, and X. Zeng  
**3209** (2019). The Community Land Model Version 5: description of new features,  
**3210** benchmarking, and impact of forcing uncertainty. *Journal of Advances in*  
**3211** *Modeling Earth Systems* 11(12), 4245–4287.
- 3212** LeBauer, D. S. and K. K. Treseder (2008). Nitrogen limitation of net primary  
**3213** productivity. *Ecology* 89(2), 371–379.
- 3214** Lefcheck, J. S. (2016). piecewiseSEM: Piecewise structural equation modelling  
**3215** in r for ecology, evolution, and systematics. *Methods in Ecology and Evolu-*  
**3216** *tion* 7(5), 573–579.
- 3217** Lenth, R. (2019). emmeans: estimated marginal means, aka least-squares  
**3218** means.
- 3219** Li, W., H. Zhang, G. Huang, R. Liu, H. Wu, C. Zhao, and N. G. McDowell  
**3220** (2020). Effects of nitrogen enrichment on tree carbon allocation: A global  
**3221** synthesis. *Global Ecology and Biogeography* 29(3), 573–589.
- 3222** Liang, J., X. Qi, L. Souza, and Y. Luo (2016). Processes regulating progressive  
**3223** nitrogen limitation under elevated carbon dioxide: a meta-analysis. *Biogeosciences*  
**3224** 13(9), 2689–2699.
- 3225** Liang, X., T. Zhang, X. Lu, D. S. Ellsworth, H. BassiriRad, C. You, D. Wang,  
**3226** P. He, Q. Deng, H. Liu, J. Mo, and Q. Ye (2020). Global response patterns of  
**3227** plant photosynthesis to nitrogen addition: A meta-analysis. *Global Change*  
**3228** *Biology* 26(6), 3585–3600.
- 3229** López, J., D. A. Way, and W. Sadok (2021). Systemic effects of rising atmo-  
**3230** spheric vapor pressure deficit on plant physiology and productivity. *Global*

- 3231** *Change Biology* 27(9), 1704–1720.
- 3232** Lu, J., J. Yang, C. Keitel, L. Yin, P. Wang, W. Cheng, and F. A. Dijkstra
- 3233** (2022). Belowground carbon efficiency for nitrogen and phosphorus acqui-
- 3234** sition varies between *Lolium perenne* and *Trifolium repens* and depends on
- 3235** phosphorus fertilization. *Frontiers in Plant Science* 13, 1–9.
- 3236** Luo, X., T. F. Keenan, J. M. Chen, H. Croft, I. C. Prentice, N. G. Smith,
- 3237** A. P. Walker, H. Wang, R. Wang, C. Xu, and Y. Zhang (2021). Global
- 3238** variation in the fraction of leaf nitrogen allocated to photosynthesis. *Nature*
- 3239** *Communications* 12(1), 4866.
- 3240** Luo, Y., W. S. Currie, J. S. Dukes, A. C. Finzi, U. A. Hartwig, B. A. Hungate,
- 3241** R. E. McMurtrie, R. Oren, W. J. Parton, D. E. Pataki, R. M. Shaw, D. R.
- 3242** Zak, and C. B. Field (2004). Progressive nitrogen limitation of ecosystem
- 3243** responses to rising atmospheric carbon dioxide. *BioScience* 54(8), 731–739.
- 3244** Maire, V., P. Martre, J. Kattge, F. Gastal, G. Esser, S. Fontaine, and J.-F.
- 3245** Soussana (2012). The coordination of leaf photosynthesis links C and N
- 3246** fluxes in C<sub>3</sub> plant species. *PLoS ONE* 7(6), e38345.
- 3247** Makino, A. (2003). Rubisco and nitrogen relationships in rice: leaf photosyn-
- 3248** thesis and plant growth. *Soil Science and Plant Nutrition* 49(3), 319–327.
- 3249** Makino, A., M. Harada, T. Sato, H. Nakano, and T. Mae (1997). Growth and N
- 3250** Allocation in Rice Plants under CO<sub>2</sub> Enrichment. *Plant Physiology* 115(1),
- 3251** 199–203.
- 3252** Markham, J. H. and C. Zekveld (2007). Nitrogen fixation makes biomass al-
- 3253** location to roots independent of soil nitrogen supply. *Canadian Journal of*

- 3254** *Botany* (9), 787–793.
- 3255** Marschner, H. and B. Dell (1994). Nutrient uptake in mycorrhizal symbiosis.
- 3256** *Plant and Soil* 159(1), 89–102.
- 3257** Matamala, R. and W. H. Schlesinger (2000). Effects of elevated atmospheric
- 3258** CO<sub>2</sub> on fine root production and activity in an intact temperate forest
- 3259** ecosystem. *Global Change Biology* 6(8), 967–979.
- 3260** Medlyn, B. E., E. Dreyer, D. S. Ellsworth, M. Forstreuter, P. C. Harley,
- 3261** M. U. F. Kirschbaum, X. Le Roux, P. Montpied, J. Strassmeyer, A. Wal-
- 3262** croft, K. Wang, and D. Loustau (2002). Temperature response of parameters
- 3263** of a biochemically based model of photosynthesis. II. A review of experimen-
- 3264** tal data. *Plant, Cell and Environment* 25(9), 1167–1179.
- 3265** Menge, D. N. L., S. A. Levin, and L. O. Hedin (2008). Evolutionary tradeoffs can
- 3266** select against nitrogen fixation and thereby maintain nitrogen limitation.
- 3267** *Proceedings of the National Academy of Sciences* 105(5), 1573–1578.
- 3268** Menne, M. J., I. Durre, R. S. Vose, B. E. Gleason, and T. G. Houston (2012).
- 3269** An overview of the global historical climatology network-daily database.
- 3270** *Journal of Atmospheric and Oceanic Technology* 29(7), 897–910.
- 3271** Meyerholt, J., K. Sickel, and S. Zaehle (2020). Ensemble projections elucidate
- 3272** effects of uncertainty in terrestrial nitrogen limitation on future carbon up-
- 3273** take. *Global Change Biology* 26(7), 3978–3996.
- 3274** Meyerholt, J., S. Zaehle, and M. J. Smith (2016). Variability of projected ter-
- 3275** restrial biosphere responses to elevated levels of atmospheric CO<sub>2</sub> due to
- 3276** uncertainty in biological nitrogen fixation. *Biogeosciences* 13(5), 1491–1518.

- 3277** Minocha, R., S. Long, A. H. Magill, J. D. Aber, and W. H. McDowell (2000).
- 3278** Foliar free polyamine and inorganic ion content in relation to soil and soil
- 3279** solution chemistry in two fertilized forest stands at the Harvard Forest,
- 3280** Massachusetts. *Plant and Soil* 222(1-2), 119–137.
- 3281** Moore, D. J., S. Aref, R. M. Ho, J. S. Pippen, J. G. Hamilton, and E. H. De
- 3282** Lucia (2006). Annual basal area increment and growth duration of *Pinus*
- 3283** *taeda* in response to eight years of free-air carbon dioxide enrichment. *Global*
- 3284** *Change Biology* 12(8), 1367–1377.
- 3285** Morgan, J. A., D. E. Pataki, C. Körner, H. Clark, S. J. Del Grosso, J. M.
- 3286** Grünzweig, A. K. Knapp, A. R. Mosier, P. C. D. Newton, P. A. Niklaus,
- 3287** J. B. Nippert, R. S. Nowak, W. J. Parton, H. W. Polley, and M. R. Shaw
- 3288** (2004). Water relations in grassland and desert ecosystems exposed to ele-
- 3289** vated atmospheric CO<sub>2</sub>. *Oecologia* 140(1), 11–25.
- 3290** Muñoz, N., X. Qi, M. W. Li, M. Xie, Y. Gao, M. Y. Cheung, F. L. Wong, and
- 3291** H.-M. Lam (2016). Improvement in nitrogen fixation capacity could be part
- 3292** of the domestication process in soybean. *Heredity* 117(2), 84–93.
- 3293** Nadelhoffer, K. J. and J. W. Raich (1992). Fine root production estimates and
- 3294** belowground carbon allocation in forest ecosystems. *Ecology* 73(4), 1139–
- 3295** 1147.
- 3296** Niinemets, Ü. and J. D. Tenhunen (1997). A model separating leaf structural
- 3297** and physiological effects on carbon gain along light gradients for the shade-
- 3298** tolerant species *Acer saccharum*. *Plant, Cell and Environment* 20(7), 845–
- 3299** 866.
- 3300** Norby, R. J., J. Ledford, C. D. Reilly, N. E. Miller, and E. G. O'Neill

- 3301 (2004). Fine-root production dominates response of a deciduous forest to  
3302 atmospheric CO<sub>2</sub> enrichment. *Proceedings of the National Academy of Sci-*  
3303 *ences* 101(26), 9689–9693.
- 3304 Norby, R. J., J. M. Warren, C. M. Iversen, B. E. Medlyn, and R. E. Mc-  
3305 Murtrie (2010). CO<sub>2</sub> enhancement of forest productivity constrained by  
3306 limited nitrogen availability. *Proceedings of the National Academy of Sci-*  
3307 *ences* 107(45), 19368–19373.
- 3308 Novick, K. A., D. L. Ficklin, P. C. Stoy, C. A. Williams, G. Bohrer, A. C.  
3309 Oishi, S. A. Papuga, P. D. Blanken, A. Noormets, B. N. Sulman, R. L.  
3310 Scott, L. Wang, and R. P. Phillips (2016). The increasing importance of  
3311 atmospheric demand for ecosystem water and carbon fluxes. *Nature Climate  
3312 Change* 6(11), 1023–1027.
- 3313 Noyce, G. L., M. L. Kirwan, R. L. Rich, and J. P. Megonigal (2019). Asyn-  
3314 chronous nitrogen supply and demand produce nonlinear plant allocation re-  
3315 sponds to warming and elevated CO<sub>2</sub>. *Proceedings of the National Academy  
3316 of Sciences* 116(43), 21623–21628.
- 3317 Onoda, Y., K. Hikosaka, and T. Hirose (2004). Allocation of nitrogen to  
3318 cell walls decreases photosynthetic nitrogen-use efficiency. *Functional Ecol-  
3319 ogy* 18(3), 419–425.
- 3320 Onoda, Y., I. J. Wright, J. R. Evans, K. Hikosaka, K. Kitajima, Ü. Niinemets,  
3321 H. Poorter, T. Tosens, and M. Westoby (2017). Physiological and structural  
3322 trade-offs underlying the leaf economics spectrum. *New Phytologist* 214(4),  
3323 1447–1463.
- 3324 Oren, R., J. S. Sperry, G. G. Katul, D. E. Pataki, B. E. Ewers, N. Phillips,

- 3325 and K. V. R. Schäfer (1999). Survey and synthesis of intra- and interspecific  
3326 variation in stomatal sensitivity to vapor pressure deficit. *Plant, Cell and*  
3327 *Environment* 22(12), 1515–1526.
- 3328 Oreskes, N., K. Shrader-Frechette, and K. Belitz (1994). Verification, vali-  
3329 dation, and confirmation of numerical models in the Earth sciences. *Sci-  
3330 ence* 263(5147), 641–646.
- 3331 Paillassa, J., I. J. Wright, I. C. Prentice, S. Pepin, N. G. Smith, G. Ethier,  
3332 A. C. Westerband, L. J. Lamarque, H. Wang, W. K. Cornwell, and V. Maire  
3333 (2020). When and where soil is important to modify the carbon and water  
3334 economy of leaves. *New Phytologist* 228(1), 121–135.
- 3335 Parvin, S., S. Uddin, S. Tausz Posch, R. Armstrong, and M. Tausz (2020). Car-  
3336 bon sink strength of nodules but not other organs modulates photosynthesis  
3337 of faba bean (*Vicia faba*) grown under elevated [CO<sub>2</sub>] and different water  
3338 supply. *New Phytologist* 227(1), 132–145.
- 3339 Paul, K. I., P. J. Polglase, A. M. O'Connell, J. C. Carlyle, P. J. Smethurst, and  
3340 P. K. Khanna (2003). Defining the relation between soil water content and  
3341 net nitrogen mineralization. *European Journal of Soil Science* 54(1), 39–48.
- 3342 Peng, Y., K. J. Bloomfield, L. A. Cernusak, T. F. Domingues, and I. C. Pren-  
3343 tice (2021). Global climate and nutrient controls of photosynthetic capacity.  
3344 *Communications Biology* 4(1), 462.
- 3345 Perkowski, E. A., E. F. Waring, and N. G. Smith (2021). Root mass carbon  
3346 costs to acquire nitrogen are determined by nitrogen and light availabil-  
3347 ity in two species with different nitrogen acquisition strategies. *Journal of  
3348 Experimental Botany* 72(15), 5766–5776.

- 3349** Phillips, R. P., E. R. Brzostek, and M. G. Midgley (2013). The mycorrhizal-  
**3350** associated nutrient economy: a new framework for predicting carbon-  
**3351** nutrient couplings in temperate forests. *New Phytologist* 199(1), 41–51.
- 3352** Phillips, R. P., A. C. Finzi, and E. S. Bernhardt (2011). Enhanced root ex-  
**3353** udation induces microbial feedbacks to N cycling in a pine forest under  
**3354** long-term CO<sub>2</sub> fumigation. *Ecology Letters* 14(2), 187–194.
- 3355** Pinheiro, J. and D. Bates (2022). nlme: linear and nonlinear mixed effects  
**3356** models.
- 3357** Poggio, L., L. M. De Sousa, N. H. Batjes, G. B. M. Heuvelink, B. Kempen,  
**3358** E. Ribeiro, and D. Rossiter (2021). SoilGrids 2.0: Producing soil information  
**3359** for the globe with quantified spatial uncertainty. *Soil* 7(1), 217–240.
- 3360** Pons, T. L. and R. W. Pearcy (1994). Nitrogen reallocation and photosynthetic  
**3361** acclimation in response to partial shading in soybean plants. *Physiologia*  
**3362** *Plantarum* 92(4), 636–644.
- 3363** Poorter, H., J. Bühler, D. Van Dusschoten, J. Climent, and J. A. Postma (2012).  
**3364** Pot size matters: A meta-analysis of the effects of rooting volume on plant  
**3365** growth. *Functional Plant Biology* 39(11), 839–850.
- 3366** Poorter, H., O. Knopf, I. J. Wright, A. A. Temme, S. W. Hogewoning, A. Graf,  
**3367** L. A. Cernusak, and T. L. Pons (2022). A meta-analysis of responses of C<sub>3</sub>  
**3368** plants to atmospheric CO<sub>2</sub>: dose-response curves for 85 traits ranging from  
**3369** the molecular to the whole-plant level. *New Phytologist* 233(4), 1560–1596.
- 3370** Prentice, I. C., N. Dong, S. M. Gleason, V. Maire, and I. J. Wright (2014).  
**3371** Balancing the costs of carbon gain and water transport: testing a new theo-

- 3372 retical framework for plant functional ecology. *Ecology Letters* 17(1), 82–91.
- 3373 Prentice, I. C., X. Liang, B. E. Medlyn, and Y.-P. Wang (2015). Reliable, ro-
- 3374 bust and realistic: The three R's of next-generation land-surface modelling.
- 3375 *Atmospheric Chemistry and Physics* 15, 5987–6005.
- 3376 Priestley, C. H. B. and R. J. Taylor (1972). On the Assessment of Surface
- 3377 Heat Flux and Evaporation Using Large-Scale Parameters. *Monthly Weather*
- 3378 *Review* 100(2), 81–92.
- 3379 Querejeta, J. I., I. Prieto, C. Armas, F. Casanoves, J. S. Diémé, M. Diouf,
- 3380 H. Yossi, B. Kaya, F. I. Pugnaire, and G. M. Rusch (2022). Higher leaf
- 3381 nitrogen content is linked to tighter stomatal regulation of transpiration
- 3382 and more efficient water use across dryland trees. *New Phytologist* 235(4),
- 3383 1351–1364.
- 3384 R Core Team (2021). R: A language and environment for statistical computing.
- 3385 Raich, J. W., D. A. Clark, L. Schwendenmann, and T. E. Wood (2014). Above-
- 3386 ground tree growth varies with belowground carbon allocation in a tropical
- 3387 rainforest environment. *PLoS ONE* 9(6), e100275.
- 3388 Rastetter, E. B., P. M. Vitousek, C. B. Field, G. R. Shaver, D. Herbert, and
- 3389 G. I. Ågren (2001). Resource optimization and symbiotic nitrogen fixation.
- 3390 *Ecosystems* 4(4), 369–388.
- 3391 Reich, P. B. (2014). The world-wide 'fast-slow' plant economics spectrum: a
- 3392 traits manifesto. *Journal of Ecology* 102(2), 275–301.
- 3393 Reich, P. B., S. E. Hobbie, T. Lee, D. S. Ellsworth, J. B. West, D. Tilman,
- 3394 J. M. H. Knops, S. Naeem, and J. Trost (2006). Nitrogen limitation con-

- 3395 strains sustainability of ecosystem response to CO<sub>2</sub>. *Nature* 440(7086), 922–  
3396 925.
- 3397 Reichman, G. A., D. L. Grunes, and F. G. Viets (1966). Effect of soil moisture  
3398 on ammonification and nitrification in two Northern Plains soils. *Soil Science  
3399 Society of America Journal* 30(3), 363–366.
- 3400 Rhine, E. D., R. L. Mulvaney, E. J. Pratt, and G. K. Sims (1998). Improving  
3401 the Berthelot reaction for determining ammonium in soil extracts and water.  
3402 *Soil Science Society of America Journal* 62(2), 473.
- 3403 Rogers, A. (2014). The use and misuse of  $V_{cmax}$  in Earth System Models. *Photo-  
3404 tosynthesis Research* 119(1-2), 15–29.
- 3405 Rogers, A., B. E. Medlyn, J. S. Dukes, G. B. Bonan, S. Caemmerer, M. C.  
3406 Dietze, J. Kattge, A. D. B. Leakey, L. M. Mercado, Ü. Niinemets, I. C.  
3407 Prentice, S. P. Serbin, S. Sitch, D. A. Way, and S. Zaehle (2017). A roadmap  
3408 for improving the representation of photosynthesis in Earth system models.  
3409 *New Phytologist* 213(1), 22–42.
- 3410 Saathoff, A. J. and J. Welles (2021). Gas exchange measurements in the un-  
3411 steady state. *Plant Cell and Environment* 44(11), 3509–3523.
- 3412 Sage, R. F. and R. W. Pearcy (1987). The nitrogen use efficiency of C<sub>3</sub> and C<sub>4</sub>  
3413 plants: I. Leaf nitrogen, growth, and biomass partitioning in *Chenopodium  
3414 album* (L.) and *Amaranthus retroflexus* (L.). *Plant Physiology* 84(3), 954–  
3415 958.
- 3416 Saleh, A. M., M. Abdel-Mawgoud, A. R. Hassan, T. H. Habeeb, R. S. Yehia,  
3417 and H. AbdElgawad (2020). Global metabolic changes induced by arbuscular

- 3418 mycorrhizal fungi in oregano plants grown under ambient and elevated levels  
3419 of atmospheric CO<sub>2</sub>. *Plant Physiology and Biochemistry* 151, 255–263.
- 3420 Saxton, K. E. and W. J. Rawls (2006). Soil water characteristic estimates by  
3421 texture and organic matter for hydrologic solutions. *Soil Science Society of  
3422 America Journal* 70(5), 1569–1578.
- 3423 Schaefer, K., C. R. Schwalm, C. Williams, M. A. Arain, A. Barr, J. M. Chen,  
3424 K. J. Davis, D. Dimitrov, T. W. Hilton, D. Y. Hollinger, E. Humphreys,  
3425 B. Poulter, B. M. Racza, A. D. Richardson, A. Sahoo, P. Thornton, R. Var-  
3426 gas, H. Verbeeck, R. Anderson, I. Baker, T. A. Black, P. Bolstad, J. Chen,  
3427 P. S. Curtis, A. R. Desai, M. C. Dietze, D. Dragoni, C. M. Gough, R. F.  
3428 Grant, L. Gu, A. K. Jain, C. Kucharik, B. E. Law, S. Liu, E. Lokipitiya,  
3429 H. A. Margolis, R. Matamala, J. H. McCaughey, R. Monson, J. W. Munger,  
3430 W. Oechel, C. Peng, D. T. Price, D. Ricciuto, W. J. Riley, N. Roulet,  
3431 H. Tian, C. Tonitto, M. Torn, E. Weng, and X. Zhou (2012). A model-  
3432 data comparison of gross primary productivity: Results from the North  
3433 American Carbon Program site synthesis. *Journal of Geophysical Research:  
3434 Biogeosciences* 117(G3), G03010.
- 3435 Schmitt, M. R. and G. E. Edwards (1981). Photosynthetic capacity and nitrogen  
3436 use efficiency of maize, wheat, and rice: A comparison between C<sub>3</sub> and C<sub>4</sub>  
3437 photosynthesis. *Journal of Experimental Botany* 32(3), 459–466.
- 3438 Schneider, C. A., W. S. Rasband, and K. W. Eliceiri (2012). NIH Image to  
3439 ImageJ: 25 years of image analysis. *Nature Methods* 9(7), 671–675.
- 3440 Scott, H. G. and N. G. Smith (2022). A Model of C<sub>4</sub> photosynthetic acclima-  
3441 tion based on least-cost optimality theory suitable for Earth system model

- 3442** incorporation. *Journal of Advances in Modeling Earth Systems* 14(3), 1–16.
- 3443** Shi, M., J. B. Fisher, E. R. Brzostek, and R. P. Phillips (2016). Carbon cost
- 3444** of plant nitrogen acquisition: Global carbon cycle impact from an improved
- 3445** plant nitrogen cycle in the Community Land Model. *Global Change Biology*
- 3446** 22(3), 1299–1314.
- 3447** Shi, M., J. B. Fisher, R. P. Phillips, and E. R. Brzostek (2019). Neglecting
- 3448** plant–microbe symbioses leads to underestimation of modeled climate im-
- 3449** pacts. *Biogeosciences* 16(2), 457–465.
- 3450** Smith, B., D. Wärllind, A. Arneth, T. Hickler, P. Leadley, J. Siltberg, and
- 3451** S. Zaehle (2014). Implications of incorporating N cycling and N limitations
- 3452** on primary production in an individual-based dynamic vegetation model.
- 3453** *Biogeosciences* 11(7), 2027–2054.
- 3454** Smith, N. G. and J. S. Dukes (2013). Plant respiration and photosynthesis in
- 3455** global-scale models: incorporating acclimation to temperature and CO<sub>2</sub>.
- 3456** *Global Change Biology* 19(1), 45–63.
- 3457** Smith, N. G. and J. S. Dukes (2018). Drivers of leaf carbon exchange capacity
- 3458** across biomes at the continental scale. *Ecology* 99(7), 1610–1620.
- 3459** Smith, N. G. and T. F. Keenan (2020). Mechanisms underlying leaf photosyn-
- 3460** thetic acclimation to warming and elevated CO<sub>2</sub> as inferred from least-cost
- 3461** optimality theory. *Global Change Biology* 26(9), 5202–5216.
- 3462** Smith, N. G., T. F. Keenan, I. C. Prentice, H. Wang, I. J. Wright, Ü. Niinemets,
- 3463** K. Y. Crous, T. F. Domingues, R. Guerrieri, F. oko Ishida, J. Kattge, E. L.
- 3464** Kruger, V. Maire, A. Rogers, S. P. Serbin, L. Tarvainen, H. F. Togashi,

- 3465** P. A. Townsend, M. Wang, L. K. Weerasinghe, and S.-X. Zhou (2019).  
**3466** Global photosynthetic capacity is optimized to the environment. *Ecology Letters* 22(3), 506–517.
- 3468** Smith, N. G., D. L. Lombardozzi, A. Tawfik, G. B. Bonan, and J. S. Dukes  
**3469** (2017). Biophysical consequences of photosynthetic temperature acclimation  
**3470** for climate. *Journal of Advances in Modeling Earth Systems* 9(1), 536–547.
- 3471** Smith, N. G., S. L. Malyshev, E. Shevliakova, J. Kattge, and J. S. Dukes  
**3472** (2016). Foliar temperature acclimation reduces simulated carbon sensitivity  
**3473** to climate. *Nature Climate Change* 6(4), 407–411.
- 3474** Smith, S. E. and D. J. Read (2008). *Mycorrhizal Symbiosis*. Academic Press.
- 3475** Soil Survey Staff (2022). Web Soil Survey.
- 3476** Soudzilovskaia, N. A., J. C. Douma, A. A. Akhmetzhanova, P. M. van Bode-  
**3477** gom, W. K. Cornwell, E. J. Moens, K. K. Treseder, and J. H. C. Cornelissen  
**3478** (2015). Global patterns of plant root colonization intensity by mycorrhizal  
**3479** fungi explained by climate and soil chemistry. *Global Ecology and Biogeogra-*  
**3480** *phy* 24(3), 371–382.
- 3481** Stark, J. M. and M. K. Firestone (1995). Mechanisms for soil moisture ef-  
**3482** fects on activity of nitrifying bacteria. *Applied and Environmental Microbiol-*  
**3483** *ogy* 61(1), 218–221.
- 3484** Stocker, B. D., H. Wang, N. G. Smith, S. P. Harrison, T. F. Keenan, D. San-  
**3485** doval, T. Davis, and I. C. Prentice (2020). P-model v1.0: An optimality-  
**3486** based light use efficiency model for simulating ecosystem gross primary pro-  
**3487** duction. *Geoscientific Model Development* 13(3), 1545–1581.

- 3488** Stocker, B. D., J. Zscheischler, T. F. Keenan, I. C. Prentice, J. Peñuelas, and  
**3489** S. I. Seneviratne (2018). Quantifying soil moisture impacts on light use  
**3490** efficiency across biomes. *New Phytologist* 218(4), 1430–1449.
- 3491** Sulman, B. N., D. T. Roman, K. Yi, L. Wang, R. P. Phillips, and K. A.  
**3492** Novick (2016). High atmospheric demand for water can limit forest car-  
**3493** bon uptake and transpiration as severely as dry soil. *Geophysical Research*  
**3494** *Letters* 43(18), 9686–9695.
- 3495** Sulman, B. N., E. Shevliakova, E. R. Brzostek, S. N. Kivlin, S. L. Malyshev,  
**3496** D. N. L. Menge, and X. Zhang (2019). Diverse mycorrhizal associations  
**3497** enhance terrestrial C storage in a global model. *Global Biogeochemical Cy-  
3498 cles* 33(4), 501–523.
- 3499** Sweet, S. K., D. W. Wolfe, A. DeGaetano, and R. Benner (2017). Anatomy  
**3500** of the 2016 drought in the Northeastern United States: Implications for  
**3501** agriculture and water resources in humid climates. *Agricultural and Forest*  
**3502** *Meteorology* 247, 571–581.
- 3503** Taylor, B. N. and D. N. L. Menge (2018). Light regulates tropical symbiotic  
**3504** nitrogen fixation more strongly than soil nitrogen. *Nature Plants* 4(9), 655–  
**3505** 661.
- 3506** Terrer, C., S. Vicca, B. A. Hungate, R. P. Phillips, and I. C. Prentice (2016).  
**3507** Mycorrhizal association as a primary control of the CO<sub>2</sub> fertilization effect.  
**3508** *Science* 353(6294), 72–74.
- 3509** Terrer, C., S. Vicca, B. D. Stocker, B. A. Hungate, R. P. Phillips, P. B. Reich,  
**3510** A. C. Finzi, and I. C. Prentice (2018). Ecosystem responses to elevated CO<sub>2</sub>  
**3511** governed by plant–soil interactions and the cost of nitrogen acquisition. *New*

- 3512      *Phytologist* 217(2), 507–522.
- 3513      Thieurmel, B. and A. Elmarhraoui (2019). suncalc: Compute sun position,
- 3514      sunlight phases, moon position, and lunar phase.
- 3515      Thomas, R. Q., E. N. J. Brookshire, and S. Gerber (2015). Nitrogen limita-
- 3516      tion on land: how can it occur in Earth system models? *Global Change*
- 3517      *Biology* 21(5), 1777–1793.
- 3518      Thomas, R. Q., S. Zaehle, P. H. Templer, and C. L. Goodale (2013). Global pat-
- 3519      terns of nitrogen limitation: confronting two global biogeochemical models
- 3520      with observations. *Global Change Biology* 19(10), 2986–2998.
- 3521      Thornton, P. E., J.-F. Lamarque, N. A. Rosenbloom, and N. M. Mahowald
- 3522      (2007). Influence of carbon-nitrogen cycle coupling on land model response
- 3523      to CO<sub>2</sub> fertilization and climate variability. *Global Biogeochemical Cy-*
- 3524      *cles* 21(4), GB4018.
- 3525      Tingey, D. T., D. L. Phillips, and M. G. Johnson (2000). Elevated CO<sub>2</sub> and
- 3526      conifer roots: effects on growth, life span and turnover. *New Phytolo-*
- 3527      *gist* 147(1), 87–103.
- 3528      Udvardi, M. and P. S. Poole (2013). Transport and metabolism in legume-
- 3529      rhizobia symbioses. *Annual Review of Plant Biology* 64, 781–805.
- 3530      USDA NRCS (2022). The PLANTS Database.
- 3531      Uselman, S. M., R. G. Qualls, and R. B. Thomas (2000). Effects of increased
- 3532      atmospheric CO<sub>2</sub>, temperature, and soil N availability on root exudation
- 3533      of dissolved organic carbon by an N-fixing tree (*Robinia pseudoacacia* L.).
- 3534      *Plant and Soil* 222, 191–202.

- 3535 van Diepen, L. T. A., E. A. Lilleskov, K. S. Pregitzer, and R. M. Miller (2007).
- 3536 Decline of arbuscular mycorrhizal fungi in northern hardwood forests ex-
- 3537 posed to chronic nitrogen additions. *New Phytologist* 176(1), 175–183.
- 3538 Vance, C. P. and G. H. Heichel (1991). Carbon in N<sub>2</sub> fixation: Limitation or
- 3539 exquisite adaptation. *Annual Review of Plant Physiology and Plant Molec-*
- 3540 *ular Biology* 42(1), 373–392.
- 3541 Viet, H. D., J.-H. Kwak, K.-S. Lee, S.-S. Lim, M. Matsushima, S. X. Chang,
- 3542 K.-H. Lee, and W.-J. Choi (2013). Foliar chemistry and tree ring δ<sup>13</sup>C of
- 3543 *Pinus densiflora* in relation to tree growth along a soil pH gradient. *Plant*
- 3544 *and Soil* 363(1-2), 101–112.
- 3545 Vitousek, P. M., K. Cassman, C. C. Cleveland, T. Crews, C. B. Field, N. B.
- 3546 Grimm, R. W. Howarth, R. Marino, L. Martinelli, E. B. Rastetter, and
- 3547 J. I. Sprent (2002). Towards an ecological understanding of biological nitro-
- 3548 gen fixation. In *The Nitrogen Cycle at Regional to Global Scales*, pp. 1–45.
- 3549 Springer Netherlands.
- 3550 Vitousek, P. M. and R. W. Howarth (1991). Nitrogen limitation on land and in
- 3551 the sea: How can it occur? *Biogeochemistry* 13(2), 87–115.
- 3552 Vitousek, P. M., S. Porder, B. Z. Houlton, and O. A. Chadwick (2010).
- 3553 Terrestrial phosphorus limitation: mechanisms, implications, and nitro-
- 3554 gen–phosphorus interactions. *Ecological Applications* 20(1), 5–15.
- 3555 Walker, A. P., A. P. Beckerman, L. Gu, J. Kattge, L. A. Cernusak, T. F.
- 3556 Domingues, J. C. Scales, G. Wohlfahrt, S. D. Wullschleger, and F. I. Wood-
- 3557 ward (2014). The relationship of leaf photosynthetic traits - V<sub>cmax</sub> and J<sub>max</sub>
- 3558 - to leaf nitrogen, leaf phosphorus, and specific leaf area: a meta-analysis

- 3559 and modeling study. *Ecology and Evolution* 4(16), 3218–3235.
- 3560 Walker, A. P., A. L. Johnson, A. Rogers, J. Anderson, R. A. Bridges, R. A.
- 3561 Fisher, D. Lu, D. M. Ricciuto, S. P. Serbin, and M. Ye (2021). Multi-
- 3562 hypothesis comparison of Farquhar and Collatz photosynthesis models re-
- 3563 veals the unexpected influence of empirical assumptions at leaf and global
- 3564 scales. *Global Change Biology* 27(4), 804–822.
- 3565 Wang, H., I. C. Prentice, T. F. Keenan, T. W. Davis, I. J. Wright, W. K.
- 3566 Cornwell, B. J. Evans, and C. Peng (2017). Towards a universal model for
- 3567 carbon dioxide uptake by plants. *Nature Plants* 3(9), 734–741.
- 3568 Wang, H., I. C. Prentice, I. J. Wright, D. I. Warton, S. Qiao, X. Xu, J. Zhou,
- 3569 Kikuzawa, and N. C. Stenseth (2023). Leaf economics fundamentals ex-
- 3570 plained by optimality principles. *Science Advances* 9(3), eadd566.
- 3571 Wang, J., J. M. Knops, C. E. Brassil, and C. Mu (2017). Increased productivity
- 3572 in wet years drives a decline in ecosystem stability with nitrogen additions
- 3573 in arid grasslands. *Ecology* 98(7), 1779–1786.
- 3574 Wang, W., Y. Wang, G. Hoch, Z. Wang, and J. Gu (2018). Linkage of root mor-
- 3575 phology to anatomy with increasing nitrogen availability in six temperate
- 3576 tree species. *Plant and Soil* 425(1-2), 189–200.
- 3577 Weatherburn, M. W. (1967). Phenol-hypochlorite reaction for determination of
- 3578 ammonia. *Analytical Chemistry* 39(8), 971–974.
- 3579 Wellburn, A. R. (1994). The spectral determination of chlorophylls a and b, as
- 3580 well as total carotenoids, using various solvents with spectrophotometers of
- 3581 different resolution. *Journal of Plant Physiology* 144(3), 307–313.

- 3582 Wen, Z., P. J. White, J. Shen, and H. Lambers (2022). Linking root exuda-  
3583 tion to belowground economic traits for resource acquisition. *New Phytolo-*  
3584 *gist* 233(4), 1620–1635.
- 3585 Westerband, A. C., I. J. Wright, V. Maire, J. Paillassa, I. C. Prentice, O. K.  
3586 Atkin, K. J. Bloomfield, L. A. Cernusak, N. Dong, S. M. Gleason, C. Guil-  
3587 herme Pereira, H. Lambers, M. R. Leishman, Y. Malhi, and R. H. Nolan  
3588 (2023). Coordination of photosynthetic traits across soil and climate gradi-  
3589 ents. *Global Change Biology* 29(3), 1–29.
- 3590 Wieder, W. R., C. C. Cleveland, W. K. Smith, and K. Todd-Brown (2015).  
3591 Future productivity and carbon storage limited by terrestrial nutrient avail-  
3592 ability. *Nature Geoscience* 8(6), 441–444.
- 3593 Wieder, W. R., D. M. Lawrence, R. A. Fisher, G. B. Bonan, S. J. Cheng, C. L.  
3594 Goodale, A. S. Grandy, C. D. Koven, D. L. Lombardozzi, K. W. Oleson,  
3595 and R. Q. Thomas (2019). Beyond static benchmarking: using experimental  
3596 manipulations to evaluate land model assumptions. *Global Biogeochemical*  
3597 *Cycles* 33(10), 1289–1309.
- 3598 Wright, I. J., P. B. Reich, and M. Westoby (2003). Least-cost input mixtures  
3599 of water and nitrogen for photosynthesis. *The American Naturalist* 161(1),  
3600 98–111.
- 3601 Wright, I. J., P. B. Reich, M. Westoby, D. D. Ackerly, Z. Baruch, F. Bongers,  
3602 J. Cavender-Bares, T. Chapin, J. H. C. Cornelissen, M. Diemer, J. Flexas,  
3603 E. Garnier, P. K. Groom, J. Gulias, K. Hikosaka, B. B. Lamont, T. Lee,  
3604 W. Lee, C. Lusk, J. J. Midgley, M.-L. Navas, Ü. Niinemets, J. Oleksyn,  
3605 N. Osada, H. Poorter, P. Poot, L. Prior, V. I. Pyankov, C. Roumet, S. C.

- 3606** Thomas, M. G. Tjoelker, E. J. Veneklaas, and R. Villar (2004). The world-wide leaf economics spectrum. *Nature* 428(6985), 821–827.
- 3607**
- 3608** Xu-Ri and I. C. Prentice (2017). Modelling the demand for new nitrogen fixation by terrestrial ecosystems. *Biogeosciences* 14(7), 2003–2017.
- 3609**
- 3610** Yahdjian, L., L. A. Gherardi, and O. E. Sala (2011). Nitrogen limitation in arid-subhumid ecosystems: A meta-analysis of fertilization studies. *Journal of Arid Environments* 75(8), 675–680.
- 3611**
- 3612**
- 3613** Zaehle, S., B. E. Medlyn, M. G. De Kauwe, A. P. Walker, M. C. Dietze, T. Hickler, Y. Luo, Y. P. Wang, B. El-Masri, P. Thornton, A. Jain, S. Wang,
- 3614**
- 3615** D. Warlind, E. Weng, W. Parton, C. M. Iversen, A. Gallet-Budynek, H. McCarthy, A. C. Finzi, P. J. Hanson, I. C. Prentice, R. Oren, and R. J. Norby
- 3616**
- 3617** (2014). Evaluation of 11 terrestrial carbon-nitrogen cycle models against observations from two temperate Free-Air CO<sub>2</sub> Enrichment studies. *New Phytologist* 202(3), 803–822.
- 3618**
- 3619**
- 3620** Zaehle, S., S. Sitch, B. Smith, and F. Hatterman (2005). Effects of parameter uncertainties on the modeling of terrestrial biosphere dynamics. *Global Biogeochemical Cycles* 19(3), GB3020.
- 3621**
- 3622**
- 3623** Zhu, Q., W. J. Riley, J. Tang, N. Collier, F. M. Hoffman, X. Yang, and G. Bisht
- 3624**
- 3625** (2019). Representing nitrogen, phosphorus, and carbon interactions in the E3SM land model: development and global benchmarking. *Journal of Advances in Modeling Earth Systems* 11(7), 2238–2258.
- 3626**
- 3627** Ziegler, C., M. E. Dusenge, B. Nyirambangutse, E. Zibera, G. Wallin, and
- 3628**
- 3629** J. Uddling (2020). Contrasting dependencies of photosynthetic capacity on leaf nitrogen in early- and late-successional tropical montane tree species.

- 3630** *Frontiers in Plant Science* 11, 1–12.
- 3631** Ziehn, T., J. Kattge, W. Knorr, and M. Scholze (2011). Improving the pre-  
**3632** dictability of global CO<sub>2</sub> assimilation rates under climate change. *Geophys-  
**3633** ical Research Letters* 38(10), L10404.

3634      **Appendix A: Supplemental material for "Structural carbon costs to**  
 3635      **acquire nitrogen are determined by nitrogen and light availability in**  
 3636      **two species with different nitrogen acquisition strategies"**

**Table A1.** Summary table containing volumes of compounds used to create modified Hoagland's solutions for each soil nitrogen fertilization treatment. All volumes are expressed as milliliters per liter (mL/L)

Compound	0 ppm N	70 ppm N	210 ppm N	630 ppm N
1 M NH <sub>4</sub> H <sub>2</sub> PO <sub>4</sub>	0	0.33	1	1
2 M KNO <sub>3</sub>	0	0.67	2	2
2 M Ca(NO <sub>3</sub> ) <sub>2</sub>	0	0.67	2	2
1 M NH <sub>4</sub> NO <sub>3</sub>	0	0.33	1	0
8 M NH <sub>4</sub> NO <sub>3</sub>	0	0	0	2
1 M KH <sub>2</sub> PO <sub>4</sub>	1	0.67	0	0
1 M KCl	4	1.33	0	0
1 M CaCO <sub>3</sub>	4	3	0	0
2 M MgSO <sub>4</sub>	1	1	1	1
10% Fe-EDTA	1	1	1	1
Trace Elements	1	1	1	1

**Table A2.** Analysis of variance results exploring species-specific effects of light availability, nitrogen fertilization, and their interactions on the ratio of whole plant biomass to pot volume (g L<sup>-1</sup>)\*

	df	Coefficient	$\chi^2$	p
<i>G. hirsutum</i>				
Intercept		0.740	-	-
Light (L)	1	-4.23E-03	189.581	<b>&lt;0.001</b>
Nitrogen (N)	1	7.86E-04	17.927	<b>&lt;0.001</b>
L*N	1	-6.61E-06	4.709	<b>0.030</b>
<i>G. max</i>				
Intercept		-0.233	-	-
Light (L)	1	-1.12E-02	69.500	<b>&lt;0.001</b>
Nitrogen (N)	1	8.29E-04	40.297	<b>&lt;0.001</b>
L*N	1	-8.51E-06	5.548	<b>0.019</b>

**3637** \*Significance determined using Wald's  $\chi^2$  tests ( $p=0.05$ ). *P*-values less than 0.05  
**3638** are in bold and *p*-values between 0.05 and 0.1 are italicized. Negative coefficients  
**3639** for light treatments indicate a positive effect of increasing light availability on  
**3640** all response variables, as light availability is treated as percent shade cover in all  
**3641** linear mixed-effects models.

**Table A3.** Slopes of the regression line describing the relationship between each dependent variable and nitrogen fertilization at each light level\*

Shade cover	Slope
<i>G. hirsutum</i>	
0%	<b>8.29E-04<sup>a</sup></b>
30%	<b>5.74E-04<sup>a</sup></b>
50%	<b>4.03E-04<sup>a</sup></b>
80%	1.48E-04 <sup>a</sup>
<i>G. max</i>	
0%	<b>7.86E-04</b>
30%	<b>5.87E-04</b>
50%	<b>4.55E-04</b>
80%	<i>2.57E-05</i>

205

**3642** \*Slopes represent estimated marginal mean slopes from linear mixed-effects models described in the Methods. Slopes  
**3643** were calculated using the ‘emmeans’ R package (Lenth 2019). Superscripts indicate slopes fit to natural-log (<sup>a</sup>) or  
**3644** square root (<sup>b</sup>) transformed data. Slopes statistically different from zero (Tukey:  $p < 0.05$ ) are indicated in bold.  
**3645** Marginally significant slopes (Tukey:  $0.05 < p < 0.1$ ) are italicized.

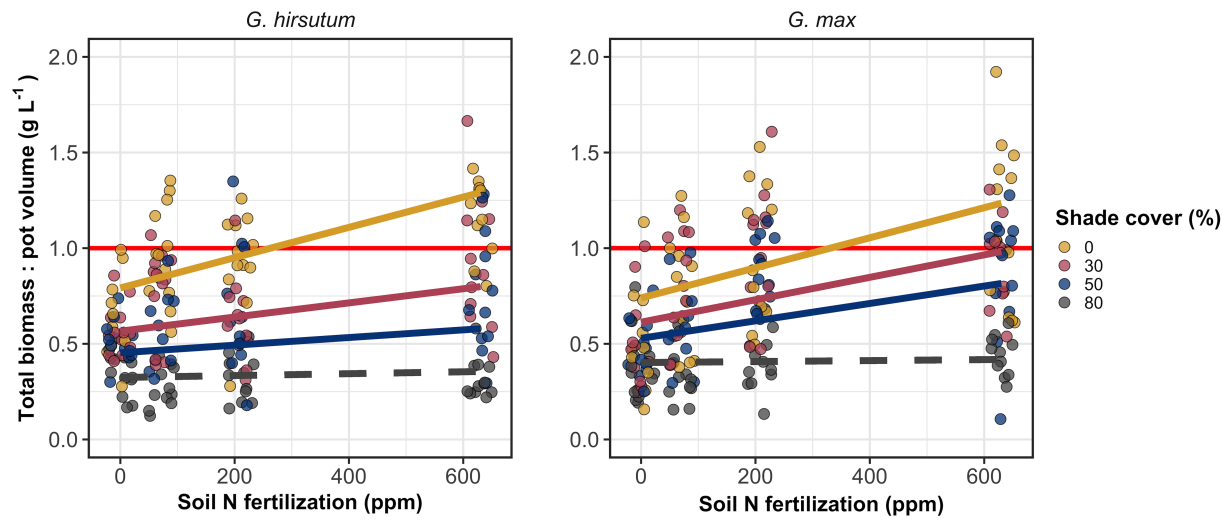


**Figure A1.** Effects of shade cover and nitrogen fertilization on the ratio of plant biomass to rooting volume in *G. hirsutum* (left panel) and *G. max* (right panel). The red horizontal line indicates the recommended  $1 \text{ g L}^{-1}$  threshold for BVR recommended by Poorter et al. (2012) to avoid pot size-induced growth limitation. Nitrogen fertilization treatments are represented on the x-axis. Shade cover treatments are represented through colored points and trendlines. Points are jittered for visibility. Yellow points and trendlines represent the 0% shade cover treatment, blue points and trendlines represent the 30% shade cover treatment, green points and trendlines represent the 50% shade cover treatment, and purple points and trendlines represent the 80% shade cover treatment. Solid trendlines indicate slopes that are significantly different from zero (Tukey:  $p < 0.05$ ), while dashed trendlines indicate slopes that are not statistically different from zero.

**3646      Appendix B: Supplemental material for "Soil nitrogen availability**  
**3647      modifies leaf nitrogen economies in mature temperate deciduous**  
**3648      forests: a direct test of photosynthetic least-cost theory"**

**Table B1.** Sample sizes of each species, abbreviated by their USDA NRCS PLANTS database code, within each plot at each site\*

	ACRU	ACSA	FAGR	FRAM	QURU	$N_{\text{plot}}$
Bald Hill						
+N; +S	0	6	1	0	1	8
+N; -S	1	2	2	0	1	6
-N; +S	2	2	0	0	2	6
-N; -S	2	3	3	0	2	10
Carter Creek						
+N; +S	0	6	1	2	0	9
+N; -S	0	4	0	2	0	6
-N; +S	0	5	1	4	0	10
-N; -S	0	7	0	0	0	7
Mount Pleasant						
+N; +S	3	2	1	0	3	9
+N; -S	0	5	4	1	0	10
-N; +S	1	2	4	0	0	7
-N; -S	3	3	1	2	1	10
$N_{\text{spp}}$	12	47	18	11	10	98

**3649** \*Plots within each site are represented based on nitrogen and sulfur addition  
**3650** status. The final column on the right depicts total sample size per plot in each  
**3651** site ( $N_{\text{plot}}$ ) and the final row on the bottom represents cumulative species sample  
**3652** size across all plots and all sites ( $N_{\text{spp}}$ ). Key: ACRU=*A. rubrum*; ACSA=*A.*  
**3653** *saccharum*; FAGR=*F. grandifolia*; FRAM=*F. americana*; QURU=*Q. rubra*

**Table B2.** Analysis of variance results exploring the linear effect of leaf temperature on net photosynthesis rate ( $A_{\text{net}}$ ;  $\mu\text{mol m}^{-2} \text{s}^{-1}$ ) and stomatal conductance ( $g_{\text{sw}}$ ;  $\mu\text{mol m}^{-2} \text{s}^{-1}$ ) measured at  $400 \mu\text{mol mol}^{-1} \text{CO}_2$

	df	$A_{\text{net}}$		$g_{\text{sw}}$	
		$\chi^2$	p	$\chi^2$	p
Leaf temperature	1	1.287	0.257	1.716	0.190

**3654** \*Results detail linear mixed effects model where temperature was regressed against  
**3655** net photosynthesis or stomatal conductance, with site and species designated as  
**3656** random intercept terms. Significance was determined using Type II Wald  $\chi^2$  tests  
**3657** ( $\alpha=0.05$ ).

**Table B3.** Second order log-polynomial regression coefficients that described the effect of leaf temperature on net photosynthesis ( $A_{\text{net}}$ ;  $\mu\text{mol m}^{-2} \text{s}^{-1}$ ) and stomatal conductance ( $g_s$ ;  $\mu\text{mol m}^{-2} \text{s}^{-1}$ ) measured at 400  $\mu\text{mol mol}^{-1} \text{CO}_2$ \*

	a	b	c
$A_{\text{net}}$	9.422	-0.573	0.010
$g_s$	-0.170	-0.186	0.003

**3658** \*Net photosynthesis and stomatal conductance values were fit to the log-polynomial  
**3659** equation  $\log(y) = a + bx + cx^2$ , where x is leaf temperature in °C.

**Table B4.** Mean, standard error, and 95% confidence interval ranges of soil nitrogen availability estimates across all measured plots. All units are expressed as  $\mu\text{g N g}^{-1}$  resin  $\text{d}^{-1}$

Site	Treatment	Mean	SE	Lower 95% CI	Upper 95% CI
Bald Hill	Ammonium sulfate	27.11	6.14	15.08	39.13
Bald Hill	Control	14.41	5.02	4.56	24.26
Bald Hill	Sodium nitrate	20.65	3.15	14.46	26.83
Bald Hill	Sulfur	6.33	2.19	2.04	10.62
Carter Creek	Ammonium sulfate	26.94	5.36	16.43	37.44
Carter Creek	Control	19.87	1.92	16.10	23.64
Carter Creek	Sodium nitrate	15.51	4.16	7.36	23.65
Carter Creek	Sulfur	5.50	1.40	2.75	8.25
Mount Pleasant	Ammonium sulfate	8.02	2.31	3.49	12.56
Mount Pleasant	Control	2.00	0.57	0.89	3.11
Mount Pleasant	Sodium nitrate	2.52	0.68	1.19	3.85
Mount Pleasant	Sulfur	2.42	0.39	1.66	3.17

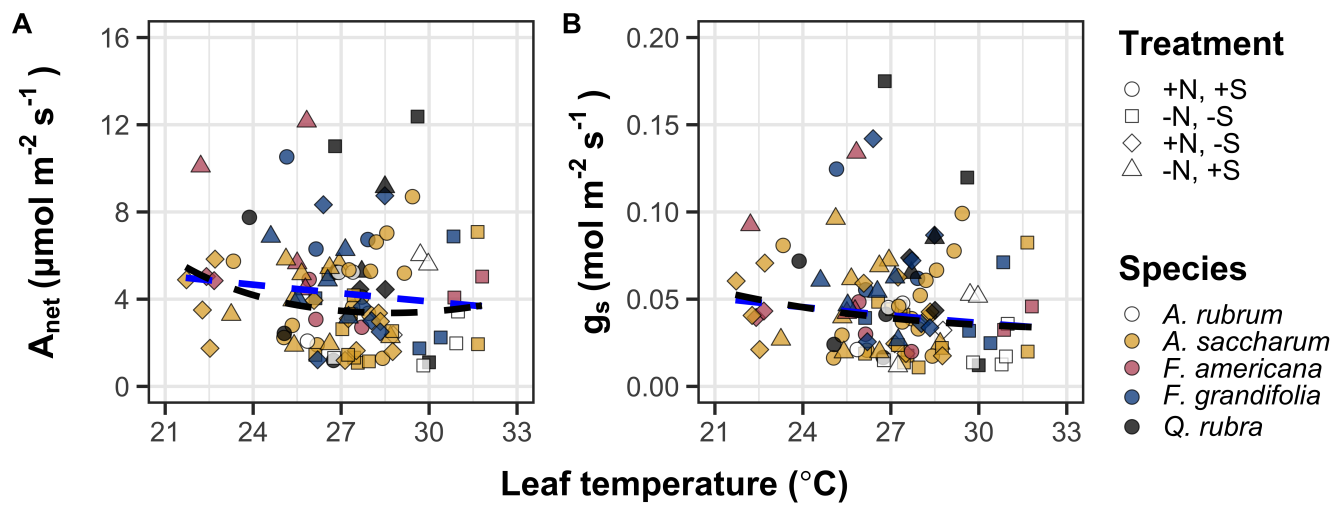


**Figure B1.** Effects of leaf temperature on net photosynthesis rate (A) and stomatal conductance (B) values when measured at  $400 \mu\text{mol mol}^{-1} \text{CO}_2$ . Leaf temperature is represented on the x-axis, while species are represented as colored points. Colored points and shapes are as explained in Figure 3.1. The dashed blue trendline describes the linear relationship between leaf temperature and each response variable, while the dashed black trendline describes the same relationship with a log-polynomial regression equation.

**3660 Appendix C: Supplemental material for "The relative cost of resource  
3661 use for photosynthesis drives variance in leaf nitrogen content across a  
3662 climate and soil resource availability gradient"**

**3663** C.1 Calculations for soil water holding capacity

**3664** Water holding capacity ( $\theta_{WHC}$ ; mm) was calculated as a function of the volumetric  
**3665** soil water storage at field capacity ( $W_{FC}$ ; m<sup>3</sup> m<sup>-3</sup>), and the volumetric soil water  
**3666** storage at wilting point ( $W_{PWP}$ ; m<sup>3</sup> m<sup>-3</sup>):

$$\theta_{WHC} = (W_{FC} - W_{PWP})(1 - f_{gravel}) * \min(z_{bedrock}, z_{max}) \quad (\text{C4.1})$$

**3667** where  $f_{gravel}$  (%) is the fraction of gravel content in soil,  $z_{bedrock}$  (mm) is the  
**3668** distance to bedrock, and  $z_{max}$  (mm) is the maximum allowable distance to bedrock,  
**3669** set to 2000mm.  $W_{FC}$  is calculated as:

$$\theta_{FC} = k_{fc} + (1.283 * (k_{fc})^2 - 0.374 * k_{fc} - 0.015) \quad (\text{C4.2})$$

**3670** where

$$\begin{aligned} k_{fc} = & -0.251 * f_{sand} + 0.195 * f_{clay} + 0.011 * f_{OM} \\ & + 0.006 * (f_{sand} * f_{OM}) - 0.027 * (f_{clay} \\ & * f_{OM}) + 0.452 * (f_{sand} * f_{clay}) + 0.299 \end{aligned} \quad (\text{C4.3})$$

**3671**  $W_{PWP}$  is calculated as:

$$W_{PWP} = k_{pwp} + (0.14 * k_{pwp} - 0.02) \quad (\text{C4.4})$$

**3672** where

$$\begin{aligned} k_{pwp} = & -0.024 * f_{sand} + 0.487 * f_{clay} + 0.006 * f_{OM} \\ & + 0.005 * (f_{sand} * f_{OM}) - 0.013 * (f_{clay} \\ & * f_{OM}) + 0.068 * (f_{sand} * f_{clay}) + 0.031 \end{aligned} \quad (\text{C4.5})$$

**3673** In Equations C4.4 and C4.5,  $f_{sand}$  (%) is the fraction of sand content in soil

**3674** (%),  $f_{clay}$  (%) is the fraction of clay content in soil (%), and  $f_{OM}$  is the fraction of

**3675** organic matter in soil (%). Organic matter in the soil was calculated by converting

**3676** soil organic carbon data extracted from SoilGrids 2.0 to soil organic matter using

**3677** the van Bemmelen factor (1.724 conversion factor).

**Table C1.** List of sampled species and their plant functional group assignment

Symbol	Species	Photo. pathway	Growth duration	Growth habit	N-fixer?	Plant functional group	Number sampled
ACAN11	<i>Acaciella angustissima</i>	c3	perennial	forb	yes	c3_legume	3
AMAR2	<i>Ambrosia artemisiifolia</i>	c3	annual	forb	no	c3_nonlegume	25
AMPS	<i>Ambrosia psilostachya</i>	c3	perennial	forb	no	c3_nonlegume	32
ARAL3	<i>Argemone albiflora</i>	c3	annual	forb	no	c3_nonlegume	3
ARPU9	<i>Aristida purpurea</i>	c4	perennial	graminoid	no	c4_nonlegume	2
ASAS	<i>Asclepias asperula</i>	c3	perennial	forb	no	c3_nonlegume	3
ASLA4	<i>Asclepias latifolia</i>	c3	perennial	forb	no	c3_nonlegume	3
ASSY	<i>Asclepias syriaca</i>	c3	perennial	forb	no	c3_nonlegume	18
BOIS	<i>Bothriochloa ischaemum</i>	c4	perennial	graminoid	no	c4_nonlegume	6
BOSA	<i>Bothriochloa saccharoides</i>	c4	perennial	graminoid	no	c4_nonlegume	6
CAPL3	<i>Carex planostachys</i>	c4	perennial	graminoid	no	c4_nonlegume	3
CAREX	<i>Carex</i> spp.	c4	perennial	graminoid	no	c4_nonlegume	16
CHFE3	<i>Chamaesyce fendleri</i>	c3	perennial	forb	no	c3_nonlegume	2
CHPI8	<i>Chrysopsis pilosa</i>	c3	annual	forb	no	c3_nonlegume	3
COCO13	<i>Conoclinium coelestinum</i>	c3	perennial	forb	no	c3_nonlegume	3
COER	<i>Commelina erecta</i>	c3	perennial	forb	no	c3_nonlegume	3
CRGLL	<i>Croton glandulosus</i>	c3	annual	forb	no	c3_nonlegume	22
CYDA	<i>Cynodon dactylon</i>	c4	perennial	graminoid	no	c4_nonlegume	15
DIAN	<i>Dichanthium annulatum</i>	c4	perennial	graminoid	no	c4_nonlegume	8
ENPE4	<i>Engelmannia peristenia</i>	c3	perennial	forb	no	c3_nonlegume	6
EUMA8	<i>Euphorbia marginata</i>	c3	annual	forb	no	c3_nonlegume	6
GAPU	<i>Gaillardia pulchella</i>	c3	annual	forb	no	c3_nonlegume	16
GLGO	<i>Glandularia gooddingii</i>	c3	perennial	forb	no	c3_nonlegume	2
HEAN3	<i>Helianthus annuus</i>	c3	annual	forb	no	c3_nonlegume	6

**Table C2.** List of sampled species and their plant functional group assignment (cont.)

Symbol	Species	Photo. pathway	Growth duration	Growth habit	N-fixer?	Plant functional group	Number sampled
HECA8	<i>Heterotheca canescens</i>	c3	perennial	forb	no	c3_nonlegume	2
HETE3	<i>Heliotropium tenellum</i>	c3	annual	forb	no	c3_nonlegume	3
IVAX	<i>Iva axillaris</i>	c3	perennial	forb	no	c3_nonlegume	4
LIAT	<i>Lilaeopsis attenuata</i>	c3	perennial	forb	no	c3_nonlegume	3
LIPU	<i>Liatris punctata</i>	c3	perennial	forb	no	c3_nonlegume	3
LOPE	<i>Lolium perenne</i>	c3	perennial	graminoid	no	c3_nonlegume	9
MIQU2	<i>Mimosa quadrivalvis</i>	c3	perennial	forb	yes	c3_legume	15
NALE3	<i>Nassella leucotricha</i>	c3	perennial	graminoid	no	c3_nonlegume	19
OECU2	<i>Oenothera curtiflora</i>	c3	annual	forb	no	c3_nonlegume	3
OENOT	<i>Oenothera</i> spp.	c3	annual	forb	no	c3_nonlegume	1
PAVI2	<i>Panicum virgatum</i>	c4	perennial	graminoid	no	c4_nonlegume	12
RACO3	<i>Ratibida columnifera</i>	c3	perennial	forb	no	c3_nonlegume	40
RHSET	<i>Rhynchosia senna</i>	c3	perennial	forb	yes	c3_legume	1
RUHI2	<i>Rudbeckia hirta</i>	c3	perennial	forb	no	c3_nonlegume	3
RUNU	<i>Ruellia nudiflora</i>	c3	perennial	forb	no	c3_nonlegume	15
RUTR	<i>Rubus trivialis</i>	c3	perennial	vine	no	c3_nonlegume	3
SAFA2	<i>Salvia farinacea</i>	c3	perennial	forb	no	c3_nonlegume	7
SCHIZ4	<i>Schizachyrium</i> spp.	c4	perennial	graminoid	no	c4_nonlegume	8
SCSC	<i>Schizachyrium scoparium</i>	c4	perennial	graminoid	no	c4_nonlegume	3
SODI	<i>Solanum dimidiatum</i>	c3	perennial	forb	no	c3_nonlegume	1
SOEL	<i>Solanum elaeagnifolium</i>	c3	perennial	forb	no	c3_nonlegume	53
SOHA	<i>Sorghum halapense</i>	c4	perennial	graminoid	no	c4_nonlegume	38
STTE3	<i>Stillingia texana</i>	c3	perennial	forb	no	c3_nonlegume	3
VEOC	<i>Verbesina occidentalis</i>	c3	perennial	forb	no	c3_nonlegume	3
VEST	<i>Verbena stricta</i>	c3	perennial	forb	no	c3_nonlegume	3

**Table C3.** Model selection results for soil moisture and vapor pressure deficit. Soil moisture was used in a bivariate regression against log-transformed  $\beta$ , while vapor pressure deficit was used in bivariate regressions against leaf  $C_l:C_a$

Day	Soil moisture		VPD	
	AICc	RMSE	AICc	RMSE
1	1431.77	0.8400	-772.71	0.0853
2	1431.76	0.8400	-775.47	0.0849
3	1431.78	0.8400	-770.86	0.0854
4	1431.79	0.8401	<b>-793.49</b>	<b>0.0839</b>
5	1431.79	0.8401	-771.66	0.0853
6	1431.78	0.8401	-771.66	0.0853
7	1431.78	0.8401	-771.05	0.0854
8	1431.76	0.8401	-770.94	0.0854
9	1431.75	0.8401	-770.11	0.0854
10	1431.74	0.8401	-770.08	0.0855
15	1431.54	0.8401	-768.64	0.0856
20	1431.40	0.8401	-769.77	0.0855
30	1431.23	0.8400	-772.18	0.0853
60	1429.84	0.8391	-779.06	0.0848
90	<b>1429.14</b>	<b>0.8385</b>	-773.99	0.0852

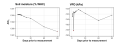


**Figure C1.** Model selection results exploring relevant timescales for soil moisture (left panel) and vapor pressure deficit (right panel). The x-axis indicates the number of days before each site visit and the y-axis notes the corrected Akaike Information Criterion value. The timescale with the lowest AICc value, and therefore most relevant timescale to include in statistical models, is noted as a red point.

**3678 Appendix D: Supplemental material for "Optimal resource investment  
 3679 to photosynthetic capacity maximizes nutrient allocation to whole  
 3680 plant growth under elevated CO<sub>2</sub>"**

**Table D1.** Summary table containing volumes of compounds used to create modified Hoagland's solutions for each soil nitrogen fertilization treatment. All volumes are expressed as milliliters per liter (mL/L)

Compound	0 ppm N	35 ppm N	70 ppm N	105 ppm N	140 ppm N
1 M NH <sub>4</sub> H <sub>2</sub> PO <sub>4</sub>	0	0.165	0.33	0.5	0.67
2 M KNO <sub>3</sub>	0	0.335	0.67	1	1.33
2 M Ca(NO <sub>3</sub> ) <sub>2</sub>	0	0.335	0.67	1	1.33
1 M NH <sub>4</sub> NO <sub>3</sub>	0	0.165	0.33	0.5	0.67
8 M NH <sub>4</sub> NO <sub>3</sub>	0	0	0	0	0
1 M KH <sub>2</sub> PO <sub>4</sub>	1	0.85	0.67	0.5	0.33
1 M KCl	3	2.45	2	1.5	1
1 M CaCO <sub>3</sub>	4	3.33	2.67	2	1.33
2 M MgSO <sub>4</sub>	1	1	1	1	1
10% Fe-EDTA	1	1	1	1	1
Trace elements	1	1	1	1	1

Compound	210 ppm N	280 ppm N	350 ppm N	630 ppm N
1 M NH <sub>4</sub> H <sub>2</sub> PO <sub>4</sub>	1	1	1	1
2 M KNO <sub>3</sub>	2	2	2	2
2 M Ca(NO <sub>3</sub> ) <sub>2</sub>	2	2	2	2
1 M NH <sub>4</sub> NO <sub>3</sub>	1	3.5	0	0
8 M NH <sub>4</sub> NO <sub>3</sub>	0	0	0.75	2
1 M KH <sub>2</sub> PO <sub>4</sub>	0	0	0	0
1 M KCl	0	0	0	0
1 M CaCO <sub>3</sub>	0	0	0	0
2 M MgSO <sub>4</sub>	1	1	1	1
10% Fe-EDTA	1	1	1	1
Trace elements	1	1	1	1

**Table D2.** Summary of the daily growth chamber growing condition program

Time	Air temperature (°C)	Light (%)
09:00	21	25
09:45		50
10:30	25	75
11:15		100
22:45	21	75
23:30		50
00:15	17	25
01:00		0

**Table D3.** Effects of CO<sub>2</sub>, fertilization, and inoculation on whole plant biomass: pot volume (BVR; g L<sup>-1</sup>)\*

	df	Coefficient	$\chi^2$	p
(Intercept)	-	1.33E-01	-	-
CO <sub>2</sub>	1	1.53E-01	146.004	<b>&lt;0.001</b>
Inoculation (I)	1	4.19E-01	19.320	<b>&lt;0.001</b>
Fertilization (N)	1	1.90E-03	279.387	<b>&lt;0.001</b>
CO <sub>2</sub> *I	1	1.03E-01	0.007	0.934
CO <sub>2</sub> *N	1	2.44E-03	49.725	<b>&lt;0.001</b>
I*N	1	-6.90E-04	9.006	<b>0.003</b>
CO <sub>2</sub> *I*N	1	-4.95E-04	0.640	0.424

**3681** \*Significance determined using Type II Wald  $\chi^2$  tests ( $\alpha=0.05$ ). P-values less  
**3682** than 0.05 are in bold. Key: df=degrees of freedom;  $\chi^2$ =Wald Type II chi-square  
**3683** test statistic.

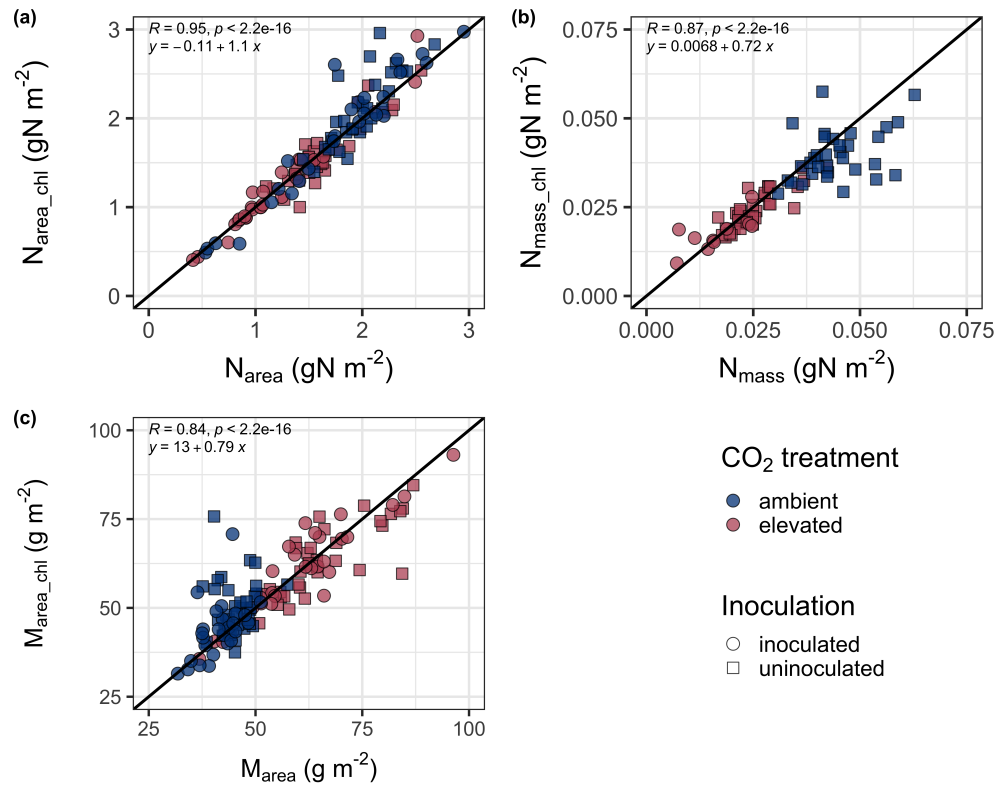


**Figure D1.** Relationships between area-based leaf nitrogen content (a), mass-based leaf nitrogen content (b), and leaf mass per unit leaf area (c) measured on the focal leaf used to generate  $A_{net}/C_i$  curves (x-axis) and leaf nitrogen content measured on the leaf used for chlorophyll extractions (y-axis). Blue points refer to leaves grown under ambient CO<sub>2</sub> and red points refer leaves grown under elevated CO<sub>2</sub>. Square points indicate uninoculated pots and circular points indicate inoculated pots. Pearson's correlation coefficient, associated *p*-values, and the line of the regression line that described each bivariate are included in the top left corner of each plot. The solid black line visualizes the trend given a 1:1 bivariate relationship.

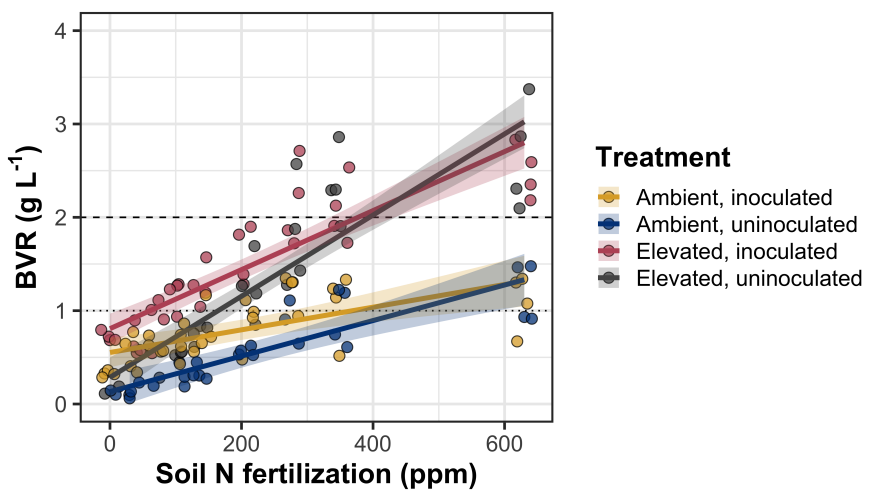


**Figure D2.** Effects of CO<sub>2</sub>, fertilization, and inoculation on the ratio of whole plant biomass to pot volume. Soil nitrogen fertilization is represented on the x-axis in all panels. Yellow points and trendlines indicate inoculated individuals grown under ambient CO<sub>2</sub>, blue points and trendlines indicate uninoculated individuals grown under ambient CO<sub>2</sub>, red points and trendlines indicate inoculated individuals grown under elevated CO<sub>2</sub>, and grey points indicate uninoculated individuals grown under elevated CO<sub>2</sub>. Solid trendlines indicate regression slopes that are different from zero ( $p<0.05$ ). The dotted horizontal line indicates the point where biomass:pot volume exceeds 1 g L<sup>-1</sup>, and the dashed line indicates the point where biomass:pot volume exceeds 2 g L<sup>-1</sup>.